Caprolactam extraction in a pulsed disc and doughnut column with a benign mixed solvent

Promotiecommissie:

Prof. dr. ir. A. Bliek, voorzitter	Universiteit Twente
Prof. dr. ir. A. B. de Haan, promotor	Universiteit Twente
Dr. ir. N. J. M. Kuipers, assistent-promotor	Universiteit Twente
Prof. dr. W. J. Briels	Universiteit Twente
Prof. dr. ir. M. M. C. G. Warmoeskerken	Universiteit Twente
Prof. dr. ir. G. J. Witkamp	Technische Universiteit Delft
Prof. dipl.-ing. dr. H.-J. Bart	Technical University of Kaiserslautern, Germany
Dr. ir. A. J. F. Simons	DSM-Research

Cover: Flooding in the top-settler of the PDDC during the forward extraction of caprolactam

CAPROLACTAM EXTRACTION IN A PULSED DISC AND DOUGHNUT COLUMN WITH A BENIGN MIXED SOLVENT

PROEFSCHRIFT

ter verkrijging van
de graad van doctor aan de Universiteit Twente,
op gezag van de rector magnificus,
prof. dr. W. H. M. Zijm,
volgens besluit van het College voor Promoties
in het openbaar te verdedigen
op vrijdag 2 september 2005 om 15.00 uur

door

Mathijs Leonard van Delden

geboren op 9 april 1977
te Hoogeveen

Dit proefschrift is goedgekeurd door de promotor

Prof. dr. ir. A. B. de Haan

en de assistent-promotor

Dr. ir. N. J. M. Kuipers

Discovery consists of looking at the same thing as everyone else and thinking something different.

(Ontdekken is zien wat iedereen heeft gezien en denken wat niemand heeft gedacht.)

Albert Szent-Györgyi, American biochemist, 1893-1986

Voorwoord

Voorjaar 2000. Informatiegesprek over een afstudeeropdracht bij Scheidingstechnologie. De (voor mij nieuwe) prof. André de Haan overtuigde me mijn heil bij zijn groep te zoeken. Ik koos uiteindelijk voor een afstudeeropdracht bij Maartje, mijn gewezen buurvrouw van de Kremersmaten. Na een paar maanden rondgelopen te hebben klampt André me aan ... 'of we even onder vier ogen konden praten' ... Hierop volgde een aanbod om na mijn afstuderen te blijven als AIO en per 1 mei 2001 liep ik dus weer rond op CT ...

Juni 2005. Het is af! Hoera! En voor het feit dat ik deze woorden nu kan intikken, wil ik een aantal mensen bedanken.

In de eerste plaats natuurlijk André, die mij verleid heeft het AIO-pad te kiezen. De vrijheid, die ik heb gekregen in mijn werk, de gezamenlijke discussies, maar zeker ook de steun in bijvoorbeeld de omgang met Bateman heb ik erg gewaardeerd. Mijn dagelijkse begeleider Norbert was altijd aanspreekbaar voor 'een klein vraagje' en heeft mij werkelijk versteld doen staan in de hoeveelheden tekst die hij kan lezen en corrigeren. De vaste staf, Wytze, Henny, Bert, Anita, Alfons, Louis, Hans, Annet en Annemiek wil ik bedanken voor de gezellige en nuttige discussies en de praktische hulp bij bijvoorbeeld de analyses of het bestellen en vervolgens weer afvoeren van chemicaliën. Een speciaal woord van dank gaat uit naar Bert, die ontzettend veel werk verzet heeft in de opbouw, het onderhoud en het werken met de pilot en andere opstellingen. Ik heb heel veel lol gehad in de samenwerking en denk met plezier terug aan alle dagen die we samen op het lab hebben rondgehangen. Onze resultaten staan in hoofdstuk 4, 5 en 8. Natuurlijk wil ik ook alle collega-AIOs bedanken voor de gezellige tijd en de steun: Boris, Fahong, Jeroen, Maartje, Bart, Johan, Paul, Meritxell, Lara, Renze, Daleen, Katarina, Natasja; en in het speciaal mijn kamergenoten, die het al die tijd met mij hebben uitgehouden: Karin, Maksym en Tanja: Bedankt!! Daarnaast hebben vele anderen binnen de faculteit hun bijdrage geleverd, zoals de mensen van de Technische Dienst, de glasinstrumentmakerij, de bibliotheek en de analysegroep.

Een groep studenten heeft mij tijdens hun stage, uitwisseling of afstuderen verder op pad geholpen in mijn onderzoek. Hartstikke bedankt daarvoor! De resultaten zijn terug te vinden in de hoofdstukken 6 en 7. Renze heeft veel werk besteed aan het modelleren en een aantal verkennende experimenten. Enric heeft goed werk verzet bij de screening van allerlei verschillende soorten oplosmiddelen. Annemarie, Milena en Rinke hebben vervolgens de screening en karakterisering van de alcohol-mengsels voor hun rekening genomen, met een mooi resultaat tot gevolg. Christian heeft tenslotte de evenwichtsverdeling van een aantal verontreinigingen onderzocht en uitgewerkt.

Natuurlijk heb ik deze jaren als AIO niet alleen op CT/TNW doorgebracht. Na de studie te hebben afgerond heb ik nog steeds contact met onder andere Daniëlle, Frans en Wouter, waarvan ik de laatste twee erg veel succes wens met hùn promotie.

In mijn vrije tijd is volleybal een grote passie en alle vrienden, teamgenoten en kennissen, die ik heb leren kennen tijdens mijn Harambee-jaren, wil ik dan ook bedanken. Met ontzettend veel plezier denk ik onder andere terug aan de teams Heren Vla, HaramGay en De Grolsche Katers of het coachen van De Barbies en Boeldoos. Natuurlijk was ook het beachen een hoogtepunt! De uitspraak 'Je hoeft echt niet te kunnen beachvolleyballen om een Master te zijn!' zal me nog lang blijven heugen. Daarnaast ben ik door Harambee ook terecht gekomen in een fantastisch studentenhuis op Kremersmaten 168. Ik hoop dan ook zeker dat het skieën met 't Gluurhuus er dit jaar weer in zit! Al met al: Inez & Mattijs, Dity & Herm, Karel, Maarten & Josien, Henny & Paul, Sonja & Vincent, Margriet & Albert, Bartje, Joris, Annick & Marco, Mark, Alex, Inge, Tobias, Benno, Hans ... en nog een heleboel anderen: Super!!

Zonder nog meer namen te gaan noemen wil ik iedereen, familie, vrienden en kennissen, die deze jaren heeft meegeleefd en belangstelling getoond, van harte bedanken.

Pap & mam, Alet & Peter, Coen & Jen, Jobien & Ad en natuurlijk alle oomzeggers, ik wil jullie ontzettend bedanken voor alle steun, al het meeleven en alle plezier: Mijn basis.

Maria, al vanaf het begin van mijn promotie ben je er altijd voor mij. Jag tackar dig för allt ...

Thijs

Contents

Summary

Introduction

Caprolactam, the monomer of nylon-6, has been known since the 19th century. Commercial interest in the caprolactam production increased in 1938, when IG Farben produced the first spinnable polymer. Large-scale industrial production of caprolactam has increased rapidly since then, resulting in a global demand of 3.5 million tons in 2001, which was expected to rise to 3.9 million tons in 2005.

Various production processes have been developed for caprolactam which is accompanied by an ongoing investigation of new or improved syntheses routes. Industrially, however, 90% of the caprolactam is produced via cyclohexanone formation, oximation and finally the Beckmann rearrangement. The recovery of caprolactam from the reaction mixture starts with neutralization, which results in the formation of a crude caprolactam top phase and an aqueous ammonium sulfate layer. Several different routes exist from this point, of which most industrial processes use solvent extraction as first step in the further recovery and purification of caprolactam.

The crude caprolactam layer is extracted with an organic solvent in the so-called forward extraction, which is followed by back-extraction with water. Nowadays, benzene, toluene or chlorinated hydrocarbons are often used as solvent in the industry. From the current market situation it follows that in the near future existing technology will remain the dominating production route for caprolactam. However, the growing awareness of the negative effects of the used solvents on health and environment results in extremely strict legislation. Thus, still an urgent need exists to improve the currently used processes, which are benchmarked in this thesis by the DSM process.

Objectives

This research was started in cooperation with Bateman Advanced Technologies (Yokneam, Israel). The first objective of the research presented in this thesis is the characterisation of their pulsed disc and doughnut column, the so-called Bateman Pulsed Column, for its applicability in the extraction of caprolactam, since it is a new type of column for the extraction of organics. The second objective of the presented research is the selection and characterization of alternative environmentally benign solvents for the extraction of caprolactam. The final objective is to compare the caprolactam extraction for the selected alternative solvent with toluene in the pilot scale pulsed disc and doughnut column.

Liquid-liquid reference systems

For the characterization of the pulsed disc and doughnut column and as reference for the alternative solvent an accurate description of the phase compositions and the physical properties of all liquid phases is required. Therefore experimental liquid-liquid equilibrium data were measured for the systems water + caprolactam + ammonium sulfate + benchmark organic solvent, where the organic solvent was either benzene or toluene. Furthermore, the

following physical properties were determined: density and viscosity of the separate phases and the interfacial tension of the two-phase systems. The equilibrium phase composition data were correlated using the Non-Random Two-Liquid (NRTL) model. The physical properties were correlated taking into account the influence of the concentration of the different solutes and the influence of temperature.

Pulsed disc and doughnut column characterization

Characteristic parameters for liquid-liquid extraction in a column are the dispersed phase hold-up, Sauter drop diameter and operational window. A theoretical model was developed capable of describing these parameters for a pulsed disc and doughnut column (PDDC) as a function of the physical properties and the operating conditions, being total flux, solvent to feed ratio, pulsation frequency and amplitude, and temperature. This model consists of an investigation of the operational window via a description of flooding due to insufficient pulsation, flooding due to a too small relative velocity between the phases and phase inversion. Within the operational window several operational regimes can be distinguished, characterising mixer-settler, dispersion and emulsion type of operation. Equations are presented for the description of the Sauter drop diameter and hold-up at each operational point. These characteristics are correlated using physical properties, operational parameters and geometrical characteristics of the column and internals.

In order to determine the above characteristics for the forward and back-extraction of caprolactam with toluene, experiments were performed in a pilot scale PDDC with a 0.04 m internal diameter and 4.24 m active column length. The experimental conditions covered the industrial range with respect to the concentrations of caprolactam and ammonium sulfate and phase continuity. The experiments were performed at equilibrium concentrations to avoid the influence of mass transfer, such that no concentration profiles existed along the column. In the determination of the operational window flooding because of too low pulsation intensity was qualitatively observed. At high pulsation intensities flooding was limiting in the forward extraction and phase inversion for the back-extraction. Application of the developed theoretical model for the description of the obtained hydraulic data resulted in an accurate description after fitting the drop diameter, hold-up and phase inversion data.

Next, the mass transfer characteristics were investigated to evaluate the contacting efficiency of a PDDC for caprolactam extraction with toluene. The concentrations of caprolactam in both phases were determined experimentally along the column length for both the forward and back-extraction. Furthermore the dispersed phase hold-up, Sauter drop diameter and operating regimes were determined and compared with the results obtained for the equilibrium situation. In the forward extraction process a significant influence of operating conditions was observed, where an increase in the flux decreased the separation efficiency, but an increase in pulsation intensity, temperature or the addition of ammonium sulfate increased the separation efficiency. HETS/m values were found between 0.42 and 0.67, depending on the conditions. In the back-extraction all concentration profiles were identical and all caprolactam was extracted after a column length of $L/m = 2$, resulting in HETS/m

values of 0.29 to 0.41. Compared to the equilibrium situation the drop diameter and pulsation intensity required for the transition of the mixer-settler to the dispersion regime were found to increase under mass transfer conditions, while the hold-up decreased. The concentration profiles were correlated with the backflow model, using a constant backflow parameter for the continuous phase and a constant overall mass transfer coefficient. The interfacial area was correlated using drop diameter and hold-up expressions derived for the equilibrium situation, taking into account the relative effect of mass transfer.

Alternative solvent selection, characterization and application

It is known that non-polar solvents are unfavourable for caprolactam extraction, because of their low caprolactam partition ratio, although they form a large binary area with water. These trends are opposite for polar solvents. As candidate alternative solvents, therefore, solvent mixtures containing a polar solvent and an alkane were proposed in order to combine the positive and eliminate the negative properties of both solvent classes. This approach was confirmed by calculations performed with the Hansen and Unifac Dortmund model, although these were not accurate enough for the selection of specific alternative solvents. In an experimental screening procedure it was found that the distribution ratio of caprolactam increased with increasing solvent (mixture) polarity. This was achieved by using a more polar functional group (ether, ester, ketone and alcohol), by a decreasing carbon chain length of the polar solvent (C_{12}-C_6) or by an increasing polar solvent fraction in the mixture. Mixtures containing heptanol (40 mass %) as polar component and methylcyclohexane or heptane as non-polar component were selected as promising candidate solvents based on a high capacity and a low mutual solvent solubility. The phase compositions of both mixed solvent systems were comparable and the data were correlated using the NRTL model. Compared to benzene an equal amount of mixed solvent is needed for both the forward and back-extraction according to the industrial DSM process lay-out. The number of theoretical stages (NTS) for the mixed solvents (m) and benzene (b) is 5 (m) and 9 (b) in the forward and 10 (m) and 5 (b) in the back-extraction, respectively. Furthermore the density and viscosity of the separate phases and the interfacial tension of the two-phase systems, were determined for both alternative solvents and correlated.

In the neutralized Beckmann rearrangement mixture impurities of inorganic and organic nature are present, of which mainly the latter are extracted along with caprolactam in the forward extraction. The effect of an alternative extraction solvent on the impurity distribution is investigated, since a different extract composition might lead to a different approach for the final purification. Equilibrium experiments were performed to determine the distribution ratio of four model impurities, aniline, n-methylcaprolactam, cyclohexanone and cyclohexane-carboxamide using toluene and the mixed solvents methylcyclohexane-heptanol (40 mass %) and heptane-heptanol (40 mass %). The experimental conditions covered the industrial case.

It was found that for all conditions the distribution to the organic phase was favourable for the impurities compared to caprolactam, resulting in all impurities being extracted in the forward extraction. Furthermore the distribution ratio of the impurities was similar for both mixed

solvents, whereas it differed relative to toluene. From equilibrium calculations the amount of each impurity in the extract of the back-extraction compared to the initial amount fed in the forward extraction was calculated for toluene and the mixed solvent at 12.9% and 26.5% for aniline, 92.0% and 85.9% for n-methylcaprolactam, 6.7% and 22.2% for cyclohexanone and 91.0% and 40.9% for cyclohexane-carboxamide, respectively. Overall, a lower amount of impurities was extracted using the mixed solvent compared to toluene.

The solvent mixture heptane-heptanol (40 mass %) was finally selected as best alternative solvent based on its beneficial physical properties, in principle allowing a higher operation capacity, since the phase compositions and the impurity distribution ratio for both candidate solvent mixtures are comparable.

Pilot plant experiments for both the forward and back-extraction of caprolactam with the mixed solvent were performed to determine the hydraulic characteristics, being hold-up, Sauter drop diameter, operational window, and separation performance as a function of the operating conditions. Furthermore the influence of mass transfer on the dispersed phase hold-up, average droplet diameter and operating regime was determined. It was found that the hydraulic characteristics were qualitatively comparable to the behaviour determined for caprolactam extraction with toluene and the obtained hydraulic data were described using the derived theoretical model. For the mass transfer experiments it was found that the mixed solvent was highly favourable in the forward extraction with HETS/m values of 0.26 to 0.37, while less theoretical stages are required as well. Toluene was favourable as solvent in the back-extraction, because less theoretical stages are required, since the HETS values are comparable for both solvents. Mass transfer profiles were described using the backflow model.

Outlook

The selected candidate solvent mixture, heptane-heptanol (40 mass %), shows beneficial behaviour relative to toluene. The developed solvent mixture might, however, be improved even further, with respect to considerations of economical nature, the ease with which it can be recovered or freed from impurities and, if required, a further decrease of the solubility of water in the organic phase.

It has furthermore been demonstrated that the use of solvent mixtures offers a possibility to create environmentally benign solvents, which can replace currently used toxic solvents in a technical and economical feasible way. Although studied for caprolactam in this thesis, it is expected that solvent mixtures can be used as well in other applications where pure solvents are not able to replace the currently used hazardous solvents. Mixed solvents can be designed to perform better than pure solvents and/or to obtain economically attractive designer solvents without the need of custom synthesizes.

Concerning the application of the selected mixed solvent relative to benzene in a PDDC, qualitatively comparable hydraulic characteristics are expected, while benzene is expected to

show almost equal characteristics compared to toluene, since only a minor difference exists between the physical properties of these two solvents.

From the performed mass transfer experiments it follows that changing experimental conditions influenced the extraction process beneficially. The forward extraction with toluene and the back-extraction from the mixed solvent were influenced beneficially by a temperature increase and decrease, respectively, because of a positive change of the system properties.

The operation and design of a column for caprolactam extraction are dominated by the concentrations and physical properties at the feed-section only, which change strongly, however, along the column length. In order to obtain the desired raffinate concentration, the required length of the column is, in contrast, dominated by the raffinate-side of the column, which is operated in the unfavourable mixer-settler regime in case of the PDDC. A customized design of the column internals along the column length might result in a more efficient operation, assuring a less intensified energy input in the top (feed-section) and a more intensified input in the bottom (raffinate-section). For a PDDC this might be obtained by decreasing disc sizes, increasing doughnut aperture sizes and a larger distance between the discs and doughnuts towards the top of the column.

In agitated columns a more even distribution of the mechanical energy input leads to a smaller drop size distribution, resulting amongst others in less formation of emulsions. A PDDC might prove beneficial compared to a RDC, since the latter shows a locally high energy input at the disc-tips.

During the operation of the column emulsion formation was observed, but not quantified, and this effect on the extract quality of especially the forward extraction might prove necessary to take into account.

Samenvatting

Inleiding

Caprolactam, het monomeer van nylon-6, is reeds bekend sinds de 19^e eeuw. Commerciële interesse in de productie van caprolactam ontstond in 1938, toen IG Farben het eerste gesponnen polymeer produceerde. Caprolactam werd al gauw belangrijker zodat de industriële productie snel toenam, wat resulteerde in een wereldwijde vraag van 3,5 miljoen ton in 2001. De verwachting is dat deze zal stijgen tot 3,9 miljoen ton in 2005.

Verschillende productieprocessen zijn ontwikkeld voor caprolactam terwijl er doorlopend onderzoek plaatsvindt naar nieuwe of verbeterde syntheseroutes. In de industrie wordt echter 90% van het caprolactam geproduceerd via de vorming van cyclohexanon, daaropvolgende oximering en uiteindelijk de Beckmann-omlegging. De winning van caprolactam uit het reactiemengsel start vervolgens met een neutralisatiestap. Dit resulteert in de vorming van de zogenaamde 'crude caprolactam' toplaag en een waterige ammoniumsulfaatlaag. Er bestaan verschillende opwerkingsprocessen vanaf dit punt waarbij de meeste industriële processen extractie gebruiken als eerste stap in de verdere winning en zuivering van caprolactam.

De 'crude caprolactam' laag wordt geëxtraheerd met een organisch oplosmiddel in de zogenaamde heen-extractie. Deze wordt gevolgd door een terugextractie met water. Tegenwoordig worden in de industrie benzeen, tolueen of gechloreerde koolwaterstoffen gebruikt als oplosmiddel. Uit de huidige marktpositie volgt dat in de nabije toekomst de bestaande technologie bepalend zal zijn als productieproces van caprolactam. Het groeiende besef van de negatieve effecten van de gebruikte oplosmiddelen op de gezondheid en het milieu resulteert echter in een zeer strenge milieuwetgeving. Daarom bestaat de behoefte om de bestaande processen te verbeteren. Het DSM-proces wordt in dit proefschrift gebruikt als referentiekader.

Doel

Dit onderzoek is gestart in samenwerking met Bateman Advanced Technologies (Yokneam, Israel). Het eerste doel van het in dit proefschrift gepresenteerde onderzoek is de karakterisering van hun gepulseerde schijf-en-ring kolom (pulsed disc and doughnut column, PDDC, ofwel Bateman Pulsed Column) voor de toepassing in de extractie van caprolactam. Dit is een nieuw type kolom voor de extractie van organische stoffen. Het tweede doel van het onderzoek is de selectie en karakterisering van alternatieve milieuvriendelijke oplosmiddelen voor de extractie van caprolactam. Het laatste doel is de vergelijking van de caprolactamextractie met het geselecteerde alternatieve oplosmiddel en tolueen in de kolom op 'pilot' schaal.

Vloeistof-vloeistof referentiesystemen

Voor de karakterisering van de PDDC en als referentie voor het alternatieve oplosmiddel, is een nauwkeurige beschrijving nodig van de samenstelling van de fasen en de fysische eigenschappen van alle vloeibare fasen. Daarom zijn experimentele vloeistof-vloeistof-

evenwichten bepaald voor de systemen water + caprolactam + ammoniumsulfaat + referentie-organisch oplosmiddel, waarbij het organische oplosmiddel benzeen of tolueen was. Verder zijn de volgende fysische eigenschappen bepaald: dichtheid en viscositeit van iedere fase apart en de grensvlakspanning van de tweefasensystemen. Met het 'Non-Random Two-Liquid' (NRTL) model is de evenwichtssamenstelling van de fasen beschreven. De fysische eigenschappen zijn gecorreleerd op basis van de invloed van de temperatuur en de concentratie van de verschillende opgeloste stoffen.

Karakterisering van de gepulseerde schijf-en-ring kolom

Karakteristieke parameters voor vloeistof-vloeistof extractie in een kolom zijn de volumefractie van de gedispergeerde fase ('hold-up'), de gemiddelde druppeldiameter (Sauterdiameter) en het operatiegebied. Een theoretisch model dat deze parameters kan beschrijven voor een PDDC werd ontwikkeld op basis van de fysische eigenschappen en de operatiecondities zijnde de totale flux, de debietverhouding van oplosmiddel en voeding, de temperatuur en de pulsatiefrequentie en -amplitude. Uit het model volgt het operatiegebied middels de beschrijving van het over- of vollopen van de kolom ('flooding') door onvoldoende pulsatie, 'flooding' door een te kleine relatieve snelheid tussen beide fasen en fase-inversie. In het operatiegebied kunnen verschillende regimes onderscheiden worden, aangeduid als 'mixer-settler-', dispersie- en emulsieregime. Vergelijkingen voor de beschrijving van de Sauterdiameter en 'hold-up' voor ieder operatiepunt zijn weergegeven. Deze karakteristieken zijn gecorreleerd via de fysische eigenschappen, operatieparameters en de geometrische karakteristieken van de kolom en 'internals'.

Om de hierboven beschreven karakteristieken te bepalen voor de heen- en terugextractie van caprolactam met tolueen zijn experimenten uitgevoerd in een 'pilot' PDDC met een interne diameter van 0,04 m en een actieve kolomlengte van 4,24 m. De experimentele condities kwamen overeen met die in de industrie wat betreft de concentraties van caprolactam en ammoniumsulfaat en de selectie van de continue fase. De experimenten zijn uitgevoerd met een systeem dat op evenwicht was om de invloed van stofoverdracht te voorkomen: er treden dus geen concentratieprofielen in de kolom op. Bij de bepaling van het operatiegebied is 'flooding' vanwege een te lage pulsatie-intensiteit kwalitatief waargenomen. Bij een hoge pulsatie-intensiteit was 'flooding' limiterend bij de heen-extractie en fase-inversie tijdens de terugextractie. Het ontwikkelde model gaf een nauwkeurige beschrijving van de verkregen hydraulische data na het correleren van de data voor de Sauterdiameter, 'hold-up' en fase-inversie.

Vervolgens zijn de stofoverdrachtskarakteristieken onderzocht om de effectiviteit te bepalen van de PDDC voor de caprolactamextractie met tolueen. De caprolactamconcentraties in beide fasen zijn experimenteel bepaald als functie van de positie langs de kolom, zowel voor de heen- als de terugextractie. Verder zijn de 'hold-up', Sauterdiameter en operatieregimes bepaald en vergeleken met de verkregen resultaten voor de evenwichtssituatie. In het heen-extractieproces werd een significante invloed van de operatiecondities waargenomen, waarbij een verhoging van de flux de effectiviteit verlaagde. Een verhoging van de pulsatie-intensiteit,

temperatuur of het toevoegen van ammoniumsulfaat vergrootte echter de effectiviteit. De hoogte van een evenwichtstrap (HETS) werd bepaald op 0,42 tot 0,67 m, afhankelijk van de operatiecondities. In de terugextractie waren alle concentratieprofielen identiek, waarbij al het caprolactam reeds was geëxtraheerd na een kolomlengte van L/m = 2, hetgeen resulteerde in waarden van HETS/m = 0,29 tot 0,41. Vergeleken met de evenwichtssituatie bleken de druppeldiameter en de pulsatie-intensiteit voor de overgang van het 'mixer-settler-' naar het dispersieregime groter tijdens stofoverdracht, terwijl de 'hold-up' juist kleiner werd. De concentratieprofielen werden beschreven met het 'backflow' model, waarbij een constante 'backflow' parameter voor de continue fase werd gebruikt en een constante totale stofoverdrachtscoëfficiënt. Het uitwisselend oppervlak tussen de fasen werd beschreven met de afgeleide relaties voor de Sauterdiameter en de 'hold-up' onder evenwichtscondities, waarbij rekening werd gehouden met het relatieve effect van stofoverdracht.

Selectie, karakterisering en toepassing van het alternatieve oplosmiddel

Het is bekend dat apolaire oplosmiddelen ongunstig zijn voor caprolactamextractie vanwege hun lage verdelingscoëfficiënt voor caprolactam, alhoewel ze een groot binair gebied vormen met water. Deze trends zijn omgekeerd voor polaire oplosmiddelen. Als mogelijke alternatieve oplosmiddelen werden daarom mengsels van een polair oplosmiddel en een alkaan voorgesteld om zo de positieve eigenschappen van beide oplosmiddelsoorten te combineren en de negatieve te elimineren. Deze aanpak werd bevestigd door berekeningen uitgevoerd met het Hansen- en Unifac Dortmund model. Deze waren echter niet nauwkeurig genoeg voor de selectie van specifieke alternatieve oplosmiddelen. Via een experimentele screeningprocedure werd bepaald dat de verdelingscoëfficiënt van caprolactam toenam met een toenemende polariteit van het oplosmiddel. Dit werd bewerkstelligd door een meer polaire functionele groep (ether, ester, keton en alcohol), afnemende lengte van de koolstofketen van het polaire oplosmiddel (C_{12}-C_6) of een toenemende fractie van het polaire oplosmiddel te gebruiken in het mengsel. Mengsels van heptanol (40 gewichts %) als polaire component en heptaan of methylcyclohexaan als niet-polaire componenten werden geselecteerd als veelbelovende mogelijke oplosmiddelen op basis van een hoge capaciteit en een lage wederzijdse oplosbaarheid. De samenstelling van de fasen was vergelijkbaar voor beide oplosmiddelen en de data werden gecorreleerd via het NRTL model. Vergeleken met benzeen in het industriële DSM-proces is een zelfde hoeveelheid mengsel nodig voor zowel de heen- als de terugextractie. De hoeveelheid evenwichtstrappen (NTS) voor het mengsel (m) en benzeen (b) is berekend op respectievelijk 5 (m) en 9 (b) in de heen- en 10 (m) en 5 (b) in de terugextractie. Verder zijn de dichtheid en viscositeit van iedere fase apart en de grensvlakspanning van de tweefasensystemen bepaald en gecorreleerd voor beide alternatieve oplosmiddelen.

In het geneutraliseerde mengsel na de Beckmann-omlegging zijn verontreinigingen van anorganische en organische aard aanwezig, waarvan voornamelijk de laatste samen met caprolactam worden geëxtraheerd in de heen-extractie. Het effect van een alternatief oplosmiddel op de verdelingscoëfficiënt van deze verontreinigingen is onderzocht, aangezien een andere samenstelling van het extract kan leiden tot een andere aanpak in de uiteindelijke

zuivering. Evenwichtsexperimenten werden uitgevoerd waarbij de verdelingscoëfficiënt voor vier modelverontreinigingen, aniline, n-methylcaprolactam, cyclohexanon en cyclohexaancarboxamide, is bepaald voor zowel tolueen als de mengsels methylcyclohexaan-heptanol (40 gewichts %) en heptaan-heptanol (40 gewichts %). De experimentele condities kwamen overeen met de industriële situatie.

Bij alle condities werd gevonden dat, vergeleken met caprolactam, de verdeling naar de organische fase hoger was voor de verontreinigingen zodat in de praktijk alle verontreinigingen volledig geëxtraheerd worden in de heen-extractie. Verder was de verdelingscoefficiënt van de verontreinigingen gelijk voor beide mengsels, maar anders dan met tolueen. Met evenwichtsberekeningen werd de hoeveelheid van iedere verontreiniging in het extract van de terugextractie bepaald voor tolueen en het mengsel in vergelijking tot de initiële hoeveelheid, die was gevoed in de heen-extractie. Deze was respectievelijk 12,9% en 26,5% voor aniline, 92% en 85,9% voor n-methylcaprolactam, 6,7% en 22,2% voor cyclohexanon en 91,0% en 40,9% voor cyclohexaan-carboxamide. In totaliteit werd een kleinere hoeveelheid verontreinigingen geëxtraheerd door het mengsel dan door tolueen.

Het mengsel heptaan-heptanol (40 gewichts %) werd uiteindelijk geselecteerd als beste alternatieve oplosmiddel op basis van de gunstige fysische eigenschappen, die in principe de mogelijkheid bieden tot een hogere operatiecapaciteit, aangezien de samenstelling van de fasen en de verdelingscoëfficiënt van de verontreinigingen voor beide kandidaatmengsels gelijk zijn.

Experimenten in de 'pilot' voor de heen- en terugextractie van caprolactam met het bovengenoemde mengsel werden uitgevoerd om de hydraulische eigenschappen, 'hold-up', Sauterdiameter en operatiegebied, en het scheidingsvermogen te bepalen als functie van de operatiecondities. Verder werd de invloed bepaald van de stofoverdracht op de genoemde karakteristieken. Het bleek dat de hydraulische karakteristieken en de invloed van stofoverdracht kwalitatief gelijk waren aan die voor de caprolactamextractie met tolueen. De bepaalde hydraulische data werden beschreven met het ontwikkelde theoretische model. Uit de stofoverdrachtsexperimenten werd bepaald dat het mengsel veel gunstiger was voor de heen-extractie, waarbij HETS-waarden van 0,26 tot 0,37 m werden berekend, terwijl ook minder theoretische trappen nodig waren. Tolueen was echter gunstiger in gebruik voor de terugextractie, omdat minder theoretische trappen nodig zijn, aangezien de HETS-waarden vergelijkbaar zijn voor beide oplosmiddelen. De stofoverdrachtsprofielen zijn beschreven met het 'backflow' model.

Nabeschouwing

Het geselecteerde mengsel, heptaan-heptanol (40 gewichts %), vertoont gunstig extractiegedrag ten opzichte van tolueen. Het ontwikkelde mengsel kan echter nog verder verbeterd worden in economisch opzicht, het gemak waarmee het teruggewonnen of van verontreinigingen ontdaan kan worden en, indien gewenst, door de oplosbaarheid van water in de organische fase verder te verlagen.

Verder is aangetoond dat het gebruik van mengsels de mogelijkheid biedt om milieuvriendelijke oplosmiddelen te creëren, die huidig toegepaste, giftige oplosmiddelen kunnen vervangen op een technisch en economisch haalbare manier. Er wordt verwacht dat mengsels ook gebruikt kunnen worden in andere toepassingen, waar een zuiver oplosmiddel niet in staat is de huidige toegepaste gevaarlijke oplosmiddelen te vervangen. Anderzijds zouden mengsels ontworpen kunnen worden voor betere prestaties en/of als een economische manier om op maat gemaakte oplosmiddelen te verkrijgen zonder specifieke synthese.

Voor de toepassing van het geselecteerde mengsel en benzeen in een PDDC worden kwalitatief gelijke hydraulische karakteristieken verwacht. Daarnaast wordt verwacht dat benzeen dezelfde karakteristieken zal vertonen als tolueen, aangezien slechts een klein verschil bestaat tussen de fysische eigenschappen van de beide oplosmiddelen.

Uit de uitgevoerde stofoverdrachtsexperimenten volgt dat het aanpassen van de experimentele condities het extractieproces gunstig beïnvloedt. De heen-extractie met tolueen en de terugextractie met het mengsel werden positief beïnvloed vanwege de positieve verandering van de systeemeigenschappen door respectievelijk een temperatuursverhoging en -verlaging.

De operatie en het ontwerp van een extractiekolom voor caprolactam wordt alleen gebaseerd op de concentraties en fysische eigenschappen aan de voedingszijde van de kolom. Langs de kolom veranderen deze echter sterk. De benodigde kolomlengte om de gewenste raffinaatconcentratie te verkrijgen, wordt met name bepaald door de raffinaatzijde van de kolom, welke wordt bedreven in het 'mixer-settler' regime voor een PDDC. Een specifiek ontwerp van de 'internals' over de kolomlengte kan resulteren in een efficiëntere operatie, waarbij energie minder intensief wordt toegevoerd in de top (voedingssectie) en meer intensief in de bodem (raffinaat-sectie). Voor een PDDC kan dit wellicht worden gerealiseerd door de schijfgrootte te verkleinen, door de ringdiameter te vergroten en door een grotere afstand tussen de schijf en de ring te introduceren in de richting van de top van de kolom.

In een mechanisch aangedreven kolom resulteert een gelijkmatiger verdeling van de energietoevoer in een smallere druppelgrootteverdeling wat onder andere een verminderde emulsievorming oplevert. Een PDDC kan hierin gunstig blijken ten opzichte van een RDC, aangezien de laatste een lokaal hoge energiedissipatie geeft aan de uiteinden van de schijf.

Tijdens het bedrijven van de kolom werd emulsievorming waargenomen, maar niet gekwantificeerd. Het zou, met name voor de heen-extractie, kunnen blijken dat het noodzakelijk is om rekening te houden met dit effect vanwege de extractkwaliteit.

Chapter 1

Current caprolactam production processes

This thesis is concerned with new technology for caprolactam extraction, namely the application of a new type of extraction column and an alternative environmentally benign solvent. In this chapter the current market situation of caprolactam, the currently applied production and recovery routes and finally a benchmark production process are discussed. For extraction, as first recovery and purification step, all applied solvents and columns are presented. The chapter is concluded with the objective and outline of this thesis.

1.1   Introduction
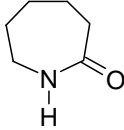
Caprolactam, 2-oxohexamethylenimine, has been known since the 19th century. Gabriel and Maas synthesized caprolactam first in 1899 by cyclization of ε-aminocaproic acid. Commercial interest in the caprolactam production increased in 1938, when IG Farben produced the first spinnable polymer. Caprolactam gained importance and large-scale industrial production has increased rapidly since then.[1,2]

Nowadays caprolactam is one of the most widely used chemical intermediates. The main producers include Allied Signal, BASF, Bayer, DSM, Leuna Werke, Mitsubishi, Montedison and Ube Industries. SNIA Viscosa and Toray produce the remaining part.[1,3] The global demand in 2001 was with 3.5 million tons covering 82% of the production capacity and is expected to rise to 3.9 million tons in 2005.[4-7] 90% of the produced amount is consumed for the production of nylon fibers.[4,5]

Caprolactam is a white, hygroscopic, crystalline solid at ambient temperature, with a characteristic odour. It is very soluble in water and in most organic solvents and is sparingly soluble in high molecular weight aliphatic hydrocarbons. The structural formula and its melting point, M_p/K, boiling point, B_p/K, and ignition point, I_p/K, are listed in Table 1.1.

Caprolactam is a cyclic amide and reacts according to this class of components. It can be subjected to oxidation, hydrolysis, N-alkylation, halogenation, nitration and various other reactions. The (industrially) most important chemical property of caprolactam is the possibility of polymerization. The ring is hydrolyzed at 533-543 K and linear polymer chains are formed by polycondensation.[1,2]

Table 1.1. Structural formula and characteristic temperatures of caprolactam.

Structure	
Molar mass/g·mol^{-1}	113.16
M_p/K	342.4
B_p/K (at 101.3 kPa)	541.7
I_p/K	648

1.2 Production routes for caprolactam

All developed production routes for caprolactam are described together with investigated improvements, alternative routes and currently performed research on (steps in the) caprolactam synthesis. Finally, a commercially applied process route is selected as reference for the process improvements discussed in this thesis.

1.2.1 Developed caprolactam synthesis routes

Various synthesis routes have been developed for caprolactam. In a great number of them cyclohexanone oxime is the main intermediate. In general, this oxime is obtained via hydroxylamine salts reacting with cyclohexanone. In a conventional synthesis route, the Raschig process, hydroxylamine sulfate is produced in several steps with ammonium sulfate as a by-product. In the following oximation section hydroxylamine sulfate reacts with cyclohexanone, where the formation of extra free sulfuric acid is avoided by the use of aqueous ammonia as a neutralizing agent while keeping the pH at a value of 4.5. The reaction is shown in Reaction 1.1.[1,2,8]

Reaction 1.1
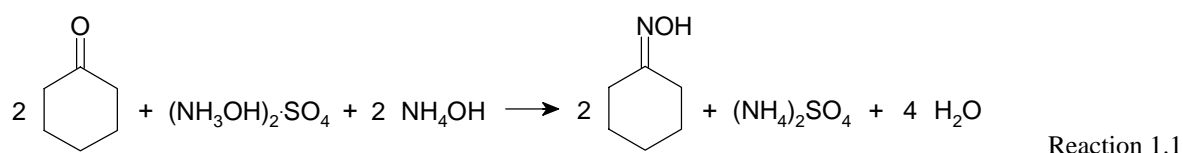
The formation of cyclohexanone oxime results in two liquid phases. The first phase, consisting of oxime, is subjected to the Beckmann rearrangement for conversion into caprolactam. The second phase is an ammonium sulfate solution.[1] The total amount of ammonium sulfate formed is 2.7 tons per ton of oxime.[2]

Several different processes have been developed for the production of hydroxylamine salts and the following formation of the oxime, mainly in order to decrease the unfavourable amount of by-product. These processes include:

- Nitrogen monoxide reduction process (BASF, Inventa), where 0.7 tons ammonium sulfate per ton of cyclohexanone oxime is produced;[1,2,9,10]

- Hydroxyl ammonium sulfate oxime (HSO) process (BASF, Inventa) where 0.1 tons ammonium sulfate per ton of oxime is produced;[10,11]

- Hydroxylamine fosfate oxime (HPO) process (DSM), where no ammonium sulfate is produced;[1,10]

- The ammoximation process of EniChem is based on the reaction of cyclohexanone with hydroxylamine, instead of a corresponding hydroxylamine salt, and no ammonium sulfate is obtained as byproduct;[12]

- In the PNC process (Toray) cyclohexane is converted by photonitrosation to cyclohexanone oxime dihydrochloride, while no ammonium sulfate is produced.[2,3,13,14]

After the oximation reaction, the obtained cyclohexanone oxime is transformed into caprolactam with sulfuric acid or oleum via the Beckmann rearrangement, as shown in Reaction 1.2, where all manufacturers use a similar approach. The molar ratio of cyclohexanone oxime compared to oleum ranges from 1.0 to 1.5.[1,2,13,15-19] The rearrangement is a very rapid, highly exothermic reaction and the rearrangement is more complete in concentrated sulfuric acid.[2] Sulphur trioxide binds the water in the moist cyclohexanone oxime to form sulfuric acid and in excess it increases the rate of the rearrangement. Free acid can be neutralized with gaseous or aqueous ammonia.[2,8]
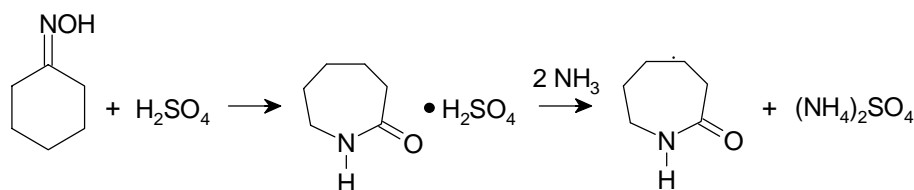
Reaction 1.2

If the acid is neutralized a total of 1.8 tons of ammonium sulfate per ton of caprolactam is obtained in the neutralization process after the rearrangement reaction.[2]

The complete process starting from benzene or cyclohexane using the production route via cyclohexanone oxime, Beckmann rearrangement and neutralization produces a maximum of 4.5 tons of ammonium sulfate per ton of product. Taking into account the improvements made in the production of cyclohexanone oxime, 2 tons of ammonium sulfate is still produced in the neutralization step following the rearrangement reaction of the oxime to caprolactam.[10]

With the formation of ammonium sulfate being the most important problem in the caprolactam production, and due to the increasing costs of its removal, extensive research was performed for new possibilities to produce caprolactam. Reduction of ammonium sulfate production was investigated by avoiding the oxime as an intermediate product.[10] The four most important processes for the production of caprolactam avoiding cyclohexanone oxime production include:

- The cyclohexane carboxylic acid process (SNIA), which is a toluene-based process, where caprolactam is obtained in three steps. Toluene is catalytically oxidated with air to benzoic acid, followed by hydrogenation to cyclohexane carboxylic acid, which is then nitrosated. One mole of carbon dioxide per mole of caprolactam is set free along with small amounts

of other gases, while 3.3 moles of sulfuric acid per mole of caprolactam are consumed;[2,10,20,21]

- The UCC process, in which cyclohexanone is oxidized with peracetic acid to caprolactone, which is a precursor to caprolactam. Since 1967 this process was in commercial use, but the caprolactam formation was given up in 1972;[10]

- The TechniChem process, in which ε-aminocaproic acid is formed from cyclohexanone in several steps, which then can be converted into caprolactam. This route was, however, never industrialized;[10]

- The BP process, where cyclohexanone reacts with H_2O_2 to 1,1-dihydroxydicyclohexyl peroxide, which is converted to caprolactam and cyclohexanone. Comparable processes are described by Inventa, Degussa and Toa Gosei.[2,10]

1.2.2   Current developments in the caprolactam synthesis

As caprolactam is an intermediate product with a large demand, there is extensive research ongoing for new synthesis routes which are more favourable due to less expensive reactants or more economical processes. One very important point is the avoidance of the production of large amounts of ammonium sulfate. As for the known process routes, the new developments can be subdivided into a group using cyclohexanone oxime as the intermediate and a group avoiding it. For the processes still using cyclohexanone oxime as an intermediate, both steps, the oximation and the Beckmann rearrangement, have to be optimized.

In the further development of the known caprolactam production processes several new routes for the production of cyclohexanone oxime have been investigated, including the oxidation of cyclohexylamine with elemental oxygen (Allied Signal), the ammoximation of cyclohexanone with ammonia and air (Allied Signal) and the reaction of cyclohexane with nitric oxide, alkyl nitrites, or nitroalkanes to bis(nitrosocyclohexane), which rearranges in situ to cyclohexanone oxime (Monsanto).[2,10]

Furthermore extensive research has been performed as well on different routes for the Beckmann rearrangement covering the non-catalytic Beckmann rearrangement in supercritical water,[22,23] catalytic vapour phase[10,24] and catalytic liquid phase rearrangement.[25] Several processes have been proposed and proved on pilot plant scale,[2,10] whereas Sumitomo Chemical now sets on caprolactam production via catalytic conversion on an industrial scale.[10]

In the development of new caprolactam production processes several routes have been investigated for an alternative formation of caprolactam from cyclohexanone. The proposed processes include:[2]

- Oxidation of cyclohexanone with air to ε-hydroxycaproic acid, which is converted to caprolactam using ammonia (Teijin);

- Reaction of cyclohexanone with excess acetic anhydride to cyclohexenyl acetate, which is converted to 2-nitrocyclohexanone followed by cracking with excess aqueous ammonia.

4

The resulting aqueous ammonium nitrocaproate solution is hydrogenated and the obtained aqueous ε-aminocaproic acid solution is converted to caprolactam (TechniChem);

- Reaction of cyclohexanone in aqueous ammonia solution with hypochlorite solution to cyclohexanone isoxime, which is heated to give caprolactam (Leuna-Werke).

Furthermore new caprolactam production processes are investigated based on alternative raw materials, being furfural, acetylene, propylene, ethylene and butadiene,[2] of which the latter is the most promising from industrial point of view.[10] DSM owns patented technology on the butadiene-based production route and a DSM/DuPont joint venture develops this production process, whereas a BASF/DuPont joint venture worked on the scale of this process. Although the latter cooperation was given up in 1999, BASF tries to realize the process alone.[10]

A different alternative raw material is nylon-6 waste, which can be depolymerised with the aid of a cracking catalyst and superheated steam. After concentration, removal of impurities and final purification, the obtained caprolactam can be re-used.[2,10] A DSM/Allied Signal joint venture managed a commercial-scale nylon recycling plant. Higher than expected production costs led to a production stop in 2001.

A completely different approach for the production of caprolactam was developed around 1960 using biological synthesis of caprolactam. DSM lately continued this research, producing caprolactam from starch via a fermentative route, and by Allied Signal, developing a microbiological process for the conversion of cyclohexane to caprolactone.[10]

1.2.3 Commercial synthesis routes

The production routes for caprolactam vary per company, but from all possible routes four basic processes that are important from commercial viewpoint can be distinguished, which are schematically shown in Figure 1.1.[19]
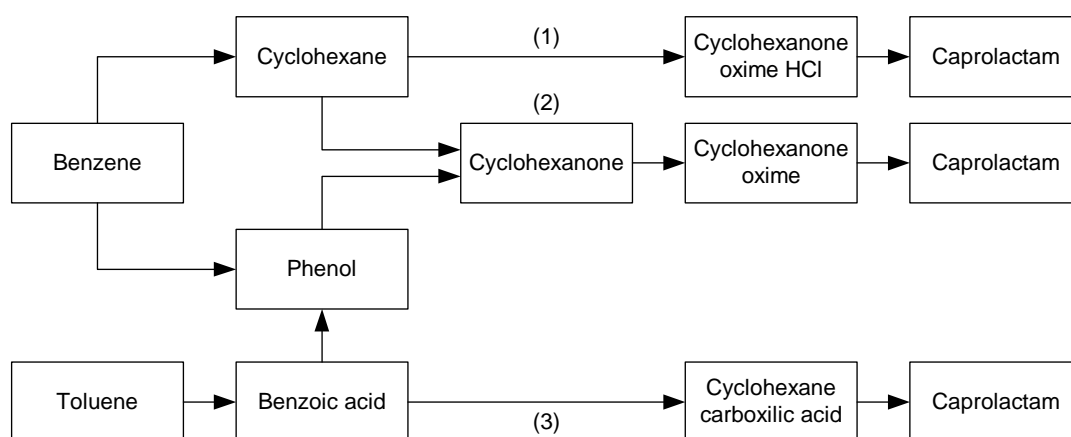
Figure 1.1. The various commercial routes for caprolactam production.[19]

The production of caprolactam via the formation of cyclohexanone followed by oximation and Beckmann rearrangement (2), is the main production route, being responsible for 90% of the produced amount (BASF, Bayer, DSM, Allied Signal, Inventa and EniChem).[1,2] The photonitrosation route (1) is used only in the Toray PNC process. Several companies including SNIA follow the cyclohexane carboxylic acid route (3).

With respect to the investments in new technology and production processes, the caprolactam market seems not favourable. A capacity utilisation of 89% is considered as the bottom-line rate for viable production and with the given demand additional production capacity is hardly needed. DSM, as one of the leading producers, believes that no new caprolactam plants need to be built at least until 2006.[6,7] Industrial facilities for caprolactam production will in the near future therefore be based on (improved) existing production routes.

1.3   Caprolactam recovery processes

Using the main production route as starting point, applied caprolactam recovery routes are described, together with alternative routes and currently performed research on caprolactam recovery. Finally, a reference recovery process is selected based on a commercial viewpoint.

1.3.1   Developed processes for caprolactam recovery

The main reaction routes for the production of caprolactam end with the Beckmann rearrangement as final step in caprolactam formation. In the resulting reaction mixture, caprolactam, which is a very weak organic nitrogen base, is bound to the sulfuric acid in its conjugated acid form.[1,16] For the separation of caprolactam from the reaction mixture two possible routes exist.

The first route is the direct extraction of caprolactam from the reaction mixture. In order to reduce the attraction between the acid and caprolactam the reaction mixture is diluted with water and possibly partly neutralized. The advantage of this approach resides in avoiding the neutralization step as described in Reaction 1.2.[1,15,19,26-29] Despite this advantage, direct extraction is commercially not applied, because of the high capital investments and a steep rise in energy costs of the process.[1,19]

For the second route, which is industrially applied, the rearrangement mixture is neutralized with gaseous or aqueous ammonia, resulting in the formation of two liquid phases. The crude caprolactam top phase, consisting of 65 to 70 mass % caprolactam, 1 to 1.5 mass % ammonium sulfate and the remainder water, is in equilibrium with a nearly saturated 40 mass % aqueous ammonium sulfate solution containing 1 to 1.5 mass % residual caprolactam. Both streams contain organic and inorganic impurities.[1] The formation of the two-phase liquid-liquid systems can be explained from the ternary diagram of the system water (1) + caprolactam (2) + ammonium sulfate (3), which is shown for 293 K in Figure 1.2. The equilibrium diagram consists of a homogeneous liquid phase, L, extending from the pure water corner of the triangle to the curve bounding the liquid two-phase area. The binodal curve, the crystallization field of caprolactam and the two crystallization fields of ammonium sulfate bound the liquid-liquid area, $L+L$. In the first crystallization field ammonium sulfate is in equilibrium with a saturated aqueous phase, which is in equilibrium with an aqueous caprolactam solution, $L+L+S_3$. In the second field ammonium sulfate is in equilibrium with the resulting liquid phase, $L+S_3$. In the last field crystallized ammonium sulfate and caprolactam are in equilibrium with the liquid phase, $L+S_2+S_3$.[31] The diagram determined for the system water + caprolactam + ammonium sulfate at 293 K does not change much with an increase of temperature up to 323 K.[30] From this diagram and the description of the

commercial processes it can be concluded that the neutralization processes results in the formation of the liquid-liquid area, *L+L*.
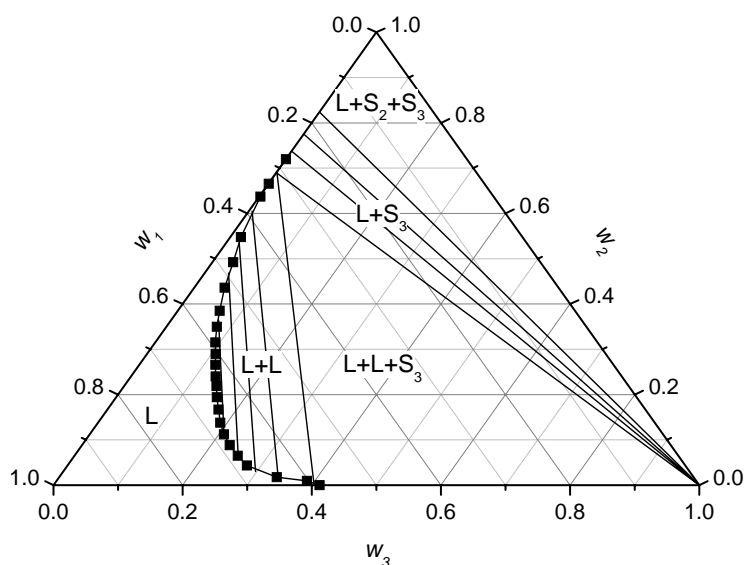
Figure 1.2. Ternary diagram for water (1) + caprolactam (2) + ammonium sulfate (3) at 293 K.[30,31]

The obtained liquid-liquid system can now either be separated, after which both streams are processed further[1,17,32-37] or the two-phase system can be pre-extracted first.[8,18,38-41] Both approaches are industrially applied.

In case the two phases are separated, caprolactam is recovered from both phases and partly purified by solvent extraction. The crude caprolactam phase is extracted with an organic solvent followed by distillation or by back-extraction with water. Advantage of this back-extraction is the removal of organic impurities and a more concentrated product stream. A drawback is the additional unit operation and that evaporation of water compared to an organic solvent requires more energy. The aqueous ammonium sulfate layer is extracted with an organic solvent or treated with evaporation followed by crystallization, filtration and recycling of the mother liquor.[1,17,32-37] A disadvantage of the direct crystallization of ammonium sulfate from this layer is the presence of impurities and therefore a product of less quality. Another disadvantage is the required energy consumption for partial evaporation of water in order to let the ammonium sulfate crystallize. An advantage of the extraction of caprolactam from the aqueous ammonium sulfate phase is the additional removal of organic impurities from this phase. A drawback is the amount of organic solvent required and the extra unit operation necessary before the ammonium sulfate phase is sent to the recovery. An example of a process layout for the extraction of crude caprolactam and crystallization of ammonium sulfate is shown in Figure 1.3.[17]
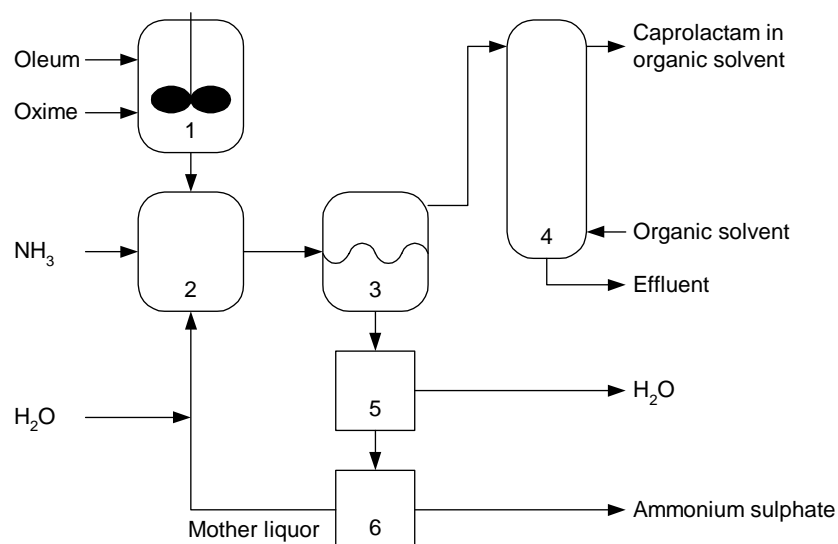
Figure 1.3. Caprolactam production followed by crude caprolactam extraction,[17] via: 1: Beckmann rearrangement; 2: Neutralization; 3: Liquid-liquid separator; 4: Crude caprolactam extraction; 5: Evaporation; 6: Filtration.

In case of the pre-extraction process, the neutralized Beckmann rearrangement mixture is treated with an organic solvent. The caprolactam is extracted and a new two-phase mixture is formed, which is separated. The organic top layer can be washed with water or an aqueous sulfuric acid solution followed by distillation or is treated with distillation only.[8,18,38-41] The advantage of the washing step is the removal of impurities like ammonium sulfate, but part of the caprolactam is washed as well and has to be processed again. Furthermore, washing requires an extra unit operation. The aqueous bottom layer from the separator can be liberated from caprolactam by extraction after which ammonium sulfate is recovered.[8,18,38-41] An example of a possible process layout for the pre-extraction process is shown in Figure 1.4.[40]
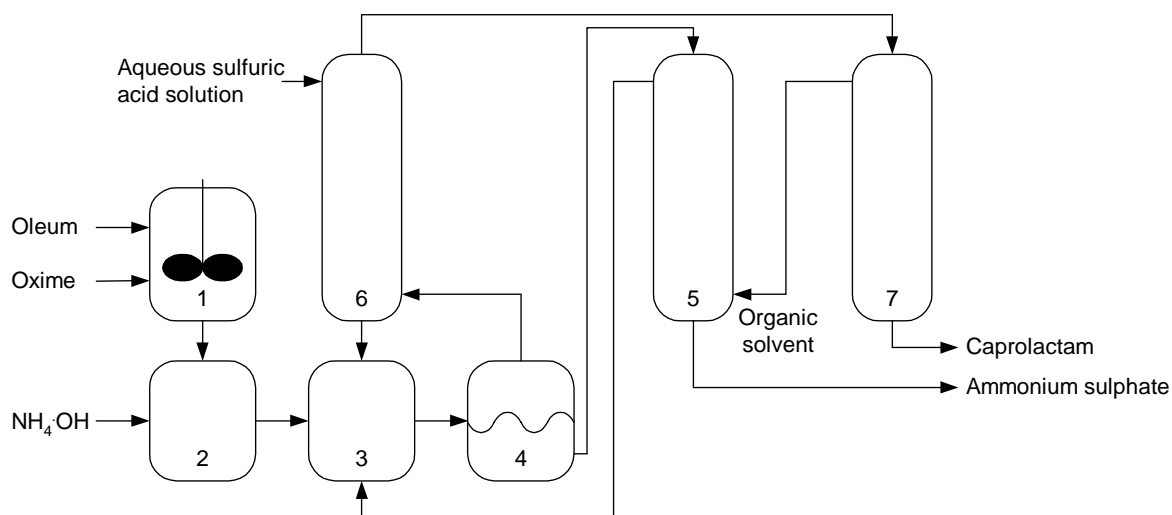
Figure 1.4. Caprolactam production followed by pre-extraction of crude caprolactam,[40] via: 1: Beckmann rearrangement; 2: Neutralization; 3: Mixer; 4: Liquid-liquid separator; 5: Ammonium sulfate extraction; 6: Washing of ammonium sulfate; 7: Caprolactam distillation.

Comparing phase separation after the neutralization step with the pre-extraction operation, an advantage of the latter is the relatively simple process layout, but a disadvantage is the presence of impurities in the caprolactam and especially the ammonium sulfate product.[2,8,40] An alternative pre-extraction process layout (EniChem) solved the latter problem, at the cost of a more complex process layout.[8]

Various new processes for caprolactam recovery from the neutralized Beckmann rearrangement mixture, aqueous solutions or waste streams are investigated, like caprolactam crystallization from crude caprolactam followed by liquid-solid separation,[42] micellar extraction of caprolactam from an aqueous stream containing ammonium sulfate[43] and caprolactam extraction from crude caprolactam using electrodialysis with ion exchange membranes.[44] However, taking into account the current caprolactam market situation,[6,7] caprolactam recovery in the near future will be based on existing processes with known technology.

1.3.2   Commercial benchmark processes

Several caprolactam production and recovery routes are discussed, but only a few of these are applied commercially. The largest commercial production processes include those of DSM, BASF, Inventa, Toray, SNIA, Bayer, EniChem and Allied Signal.[3,19] They are all multi-step processes with co-production of different amounts of ammonium sulfate and organic by-products. All commercial production processes use benzene or toluene as the main starting materials for caprolactam.[1-3,8] Of the worldwide production capacity of caprolactam up to 90% is based on the synthesis of cyclohexanone oxime from cyclohexanone and a hydroxylamine derivate followed by Beckmann rearrangement.[1,2,8] Caprolactam is recovered from the rearrangement mixture by neutralization with gaseous or aqueous ammonia, after which the resulting two-phase system is either pre-extracted with an organic solvent or separated followed by caprolactam extraction from both phases.

The commercial recovery processes of DSM, BASF/Inventa and SNIA are based on the extraction of the crude caprolactam followed by back-extraction and solvent distillation (DSM[1,2], SNIA[2,20,21]) or solvent and lactam distillation (BASF/Inventa[1,2,9]). The Bayer/EniChem and Allied Signal recovery processes are based on pre-extraction of the neutralized rearrangement mixture, separation of the obtained two-phase system, followed by washing of the separated solvent phase and distillation (Bayer/EniChem[2,8,40]) or distillation only (Allied Signal[2,3,19,45]). In the Toray PNC process caprolactam is recovered from crude caprolactam, but it is the only process where the recovery is based on other separation techniques then solvent extraction.[2,13,14]

All commercial processes applying pre-extraction (Bayer/EniChem and Allied Signal) use extraction to remove the residual amounts caprolactam from the aqueous ammonium sulfate layer, as does DSM, which uses phase separation and crude caprolactam extraction. The other commercial processes (BASF/Inventa and Toray) use crystallization after phase separation and in the SNIA process phase separation is achieved by ammonium sulfate crystallization.

As one of the caprolactam main producers for the last 50 years and a capacity of over 500 000 tons,[6,7] the DSM process was chosen in this thesis as commercial benchmark process for the recovery of caprolactam. The DSM caprolactam recovery process is shown in Figure 1.5.[1]
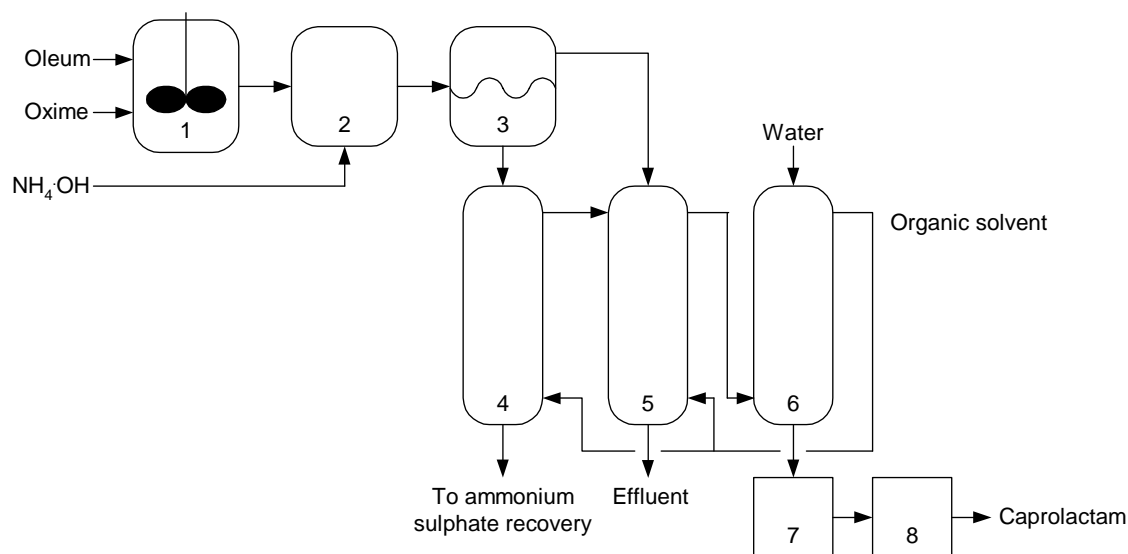
Figure 1.5. DSM process for the recovery of caprolactam:[1] 1: Beckmann rearrangement; 2: Neutralization; 3: Liquid-liquid separation; 4: Ammonium sulfate extraction with an organic solvent; 5: Crude caprolactam extraction with an organic solvent; 6: Back-extraction with water; 7: Hydrogenation; 8: Ion exchange.

1.4   Solvents for caprolactam extraction

1.4.1   Investigated solvents

In the selection procedure of a suitable solvent for a liquid-liquid extraction process several factors have to be taken into account. The solvent must have favourable selectivity in order to give a good separation and high capacity in order to reduce the amount of solvent required. In addition the solvent must preferably be chemically stable, of low toxicity, non-corrosive, cheap, easily recoverable from the extract and the loss of solvent in the raffinate phase should be as small as possible.[46,47]

Solvents proposed in literature for crude caprolactam extraction, pre-extraction and extraction of caprolactam from aqueous ammonium sulfate solutions include aromatics and their derivates, alcohols, ethers and chlorinated hydrocarbons. Specific proposed components are:

- Benzene,[1,8,15-17,26,28,32-36,38-41,48-58] xylene,[34,39,41] toluene,[1,15,20,21,26,28,32,34-39,41,48-50,53,59-61] and nitrobenzene;[1,48,49,52]

- R-phenol (where $R > C_3$),[19,29] aliphatic alcohols (C_4 to C_{10}),[38,62,63] cyclohexanol[52] and dibutyl carbinol;[26,41]

- 2-Heptanone;[64]

- Diethyl ether;[26,41]

- dichloroethane,[1,15,26-28,41,48,51] dichloroethene,[34] chloroform,[1,15,18,26-28,34,35,38,41,48,49,52] tetrachloroethane,[15,18,26,28] trichloroethene,[1,30,34,38,48,49,52-54] tetrachloromethane,[1,48,49,51,52] trichloroethane[34,41] and dichloromethane.[1,34,48]

For these extraction processes, as alternative for the pure organic solvents, it is claimed that also mixtures of proposed solvents, being benzene, toluene, xylene, chlorinated hydrocarbons and alcohols, can be applied, although mixture compositions are not specified.[34,38,48,65,66]

1.4.2   Properties of investigated solvents

The solubility of a solute is a first indication of the extraction capacity of a solvent and shows whether a favourable solvent-solute interaction exists. The caprolactam solubility as function of temperature for several proposed solvents is shown in Figure 1.6.
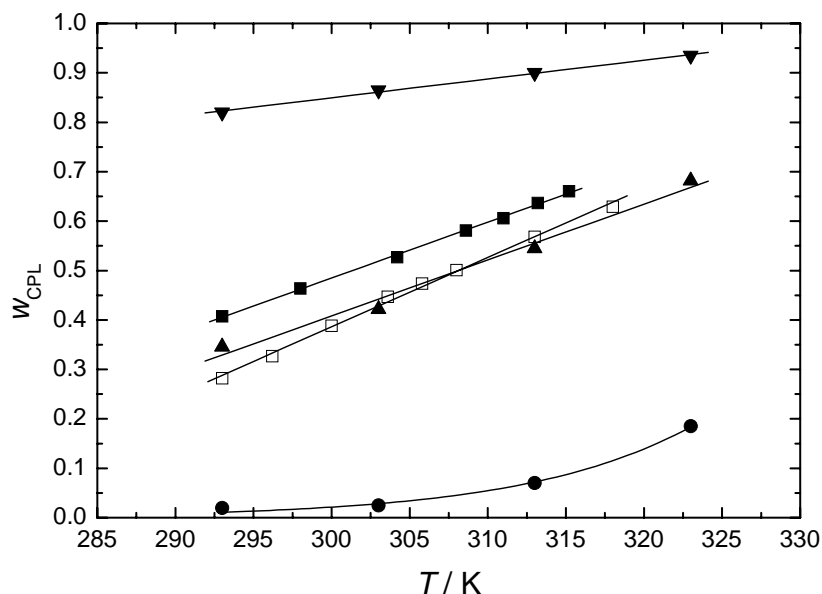
Figure 1.6. Solubility of caprolactam, w_{CPL}, as function of temperature, T/K, for various solvents: ■, benzene;[50] □, toluene;[50] ●, cyclohexane;[2] ▲, cyclohexanone;[2] ▼, water.[2]

Figure 1.6 shows that the solubility of caprolactam is the highest in water, while it is comparable for benzene, toluene and cyclohexanone, whereas it is low for cyclohexane. Therefore the interaction of caprolactam with water is expected to be strong, moderate with benzene, toluene and cyclohexanone and weak with cyclohexane.

In Figure 1.7 the ternary diagram is shown for the system water (1) + caprolactam (2) + benzene (3) at 293 K.[51] The ternary diagram shows the binodal curve, representing the boundary line between the liquid single-phase region and the two-phase area. Every point on the binodal curve, except the plait point in systems with a complete binodal curve, is in equilibrium with another binodal point and the lines connecting points in equilibrium with one another are called tie lines. From the bimodal curve follows furthermore the miscibility gap between the solvents, representing the mutual solubility of the phases. The liquid one phase region is limited furthermore by the solubility curve. For extraction operation a solvent creating a large two-phase area, with a minimum mutual solubility and distribution in favour of the solvent is desired.

For the solvents benzene,[51] toluene,[59] and nitrobenzene[52] the ternary diagrams are much alike. For low concentrations of caprolactam the mutual solubility of water and the organic solvent is very low. An increase of the mutual solubility with an increasing amount of caprolactam is

shown first for the organic solvent and at higher concentrations of caprolactam also for the aqueous phase. The tie lines show a distribution of caprolactam at equilibrium in favour of the aqueous phase.
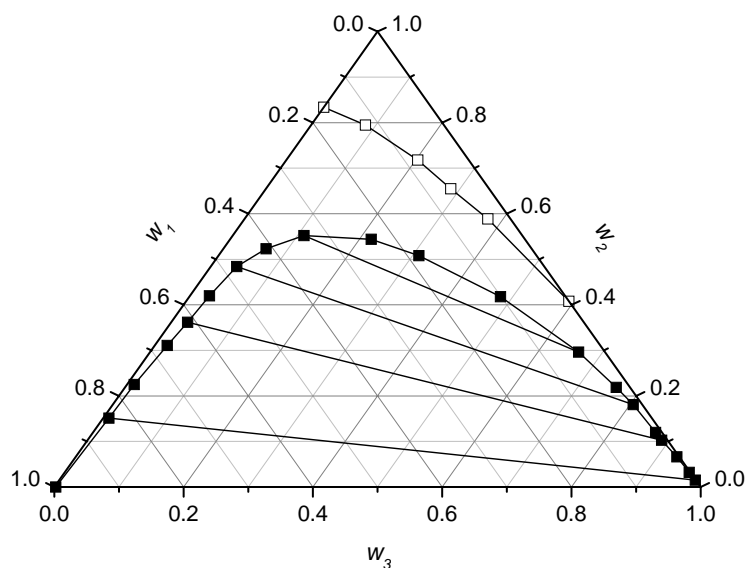
Figure 1.7. Ternary diagram for the system water (1) + caprolactam (2) + benzene (3) at 293 K,[51] where: ■, binodal curve; □, solubility line, —, tie line.

Compared to benzene the ternary diagrams for 1-heptanol[62] and cyclohexanol[52] show a smaller two-phase area and a larger mutual solubility. Therefore, using these solvents no two-phase system is formed for an aqueous 70 mass % caprolactam feed. The pure solvents can therefore not be used in the extraction process. Within the two-phase area the equilibrium distribution of caprolactam is slightly in favour of the organic phase. The temperature shows only a slight influence on the two-phase area and a temperature increase results in a shift of the distribution of caprolactam in favour of the organic phase.[62]

The systems water + caprolactam + chlorinated hydrocarbon show two-phase areas comparable to the benzene system. The tie lines show, however, a different behaviour. For chloroform[52] the distribution of caprolactam is highly in favour of the organic phase, while this is only slightly the case for dichloroethane[51] and trichloroethylene.[52] For tetrachloromethane the distribution is even highly in favour of the aqueous phase.[51]

The distribution of caprolactam between the two phases represents the capacity of a solvent system for the extraction of caprolactam. For different systems the distribution is presented in Figure 1.8. From Figure 1.8 it can be concluded that the distribution is most favourable to the organic phase for chloroform, followed by 1-heptanol and dichloroethane, while the distribution is most in favour of the aqueous phase for tetrachloromethane. A high distribution to the organic phase is desired for the crude caprolactam extraction, pre-extraction and extraction of the aqueous ammonium sulfate layer, but is also unfavourable for the back-extraction.
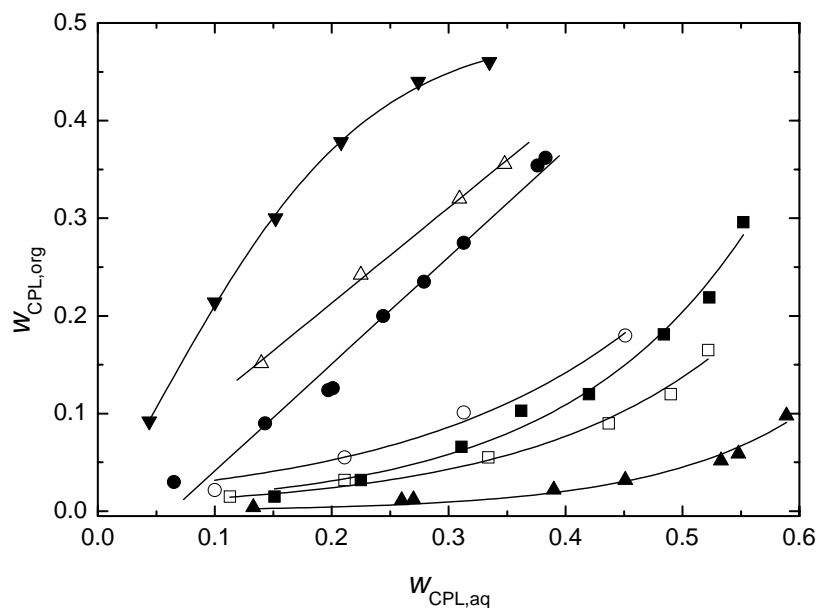
Figure 1.8. Mass fraction of caprolactam in the organic phase as function of that in the aqueous phase at 293 K for: ■, benzene;[51] □, nitrobenzene;[52] ▲, tetrachloromethane;[51] ○, trichloroethylene;[52] ●, dichloroethane;[51] △, 1-heptanol;[62] ▼, chloroform.[52]

Furthermore the selectivity of the various solvents is compared. The extracted amount of caprolactam (CPL) is therefore compared to the amount of water (W) that is co-extracted to the organic phase, relating therefore the selectivity and the mutual solvent solubility. This calculated selectivity is assumed to give an indication on the extraction of caprolactam compared to polar impurities[49] and is shown in Figure 1.9.
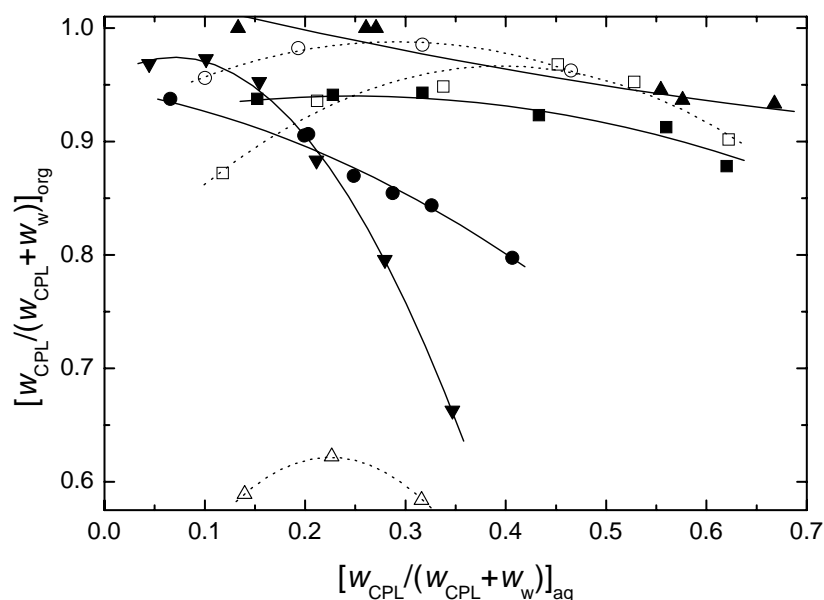
Figure 1.9. Caprolactam selectivity at 293 K for: ■, benzene;[51] □, nitrobenzene;[52] ▲, tetrachloromethane;[51] ○, trichloroethylene;[52] ●, dichloroethane;[51] △, 1-heptanol;[62] ▼, chloroform.[52]

From Figure 1.9 it can be concluded that several solvents, being benzene, trichloroethylene and tetrachloromethane, have selectivities over 0.9 for all concentrations of caprolactam, while the selectivity for the other solvents is lower in a certain range of caprolactam

concentrations, for nitrobenzene, chloroform and dichloroethane, or over the full range, for 1-heptanol.

In the industrial caprolactam extraction process, a certain amount of ammonium sulfate is present in the feed for the crude caprolactam extraction, pre-extraction and the extraction of the ammonium sulfate solution. The amounts of caprolactam and ammonium sulfate present vary from 70 mass % caprolactam and 1 to 1.5 mass % ammonium sulfate in crude caprolactam to 1 to 1.5 mass % and 40 mass % in the aqueous ammonium sulfate solution, respectively. The influence of ammonium sulfate on the distribution of caprolactam is shown in Figure 1.10 for the quaternary systems water (1) + caprolactam (2) + ammonium sulfate (3) + trichloroethylene (4).[30,31]
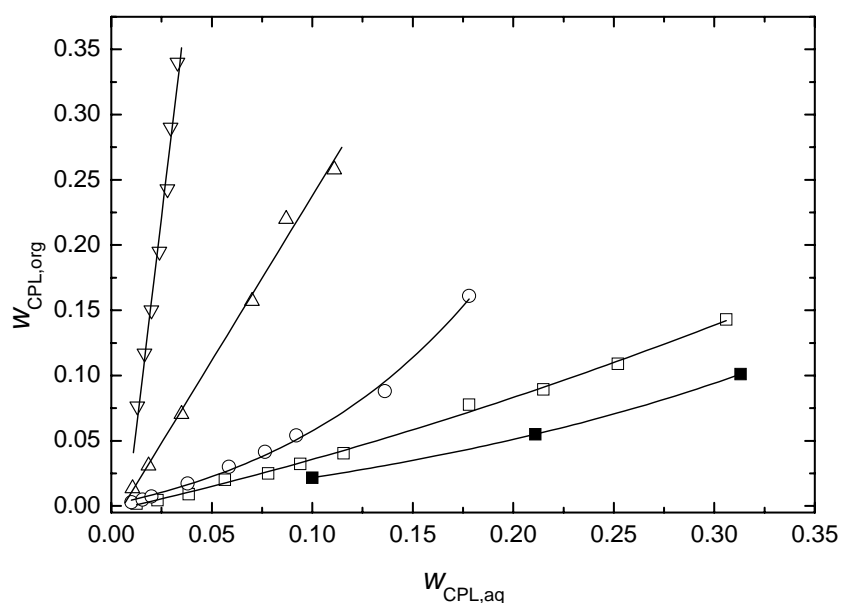
Figure 1.10. Caprolactam equilibrium distribution for the quaternary system water (1) + caprolactam (2) + ammonium sulfate (3) + trichloroethylene (4) at 293 K,[30,52] where: ■, $w_3 = 0.00$; □, $w_3 = 0.05$; ○, $w_3 = 0.10$; △, $w_3 = 0.20$; ▽, $w_3 = 0.30$.

It can be concluded that the presence of ammonium sulfate in the aqueous phase results in a shift of the equilibrium distribution of caprolactam in favour of the organic phase. This effect is known as the salting out effect[48,49] and is also observed for other solvents.[62]

1.4.3   Commercially applied solvents

In the commercial extraction processes especially benzene is often applied as extraction solvent,[1,2,8,17,53] next to toluene and chlorinated hydrocarbons.[1,2,53] This can be understood from the combined mutual solubility, equilibrium distribution and selectivity data.[48]

Because of the growing awareness of the negative effects of benzene on health and environment and the resulting extremely strict legislation on the use of benzene,[67-69] toluene has become an important alternative solvent.[20,37,53,59,60] However, because of unfavourable properties the application of toluene and chlorinated hydrocarbons becomes more restricted as well.[70]

1.5 Extraction columns used for caprolactam extraction

1.5.1 General extractor selection

The earliest large-scale continuous extraction equipment consisted of mixer-settlers and open-spray columns and the vertical stacking of a series of mixer-settlers was a feature of a patented column in 1935.[71] Over the years a lot of different contactors are developed and it is estimated that at least 25 different types of extractors are applied in commercial processes. The two main reasons for this diversification are that the equipment must suit the individual characteristics of each process and that a lot of extractors are developed for a specific process by a specific company.[72]

The following criteria should be considered when selecting a contactor for a particular process: (1) stability and residence time, (2) settling characteristics of the solvent system (3) number of stages required, (4) capital cost and maintenance, (5) available space and building height and (6) throughput. The preliminary choice of an extractor for a process is primarily based on consideration of the system properties and the number of stages required for the extraction.[2,71,73]

Extractors can be classified according to methods applied for dispersing the phases and producing the counter-current flow pattern.[2,71,73] Extractors can be divided first into gravity-separated and centrifugally separated types. Of these the former, which greatly predominate, are subdivided into unagitated-, pulsed-, mechanically agitated- and miscellaneous columns. In each of these subdivisions the apparatus can be divided in continuous contact (differential) types, discontinuous (discrete) contact types or mixer-settlers.[71,73]

Most modern differential contactors use an external energy input because the mechanical energy will improve formation of new and smaller droplets and increase interfacial turbulence, resulting in greater efficiency. The required energy can be introduced via agitation or pulsation.

1.5.2 Extraction columns used for caprolactam extraction

The extraction of caprolactam in the possible process layouts is in most cases carried out in extraction columns with an external energy supply like those equipped with rotary inserts or means for pulsating the liquid column or inserts.[39] The pre-extraction is, however, performed in a type of mixer-settler combination.[8,40] Extraction columns proposed in literature for crude caprolactam extraction, pre-extraction and extraction of caprolactam from aqueous ammonium sulfate solutions include:

- Columns without energy supply: packed columns[33,60] and perforated plate or sieve plate columns;[17,32,33]

- Rotary agitated columns: Scheibel column,[39] Rotating Disc Contactor,[1,35,37,49] Asymmetric Rotating Disc Contactor[1,39,49] and the Kühni column;[39]

- Pulsed columns: pulsed packed column,[1,34,39,58] reciprocating plate column[53,74] and the pulsed sieve plate column.[39,56]

The rotary agitated columns proposed for caprolactam extraction are shown in Figure 1.11.
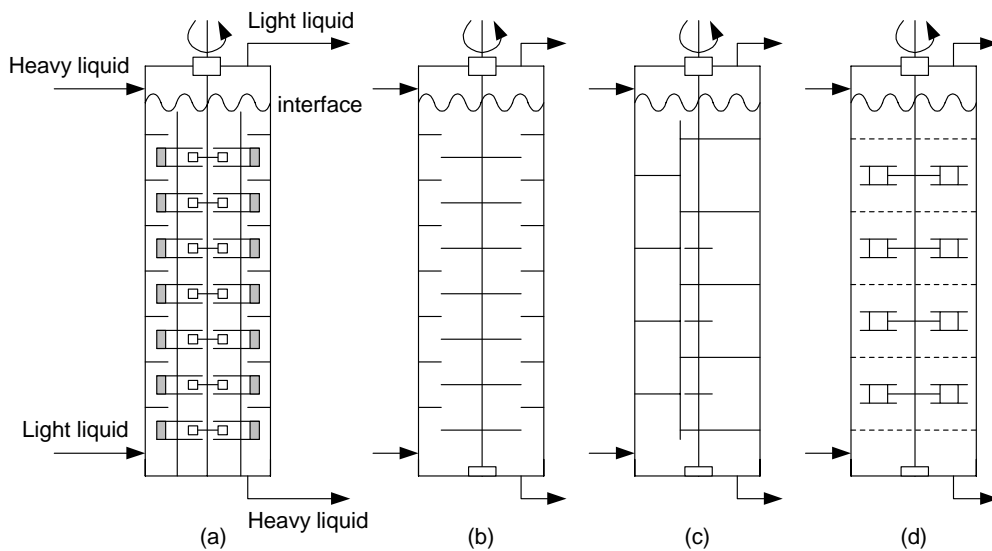
Figure 1.11. Rotary agitated columns: (a) Scheibel column; (b) Rotating Disc Contactor (c) Asymmetric Rotating Disc Contactor; (d) Kühni column.[71]

In the Scheibel column double-bladed agitators are mounted on a shaft and the impeller agitates every alternate compartment. The unagitated compartments act as settling zones and are packed with open woven wired mesh in order to improve coalescence. Other designs use horizontal baffles with or without wire mesh packing or a pumping impeller instead of a turbine.[71]

In the rotating disk contactor (RDC) stator rings are mounted at close intervals in the column and disks are fitted between the rings to a rotating shaft. The disks have a smaller diameter than the aperture of the rings and the RDC uses the shearing action of the rapidly rotating disks to disperse the phases. This construction results in a free cross-sectional area favorable for large throughputs, but as well backmixing of the phases. An advanced development of the RDC is the asymmetric rotating disk contactor (ARD). In this construction the shaft with the agitator disks is located asymmetrically to the column axis. Non-perforated plates separate the agitation zones and settling zones are separated from the agitation zones by a vertical wall. The throughput of the ARD is smaller than for the RDC because of the subdivision of the column.[71,75]

The Kühni contactor is based on similar principles as the Scheibel column. It uses a shrouded impeller to promote radial discharge within the compartments and a variable arrangement to allow flexibility of design for different process applications.[2,71,75]

As an alternative to rotary agitated columns, mechanical energy can also be introduced by pulsation. Either the liquids in the column or the inserts can be pulsated, as shown via the pulsed sieve plate and (Karr) reciprocating plate column in Figure 1.12.
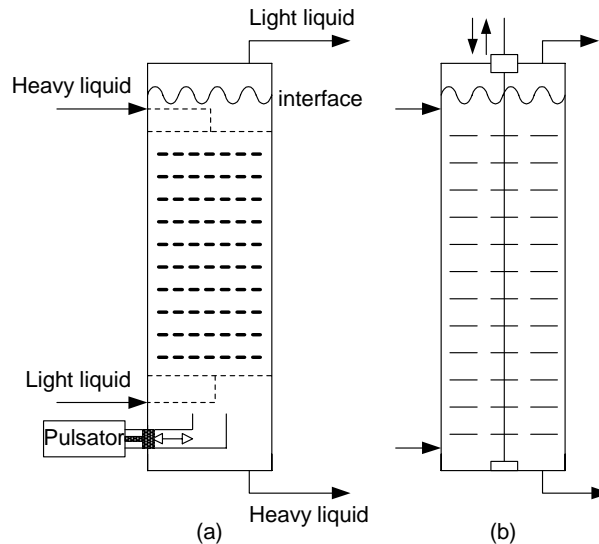
Figure 1.12. Pulsed columns: (a) Pulsed sieve plate column, (b) Karr reciprocating plate column.[71]

The pulsed sieve plate column is fitted with horizontal perforated or sieve plates, which occupy the entire cross section of the column. The total free area of the plate varies typically from 20% to 40%.[2,75] The columns are operated at frequencies varying from 0.5 to 4 Hz and with an amplitude of 0.5 to 2.5 cm.[502,71,75] The range of throughputs pulsed sieve plate columns can handle is, however, rather small.

Pulsed packed columns (PPC) consist of vertical cylindrical vessels filled with packing. The light and dense liquids passing counter currently through the packing are acted on by pulsations to form a dispersion of drops.[2,71]

In contrast to pulsed sieve plate or packed columns where the liquid contents is pulsed, in a reciprocating or vibrating plate column the internals are subjected to a pulsing motion. Many different types of columns exist, mainly because of different plate types.[71]

The application of pulsed columns is limited by the physical properties of the substances concerned and the rather small range of throughputs these columns can handle. Systems that emulsify easily and viscous liquids cannot be processed.[2,75]

In the pre-extraction process a mixer and liquid-liquid separator are applied for the caprolactam extraction.[8] Each mixer-settler stage consists of a stirring vessel and a settling vessel and a typical mixer-settler configuration is shown in Figure 1.13.
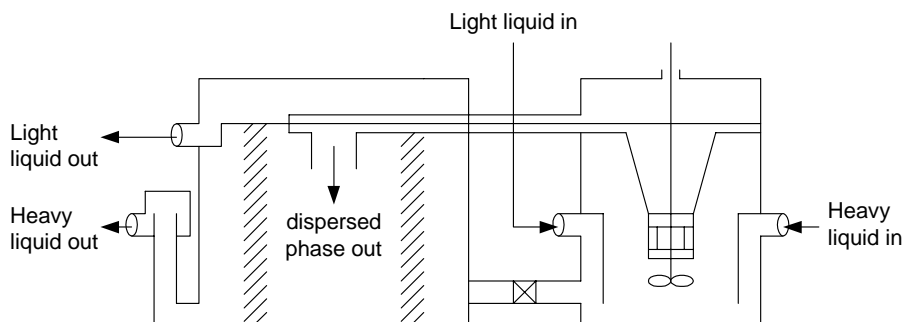
Figure 1.13. IMI type mixer-settler.[71]

17

The IMI mixer-settler is widely used in the industry. The basic design of a mixer-settler is the simple box-type. The mixing and separation zone are combined in a single unit and an impeller mounted on a shaft disperses the two phases.[2,71] For processes requiring several stages various arrangements are possible such as co-current, countercurrent or cross-flow. Mixer-settlers are widely used in the chemical process industry because of reliability, flexibility and high capacity and these extractors are particularly favorable for operations that require high throughputs and few stages. Mixer-settlers reach almost 100% stage efficiency and are almost insensitive for load fluctuations. The main disadvantages of mixer-settlers are the size and the inventory of material held up in the equipment.[2,71]

1.6   Scope and outline of this thesis

From the current market situation it follows that in the near future existing technology will be the dominating production route for caprolactam. Therefore, there is a drive to improve the currently used processes, which consist of cyclohexanone formation, oximation, Beckmann rearrangement and finally caprolactam recovery. The latter is based on neutralization of the rearrangement mixture, separation of the resulting two-phase system after which both phases are treated with solvent extraction, according to the industrial DSM process, which is used in this thesis as benchmark. In the extraction process, however, toxic and carcinogenic solvents are used. The replacement of these with environmentally benign alternatives is therefore an important improvement with respect to the sustainability of the current recovery process.

This research was started in cooperation with Bateman Advanced Technologies (Yokneam, Israel). The first objective of the research presented in this thesis is the characterisation of their pulsed disc and doughnut column, the so-called Bateman Pulsed Column, for its applicability in the extraction of caprolactam, since it is a new column type for the extraction of organics. The column operation and separation performance is therefore investigated on pilot scale for caprolactam extraction with the conventional solvent toluene. The second objective of the presented research is the selection and characterization of alternative environmentally benign solvents for caprolactam extraction. Finally, caprolactam extraction with the selected alternative solvent is compared with toluene in the pilot scale column.

In order to achieve these objectives the experimentally determined equilibrium phase compositions and physical properties of the quaternary systems water + caprolactam + ammonium sulfate + solvent, where the solvent is benzene or toluene, is described in Chapter 2. These data are required for the characterization of the operation and separation performance in an extraction column and as reference for the alternative solvent. In Chapter 3 a theoretical model is developed for the description of the operational characteristics of the pilot scale extraction column and this model is evaluated based on experiments with toluene in Chapter 4. The separation performance of the pulsed disc and doughnut column for caprolactam extraction with toluene is determined and modelled in Chapter 5. The selection of alternative solvents as described in Chapter 6 is based on solvent capacity and selectivity and makes use of the Hanson solubility and the Unifac Dortmund thermodynamic models and an experimental screening procedure. For the alternative candidate solvents, phase equilibria

and physical properties are determined for the quaternary systems water + caprolactam + ammonium sulfate + alternative solvent. In Chapter 7 the impurity distribution for four model impurities in the system water + caprolactam + best alternative solvent in comparison to toluene is described, since the impurity profile determines the final lay-out of the purification section after the caprolactam extraction. In Chapter 8 the extraction performance of the most promising alternative solvent is experimentally evaluated and compared to that of toluene. In Chapter 9, finally, the main findings of this research are summarized, whereas main issues are discussed that should be further addressed in the future.

Literature cited

1. Simons, A. J. F.; Haasen, N. F. Extraction of Caprolactam. In *Handbook of Solvent Extraction*; Lo, T. C.; Baird, M. H. I.; Hanson, C., Eds.; Wiley: New York, 1983, pp 557-566.

2. Ullmann, F. *Ullmann's Encyclopedia of Industrial Chemistry*; Wiley-Interscience: New York, 2004; electronic version.

3. Fisher, W. B.; Crecentini, L. Caprolactam. In *Kirk-Othmer, Encyclopedia of Chemical Technology, Vol. 4*; Kroschwitz, J. I; Howe-Grant, M., Eds., John Wiley & Sons: New York, 1993, pp. 827-839.

4. Product Focus-Caprolactam. *European Chemical News* **1999**, *71*, 18.

5. Product Focus-Caprolactam. *Chemical Week* **1999**, *161*, 48.

6. Fisher, G. No Room for New Caprolactam Plants. *Fibres & Textiles in Eastern Europe* **2003**, *11*, 14-15.

7. Van der Linde, S.; Fisher, G. The Caprolactam Business Must Change: New Production Plants Cannot Be Justified. *Fibres & Textiles in Eastern Europe* **2004**, *12*, 17-18.

8. Alessi, V.; Penzo, R.; Slater, M. J.; Tessari, R. Caprolactam Production: a Comparison of Different Layouts of the Liquid-Liquid Extraction Section. *Chem. Eng. Technol.* **1997**, *20*, 445-454.

9. Petrochemical processes: Caprolactam-Inventa. *Hydrocarbon processing* Nov. **1975**, 119.

10. Dahlhoff, G.; Niederer, J. P. M.; Hoelderich, W. F. ε-Caprolactam: New By-Product Free Synthesis Routes. *Cat. Rev.* **2001**, *43*, 381-441.

11. BASF, GB 1528513, 1978.

12. Prasad, R.; Vashisht, S. Ammoximation of Cyclohexanone over Al_2O_3 Supported Titanium Silicates. *J. of Chem. Tech. Biotech.* **1997**, *68(3)*, 310-314.

13. Petrochemical processes: Caprolactam-Toray. *Hydrocarbon processing* Nov. **1989**, 97.

14. Petrochemical processes: Caprolactam-Toray. *Hydrocarbon processing* Nov. **1983**, 85.

15. Stamicarbon, NL 7106341, 1972.

16. Stamicarbon, US 3336298, 1967.

17. BASF, DE 1194863, 1961.

18. Stamicarbon, GB 1401094, 1975.

19. Caprolactam production: a survey of current technology. *European Chemical News* April 30 **1976**, 24-26.

20. Petrochemical processes: Caprolactam-SNIA. *Hydrocarbon processing* March **1999**, 103.

21. Petrochemical processes: Caprolactam-SNIA. *Hydrocarbon processing* Nov. **1973**, 109.

22. Sato, O.; Ikushima, Y.; Yokoyama, T. Noncatalytic Beckmann Rearrangement of Cyclohexanone-Oxime in Supercritical Water. *J. Org. Chem.* **1998**, *63*, 9100-9102.

23. Ikushimaa, Y.; Sato, O.; Sato, M.; Hatakeda, K.; Arai, M. Innovations in Chemical Reaction Processes Using Supercritical Water: an Environmental Application to the Production of ε-Caprolactam. *Chem. Eng. Sci.* **2003**, *58*, 935-941.

24. Mao, D.; Chen, Q.; Lu, G. Vapor-Phase Beckmann Rearrangement of Cyclohexanone Oxime over B2O3/TiO2-ZrO2. *App. Cat. A: General* **2003**, *244*, 273-282.

25. Sato, H.; Yoshioka, H.; Izumi, Y. Homogeneous Liquid-Phase Beckmann Rearrangement of Oxime Catalyzed by Phosphorous Pentaoxide and Accelerated by Fluorine-Containing Strong Acid. *J. Mol. Cat. A: Chemical* **1999**, *149*, 25-32.

26. Stamicarbon, US 4140685, 1979.

27. Stamicarbon, US 3944543, 1976.

28. Stamicarbon, NL 7106343, 1972.

29. SNIA, US 3912721, 1975.

30. Tettamanti, K.; Nogradi, M. The Influence of Ammonium Sulfate on the Distribution of Caprolactam in the Water/Trichloro Ethylene System. *Period. Polytech. Chem. Eng.* **1960**, *5*, 15-23.

31. Shubtsova, I. G.; Nikurashina, N. I.; Rybalov, S. K. The Caprolactam-Water-Ammonium Sulfate System Investigated by the Method of Sections. *Russ. J. Phys. Chem.* **1975**, *49*, 35-37.

32. BASF, US 4301073, 1981.

33. BASF, DE 2656182, 1978.

34. Stamicarbon, US 4036830, 1977.

35. Stamicarbon, US 2993889, 1961.

36. Stamicarbon, DE 930447, 1955.

37. SNIA, US 4606858, 1986.

38. DSM, WO 9849140, 1998.

39. Bayer, US 4170592, 1979.

40. Bayer, DE 1031308, 1956.

41. Allied Chemical, US 3694433, 1972.

42. Sumitomo Chemical Company, EP 1167350 A1, 2002.

43. Pajak, M.; Blaszczyk, A. Micellar Extraction of Caprolactam from Aqueous Solutions. *Third Distillation, Absorption and Extraction Conference, 1999*, Pohorecki, R.; Kuzniara, J. J.; Krolikowski, L. J. Silesia: W., Eds.; Wroclaw, Poland, 1999, pp. 251-263.

44. EuroScience. Caprolactam. http://www.georgia.technology-transfer.net/ (accessed April 2005).

45. Process survey: Caprolactam. *European Chemical News-Supplement* May 2, **1969**.

46. Meniai A.-H.; Newsham, D. M. T. The Selection of Solvents for Liquid-Liquid Extraction. *Chem. Eng. Res. Des.* **1998**, *76*, 361.

47. Cusack, R. W.; Fremeaux, P.; Glatz, D. A Fresh Look at Liquid-Liquid Extraction, Part 1: Extraction Systems. *Chem. Eng.* February **1991**, 66-76.

48. Pandya, H. P.; Puranik, S.A. Liquid-Liquid Extraction of Caprolactam. *IE(1) Journal-CH* **1995**, *76*, 1-4.

49. Pandya, H. P. Solvent System for Liquid-Liquid Extraction of Caprolactam with Salting Out Effect. *Advances in Chemical Engineering in Nuclear and Process Industries: June 9-11, 1994. Vol. 2.* Bhabha At. Res. Cent.: Bombay, 1994; pp 504-516.

50. Chang, R.-Y.; Yang, H.-M.; Wang, M.-L. Solubility of ε-Caprolactam in Benzene and Toluene Solvents. *J. Chin. Inst. Chem. Eng.* **1981**, *12*, 141-145.

51. Morachevskii, A. C.; Sabinin, V. E. Solubility Diagrams for the Ternary Systems Caprolactam-Water-Benzene, Caprolactam-Water-Carbon Tetrachloride and Caprolactam-Water-Dichloroethane. *J. Appl. Chem. (USSR)* **1960**, *33*, 1775-1779.

52. Tettamanti, K.; Nogradi, M.; Sawinsky, J. Equilibria of the Ternary System Caprolactam-Water-Organic Solvent, in the Liquid State. *Period. Polytech., Chem. Eng.* **1960**, *4*, 201-218.

53. Prochazka, J.; Landau, J.; Souhrada, F.; Heyberger, A. Reciprocating-Plate Extraction Column. *British Chem. Eng.* **1971**, *16*, 42-44.

54. Stratula, C.; Mihai, T.; Cheta, I.; Oprea, F. Comparative-Study on Caprolactam Purification with 2 Solvents. 1. Liquid-Liquid Equilibrium Study. *Rev. Chem.* **1992**, *43*, 372-381.

55. De Haan, A. B.; Niemann, S. H. Modelling Phase Equilibria in Industrial Caprolactam Recovery from Aqueous Ammonium Sulfate Solutions with Benzene. *Solvent Extraction for the 21st Century. Proceedings of ISEC 1999. Vol. 2*; Cox, M.; Hidalago, M.; Valiente, M., Eds.; Society of Chemical Industry: London, 2001; pp 1537-1542.

56. Liu, J.; Xie, F.; He, C.; Zhu, M. Recovery of Caprolactam from Wastewater in Caprolactam Production Using Pulsed-Sieve-Plate Extraction Column. *Chinese J. Chem. Eng.* **2002**, *10*, 371-373.

57. Huan, Z.; Van Bochove, G. H.; De Loos, Th. W. Three-Liquid-Phase Equilibria in Water + Benzene + Caprolactam + $(NH_4)_2SO_4$ Mixtures. *AIChE J.* **2003**, *49*, 745-752.

58. Xie, F.; Zhu, M.; Liu, J.; He, C. Extraction of Caprolactam from Aqueous Ammonium Sulfate Solution in Pulsed Packed Column Using 250Y Mellapak Packing. *Chinese J. Chem. Eng.* **2002**, *10*, 677-680.

59. Zheleznova, N. I.; Popov, D. M.; Kanakina, S. V. Phase Equilibrium in the Caprolactam-Toluene-Water System. *Z. Prikl. Khim.* **1985**, *58*, 1900-1903.

60. Pajak, M.; Piotrowicz, J.; Skrzypinski, W. Extraction of Caprolactam in Packed Columns. *Przem. Chem.* **1992**, *71(3)*, 107-110.

61. Pajak, M.; Piotrowicz, J.; Skrzypinski, W. Extractive Equilibra in Technology of Caprolactam Production. *Przem. Chem.* **1991**, *70*, 72-74.

62. Wijtkamp, M.; Van Bochove, G. H.; De Loos, Th. W.; Niemann, S. H. Measurements of Liquid-Liquid Equilibra of Water + ε-Caprolactam + Electrolyte + Organic Solvent Systems. *Fluid Phase Equilib.* **1999**, *158-160*, 939-947.

63. Poraicu, M.; Davidescu, C.; Pacurariu, C. Studies on Partition Equilibria. The Extraction of ε-Caprolactam from Aqueous Solutions. *Chem. Bull. Politehnica* **1997**, *42*, 139-143.

64. Van Bochove, G. H.; Krooshof, G. J. P.; de Loos, Th. W. Two- and Three-Liquid Phase Equilibria in the System Water + 2-Heptanone + Caprolactam + Ammonium sulfate: Experiments and Modeling. *Fluid Phase Equilib.* **2002**, *194-197*, 1029-1044.

65. DSM, WO 9841502, 1998.

66. BASF, US 4350630, 1982.

67. European Environment Agency. Reports - Page 5. Environmental Issue Report No 22. Content. Chapter 4 - Benzene. http://reports.eea.eu.int/ (accessed May 2003).

68. U.S. Environmental Protection Agency. Pollutants/Toxics. Benzene. http://www.epa.gov/ (accessed May 2003).

69. Environment Canada. CEPA Registry. Agreements. Related Federal/Provincial Agreements. Canada-wide Standards for Benzene. http://www.ec.gc.ca/envhome.html (accessed May 2003).

70. Directive of the EPC, Relating to restrictions on the Marketing and Use of Toluene and Trichlorobenzene, 2004, http://europa.eu.int/eurlex/en/.

71. Lo, T. C.; Baird, M. H. I. Extraction (liquid-liquid). In *Kirk-Othmer, Encyclopedia of Chemical Technology, Vol. 10*; Kroschwitz, J. I; Howe-Grant, M., Eds., John Wiley & Sons: New York, 1993, pp. 125-180

72. Baird M. H. I. Solvent Extraction – The Challenges of a "Mature" Technology. *Can. J. Chem. Eng.* **1991**, *69*, 1287-1301.

73. Pratt, H. R. C.; Hanson, C. Selection pilot testing, and scale-up of commercial extractors. In *Handbook of Solvent Extraction*; Lo, T. C., Baird, M. H. I., Hanson, C., Eds.; Wiley: New York, 1983; pp 475-495

74. Vasin, A. A.; Legochkina, L.A. Caprolactam Extraction from an Ammonium Sulfate Solution in a Vibrating Plate Column. *Khim. Prom-st.* **1989**, *12*, 900-903.

75. Reissinger, K.-H.; Schröter, J. Selection Criteria for Liquid-Liquid Extractors. *Chem. Eng.* November **1978**, 109-118.

Chapter 2

Liquid-liquid equilibria and physical properties of the quaternary systems water + caprolactam + ammonium sulfate + benzene and toluene

2.1   Introduction

Caprolactam is recovered from the neutralized Beckmann rearrangement mixture by phase separation followed by solvent extraction of the resulting crude caprolactam and aqueous ammonium sulfate layer, for which in industry benzene is often used as the organic solvent, as described in Chapter 1. Several experimental studies on the ternary systems water + caprolactam + ammonium sulfate and water + caprolactam + benzene and the quaternary systems water + caprolactam + ammonium sulfate + benzene at 293 K exist.[1-4] However, in most cases, the industrial caprolactam extraction is performed at elevated temperatures. Although the effect of temperature, in some cases combined with the effect of ammonium sulfate, has been measured,[4-10] data on liquid-liquid equilibrium (LLE) phase compositions covering all industrially applied concentrations and temperatures are limited. Next to phase composition data, physical properties, being density and viscosity of the separate liquid phases and interfacial tension of the liquid-liquid system, are needed for the description of extraction processes.[11] Although the data for pure liquids and pure liquid-liquid systems have been reported,[11] the influence of caprolactam and ammonium sulfate on these physical properties is unknown.

As described in Chapter 1, toluene has been proposed and applied as an alternative solvent, because of the growing awareness of the negative effects of benzene on health and environment and the resulting extremely strict legislation on the use of benzene. Experimental data on the system water + caprolactam + toluene at some temperatures are available,[16-18] but extensive data on phase compositions of the system water + caprolactam + ammonium sulfate + toluene at various temperatures are not reported, whereas physical properties are available for the pure liquids and the binary liquid-liquid system only.

In this chapter the equilibrium phase compositions of the systems water + caprolactam + ammonium sulfate + organic solvent are determined at 293 K, 313 K and 333 K, where the organic solvent was benzene or toluene. The determined phase compositions were described

using the Non-Random Two-Liquid (NRTL) model. Furthermore, density and viscosity data of the separate phases and interfacial tension data of the systems studied were determined and correlated.

2.2   Experimental section

Chemicals. Toluene (purity > 99%) was supplied by Fluka (USA), benzene (purity > 99.5%) by Riedel de Haën (USA), ε-caprolactam (purity 99%) and ammonium sulfate (purity > 99%) by Sigma-Aldrich (USA), ethanol (purity 99.8%) and methanol (purity > 99.8%) by Merck (Germany), and 1-methyl-2-pyrrolidinone (purity 99%) by Acros (Belgium). All chemicals were used as received. MiliQ water was used in all experiments.

Equilibrium measurements. The experimental setup consisted of an equilibrium cell, which had an inner chamber of about 55 mL. The cell was surrounded by a jacket for temperature control. The jacket was connected to a Julabo F12 heating/cooling bath (Julabo Labortechnik, Germany), and water was used as the heating/cooling fluid. The inner chamber had two sampling ports, one in the upper half and the other in the lower half of the cell, allowing sampling of both phases. The cell was placed on the plate of a multiple point magnetic stirrer (Variomag) and a magnetic bar (30 mm length) was used for agitation.

Equilibrium measurements were performed as follows. The organic solvent (20 mL, toluene or benzene) and 20 mL of an aqueous caprolactam solution were introduced in the vessel by a pipette. The mass fraction of caprolactam in the initial aqueous solution was in the range from 0 to 60 mass %. After introduction of the solutions, the mixture was stirred for at least 45 min at 450 rpm at an alternating regime of 90 s stirring and 20 s pause. The time of agitation required to reach equilibrium was determined by measuring the change in concentration of caprolactam for different stirring times and was found to be 25 min using the described regime. After equilibrium was reached, the mixture was left to settle for at least 1 h. During the agitation and settling, the temperature of the fluid in the vessels was kept constant at the required value with an uncertainty of 0.1 K. After the phases settled, a sample from the organic (100 μL) and two samples from the aqueous layer (both 20 μL) were taken with a syringe. Finally, a sample from the organic layer (1000 μL) was taken with a pipette. The 100 μL organic phase sample and one aqueous phase sample were diluted with 1000 μL of ethanol (in case of toluene as solvent) or methanol (in case of benzene as solvent). After that, 50 μL of the internal standard was added for determination of the concentration of caprolactam in the organic solvent and of the concentrations of organic solvent and caprolactam in water. The second aqueous phase sample was diluted with 1000 μL of water. Of this solution, 50 μL was diluted 500 times for analytical determination of the concentration of ammonium sulfate. The 1000 μL of the organic phase sample was used for analytical determination of the concentration of water.

Density measurements. Densities were determined for the ternary system water + caprolactam + ammonium sulfate and the binary systems benzene + caprolactam and toluene + caprolactam at 293 K, 313 K and 333 K using a DMA 5000 automatic density meter (Anton Paar, Austria). Solutions of known composition (in mass fractions) were prepared and a

sample was sucked up automatically via the SHx/SCx sample changer mode into the measuring cell, having a volume of 1 mL, and heated until the desired temperature with an uncertainty of 0.01 K. After measurement, the sample was ejected, whereas the cell was rinsed two times with water and acetone and finally it was dried with air for 2 min. The density was measured with an uncertainty of 1×10^{-2} kg·m^{-3}.

Viscosity measurements. Kinematic viscosities were determined for the ternary system water + caprolactam + ammonium sulfate and the binary systems benzene + caprolactam and toluene + caprolactam at 293 K, 313 K and 333 K using capillary Ubbelohde viscosimeters 501 13/Ic, having a capillary constant of 0.02887 mm^2·s^{-2} ± 0.65%, and 501 03/0c, having a capillary constant of 0.003162 mm^2·s^{-2} ± 0.65% (Schott, Germany). The capillaries were immersed in a Lauda 015T water bath (Lauda, Germany), and the temperature was controlled using a Lauda E200 thermostat (Lauda, Germany) with an uncertainty of 0.1 K. Solutions of known composition (in mass fractions) were prepared, and a sample was sucked up in the capillary. The time needed for the meniscus of the sample to descend from the first to the second marker on the capillary was measured and corrected if necessary according to the kinetic energy correction tables supplied with the respective capillaries. Measuring ranges for both capillaries were 3 to 30 mm^2·s^{-1} and 0.3 to 3 mm^2·s^{-1}, respectively. The measurement uncertainty was 1×10^{-2} mm^2·s^{-1}.

Interfacial tension measurements. Interfacial tensions were determined of the ternary system water + caprolactam + toluene and the quaternary system water + caprolactam + ammonium sulfate + toluene at 293 K, 313 K and 333 K using a Krüss K11 automatic tensiometer with a thermostated vessel (Wilten Physica, Belgium). The thermostated vessel was connected to a Julabo F12 heating/cooling bath (Julabo Labortechnik, Germany), and the temperature was controlled with an uncertainty of 1 K. Interfacial tensions were determined via the Du Noüy Ring method using a standard ring and corrected by the Huh & Mason method. The aqueous and organic phases were prepared at various pre-calculated equilibrium compositions (in mass fractions) and brought to the desired temperature in the water bath. After cleaning, the ring was immersed in the light phase and the balance was set to zero. After removal of the light phase and cleaning of the ring, the sample vessel containing the heavy phase was placed in the thermostat vessel. The ring was placed above the surface, which was then searched for with a speed varying from 20 to 1 mm·min^{-1}. After detection, the ring was immersed to 3 mm in the heavy phase with a speed varying from 100 to 1 mm·min^{-1}. The heavy phase was covered with the light phase using a 10-mL pipette. The determination of the interfacial tension was performed at a speed varying from 2 to 0.2 mm·min^{-1} with a relaxation of 10% and the experiment was continued for 20 measurements or until a standard deviation of the last five values ≤ 0.3 mN·m^{-1}. The range applied for the experimental method settings covered concentrations of caprolactam in the aqueous phase from 0 to 30 mass %. The measurement uncertainty was 0.3 mN·m^{-1} for low concentrations of solute ($w_i < 0.10$) up to 1 mN·m^{-1} for high concentrations of solute ($w_i > 0.20$).

Chemical analysis. The mass fraction of caprolactam in both the organic and the aqueous phases and of toluene in the aqueous phase was determined in a gas chromatograph, CP-3800

(Varian, USA), equipped with an EC-WAX column (30 m, 0.32 mm, 0.25 μm film thickness) using a flame ionization detector. During the analysis of caprolactam in the organic phase and of caprolactam and toluene or benzene in the aqueous phase, the column temperature was raised from 333 K to 343 K with an increment of 10 K·min^{-1} and then from 343 K to 523 K with an increment of 50 K·min^{-1}. The temperatures of the injector and detector were kept constant at 498 K and 523 K, respectively, using a pressure in the injector of 275 kPa with an initial flow of 14.2 mL·min^{-1} (in case of toluene as solvent) or with a constant flow of 5 mL·min^{-1} with an initial pressure of 97 kPa (in case of benzene as solvent). A split ratio of 10 was used. Helium was used as the carrier gas, and a sample of 0.3 μL was injected into the column. Quantification of caprolactam and toluene or benzene in the sample was done by using an internal standard method where 1-methyl-2-pyrrolidinone was used as the internal standard. A 10 mass % aqueous caprolactam solution was prepared and analyzed 4 times to test the repeatability and the uncertainty of the GC analysis. The mean value of 9.8 mass % is found with an uncertainty of 0.2 mass % (determined as standard deviation).

The mass fraction of ammonium sulfate in the aqueous phase was determined by ion chromatography using a Metrohm 733 IC Separation Center (Applikon, The Netherlands) connected to a Metrohm 709 IC Pump (Applikon, The Netherlands) and a Metrohm 732 IC Detector (Applikon, The Netherlands). The separation center was equipped with a ICSep AN2 column (250 mm, 4.6 mm) (CETAC Technologies, USA). Sulfate was determined via conductivity measurement with chemical suppression. Eluent consisting of 1×10^{-3} mol·L^{-1} NaHCO$_3$ and 3.5×10^{-3} mol·L^{-1} Na$_2$CO$_3$ was used at a flow of 1200 μL·min^{-1}. A temperature of 308 K in the detector and a pressure of 800 kPa were applied. Quantification of the amount of sulfate was performed using Metrohm IC Metrodata for Windows 95 version 1.44 (Applikon, The Netherlands) and a calibration line of sodium sulfate. Sulfate was determined with an uncertainty of 0.01 mass %.

The mass fraction of water in the organic phase was measured by coulometric Karl Fischer determination with a Metrohm 652 KF Coulometer (Applikon, The Netherlands), where controlled-current potentiometry with two platinum indicator electrodes was used for determination of the end-point, which was fixed at 250 mV. In the reaction vessel, 200 mL of Hydranal-AK anode-liquid (Riedel-de Haën, USA) was transferred, and in the generation electrode, 5 mL Hydranal CK-G cathode liquid from an ampule (Riedel-de Haën, USA) was placed. When water was present at the start, iodine was automatically generated until equilibrium was reached. For determination of water in a sample, a fixed amount of sample was added to the Hydranal-AK liquid, whereas iodine was automatically generated until the end point was reached. Water was determined with an uncertainty of 0.005 mass %.

Data analysis. By use of the described analytical methods, the amount of solute and the mutual solvent solubility (in mass fractions) were determined in the organic and aqueous phase with the described uncertainties. The mass fraction of water in the aqueous phase and of toluene or benzene in the organic phase was finally determined using mass balance. The mass fraction of ammonium sulfate in the organic phase was assumed to be negligible. This assumption was based on the results of Huan *et al.*,[10] where a very small amount of

ammonium sulfate (AS) was detected in the organic phase near the phase boundary. The amount detected was $w_{AS} < 0.004$ at the highest amounts of caprolactam (CPL) and water (W) in the organic phase ($w_{CPL,org} = 0.52$ and $w_{W,org} = 0.23$) at 333 K. In the determination of the physical properties, phase compositions were directly calculated from the weighted amounts and, in case of interfacial tension measurements, from the determined phase equilibria.

2.3 Results and data correlation

2.3.1 Equilibrium experiments

Tables A1 and A2 (see Appendix A) present the LLE data of the systems water + caprolactam + ammonium sulfate + benzene and toluene, respectively, at 293 K, 313 K and 333 K. The determined phase equilibrium data for the described systems were correlated with the classical NRTL model using the approach of de Haan and Niemann.[8] This model was reported to provide a good representation of the experimental LLE data for the ternary and quaternary systems water + caprolactam + ammonium sulfate + benzene at 293 K, 313 K and 333 K, when ammonium sulfate was treated as a fully dissociated pseudo-component and the non-randomness parameter was determined in the fitting procedure and not set at the default value of 0.2 or 0.3.[8] This approach results, however, in values for α_{ij} that are physically unrealistic and reduces the NRTL model to a fit procedure. The NRTL electrolyte model[19] or the extended NRTL electrolyte model[10,20] are capable of describing LLE and even LLLE systems containing salts, but these models are more complicated. The classical NRTL model using the described approach is, however, a simple and direct model available in ASPEN Plus. Applying the classical NRTL model in fitting phase composition data of the quaternary systems described here provided a calculation tool, which was sufficiently accurate for our purposes of extraction column modelling. The binary interactions were calculated using Equation (2–1)[19]

$$\tau_{ij} = a_{ij} + \frac{b_{ij}}{T} \qquad G_{ij} = \exp\left(-\alpha_{ij} \cdot \tau_{ij}\right) \qquad \alpha_{ij} = \alpha_{ji} \qquad (2\text{–}1)$$

where G_{ij} and τ_{ij} are NRTL parameters, which are calculated via the non-randomness parameter α_{ij} and the parameters a_{ij} and b_{ij}/K. The five NRTL parameters (α_{ij}, a_{ij}, a_{ji}, b_{ij}/K and b_{ji}/K) for all component pairs were determined via data regression using ASPEN Plus 11.1. Initial values for the solvent-solvent interactions were determined from binary solubility data.[21] The interactions for the ternary system, and after initial regression also the solvent-solvent interactions, were determined from the ternary phase equilibria data. Interactions of all components with ammonium sulfate were determined from the quaternary phase equilibrium data. In the determination of the interactions with ammonium sulfate, it was found that the value of the non-randomness parameter was critical for obtaining a good description of the system, which was also concluded by de Haan and Niemann.[8] The values of the fitted parameters are listed in Table 2.1.

Table 2.1. Fitted NRTL interaction parameters for the description of LLE of the systems water (1) + caprolactam (CPL) (2) + ammonium sulfate (AS) (3) + solvent (4) at (293 to 333) K, with benzene or toluene as solvent.

Binary parameter	α_{ij}	a_{ij}	a_{ji}	b_{ij}/K	b_{ji}/K
water + benzene	0.200	2.280	2.272	1340	359.2
water + toluene	0.200	0.479	4.383	1963	-428.3
CPL + benzene	0.300	-6.050	1.139	1242	432.6
CPL + toluene	0.300	-6.965	3.159	1657	-327.3
CPL + water	0.300	24.89	-6.166	-6123	1147
CPL + AS	0.0063	45.90	23.56	3016	-24105
water + AS	0.118	3.682	-15.88	1921	2245
benzene + AS	-0.260	-6.203	7.363	307.9	-629.3
toluene + AS	-0.294	2.384	-14.24	-2345	4845

The uncertainty in the fitted data was described with an average absolute deviation (AAD). For the benzene systems without and with ammonium sulfate, respectively, the AAD for the mass fractions of caprolactam in both phases combined was 4.6×10^{-3} and 6.9×10^{-3}, the AAD for water in the organic phase was 1.7×10^{-3} and 8.7×10^{-3}, the AAD for benzene in the aqueous phase was 2.4×10^{-3} and 2.7×10^{-3}, and the AAD for ammonium sulfate in the aqueous phase was 9.0×10^{-3}. For the toluene systems without and with ammonium sulfate, respectively, the AAD for the mass fractions of caprolactam in both phases combined was 3.7×10^{-3} and 2.4×10^{-3}, the AAD for water in the organic phase was 2.1×10^{-3} and 2.3×10^{-3}, the AAD for toluene in the aqueous phase was 3.0×10^{-3} and 3.7×10^{-3}, and the AAD for ammonium sulfate in the aqueous phase was 1.6×10^{-3}.

Experimental and calculated phase compositions of the ternary systems water + caprolactam + benzene and toluene at 293 K are presented in parts (a) and (b) of Figure 2.1.

(a)

(b)
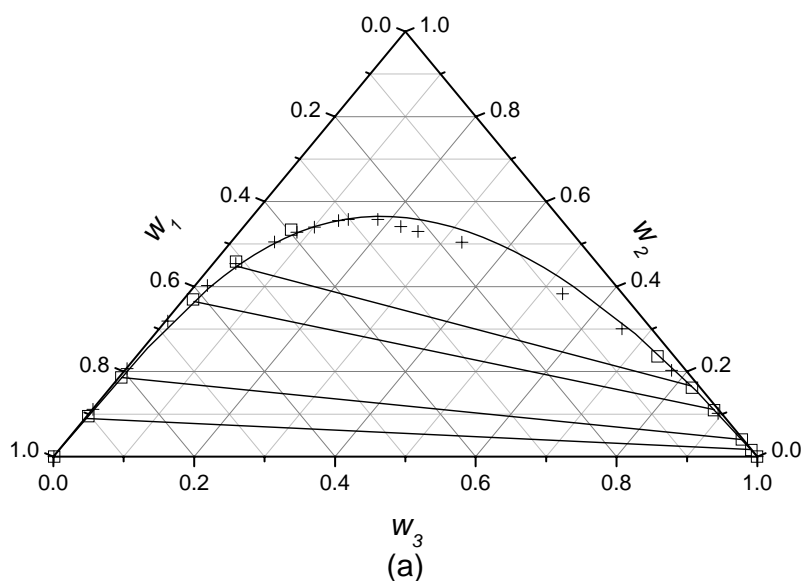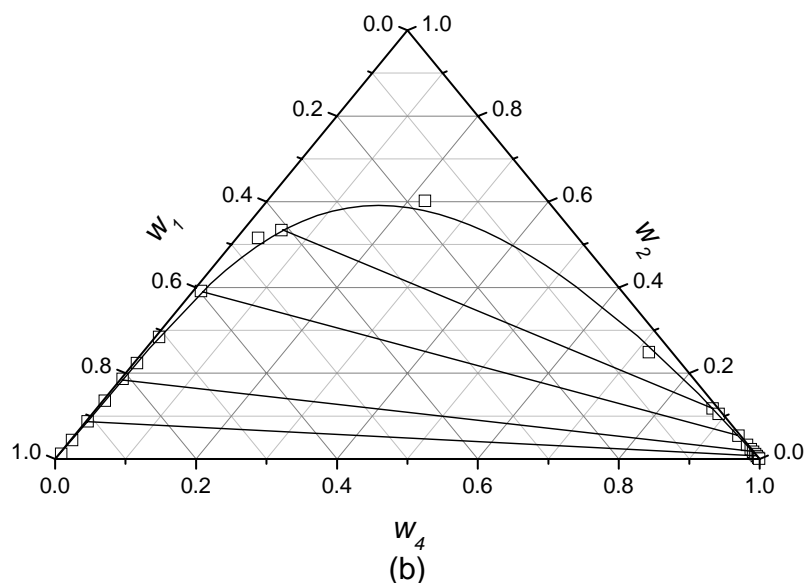
Figure 2.1. Equilibrium phase compositions (mass fractions) for the ternary systems water (1) + caprolactam (2) + benzene (3) (a) and toluene (4) (b) at 293 K: □, this work; +, Tettamanti *et al.*[2]; —, fitted values using the NRTL model.

In this figure, the data measured for the system water + caprolactam + benzene are compared to those reported by Tettamanti *et al.*[2] It can be concluded that all data are in good agreement. The figure shows, furthermore, that the two-phase region for both solvents is comparable and well correlated by the NRTL model. The influence of temperature on the experimental and calculated equilibrium data for caprolactam for both ternary systems is shown in parts (a) and (b) of Figure 2.2. The data for the benzene system at 293 K are compared to literature data reported by Tettamanti *et al.*,[2] whereas the data for the toluene system at 313 K are compared to literature data reported by Pajak *et al.*[14]

(a)

(b)
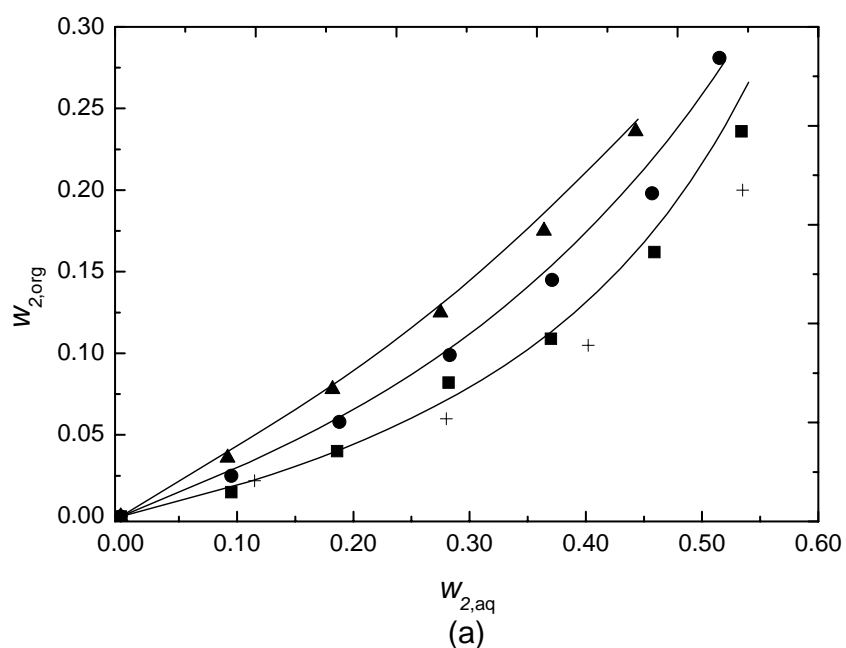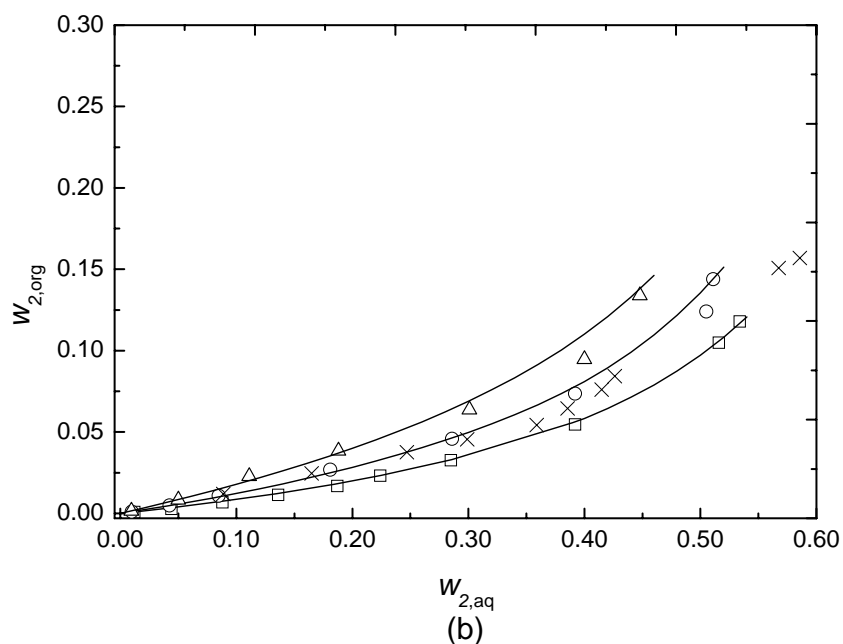
Figure 2.2. Organic equilibrium mass fraction of caprolactam as a function of the aqueous equilibrium mass fraction for the ternary system water (1) + caprolactam (2) + benzene (3) (a): ■, 293 K; ●, 313 K; ▲, 333 K; +, 293 K reported by Tettamanti *et al.*;[2] —, fitted equilibria according to the NRTL model; for the ternary system water (1) + caprolactam (2) + toluene (3) (b): □, 293 K; ○, 313 K; △, 333 K; ×, 313 K reported by Pajak *et al.*;[14] —, fitted equilibria according to the NRTL model.

From this figure, it can be concluded that the measured data show good agreement with the literature data and that the temperature influence on the distribution of caprolactam is represented well by the NRTL model for both solvents. It is clearly shown that for both solvents the concentration of caprolactam in the organic phase is increased considerably at elevated temperatures and that the concentration of caprolactam in the organic phase is always higher for benzene than for toluene at equal conditions. The influence of ammonium sulfate on the experimental and fitted equilibrium data for caprolactam for both ternary systems is presented in parts (a) and (b) of Figure 2.3. It shows that the influence of ammonium sulfate on the distribution of caprolactam is fitted well with the NRTL model. Furthermore, it can be concluded that the addition of ammonium sulfate to the system causes considerable salting out of caprolactam for both solvents, resulting in significant changes of the distribution of caprolactam between the two liquid phases. The concentration of caprolactam in the organic phase is, however, still always higher for benzene than for toluene at equal conditions. For the 15 mass % ammonium sulfate system with benzene and the 5 mass % ammonium sulfate system with toluene a three liquid-phase equilibrium region was observed at concentrations of caprolactam higher than the presented experimental range in Tables A1 and A2. This appearance of three-phase equilibria for the quaternary system water + caprolactam + ammonium sulfate + benzene at 293 K, 313 K and 333 K was studied and fitted in more detail by van Bochove *et al.*[10,20] However, three-phase equilibria do not occur in the industrial caprolactam extraction process and were therefore not investigated further here. The three-phase systems disappeared when going to the 40 mass % ammonium sulfate systems.
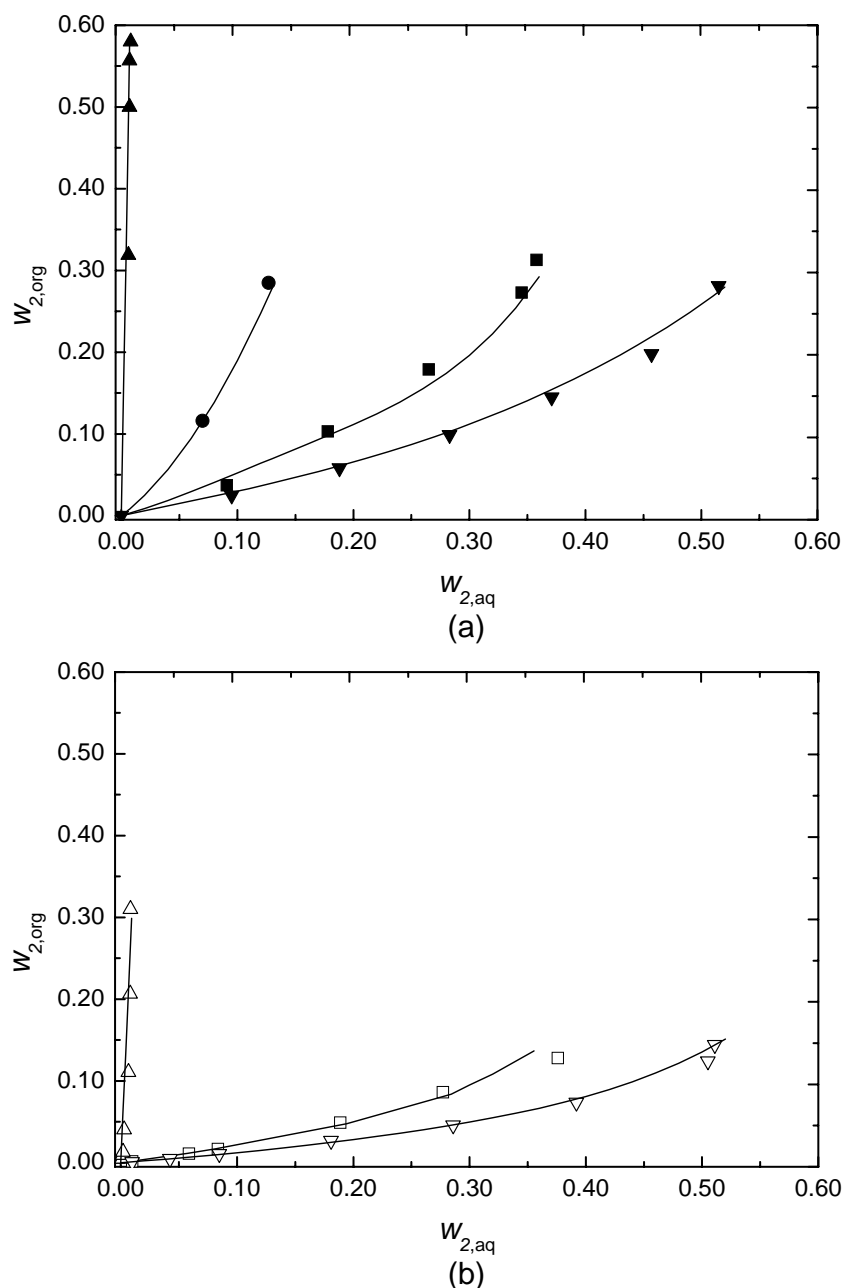
Figure 2.3. Organic equilibrium mass fraction of caprolactam as a function of the aqueous equilibrium mass fraction for the quaternary system water (1) + caprolactam (2) + ammonium sulfate (3) + benzene (4) (a) at 313 K: ▼, 0 mass % ammonium sulfate; ■, 5 mass %, ●, 15 mass %; ▲, 40 mass %; —, fitted equilibria according to the NRTL model; and for the quaternary system water (1) + caprolactam (2) + ammonium sulfate (3) + toluene (4) (b) at 313 K: ▽, 0 mass % ammonium sulfate; □, 5 mass %; △, 40 mass %; —, fitted equilibria according to the NRTL model.

2.3.2   Physical properties

Density. In Table A3 (see Appendix A), the results are given for the density data at 293 K, 313 K and 333 K of the systems water + caprolactam + ammonium sulfate, benzene + caprolactam, and toluene + caprolactam. The presented density data were correlated using Equation (2–2), which represents a linear effect of the solute mass fraction and a temperature effect that is described with the volumetric expansion coefficient[11]

$$\frac{\rho_{i,T}}{\rho_{0,293}} = \frac{1}{1+\alpha \cdot (T-293)} + \sum_i \frac{A_i \cdot w_i}{1+\alpha \cdot (T-293)^{b_i}}$$

(2–2)

where $\rho_{i,T}$/kg·m^{-3} is the density for given mass fractions w of solute i in the solvent at the system temperature T/K, $\rho_{0,293}$/kg·m^{-3} is the density of pure solvent ($w_i = 0$) at the reference temperature of 293 K, A_i is an adjustable parameter describing the influence of the mass fraction of solute i on the mixture volume, α/K^{-1} is the volumetric thermal expansion coefficient, and b_i is an adjustable parameter describing the influence of the temperature on the mixture volume expansion as result of the addition of solute i. In the case of $b_i = 1$, the temperature influence simplifies to the standard volumetric thermal expansion expression.[22] The coefficients A_i, b_i, and the volumetric thermal expansion coefficient were determined by minimization of the standard error in fitting the density data for various amounts of solute at 293 K, 313 K, and 333 K using the program Origin 6.0. The determined parameters are shown in Table 2.2.

Table 2.2. Fitted parameters for the description of densities according to Equation (2–2) of the systems solvent (1) + caprolactam (CPL) (2) + ammonium sulfate (AS) (3) at 293 K, 313 K and 333 K, where the solvent is water, benzene or toluene.

	Water-system[a]	Benzene-system[b]	Toluene-system[c]
$\rho_{0,293}$/kg·m^{-3}	998.4	879.0	867.6
A_{CPL}/kg·m^{-3}	0.086	0.204	0.216
b_{CPL}	2	1	1
A_{AS}/kg·m^{-3}	0.580	-	-
b_{AS}	1	-	-
α/K^{-1}	0.366×10^{-3}	1.26×10^{-3}	1.15×10^{-3}

[a] water (1) + caprolactam (2) + ammonium sulfate (3)
[b] benzene (1) + caprolactam (2)
[c] toluene (1) + caprolactam (2)

The average of the ratio of the measured and calculated density data and its standard deviation is $0.9999 \pm 8 \times 10^{-4}$, $1.0000 \pm 3 \times 10^{-4}$ and $1.0001 \pm 8 \times 10^{-4}$ for the water, toluene, and benzene systems, respectively. Experimental and calculated density data for the binary systems water + caprolactam, benzene + caprolactam, and toluene + caprolactam as a function of the mass fraction of caprolactam, for the binary system water + ammonium sulfate as function of the mass fraction of ammonium sulfate, and for the ternary system water + caprolactam + ammonium sulfate as function of the concentration of caprolactam at 293 K and 333 K are presented in Figure 2.4. Comparison of the calculated and experimental results shows that the experimental data are very well represented by Equation (2–2). Figure 2.4 shows that for all solvents and all solutes the density increases linearly with increasing solute

mass fraction. This increase is equal at different temperatures, except for the binary and ternary solutions containing water and caprolactam, where the density increase with a higher solute mass fraction was lower at elevated temperatures. From the figure, it can furthermore be seen that an increase of the temperature resulted in a decrease of density. From the results for the binary water + caprolactam and ternary water + caprolactam + ammonium sulfate systems, it was concluded that the influence of solute mass fraction on the density was additive.
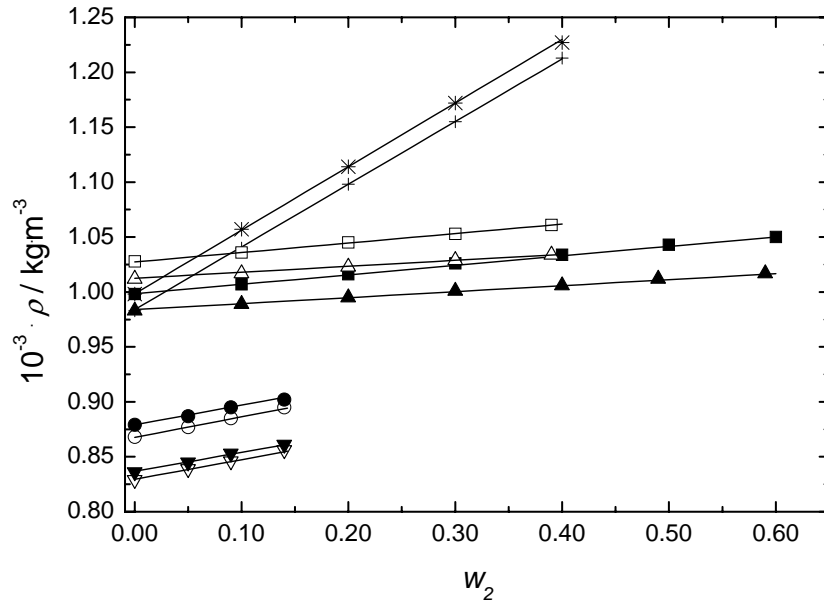
Figure 2.4. Densities as a function of the solute concentration of the binary systems water (1) + caprolactam (2): ■, 293 K; ▲, 333 K; of benzene (1) + caprolactam (2): ●, 293 K; ▼, 333 K; of toluene (1) + caprolactam (2): ○, 293 K; ▽, 333 K; of water (1) + ammonium sulfate (2): ✳, 293 K; +, 333 K; and of the ternary system water (1) + caprolactam (2) + ammonium sulfate (5 mass %) (3): □, 293 K; △, 333 K; —, fitted values according to Equation (2–2).

Viscosity. In Table A4 (see Appendix A), the results are shown for the kinematic viscosity data of the systems water + caprolactam + ammonium sulfate, benzene + caprolactam, and toluene + caprolactam at 293 K, 313 K and 333 K. The presented viscosity data were correlated using the (extended) Dole-Jones equation as shown in Equation (2–3), which is capable of correlating the influence of the concentration of solute on the viscosity for both electrolyte[23] as well as for non-electrolyte solutions[24,25]

$$\frac{v_{i,T} \cdot \rho_{i,T}}{v_{0,T} \cdot \rho_{0,T}} = \frac{\eta_{i,T}}{\eta_{0,T}} = 1 + A_{DJ,T} \cdot \sqrt{c_i} + B_{DJ,T} \cdot c_i + D_{DJ,T} \cdot c_i^{F_{DJ,T}} \qquad (2\text{–}3)$$

where $v_{i,T}$/m^2·s^{-1} and $\eta_{i,T}$/kg·m^{-1}·s^{-1} are the kinematic and dynamic viscosities for a given concentration c/mol·L^{-1} of solute i at the system temperature T/K, $v_{0,T}$/m^2·s^{-1} and $\eta_{0,T}$/kg·m^{-1}·s^{-1} are the kinematic and dynamic viscosities for the pure solvent (c_i/mol·L^{-1} = 0) at the system temperature T/K, A_{DJ}/L$^{1/2}$·mol$^{-1/2}$ accounts for the ion-ion interaction, B_{DJ}/L·mol^{-1} accounts for ion-solvent interaction (in case of an electrolyte solution) or solvent-solvent interaction and

viscosity difference of pure solvents (in case of a mixture of solvents), $D_{DJ}/L^F \cdot mol^{-F}$ is an adjustable parameter, which extends the validity of the empirical expression from 0.1 mol·L^{-1} up to 1 to 2 mol·L^{-1} [23,24] in combination with parameter F_{DJ}, which is generally set to $F_{DJ} = 2$. The electrolyte ion-ion interaction, expressed in parameter A_{DJ}, is zero for non-electrolyte solutes[24,25] and shows an influence for electrolyte solutes up to $c_i/mol \cdot L^{-1} = 0.05$.[23] Since the concentrations of NH_4^+ and SO_4^{2-} in this study reached up to 3 to 6 mol·L^{-1}, the effect of parameter A_{DJ} was neglected.

The temperature influence on the pure solvent viscosity was described by the Guzman-Andrade equation as shown in Equation (2–4)[22]

$$\frac{v_{0,T} \cdot \rho_{0,T}}{v_{0,293} \cdot \rho_{0,293}} = \frac{\eta_{0,T}}{\eta_{0,293}} = \exp\left(B_{AG} \cdot \left(\frac{1}{T} - \frac{1}{293} \right) \right) \tag{2–4}$$

where $v_{0,293}/$ m$^2 \cdot$s^{-1} and $\eta_{0,T}/$kg·m$^{-1} \cdot$s^{-1} are the kinematic and dynamic viscosities of the pure solvent at the reference temperature of 293 K and $B_{AG}/$K represents the Andrade-Guzman coefficient. In binary solutions, the Dole-Jones coefficients B_{DJ} and D_{DJ} can be determined graphically from the linear relation between $(B_{DJ} + D_{DJ} \cdot c_i)$ and c_i, according to Equation (2–3) when $F_{DJ} = 2$.[24] This method was found to be valid for all caprolactam solutions but not for aqueous ammonium sulfate solutions. Since the NH_4^+ and SO_4^{2-} ions were always present in the same ratio, their separate influence could not be distinguished. In the determination of the Dole-Jones parameters for the NH_4^+ and SO_4^{2-} ions it was therefore assumed that ammonium sulfate is fully dissociated and that the influence of all solutes is additive. The parameters B_{DJ} for the NH_4^+ and SO_4^{2-} ions and the temperature influence on these parameters were taken from literature.[23] The remaining Dole-Jones coefficients, D_{DJ} for both ions, were determined by minimization of the standard error in fitting the viscosity data for various amounts of solute at 293 K, 313 K and 333 K using the program Origin 6.0. The Andrade-Guzman coefficient for the pure solvents was also determined using this approach. As expected from literature,[23-25] a temperature influence on the Dole-Jones parameters was observed both from the graphical interpretation as from the fitting method. The temperature influence was assumed to be linear. The determined parameters are listed in Table 2.3, where the Dole-Jones parameters determined for caprolactam are based on the combined data of the aqueous caprolactam solution and the aqueous ammonium sulfate solution containing caprolactam. All parameters were initially determined for data at $c_i/mol \cdot L^{-1} < 3$ and $F_{DJ} = 2$. The average of the ratio of the fitted and measured viscosity data and its standard deviation for the Dole-Jones equation is $0.96 \pm 7.0 \times 10^{-2}$, $1.001 \pm 3.7 \times 10^{-3}$, and $1.000 \pm 3.8 \times 10^{-3}$ for the water, toluene, and benzene systems, respectively.

Table 2.3. Fitted parameters for the description of dynamic viscosities according to Equation (2–3) and (2–4) of the systems solvent (1) + caprolactam (CPL) (2) + ammonium sulfate (3) at 293 K, 313 K and 333 K, where the solvent is water, benzene, or toluene.

Dole-Jones parameters		
$\eta_{0,293}/\text{kg} \cdot \text{m}^{-1} \cdot \text{s}^{-1}$		
1.02×10^{-3} [a]	0.66×10^{-3} [b]	0.59×10^{-3} [c]

$$B_{DJ}=k_1 \cdot (T-273)+k_2$$

SO_4^{2-}	$k_1=19.8 \times 10^{-4}$		
	$k_2=0.1570$ [d]		
NH_4^+	$k_1=7.8 \times 10^{-4}$		
	$k_2=-0.0282$ [d]		
CPL	$k_1=-29.3 \times 10^{-4}$	$k_1=-2.8 \times 10^{-4}$	$k_1=-15.8 \times 10^{-4}$
	$k_2=0.3960$	$k_2=0.2388$	$k_2=0.2944$

$$D_{DJ}=m_1 \cdot (T-273)+m_2 \; ; \; F_{DJ}=2$$

SO_4^{2-}	$m_1=-3.0 \times 10^{-4}$		
	$m_2=-1.4628$		
NH_4^+	$m_1=-0.7 \times 10^{-4}$		
	$m_2=0.3843$		
CPL	$m_1=-10.2 \times 10^{-4}$	$m_1=-7.7 \times 10^{-4}$	$m_1=-3.0 \times 10^{-4}$
	$m_2=0.1353$	$m_2=0.0929$	$m_2=0.0892$

$$D_{DJ}=m_1 \cdot (T-273)+m_2 \; ; \; F_{DJ}=n_1 \cdot (T-273)+n_2$$

CPL	$m_1=4.9 \times 10^{-4}$
	$m_2=0.0555$
	$n_1=-1.5 \times 10^{-2}$
	$n_2=2.960$

B_{AG}/K	1943 [e]	1266	1048

[a] water (1) + caprolactam (2) + ammonium sulfate (3)
[b] benzene (1) + caprolactam (2)
[c] toluene (1) + caprolactam (2)
[d/e] based on literature data[23/11]

Since it appeared that the description of the viscosity data using the Dole-Jones equation showed a large deviation at concentrations of caprolactam of $c_i/\text{mol} \cdot \text{L}^{-1} > 3$, Equation (2–3) was adjusted for the description of caprolactam solutions in order to ensure the validity over an extended concentration range. The determined values for parameters B_{DJ} and B_{AG} were kept constant, but the values for the parameters D_{DJ} and F_{DJ} were determined by minimization of the standard error in fitting the viscosity data for various amounts of caprolactam at 293 K, 313 K and 333 K using the program Origin 6.0. The determined parameters are listed in Table

2.3, where these parameters are obtained from the combined data of the aqueous caprolactam solution and the aqueous ammonium sulfate solution containing caprolactam. The average ratio of the fitted and measured viscosity data and its standard deviation for the Dole-Jones equation is $0.99 \pm 4.5 \times 10^{-2}$ for the water system. Experimental and fitted viscosity data for the systems water + caprolactam, benzene + caprolactam, toluene + caprolactam and water + caprolactam + ammonium sulfate as function of the concentration of caprolactam and for the system water + ammonium sulfate as function of the concentration of ammonium sulfate at 293 K and 333 K are presented in Figure 2.5.
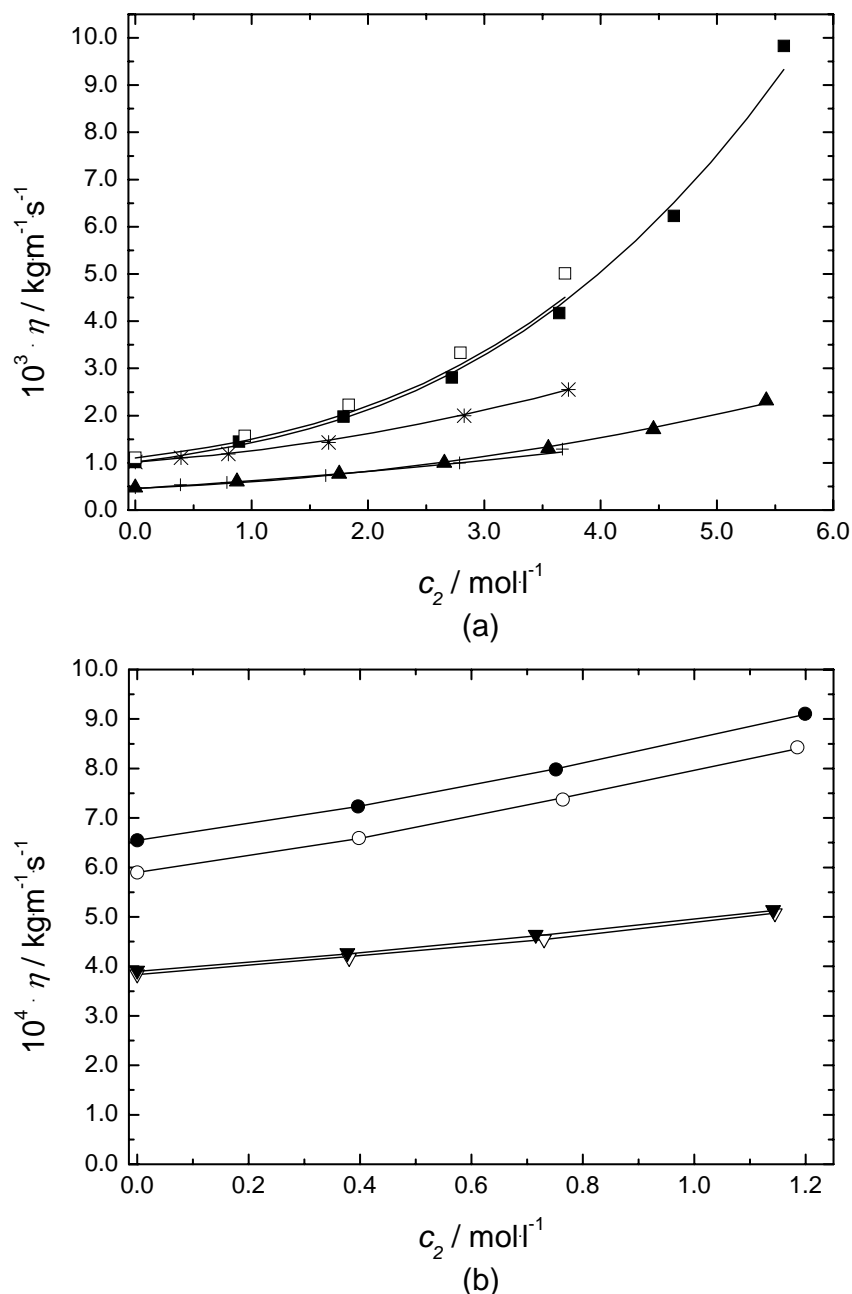
Figure 2.5. Dynamic viscosities as function of solute concentration of water (1) + caprolactam (2): ■, 293 K; ▲, 333 K; of water (1) + ammonium sulfate (2): ✳, 293 K; +, 333 K; of water (1) + caprolactam (2) + ammonium sulfate (3): □, 293 K; —, fitted values via Equation (2–3) and (2–4) (a) and of benzene (1) + caprolactam (2): ●, 293 K; ▼, 333 K; and toluene (1) + caprolactam (2) (b): ○, 293 K; ▽, 333 K; —, fitted values via Equation (2–3) and (2–4) (b).

Comparison of the calculated and experimental results shows that the experimental data are very well represented with the modified extended Dole-Jones and the Andrade-Guzman equations. Figure 2.5 shows that for all solvents and all solutes the viscosity increases with increasing solute concentration, but the increase is lower at elevated temperatures. Obviously, it can be seen that an increase of temperature results in a decrease of viscosity.

Interfacial tension. In Table A5 (see Appendix A), the results are shown for the interfacial tension of the system water + caprolactam + ammonium sulfate + organic solvent at 293 K, 313 K and 333 K, where the organic solvent is benzene or toluene. The presented interfacial tension data were correlated using the Szyzkowski isotherm as described in Equation (2–5)[26]

$$\gamma_{i,T} = \gamma_{0,T} \cdot \left[1 - B_{SZ} \cdot \ln\left(\frac{c_i}{A_{SZ}} + 1 \right) \right] \tag{2–5}$$

where $\gamma_{i,T}$/N·m^{-1} is the interfacial tension for a given concentration c/mol·L^{-1} of solute i at system temperature T/K, $\gamma_{0,T}$/N·m^{-1} is the interfacial tension for the system without solute present (c_i/mol·L^{-1} = 0) at system temperature T/K, and A_{SZ}/mol·L^{-1} and B_{SZ} are so-called Szyzkowski adsorption coefficients. The influence of the concentration of ammonium sulfate on the interfacial tension was described via the concentration of ammonium sulfate in the aqueous phase, since ammonium sulfate was assumed not to be present in the organic phase. The influence of the concentration of caprolactam on the interfacial tension of the ternary system was described either via the concentration of caprolactam in the aqueous or the organic phase. Both methods resulted in a good fit. For the quaternary system, an influence of both solutes on the interfacial tension was expected, based on experimental data for the ternary systems as shown in Table A5, although the influence of ammonium sulfate would be small compared to caprolactam. Salting out of caprolactam caused by the presence of ammonium sulfate would result in a large influence however. The water + caprolactam + ammonium sulfate + toluene system was therefore described as the ternary caprolactam system, where the concentration influence was based on the concentration of caprolactam in the organic phase, assuming that the influence of caprolactam and the salting-out effect would cover almost fully the influence of both solutes on the interfacial tension. The temperature influence on the interfacial tension of the system without solute present was described by the Jasper correlation as shown in Equation (2–6)[22]

$$\gamma_{0,T} = \gamma_{0,293} - A_J \cdot (T - 293) \tag{2–6}$$

where $\gamma_{0,293}$/N·m^{-1} is the interfacial tension of the system without solute present (c_i/mol·L^{-1} = 0) at the reference temperature of 293 K and A_J/N·m^{-1}·K^{-1} represents the Jasper coefficient. The adsorption and Jasper coefficients were determined by minimization of the standard error in fitting the interfacial tension data for various amounts of solute at 293 K, 313 K and 333 K

using the program Origin 6.0. The determined parameters are shown in Table 2.4, where the results showed a temperature influence on the caprolactam adsorption coefficients.

Table 2.4. Fitted parameters for the description of interfacial tension data based on the concentrations of caprolactam (CPL) in the organic (org) and of ammonium sulfate (AS) in the aqueous (aq) phase according to Equation (2–5) and (2–6) of the systems water (1) + caprolactam (2) + ammonium sulfate (3) + toluene (4) at 293 K, 313 K and 333 K

	$\gamma_{0,293}$/N·m^{-1}	A_J/N·m^{-1}·K^{-1}
Water+Toluene	$35.8 \cdot 10^{-3}$	$5.75 \cdot 10^{-5}$
	A_{SZ}/mol·L^{-1}	B_{SZ}
CPL$_{org}$	$-5.8 \cdot 10^{-4} +$ $7.63 \cdot 10^{-5} \cdot (T\text{-}273)$	$0.125 +$ $9.06 \cdot 10^{-4} \cdot (T\text{-}273)$
AS$_{aq}$	5.1	$-2.15 \cdot 10^{-1}$

The averages of the ratio of the fitted and measured interfacial tension data and its standard deviation are $1.00 \pm 1.1 \times 10^{-2}$, $1.02 \pm 9.1 \times 10$-2, and $0.98 \pm 1.0 \times 10$-1 for the systems water + ammonium sulfate toluene, water + caprolactam + toluene, and water + caprolactam + ammonium sulfate + toluene, respectively. Experimental and calculated interfacial tension data for the ternary system water + caprolactam + toluene as function of the concentration of caprolactam in the organic phase and water + ammonium sulfate + toluene as function of the concentration of ammonium sulfate in the aqueous phase and for the quaternary system water + caprolactam + ammonium sulfate + toluene as function of the concentration of caprolactam in the organic phase at 293 K and 333 K are presented in Figure 2.6. Comparison of the calculated and experimental results shows that the experimental data are very well represented with the Szyzkowski and the Jasper equations. Figure 2.6 shows that for the ternary system water + ammonium sulfate + toluene the interfacial tension increased with solute concentration, where it decreased for the ternary and quaternary systems containing caprolactam. The figure illustrates furthermore the opposite behaviour with temperature, since the interfacial tension decreases with increasing temperature for the binary system water + toluene and the ternary system water + ammonium sulfate + toluene as expected from the Jasper equation. It increases, however, with increasing temperature for the ternary and quaternary systems containing caprolactam. The reason for this behaviour can probably be found in the increase of the distribution ratio of caprolactam with increasing temperature as presented in part (b) of Figure 2.2. At equal concentrations of caprolactam in the organic phase this change results in decreasing concentrations of caprolactam in the aqueous phase with increasing temperature. These lower concentrations of caprolactam in the aqueous phase have an effect on the interfacial tension. The combined effect of temperature and the phase compositions at that temperature then results in the increase of the interfacial tension with increasing temperature. Figure 2.6 shows also that the experimental interfacial tension data for the ternary system water + caprolactam + toluene and the quaternary system water +

caprolactam + ammonium sulfate + toluene were comparable at equal equilibrium concentrations of caprolactam in the organic phase, which supports the assumption that the interfacial tension of the quaternary system could be described as the ternary system water + caprolactam + toluene, where the influence of ammonium sulfate was taken into account via the salting-out effect on the equilibrium distribution of caprolactam.
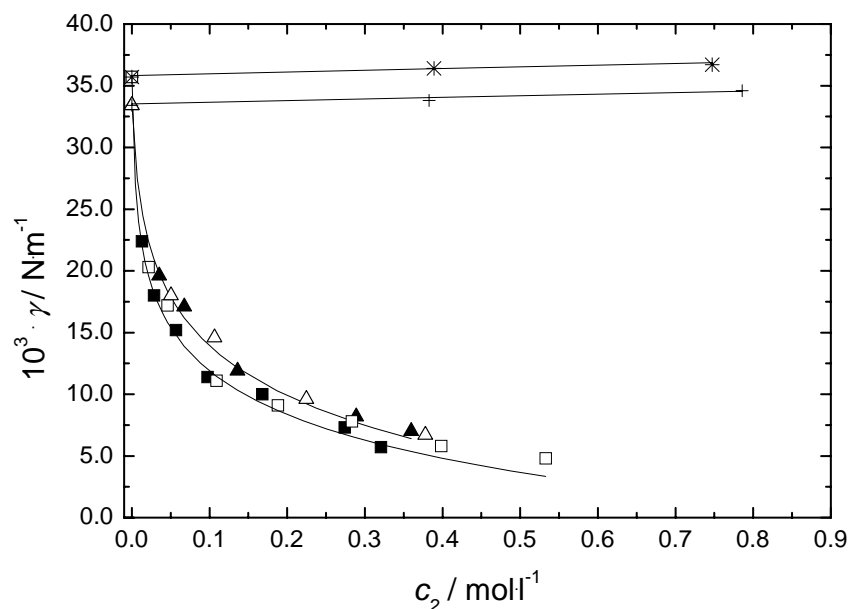
Figure 2.6. Interfacial tension data of the ternary systems water (1) + caprolactam (2) + toluene (3) as function of the concentration of caprolactam in the organic phase: ■, 293 K; ▲, 333 K; of water (1) + ammonium sulfate (2) + toluene (3) as function of the concentration of ammonium sulfate in the aqueous phase: ✳, 293 K; +, 333 K; and of the quaternary system water (1) + caprolactam (2) + ammonium sulfate (3) + toluene (4) as function of the concentration of caprolactam in the organic phase: □, 293 K; △, 333 K; —, model fits according to Equation (2–5) and (2–6).

2.4   Conclusions

LLE phase compositions for the quaternary system water + caprolactam + ammonium sulfate + solvent, where the solvent was benzene or toluene, and density, viscosity, and interfacial tension data for the respective phases were determined at 293 K, 313 K and 333 K, covering the full concentration and temperature range as present in the industrial process. Data were determined for the two liquid phase systems, where three liquid phases were observed for the benzene and toluene system at, respectively, 15 mass % and 5 mass % of ammonium sulfate. The measured data showed good agreement with results reported in the literature by Tettamanti *et al.*[2] and Pajak *et al.*[14]

Phase equilibria were correlated with the classical NRTL model, and a good representation was obtained for both ternary and quaternary systems, when ammonium sulfate was treated as a fully dissociated pseudo-component and the non-randomness parameter was determined in the fitting procedure and not set at the default value of 0.2 or 0.3. This approach resulted in a simple and direct applicable model in ASPEN Plus 11.1, although the developed model by van Bochove *et al.*[20] and applied in Huan *et al.*[10] might give an even better representation and holds also the possibility of describing LLLE data. Three-phase systems, however, do not

occur in the industrial caprolactam extraction process and were therefore not further investigated here.

Density data were correlated well using a linear relation for the influence of the concentration of solute, whereas the volumetric thermal expansion coefficient is used to describe the temperature influence on the system. Viscosity data were correlated using the adapted Dole-Jones equation for the influence of concentration, taking into account the influence of temperature on the Dole-Jones parameters. The Andrade-Guzman equation was used to accurately describe the influence of temperature on the viscosity of the pure solvents. Interfacial tension data were fitted with the Szyzkowski equation and the Jasper equation for the temperature influence on the binary system. The influence of concentration on ternary systems was described via the concentration of ammonium sulfate in the aqueous phase and both the concentrations of caprolactam in the aqueous and organic phase, which resulted in good fits. The concentration influence on the quaternary system, however, was described via the concentration of caprolactam in the organic phase assuming that the influence of caprolactam and the salting-out effect would cover almost fully the influence of both solutes on the interfacial tension. An influence of the temperature on the Szyzkowski coefficients for caprolactam was observed, but for ammonium sulfate, this influence was not clearly present. A good representation of the interfacial tension for all systems was obtained using this approach.

Literature cited

1. Morachevskii, A. C.; Sabinin, V. E. Solubility Diagrams for the Ternary Systems Caprolactam-Water-Benzene, Caprolactam-Water-Carbon Tetrachloride and Caprolactam-Water-Dichloroethane. *J. Appl. Chem.* **1960**, *33*, 1775-1779.

2. Tettamanti, K.; Nogradi, M.; Sawinsky, J. Equilibria of the Ternary System Caprolactam-Water-Organic Solvent, in the Liquid State. *Period. Polytech.*, *Chem. Eng*. **1960**, *4*, 201-218.

3. Tettamanti, K.; Nogradi, M. The Influence of Ammonium Sulfate on the Distribution of Caprolactam in the Water/Trichloro Ethylene System. *Period. Polytech. Chem. Eng*. **1960**, *5*, 15-23.

4. Shubtsova, I. G.; Nikurashina, N. I.; Rybalov, S. K. The Caprolactam-Water-Ammonium Sulfate System Investigated by the Method of Sections. *Russ. J. Phys. Chem.* **1975**, *49*, 35-37.

5. Pandya, H. P. Solvent System for Liquid-Liquid Extraction of Caprolactam with Salting Out Effect. *Advances in Chemical Engineering in Nuclear and Process Industries: June 9-11, 1994. Vol. 2*. Bhabha At. Res. Cent.: Bombay, 1994; pp 504-516.

6. Pandya, H. P.; Puranik, S.A. Liquid-Liquid Extraction of Caprolactam. *IE(1) Journal-CH* **1995**, *76*, 1-4.

7. Stratula, C.; Mihai, T.; Cheta, I.; Oprea, F. Comparative-Study on Caprolactam Purification with 2 Solvents. 1. Liquid-Liquid Equilibrium Study. *Rev. Chem.* **1992**, *43*, 372-381.

8. de Haan, A. B.; Niemann, S. H. Modelling Phase Equilibria in Industrial Caprolactam Recovery from Aqueous Ammonium Sulfate Solutions with Benzene. *Solvent Extraction for the 21st Century. Proceedings of ISEC 1999. Vol. 2*; Cox, M., Hidalago, M., Valiente, M., Eds.; Society of Chemical Industry: London, 2001; pp 1537-1542.

9. Liu, J.; Xie, F.; He, C.; Zhu, M. Recovery of Caprolactam from Wastewater in Caprolactam Production Using Pulsed-Sieve-Plate Extraction Column. *Chin. J. Chem. Eng.* **2002**, *10*, 371-373.

10. Huan, Z.; van Bochove, G. H.; de Loos, Th. W. Three-Liquid-Phase Equilibria in Water + Benzene + Caprolactam + $(NH_4)_2SO_4$ Mixtures. *AIChE J.* **2003**, *49*, 745-752.

11. Ullmann, F. *Ullmann's Encyclopedia of Industrial Chemistry*; Wiley-Interscience: New York, 2004; electronic version.

12. SNIA. US 4606858, 1986.

13. Petrochemical processes: Caprolactam-SNIA. *Hydrocarbon Processing* **1999**, 103.

14. Pajak, M.; Piotrowicz, J.; Skrzypinski, W. Extraction of Caprolactam in Packed Columns. *Przem. Chem.* **1991**, *71*, 107-110.

15. Prochazka, J.; Landau, J.; Souhrada, F.; Heyberger, A. Reciprocating-Plate Extraction Column. *British Chem. Eng.* **1971**, *16*, 42-44.

16. Chang, R.-Y.; Yang, H.-M.; Wang, M.-L. Solubility of ε-Caprolactam in Benzene and Toluene Solvents. *J. Chin. Inst. Chem. Eng.* **1981**, *12*, 141-145.

17. Zheleznova, N. I.; Popov, D. M.; Kanakina, S. V. Phase Equilibrium in the Caprolactam-Toluene-Water System. *Z. Prikl. Khim.* **1985**, *58*, 1900-1903.

18. Pajak, M.; Piotrowicz, J.; Skrzypinski, W. Extractive Equilibria in Technology of Caprolactam Production. *Przem. Chem.* **1991**, *70*, 72-74.

19. Aspen Technology, Inc. *Aspen Physical Property System*; ASPEN PLUS User Manual, Release 11.1: Cambridge, MA, 2001.

20. Van Bochove, G. H.; Krooshof, G. J. P.; De Loos, T. W. Modelling of Liquid-Liquid Equilibria of Mixed Solvent Electrolyte Systems Using the Extended Electrolyte NRTL. *Fluid Phase Equilib.* **2000**, *171*, 45-58.

21. Shaw, D. G. *Solubility Data Series*; Pergamon Press: Oxford, 1989.

22. Poling, B. E.; Prausnitz J. M.; O'Connell J. P. *The Properties of Gases and Liquids*; McGraw-Hill International Editions: Singapore, 2001.

23. Donald, H.; Jenkins, B.; Marcus, Y. Viscosity B-Coefficients of Ions in Solution. *Chem. Rev.* **1995**, *95*, 2695-2724.

24. Nakagawa, T. Is Viscosity B-Coefficient Characteristic for Solute-Solvent Interaction. *J. Mol. Liq.* **1995**, *63*, 303-316.

25. De Ruiz Holgado, M. E.; de Schaeffer, C. R.; Arancibia, E. L. Viscosity Study of 1-Propanol with Polyethylene Glycol 350 Monomethyl Ether Systems at Different Temperatures. *J. Mol. Liq.* **1999**, *79*, 257-267.

26. Prochaska, K. Interfacial Activity of Metal Ion Extractants. Adv. *Coll*. *Int*. *Sci*. **2002**, *95*, 51-72.

Chapter 3

Extraction of caprolactam with toluene in a pulsed disc and doughnut column: model development for hydraulic characteristics

3.1   Introduction

Caprolactam is recovered from the neutralized Beckmann rearrangement mixture by phase separation followed by solvent extraction of the resulting crude caprolactam phase, the so-called forward extraction (FE), and the aqueous ammonium sulfate layer. Currently, benzene, toluene and chlorinated hydrocarbons are used as solvent. After the forward extraction caprolactam is recovered by back-extraction (BE) with water and for both extraction processes columns like the Rotating Disk Contactor (RDC), Asymmetric Rotating Disc Contactor (ARD) and Pulsed Packed Column (PPC) are applied, as described in Chapter 1.

In this research a novel type of extraction column for the extraction of organics, a Pulsed Disc and Doughnut Column (PDDC), was investigated for its applicability in the caprolactam extraction process. This column was analysed since it is simpler and cheaper to construct compared to the rotating internals of the RDC and ARD, whereas the PDDC is less susceptible to fouling than a PPC.

The PDDC is already applied in metal extraction for which the operational characteristics of this column are therefore known.[1-3] Furthermore fundamental research has been performed on hydrodynamics, mass transfer and axial dispersion by means of numerical simulation[4-14], whereas also some literature is available on experimental data for hydrodynamics and mass transfer in a PDDC.[15,16] However, for the extraction of organics, like caprolactam, which possess different physical characteristics than metal extraction systems, no information is available.

In the design of an extraction column, besides the separation performance, the hydraulic characteristics, being hold-up and drop size, which determine operating regimes and operational window, are key parameters in order to determine the column capacity and the required column diameter to provide the desired throughput.[17,18]

In the present study a mathematical model is developed describing the hydraulic characteristics of a PDDC for both the caprolactam forward and back-extraction configuration with and from toluene, respectively. This model is developed based on existing column-

independent equations and equations derived for pulsed sieve-plate and Karr columns. These need to be valid for the industrial operating range with respect to the concentrations of caprolactam and ammonium sulfate, solvent to feed ratio, phase continuity and operating parameters, being temperature, flow rates, pulsation frequency and amplitude. It is furthermore necessary that the geometrical characteristics used in the equations can be easily translated to a PDDC. Based on these constraints, finally, one equation is selected for each of the hydraulic characteristics.

3.2 Experimental set-up

The experimental PDDC pilot set-up is shown in Chapter 4 of this study, but the geometrical characteristics necessary for the model development are shown in Figure 3.1.

		PVDF	SS
D_c	/mm	40	40
H	/mm	8.4	9.9
D_r	/mm	39.4	39.4
D_d	/mm	19.9	20.0
e	$(=1-D_d^2/D_c^2)$	0.263	0.267
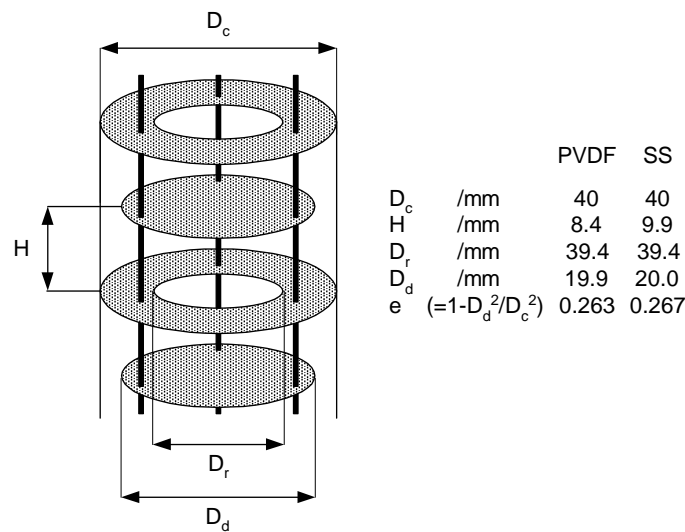
Figure 3.1. Schematic presentation of the PDDC internals with characteristic dimensions.

3.3 Pulsed Disc and Doughnut Column operational window

In the operation of pulsed and reciprocating extraction columns various regimes can be distinguished.[17,19,20] The operating regimes are generally described as mixer-settler (MS), dispersion (D) and emulsion (E) as presented schematically in Figure 3.2.[17,19,20] Comparable operational characteristics have been reported for a binary water-kerosene system in a pulsed disc and doughnut column.[15] The mixer-settler regime is limited by flooding due to a too low amount of energy applied. The other two regimes are limited either by flooding due to a too small relative velocity between the phases, phase inversion in which the original continuous phase becomes dispersed or when the maximal allowable entrainment level is reached.[17] Depending on the desired flow ratio, $R = V_d/V_c$, the dispersed phase hold-up, x, and the maximum allowable entrainment level either regime can be limiting.[17] In Figure 3.2 four possible operating points are shown, denoted by steady state operation point (A), maximum throughput (B), minimal pulsation intensity (C) and maximum pulsation intensity (D).

44
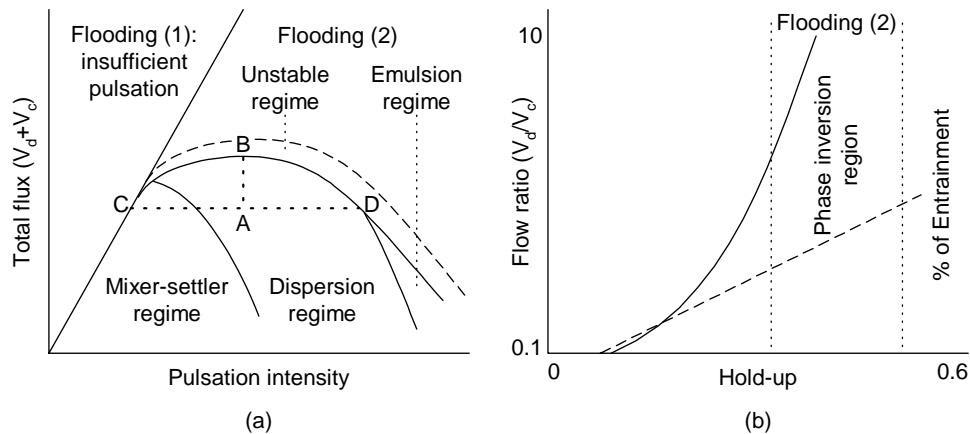
Figure 3.2. Pulsed column operational regimes (a)[17,19,20] and limiting processes (b).[17]

The mixer-settler regime is observed for systems with high interfacial tension operated at low pulsation intensities (being the product of pulsation frequency and stroke). It is created when drops rise faster than the next pulsation stroke is performed, resulting in drops to be retarded and to coalesce at the internals.[17] The characteristics for pulsed sieve-plate columns operated in this regime with the light phase being dispersed are schematically presented in Figure 3.3.[20]
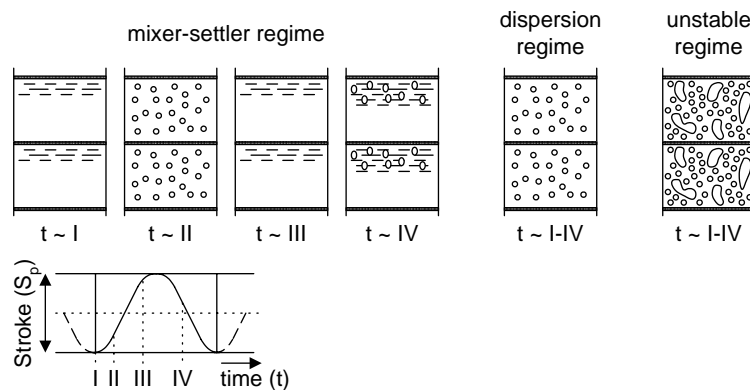
Figure 3.3. Schematic presentation of operational regimes for pulsed sieve-plate columns, where the light phase is dispersed.[20]

At the quiescent time of the pulsation cycle (time I) a zone almost without drops exists together with a layer of densely packed or coalesced drops. At the start of the first half of the pulsation cycle (time II) the layer of dispersed phase is forced through the internals. The drops coalesce again at the second quiescent time of the pulsation cycle (time III). With the pulsation stroke in reverse direction (time IV) the continuous (heavy) phase is transported through the internals with the possibility of phase inversion to occur.

The dispersion regime is characterized by (uniform) drops also rising in the quiescent times, which are accelerated at the start of the first half of the pulsation cycle and retarded in the second half of the pulsation cycle. The emulsion regime behaves like the dispersion regime, except for the second half of the pulsation cycle where the drops are not only retarded, but also dragged in opposite direction by the continuous phase flow. In the unstable regime slugs are formed, which are the onset for flooding.[20]

The behaviour of the dispersed phase hold-up, x, and the Sauter drop diameter, d_{32}/m, in relation to the total flux (Flux/m·h^{-1} = $V_d + V_c$) and pulsation intensity (pulsation intensity = $f \cdot S_p$/m·s^{-1}) is schematically represented in Figure 3.4.[21]
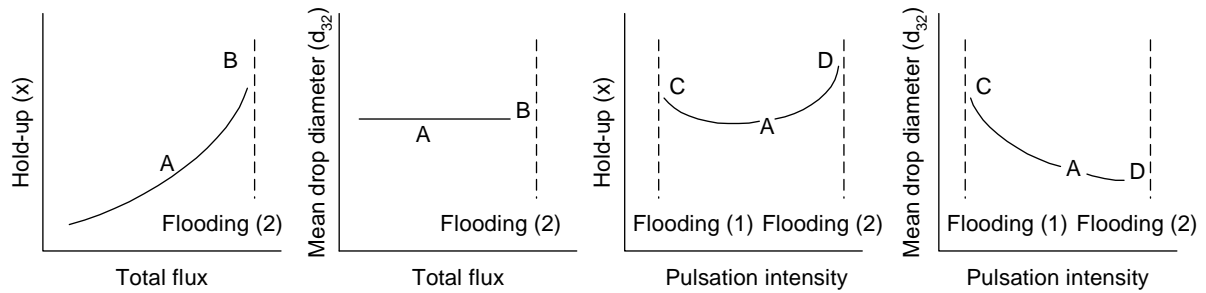
Figure 3.4. Hold-up, x, and Sauter drop diameter, d_{32}, as function of total flux and pulsation intensity in pulsed column operation at constant flow ratio.[21]

When the total flux is increased at constant pulsation intensity (line A to B in Figure 3.2) an increase of the dispersed phase hold-up is observed until flooding is reached. The drop diameter remains constant, but, however, near the flooding limit extra coalescence results in larger average drop diameters.[17] Decreasing the pulsation intensity at a constant total flux (A to C) will initially result in a decrease of the hold-up, because of a larger drop size, but finally results in an increase of the hold-up near the flooding line due to a too low pulsation intensity. Increasing the pulsation intensity at a constant total flux (A to D) will result in an increase of the hold-up, because of a decreasing average drop size with pulsation intensity, until flooding due to a too low relative velocity between the phases occurs.[21] Extraction column operation is generally performed around point A.

3.4   Model development

According to the theory for pulsed sieve-plate columns, pulsed column operation can be characterized by the dispersed phase drop diameter, d_{32}, the dispersed phase hold-up, x, of which the latter is dependent on the operational regime in the column. The column can be operated within a certain window covering a range of operational parameters, which is limited by flooding (1) due to too low pulsation and by flooding (2), phase inversion or entrainment at high pulsation. Equations describing the characteristics within the operational window, being drop diameter, operational regime and hold-up, are selected first, after which the equations describing the limitations of this window are selected.

The parameters on which the equations are based can be divided into three categories: physical properties, operational parameters and geometrical characteristics of the column and internals. The physical properties cover the densities of the phases, ρ_c and ρ_d, and thus the corresponding density difference, $\Delta\rho = |\rho_c - \rho_d|$, the dynamic viscosities of the phases, η_c and η_d, and the interfacial tension, γ. These properties are dependent on the concentrations of caprolactam and ammonium sulfate and the temperature, T, as operational parameter. The conditions used in the experimental pilot set-up and the corresponding physical properties of the quaternary system water + caprolactam + ammonium sulfate + toluene are described in Chapter 4. The physical properties were correlated by the equations as presented in Chapter 2.

The operational parameters cover furthermore the phase velocities, V_c and V_d, and thus the corresponding flux and flow ratio, phase continuity and the pulsation intensity, $f \cdot S_p$. The geometrical characteristics are determined by the internals as presented in Figure 3.1 and cover amongst others the disc to doughnut spacing, H, and the fractional free area, e.

The model is developed for the hydraulic situation and therefore assumes equilibrium conditions in order to avoid the influence of mass transfer. When the forward and back-extraction processes are addressed, therefore the configuration used in these processes is referred to, not the actual transfer of caprolactam.

3.4.1 Sauter drop diameter

Since (empirical) correlations for the drop size, d_{32}, in a PDDC column are not available, the description for all operational regimes was based on unified equations or equations derived for pulsed sieve-plate and Karr columns. From the large set of possible equations, however, several are not directly applicable or only partly valid since they make use of the plate hole diameter, which is not present in the PDDC (Pietzsch and Pilhofer[17] and Boyadzhiev and Spassov[22]) or are only valid in one of the operating regimes (the emulsion regime for Baird and Shen[23], Baird and Lane[24] and Boyadzhiev and Spassov[22]).

The correct description of the influence of the energy input on drop size (and hold-up) via pulsation is an ongoing discussion.[19] In many studies, however, pulsation intensity, $f \cdot S_p / \text{m} \cdot \text{s}^{-1}$, is used to describe the energy input.[22-29] Furthermore, most equations state that hold-up, flow ratio and total flux do not influence the drop diameter.[17,22-26] The equations considered for the description of drop size in a PDDC are shown in Equation (3–1) and (3–2)[25,26]

$$\frac{d_{32}}{H} = \frac{C_\Psi \cdot e^n}{\dfrac{1}{C_\Omega \cdot \left(\dfrac{\gamma}{\Delta\rho \cdot g \cdot H^2}\right)^{0.5}} + \dfrac{1}{C_\Pi \cdot \left[\left(\dfrac{\varepsilon}{g}\right) \cdot \left(\dfrac{\Delta\rho}{g \cdot \gamma}\right)^{0.25}\right]^{n_1} \cdot \left[H \cdot \left(\dfrac{\Delta\rho \cdot g}{\gamma}\right)^{0.5}\right]^{n_2}}} \tag{3–1}$$

$$\text{where} \quad \varepsilon = \frac{2 \cdot \pi^2 \cdot \left(1 - e^2\right)}{3 \cdot H \cdot C_0^{\,2} \cdot e^2} \cdot \left(S_p \cdot f\right)^3$$

$$\frac{d_{32}}{\sqrt{\dfrac{\gamma}{\Delta\rho \cdot g}}} = C_1 \cdot e^{n_1} \cdot \left(H \cdot \sqrt{\dfrac{\rho_* \cdot g}{\sigma_*}}\right)^{n_2} \cdot \left(\dfrac{\eta_d \cdot g^{0.25}}{\sigma_*^{0.75} \cdot \rho_*^{0.25}}\right)^{n_3} \cdot \left(\dfrac{\gamma}{\sigma_*}\right)^{n_4} \cdot \left[C_2 + \exp^{\frac{C_3 \cdot S_p \cdot f}{e}\left(\frac{\rho_*}{\sigma_* \cdot g}\right)^{\frac{1}{4}}}\right] \tag{3–2}$$

where C_Ψ accounts for the influence of mass transfer. In the equilibrium situation $C_\Psi = 1$. The parameters C_Ω, C_Π, n, n_1, n_2 and C_0 in Equation (3–1) are 1.55, 0.42, 0.32, -0.35, -1.15 and 0.6, respectively, whereas C_1, C_2, C_3, n_1, n_2, n_3 and n_4 in Equation (3–2) have the values of 1.38, 0.16, -1.25, 0.30, 0.18, 0.14 and 0.06, respectively. The parameters ρ_* and σ_* represent

reference density and surface tension values of water at 293 K, where $\rho_*/kg \cdot m^{-3} = 998.2$ and $\sigma_*/N \cdot m^{-1} = 0.0728$.

Comparing both equations it can be seen that they are composed of comparable groups. They are valid in all operating regimes, take the energy input into account via the pulsation intensity, are based on the system physical properties and geometrical variables of the column, these geometrical characteristics can be translated to a PDDC and the original equations are derived for a wide range of experimental conditions.[25,26] The fundamental difference between both equations is therefore the influence of the dispersed phase viscosity, η_d, which is present in Equation (3–2), but not in (3–1). It has to be taken into account that in liquid-liquid dispersions a higher interfacial tension and a higher dispersed phase viscosity both counter-act drop deformation and therefore drop break-up.[30,31] In many liquid-liquid extraction systems interfacial tension is the dominant cohesive force,[25] but according to Arai *et al.*[31] the dispersed phase viscosity becomes an important parameter in a system for which $\eta_d/kg \cdot s^{-1} \cdot m^{-1} > 10^{-2}$ (at $\gamma/N \cdot m^{-1} = 22 \times 10^{-3}$). Arai *et al.* derived an expression relating the influence of the dispersed phase viscosity and interfacial tension via the dimensionless viscosity number, $N_{vi} = \eta_d \cdot \varepsilon^{1/3} \cdot d_{max}^{1/3}/\gamma$. For stirred vessels it was found that for $N_{vi} < 10^{-2}$ there was no influence of η_d on d_{max} but for $N_{vi} > 10^{-2}$ the influence became distinct.[31] In order to determine whether the dispersed phase viscosity is needed to be taken into account, the value of N_{vi} was calculated using both Equation (3–1) and (3–2) for the Sauter drop diameter, d_{32}. The application of d_{32} in N_{vi} results, however, in smaller values than using d_{max} and therefore lower values for N_{vi} are obtained. The calculated values for N_{vi} are shown in Figure 3.5.
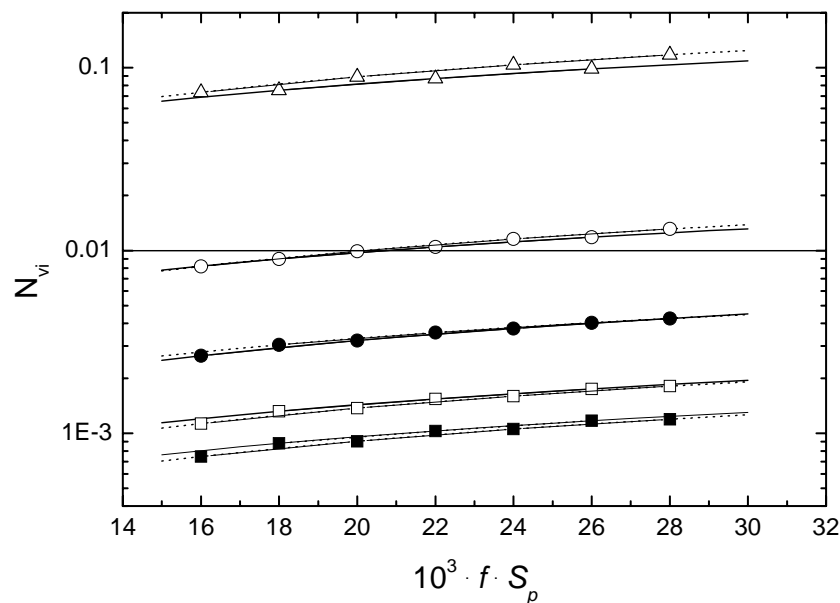
Figure 3.5. N_{vi} values as function of the pulsation intensity for FE: $\square$, $w_{CPL,aq} = 0.00$; $\bigcirc$, $w_{CPL,aq} = 0.25$; $\triangle$, $w_{CPL,aq} = 0.50$; and BE: $\blacksquare$, $w_{CPL,aq} = 0.00$; $\bullet$, $w_{CPL,aq} = 0.25$; and d_{32}/m calculated with: —, Equation (3–1); --, Equation (3–2).

It was found that $10^{-3} < N_{vi} < 10^{-1}$ for all experimental conditions. The values for N_{vi} make it therefore reasonable to believe that the dispersed phase viscosity should be taken into account when fitting the Sauter drop diameter data. Equation (3–2) was therefore used for the

calculation of Sauter drop diameter data for the caprolactam forward and back-extraction in a PDDC. However, the characteristic internal sizes, *e* and *H*, are different for a PDDC compared to sieve-plate internals and the resulting energy input is thus different as well. Therefore the parameters C_1, C_3, n_1 and n_2 might differ from the original values, which topic will be investigated in Chapter 4.

3.4.2   Operating regimes

In the operation of a pulsed column several regimes can be distinguished as shown in Figure 3.2. The transition from the mixer-settler (MS) to the dispersion (D) regime, characterized by a minimum value for the dispersed phase hold-up,[17,27] and the onset for the emulsion regime (E) are predicted by Equation (3–3a) and (b), respectively,[17,22]

$$\left(f \cdot S_p \right)_{MS/D} = k_3 \cdot \left(\frac{\gamma \cdot \Delta \rho^{0.25} \cdot e}{\eta_d^{0.75}} \right)^{0.33} \tag{3–3a}$$

$$\left(f \cdot S_p \right)_{D/E} = 0.5 \cdot \sqrt[3]{\frac{0.96 \cdot e^2}{\rho_c}} \tag{3–3b}$$

where the constant k_3/m·kg$^{-1/6}$·s$^{-7/12}$ = 9.69 × 10^{-3}.[27] The derivation of Equation (3–3a) by Kumar and Hartland, however, was based on fitting hold-up data, the influence of parameters on the regime transition was empirically determined, whereas the influence of ρ_c and η_c was not investigated.[27] Furthermore, the influence of the fractional free cross-sectional area, *e*, on the energy input might be different compared to sieve-plate or Karr columns. The theoretical basis of both equations is therefore questionable, which is further investigated in Chapter 4.

3.4.3   Dispersed phase hold-up

Theoretical or empirical equations for the description of the dispersed phase hold-up in a PDDC are not reported. The description of the hold-up was, therefore, based on unified equations or equations derived for pulsed sieve-plate and Karr columns, like those of Godfrey and Slater,[32] Kumar and Hartland,[27-29,33] which was applied by Jahya *et al*. for the description of a water-kerosene system in a pulsed disc and doughnut column,[15] and also Baird and coworkers.[23,24] The equations vary in approach from empirical to semi-empirical and theoretical. Furthermore, the presented equations apply different approaches with respect to the parameter that is fitted. In the first place the hold-up is related to the phase flow rates and a characteristic velocity using the slip velocity concept as introduced by Gayler *et al*.[34,35] and Thornton,[36] as shown in Equation (3–4). Alternatively the hold-up itself is correlated directly and finally it can also be calculated via numerical iteration. Although only one of these equations is valid in all operating regimes,[27,33] all mentioned equations will be evaluated.

$$V_{slip} = \frac{V_d}{x} + \frac{V_c}{1-x} = V_o \cdot (1-x)^m \tag{3–4}$$

The presented equation is generally applied for the interpretation of hold-up data by fitting the characteristic velocity V_o at $m = 1$ or fitting both V_o and m. These parameters, however, are dependent on the system used[32] and, since the physical properties change appreciable in the caprolactam system, this would result in multiple values for V_o and m, for which a correlation would have to be developed in order to take into account the effects of system properties. The only correlations for V_o and m that were not purely empirical were presented by Godfrey and Slater, relating the characteristic velocity, V_o, to the terminal velocity, V_t, and m to the Reynolds number.[32]

Via the terminal velocity (Godfrey and Slater;[32] Kumar and Hartland[28]) or a balance of forces based on the Ergun packed bed equation (Baird and Lane;[23] Baird and Shen[24]) the hold-up is correlated using a drag coefficient, C_D. Calculating C_D for the terminal velocity of a drop in the intermediate turbulent regime[37] for all systems in the forward and back-extraction where $w_{CPL,aq} < 0.45$ and $w_{CPL,aq} < 0.20$, respectively, it is found that $0.5 < C_D < 5$, as shown in Figure 3.6. In this figure a strong increase in the value of C_D is visible for systems with an increased concentration of caprolactam, especially for the back-extraction and at increased pulsation intensities. The high drag coefficients correspond to unrealistically low terminal velocities and consequently too high hold-up values and too low flux values when predicting the flooding (2) line as boundary of the operational area. Therefore, relations based on a drag coefficient, including Equation (3–4), were not used for the correlation of the hold-up data.
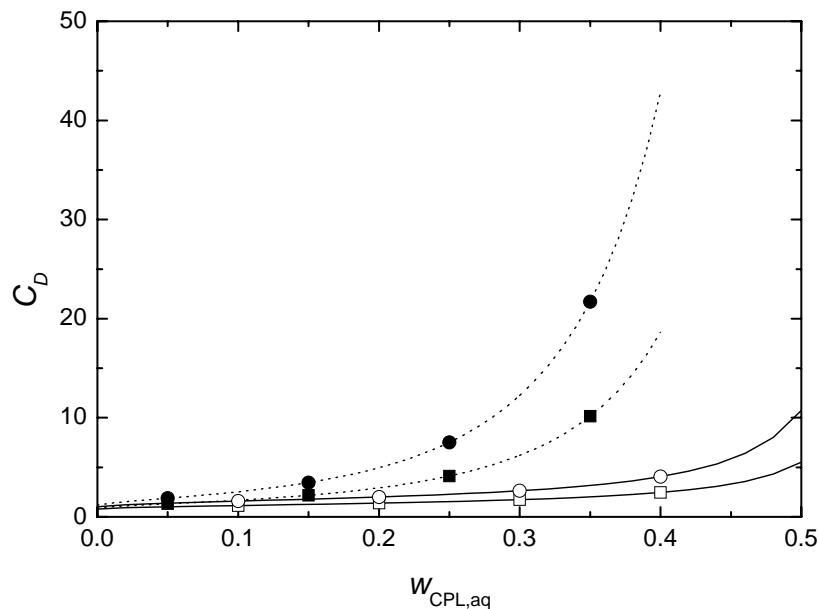
Figure 3.6. C_D values as function of the aqueous caprolactam weight fraction for FE: □, $f \cdot S_p / \text{m} \cdot \text{s}^{-1} = 0.015$; ○, $f \cdot S_p / \text{m} \cdot \text{s}^{-1} = 0.030$; and BE: ■, $f \cdot S_p / \text{m} \cdot \text{s}^{-1} = 0.015$; ●, $f \cdot S_p / \text{m} \cdot \text{s}^{-1} = 0.030$.

In the relations derived by Kumar and Hartland the influence of the continuous phase density, ρ_c,[27,33] and viscosity, η_c,[27,29,33] was not considered since their values vary not appreciably in the available data.[27,33] It is, however, stated that these parameters have a significant effect.[27]

From a unified equation, however, η_c is excluded since it proved statistically insignificant and η_* is introduced as reference viscosity,[29] but for the data on pulsed columns used in this study $\eta_c \approx \eta_*$. Since the continuous phase density and viscosity in the caprolactam system vary appreciable it was assumed that these parameters needed to be taken into account when fitting hold-up data. Therefore Equation (3–5) was applied for the description of the hold-up in the forward and back-extraction of caprolactam, where the continuous phase viscosity was introduced instead of the reference viscosity of water at 293 K.

$$x = \Pi \cdot \Phi \cdot \Psi \cdot \Gamma \tag{3–5}$$

where

$$\Pi = C_{\Pi} + \left[\frac{\varepsilon}{g} \cdot \left(\frac{\rho_c}{g \cdot \gamma} \right)^{0.25} \right]^{n_1} \qquad \Phi = \left[V_d \cdot \left(\frac{\rho_c}{g \cdot \gamma} \right)^{0.25} \right]^{n_2} \cdot \exp\left[n_3 \cdot V_c \cdot \left(\frac{\rho_c}{g \cdot \gamma} \right)^{0.25} \right]$$

$$\Psi = C_{\Psi} \cdot \left(\frac{\Delta\rho}{\rho_c} \right)^{n_4} \cdot \left(\frac{\eta_d}{\eta_c} \right)^{n_5} \qquad \Gamma = C_{\Gamma} \cdot e^{n_6} \cdot \left[H \cdot \left(\frac{\rho_c \cdot g}{\gamma} \right)^{0.5} \right]^{n_7}$$

Equation (3–5) is a semi-empirical relation valid in the dispersion and emulsion operational regime. The critical pulsation intensity for the transition from the mixer-settler to the dispersion regime is described by Equation (3–3a). The group Π allows for the influence of the energy input per unit mass, Φ for the effect of phase velocities, Ψ for the influence of the physical properties and Γ for the dimensions of the internals. The literature values for the parameters, being C_{Π}, C_{Γ}, n_1, n_2, n_3, n_4, n_5 and n_7, were 0.27, 6.87, 0.78, 0.87, 3.34, -0.58, 0.18 and -0.39, respectively. The value for C_{Ψ} was taken unity since the system operated without mass transfer and $n_6 = 0$, which was the value in the unified equation for all types of pulsed columns.[29] However, just as for the drop diameter description, the energy input is different for a PDDC compared to a pulsed sieve-plate or Karr column. Therefore, the parameters C_{Π}, C_{Γ} and n_1 might differ for a PDDC compared to the literature values. The same accounts for n_5 since the viscosity influence in Equation (3–5) changed compared to literature, although the deviation in n_5 is probably not large as long as the continuous phase viscosity is close to the value of water. The influence of these parameters on the hold-up in a PDDC is investigated in Chapter 4.

3.4.4 Operational window

From Figure 3.2 it was concluded that several regimes could be limiting for the operation of an extraction column. At low pulsation intensities flooding (1) limits the column operation, while at high pulsation intensities flooding (2), phase inversion or entrainment is limiting for the extraction process. The maximum amount of entrainment, however, is related to the desired purity of the extract and does not imply whether the extraction process itself is operable or not. Entrainment as limiting criterion for a process was therefore not considered.

Equations describing flooding (1) were selected first after which correlations for flooding (2) and phase inversion were selected.

Flooding (1). At low pulsation intensities flooding (1) limits column operation. In perforated plate-columns this flooding line is often approximated by a linear relationship between the volume displaced by pulsation and the total flux,[17,19] as shown in Equation (3–6a). However, for systems with low interfacial tensions or systems with drop diameters smaller than the plate hole diameter higher fluxes than this approximated flooding line are reported.[17] Edwards and Beyer therefore theoretically related the pulsation cycle in a perforated plate column to the pulsed volume of a light and heavy phase, which implies the organic and aqueous phase in the caprolactam system, respectively, resulting in Equation (3–6b).[38]

$$\left(V_d + V_c\right) = f \cdot S_p \tag{3–6a}$$

$$\left(V_{org} + V_{aq}\right) = f \cdot S_p \cdot \left(\cosh\left[\frac{V_{org}}{\pi \cdot f \cdot S_p}\right]\right) + \frac{V_{org}}{2} \tag{3–6b}$$

Because of its simplicity Equation (3–6a) is used for the estimation of the minimum amount of pulsation required in order to operate the column, although this amount might be over-predicted.[17,38]

Flooding (2). At the flooding point the maximum value for the hold-up, x_f, is reached. This criterion can be related to the superficial velocity of both phases, V_c and V_d, which do not increase anymore at this point, according to Equation (3–7).[36]

$$\left(\frac{d\left(V_d\right)}{dx}\right)_f = \left(\frac{d\left(V_c\right)}{dx}\right)_f = 0 \tag{3–7}$$

Godfrey and Slater,[32] Kumar and Hartland,[28] Baird and Lane[23] and Baird and Shen[24] derived their flooding equations based on the above procedure, but since the latter three are predictive equations these were only considered. The hold-up equations of Baird and Lane[23] and Kumar and Hartland,[28] however, are of comparable form, as shown in Equation (3–8a) and (b).[23,28] Baird and Shen[24] used a simplified form of Equation (3–8a).

$$\frac{d_{32} \cdot g \cdot \Delta\rho}{\rho_c \cdot V_{slip}^2} \cdot \left(1 - x\right) = \frac{150 \cdot x}{Re_{slip} \cdot \left(1 - x\right)} + 1.75 \tag{3–8a}$$

$$\frac{d_{32} \cdot g \cdot \Delta\rho}{\rho_c \cdot V_{slip}^2} \cdot \frac{\frac{4}{3} \cdot \left(1 - x\right)}{1 + 4.56 \cdot x^{0.73}} = \frac{24}{Re_{slip}} + 0.53 \tag{3–8b}$$

Since all hold-up equations are of comparable form and Kumar and Hartland already derived the correlation at flooding by applying the criterion in Equation (3–7) to Equation (3–8a),[28] this correlation was used. It has to be taken into account, however, that the application might be limited to a certain range of physical properties, as discussed in Figure 3.6. The resulting correlation for the hold-up at flooding is shown in Equation (3–9).[28]

$$
\left[x_f + R \cdot \left(1 - x_f\right)\right] \cdot \left[\left(\beta_3 - \beta_1\right) \cdot \left(1 - 2 \cdot x_f\right) - \frac{2 \cdot \beta_2 \cdot x_f \cdot \left(1 - x_f\right)}{\beta_3 \cdot \left(1 + 4.56 \cdot x_f^{0.73}\right)^2} \cdot \right.
$$
$$
\left.\left(1 + 4.56 \cdot x_f^{0.73} + 3.33 \cdot x_f^{-0.27} \cdot \left(1 - x_f\right)\right)\right] + \left(\beta_3 - \beta_1\right) \cdot x_f \cdot \left(1 - x_f\right) \cdot \left(R - 1\right) = 0 \tag{3–9}
$$

where

$$
\beta_1 = \frac{24 \cdot \eta_c}{0.53 \cdot d_{32} \cdot \rho_c} \quad ; \quad \beta_2 = \frac{4 \cdot d_{32} \cdot g \cdot \Delta\rho}{1.59 \cdot \rho_c} \quad ; \quad \beta_3 = \left(\beta_1^2 + \frac{4 \cdot \beta_2 \cdot \left(1 - x_f\right)}{\left(1 + 4.56 \cdot x_f^{0.73}\right)}\right)^{0.5}
$$

Using Equation (3–9) the hold-up at flooding conditions can be calculated from physical properties and the Sauter drop diameter, which is described via Equation (3–2). Substituting the calculated hold-up in Equation (3–8b), the slip velocity corresponding to the flooding conditions can be found and via the flow ratio thus the flux at flooding. The behaviour of the liquid-liquid system near the operational boundary changes, however, especially with respect to drop coalescence.[17] The validity of Equation (3–2) at flooding conditions is therefore questionable and application of this equation will affect the uncertainty of the description.

Phase inversion. Next to flooding (2), phase inversion is a possible process limitation for the operation of an extraction column. From simple batch-experiments, where phase continuity of pure immiscible liquids was studied, it is known that a large hold-up region exists in which either of the two phases can be the continuous phase. Which phase is the continuous one within this region depends on how the dispersion is created. This region of ambivalence is limited by a critical hold-up above which phase inversion spontaneously occurs.[39,40] The critical hold-up in a batch system of a specified construction is therefore only dependent on the physical properties of the two phases and at sufficiently high agitation the critical hold-up becomes constant.[39-41] The parameters influencing the critical hold-up in batch-experiments were assumed to determine phase inversion in extraction columns as well.

Yeo *et al.*[42] related the critical hold-up at phase inversion to the interfacial energy in a system. Deshpande and Kumar[41] related this phenomena qualitatively to the packing of drops in a liquid-liquid system whereas Kumar qualitatively argued that drops in dispersions are charged due to a difference in dielectric constant, which should be included the phase inversion description since in the first two methods certain problems remain unaccounted for.[43]

The approach suggested by Yeo *et al.*[42] states that if the magnitude of the change in interfacial energy is comparable to the total energy of the system, minimization of the interfacial energy satisfies the criterion for phase inversion, PI. Assuming that the liquid-liquid interfacial

energy is comparable to the total interfacial energy and that the interfacial tension does not change with phase inversion, Equation (3–10a) results as correlation for the hold-up at phase inversion. Equation (3–10b) is obtained after substitution of Equation (3–2), describing the Sauter drop diameter.

$$\frac{x_{org,PI}}{\left(1 - x_{org,PI}\right)} = \frac{d_{32,aq=c}}{d_{32,org=c}} \tag{3–10a}$$

$$\frac{x_{org,PI}}{\left(1 - x_{org,PI}\right)} = \left(\frac{\eta_{d,org}}{\eta_{d,aq}}\right)^{n_3} \tag{3–10b}$$

Using Equation (3–10b) the hold-up at phase inversion can be calculated from the drop diameter. Substituting the calculated hold-up in Equation (3–5), phase velocities corresponding to the phase inversion conditions can be found and via the flow ratio thus the flux at phase inversion. Since the behaviour of the liquid-liquid system changes near the operational boundary[17] the validity of Equation (3–2) and (3–5) at phase inversion conditions is questionable such that the application of these equations will affect the uncertainty of the description.

3.5   Conclusions

Using existing theory on pulsed columns, unified equations and equations derived for pulsed sieve-plate and Karr columns a theoretical model was developed describing the operational characteristics of a PDDC. For all applied equations it has to be taken into account, however, that they were originally not derived for a PDDC and therefore corrections might be necessary, which need to be established by pilot experiments.

The final model consists of three equations describing the boundaries of the operational window, being flooding (1) at low pulsation intensity and flooding (2) or phase inversion at high pulsation levels. Furthermore, the Sauter drop diameter, hold-up and operational regimes can be described within this operational window. The model therefore results in a quantitative description of the operational window. All equations are based on the physical properties and operational parameters of the system, geometrical characteristics of the column and internals as well as certain fit parameters, describing the influence of each variable.

Using this approach the difference in operation between the back- and forward extraction can be understood, just as the influence of the physical parameters on the operation.

Nomenclature

C_D — Drag coefficient

D, E, MS — Dispersion, Emulsion and Mixer-settler operating regime, respectively

d_{32}, d_{max} — Sauter drop diameter and Maximum drop diameter, respectively, m

D_c — Internal column diameter, m

D_d	Disc diameter, m
D_r	Diameter of ring aperture in doughnut, m
e	Fractional free cross-sectional area, $e = 1-D_d^2/D_c^2$
f	Frequency, s^{-1}
$f \cdot S_p$	Pulsation intensity, $m \cdot s^{-1}$
Flux	Total throughput, Flux $= V_d + V_c$, $m \cdot h^{-1}$
g	Gravitational constant, $g/m^2 \cdot s^{-1} = 9.81$
H	Disc to doughnut spacing, m
N_{vi}	Dimensionless viscosity group, $N_{vi} = \eta_d \cdot \varepsilon^{1/3} \cdot d_{max}^{1/3}/\gamma$
R	Flow ratio, $R = V_d/V_c$
Re	Reynolds number, $Re_i = d_{32} \cdot V_i \cdot \rho_c/\eta_c$
S_p	Stroke of pulsation (twice the pulsation amplitude), m
T	Temperature, K
V_i	Velocity of phase or component i, $m \cdot s^{-1}$
V_{slip}, V_o, V_t	Slip velocity, characteristic velocity and terminal velocity, respectively, $m \cdot s^{-1}$
w	Weight fraction
x	Dispersed phase hold-up defined as volume fraction of the dispersed phase

Greek letters

γ	Interfacial tension, $N \cdot m^{-1}$
ε	Mechanical power dissipation per unit mass, $W \cdot kg^{-1}$
η	Dynamic viscosity, $kg \cdot m^{-1} \cdot s^{-1}$
η_*	Reference dynamic viscosity of water at 293 K, $\eta_* = 0.001$ $kg \cdot m^{-1} \cdot s^{-1}$
ρ	Density [$kg \cdot m^{-3}$]
ρ_*	Reference density of water at 293 K, $\rho_* = 998.2$ $kg \cdot m^{-3}$
$\Delta\rho$	Density difference, $kg \cdot m^{-3}$
σ_*	Reference surface tension of water at 293 K, $\sigma_* = 0.0728$ $N \cdot m^{-1}$

Subscript

aq, org	Aqueous and organic phase, respectively
c, d	Continuous and dispersed phase, respectively
f	Denoting flooding
PI	Denoting phase inversion

Literature cited

1. Kleinberger, R. Zinc Sulfate Extraction by Bateman Pulsed Column Technology, In *Proceedings of the Copper, Cobalt, Nickel and Zinc Recovery conference, 2001*; South African Institute of Mining and Metallurgy: Johannesburg, 2001, K1-K13.

2. Buchalter, E. M.; Kleinberger, R.; Grinbaum, B. Copper Solvent Extraction Using a Bateman Pulsed Column, In *Proceedings of the Extraction Metallurgy Africa conference, 1998*; South African Institute of Mining and Metallurgy: Johannesburg, 1998, 185-199.

3. Jahya, A. B.; Stevens, G. W.; Pratt, H. R. C. Mass Transfer Studies for a Pulsed Disc and Doughnut Extraction Column, In *Proceedings of the International Congress on Mineral Processing and Extractive Metallurgy, 2000*; Australasian Institute of Mining and Metallurgy: Melbourne, 2000, pp. 281-284.

4. Angelov, G.; Gourdon, C.; Liné, A. Simulation of Flow Hydrodynamics in a Pulsed Solvent Extraction Column under Turbulent Regimes. *Chem. Eng. J.* **1998**, *71*, 1-9.

5. Mate, A.; Masbernat, O.; Gourdon, C. Detachment of a Drop from an Internal Wall in a Pulsed Liquid-Liquid Column. *Chem. Eng. Sci.* **2000**, *55*, 2073-2088.

6. Mate, A.; Morchain, J.; Masbernat, O.; Gourdon, C. A Transient Method for the Study of Wetting in a Liquid-Liquid Contactor. *Chem. Eng. Sci.* **1996**, *51*, 5313-5323.

7. Aoun Nabli, M. S.; Guiraud, P.; Gourdon, C. CFD Contribution to a Design Procedure for Discs and Doughnuts Extraction Columns. *Trans. IChemE.* **1998**, *76*, 951-960.

8. Milot, J. F.; Duhamet, J.; Gourdon, C.; Casamatta, G. Simulation of a Pneumatically Pulsed Liquid-Liquid Extraction Column. *Chem. Eng. J.* **1990**, *45*, 111-122.

9. Angelov, G.; Gourdon, C. Turbulent Viscosity in Pulsed Stagewise Extraction Columns. *Bulgarian Chem. Comm.* **2002**, *34*, 124-134.

10. Angelov, G.; Gourdon, C. Study on the Turbulence in Pulsed Stagewise Extraction Columns: Turbulence Macroscale. *Hungarian J. Ind. Chem.* **2002**, *30*, 137-142.

11. Bardin-Monnier, N.; Guiraud, P.; Gourdon, C. Langrangian Simulations Contribution to the Knowledge of Discs and Doughnuts Pulsed Solvent Extraction Columns Hydrodynamics. *Chem. Eng. Proc.* **2003**, *42*, 503-516.

12. Bardin-Monnier, N.; Guiraud, P.; Gourdon, C. Residence Time Distribution of Droplets within Discs and Doughnuts Pulsed Extraction Columns via Langrangian Experiments and Simulations. *Chem. Eng. J.* **2003**, *94*, 241-254.

13. Aoun Nabli, M. S.; Guiraud, P.; Gourdon, C. Numerical Experimentation: a Tool to Calculate the Axial Dispersion Coefficient in Discs and Doughnuts Pulsed Extraction Columns. *Chem. Eng. Sci.* **1997**, *52*, 2353-2368.

14. Angelov, G.; Gourdon, C. Influence of Stage Configuration on Flow Parameters in a Stagewise Extraction Column. *Hungarian J. Ind. Chem.* **1999**, *27*, 281-286.

15. Jahya, A. B.; Stevens, G. W.; Pratt, H. R. C. Flood Point and Dispersed Phase Hold-up in a Pulsed Disc and Doughnut Liquid-Liquid Extraction Column, In *Proceedings of the Chemeca'99 conference*. 1999.

16. Al Khani, S. D.; Gourdon, C.; Gasamatta, G. Simulation of Hydrodynamics and Mass Transfer of a Disks and Rings Pulsed Column. *Ind. Eng. Chem. Res.* **1988**, *27*, 329-333.

17. Godfrey, J. C. Slater, M. J. *Liquid-Liquid Extraction Equipment*; John Wiley & Sons, Inc.: New York, 1994.

18. Pratt, H. R. C.; Stevens, G. W. Selection, Design and Pilot Testing of Equipment. In *Science and Practice of Liquid-Liquid Extraction*; Thornton, J. D., Eds.; Clarendon Press: Oxford, 1992.

19. Logsdail, D. H.; Slater, M. J. Pulsed Perforated-Plate Columns. In *Handbook of Solvent Extraction*; Lo, T. C.; Baird, M. H. I.; Hanson, C., Eds.; Wiley: New York, 1983, 355-372.

20. Klicka, V.; Cermak, J. Zweiphasenströmung in der Pulsier-Extraktionskolonne. *Verfahrenstechnik* **1971**, *5*, 320-327.

21. Berger, R.; Walter, K. Flooding in Pulsed Sieve Plate Extractors. *Chem. Eng. Sci.* **1985**, *40*, 2175-2184.

22. Boyadzhiev, L.; Spassov, M. On the Size of Drops in Pulsed and Vibrating Plate Extraction Columns. *Chem. Eng. Sci.* **1982**, *37*, 337-340.

23. Baird, M. H. I.; Lane, S. J. Drop Size and Hold-up in a Reciprocating Plate Extraction Column. *Chem. Eng. Sci.* **1973**, *28*, 947-957.

24. Baird, M. H. I.; Shen, Z. J. Holdup and Flooding in Reciprocating Plate Extraction Columns. *Can. J. Chem. Eng.* **1984**, *62*, 218-227.

25. Kumar, A.; Hartland, S. Unified Correlations for the Prediction of Drop Size in Liquid-Liquid Extraction Columns. *Ind. Eng. Chem. Res.* **1996**, *35*, 2682-2695.

26. Kumar, A.; Hartland, S. Prediction of Drop Size in Pulsed Perforated-Plate Extraction Columns. *Chem. Eng. Comm.* **1986**, *44*, 163-182.

27. Kumar, A.; Hartland, S. Prediction of Dispersed Phase Hold-up in Pulsed Perforated-Plate Extraction Columns. *Chem. Eng. Process*. 23, 1988, 41-59.

28. Kumar, A.; Hartland, S. Prediction of Dispersed Phase Hold-up and Flooding Velocities in Karr Reciprocating-Plate Extraction Columns. *Ind. Eng. Chem. Res.* **1988**, *27*, 131-138.

29. Kumar, A.; Hartland, S. A Unified Correlation for the Prediction of Dispersed-Phase Hold-up in Liquid-Liquid Extraction Equipment. *Ind. Eng. Chem. Res.* **1995**, *34*, 3925-3940.

30. Hinze, J. O. Fundamentals of the Hydrodynamic Mechanism of Splitting in Dispersion Processes. *AIChE J.* **1955**, *1*, 289-295.

31. Arai, K.; Konno, M.; Matunaga, Y.; Saito, S. Effect of Dispersed-Phase Viscosity on the maximum Stable Drop Size for Breakup in Turbulent Flow. *J. Chem. Eng. Japan* **1977**, *10*, 325-330.

32. Godfrey, J. C.; Slater, M. J. Slip Velocity Relationships for Liquid-Liquid Extraction Columns. *Trans. IChemE.* **1991**, *69*, 130-141.

33. Kumar, A.; Hartland, S. Independent Prediction of Slip Velocity and Hold-up in Liquid-Liquid Extraction Columns. *Can. J. Chem. Eng.* **1989**, *67*, 17-25.

34. Gayler, R.; Pratt, H. R. C. Hold-up and Pressure Drop in Packed Columns. *Trans. IChemE.* **1951**, *29*, 110-125.

35. Gayler, R.; Roberts, N. W.; Pratt, H. R. C. Liquid-Liquid Extraction Studies: Part IV. A Further Study of Hold-up in Packed Columns. *Trans. IChemE.* **1953**, *31*, 57-68.

36. Thornton, J. D. Spray Liquid Extraction Columns: Prediction of Limiting Hold-up and Flooding Rates. *Chem. Eng. Sci.* **1956**, *5*, 201-208.

37. Sakiadis, B. C. Fluid and Particle Mechanics. In *Perry's Chemical Engineer's Handbook*; Perry, R. H., Green, D., Eds.; McGraw-Hill Book Co.: Singapore, 1984.

38. Edwards, R. B.; Beyer, G. H. Flooding Characteristics of a Pulse Extraction Column. *AIChE J.* **1956**, *2*, 148-152.

39. Selker, A. H.; Sleicher, C. A. Factors Affecting which Phase will Disperse when Immiscible Liquids are Stirred Together. *Can. J. Chem. Eng.* **1965**, *43*, 298-301.

40. Quinn, J. A.; Sigloh, D. B. Phase Inversion in the Mixing of Immiscible Liquids. *Can. J. Chem. Eng.* **1963**, *41*, 15-18.

41. Deshpande, K. B.; Kumar, S. A New Characteristic of Liquid-Liquid Systems – Inversion Holdup of Intensely Agitated Dispersions. *Chem. Eng. Sci.* **2003**, *58*, 3829-3835.

42. Yeo, L. Y.; Matar, O. K.; Perez de Ortiz, E. S.; Hewitt, G. F. A Simple Predictive Tool for Modelling Phase Inversion in Liquid-Liquid Dispersions. *Chem. Eng. Sci.* **2002**, *57*, 1069-1072.

43. Kumar, S. On Phase Inversion Characteristics of Stirred Dispersions. *Chem. Eng. Sci.* **1996**, *51*, 831-834.

Chapter 4

Extraction of caprolactam with toluene in a pulsed disc and doughnut column: experimental evaluation of the hydraulic characteristics

4.1   Introduction

The hydraulic characteristics of an extraction column, being hold-up and drop size, determine its operating regimes and operational window. These are key parameters in order to determine column capacity and the required column diameter to provide the desired throughput.[1] In Chapter 3 a theoretical model describing the hydraulic characteristics of a pulsed disc and doughnut column (PDDC) was developed.

In this chapter the hydraulic characteristics of the PDDC are determined for both the forward and back-extraction of caprolactam with and from toluene, respectively, as a function of the operating conditions, being total flux, solvent to feed ratio, temperature, pulsation frequency and amplitude. The experiments were performed at equilibrium conditions to avoid the influence of mass transfer. When the forward and back-extraction processes are addressed, therefore the configuration used in these processes is referred to, and not the actual transfer of caprolactam. The experimental conditions covered the whole industrial operating range with respect to the concentrations of caprolactam and ammonium sulfate and phase continuity.

The obtained results were described using the developed theoretical model. Initially the model equations as presented in literature were used for the prediction of the hydraulic data. Since the original equations were derived for different pulsed column types, relevant parameters were fitted in order to obtain an improved description.

4.2   Experimental set-up

The PDDC pilot set-up is schematically shown in Figure 4.1. The active column section consisted of four jacketed glass segments of each 1.04 m length and 40 mm internal diameter, resulting in an empty column volume of 5.20 L. This active section was enclosed on both sides by 42 cm long settlers, both having an inner diameter of 80 mm and a volume of 2.15 L. All segments were connected using 20 mm Stainless Steel (SS) flenses. The column internals consisted of alternately placed disc and doughnut baffles held in place by means of three tie

rods with spacer sleeves located in a triangular pitch as already presented in Chapter 3. The internals and space sleeves were made of PVDF or SS material to prevent wetting in processes with the aqueous or organic phase as dispersed phase, respectively. In the bottom settler a piston type pulsator was placed, which could apply a certain sinusoidal stroke to the liquid contents of the column at a desired frequency and amplitude. The stroke applied by the pulsator was related to the stroke in the column by observation of the two extreme points in the empty column. The influence of the internals on the column volume and therefore the empty column stroke was adjusted for. Each phase was pumped from its storage vessel (1 and 2, respectively) via a mass flow controller (MF) and heat exchanger (HE) to the column, where the aqueous (heavy) phase (1) was introduced in the top and the organic (light) phase (2) at the bottom both via a single glass tube. Both phases leaving the top and bottom of the column returned to storage vessel 1 and 2, respectively, for reuse. The storage vessels were kept under nitrogen purge in order to avoid a build-up of organic vapour. The heat exchangers and the jacket of the column were connected to a Julabo 6 heating bath and a Julabo 26 heating bath (HE), respectively (Julabo Labortechnik, Germany) with water used as the heating fluid. The temperature in the column was monitored via three Pt100 temperature sensors (Pt100) in the top, middle and bottom of the column, which were connected to a computer. When the aqueous phase was the continuous phase, as in Figure 4.1, the interface level in the top of the column was continuously observed via a LG DSP colour camera (C) (Philips, The Netherlands). It was displayed on a computer via the program WinTV 2000 (Hauppauge Computer, USA). The interface level at the bottom of the column, when the organic phase was the continuous phase, was observed visually. The interface level was controlled via a manually operated valve in the aqueous stream leaving the bottom, where the organic top stream was allowed to leave the column via an overflow.
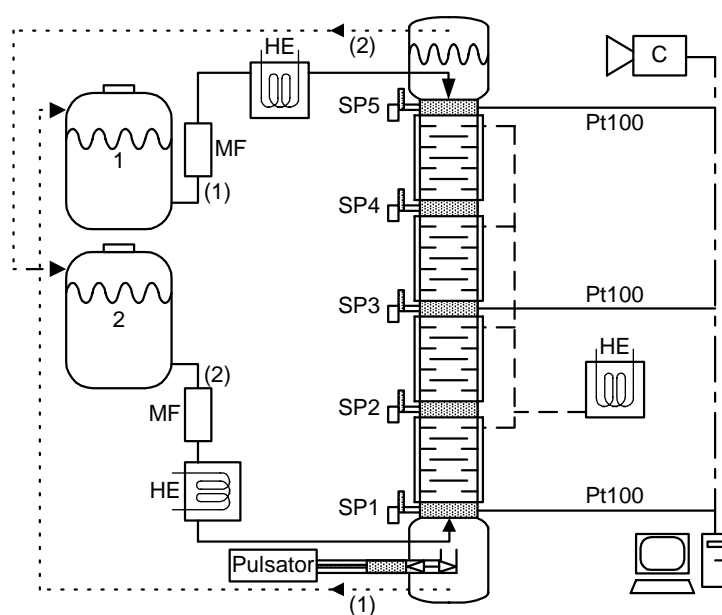
Figure 4.1. Schematic presentation of the PDDC with the aqueous phase (1) continuous and the organic phase (2) dispersed (back-extraction operation).

4.3 Experimental procedure

Chemicals. All chemicals were used as received. Toluene (purity > 99%) was supplied by Fluka (USA), ε-caprolactam (CPL) (purity grade) by DSM (The Netherlands) and ammonium sulfate (AS) (purity > 99%) by Sigma-Aldrich (USA). Demineralised water was used in all experiments.

Conditions. The experimental conditions covered the full industrial range with respect to the concentrations of caprolactam and ammonium sulfate, solvent to feed ratio, temperature and phase continuity. In Table 4.1 the studied operational conditions for both the forward and back-extraction process are presented for each experiment (Exp.). In Table 4.2 the physical properties, being densities and viscosities of both separate phases and the interfacial tension between the phases, are presented dependent on the caprolactam (CPL) and ammonium sulfate (AS) mass fractions and temperatures used.

Table 4.1. Experimental conditions regarding the forward and back-extraction of caprolactam.

Exp.	Energy input				Phase flows	
	$10^3 \cdot S_p$	f	$10^3 \cdot f \cdot S_p$	Phase	Flux = $V_d + V_c$	$R = V_d/V_c$
	m	s^{-1}	$m \cdot s^{-1}$	[c]	$m \cdot h^{-1}$	
	Forward extraction					
1-8	13.9-15.8	1.15	15.8-39.4	org	14.7-30.2	0.20; 0.33; 1.0
	8.8-15.8	1.84				
	6.3-15.8	2.49				
	Back-extraction					
1-7	12.7-14.4	1.15	14.4-36.0	aq	12.9-35.1	1.0; 3.0
	8.0-14.4	1.84				
	5.8-14.4	2.49				

Table 4.2. Physical properties regarding the forward and back-extraction of caprolactam.

Exp.	T	extract / solvent			feed / raffinate				
		w_{CPL}	$10^{-3} \cdot \rho_c$	$10^3 \cdot \eta_c$	w_{CPL}	w_{AS}	$10^{-3} \cdot \rho_d$	$10^3 \cdot \eta_d$	$10^3 \cdot \gamma$
	K	(org)	$kg \cdot m^{-3}$	$kg \cdot m^{-1} \cdot s^{-1}$	(aq)	(aq)	$kg \cdot m^{-3}$	$kg \cdot m^{-1} \cdot s^{-1}$	$N \cdot m^{-1}$
1		0.000	0.848	0.47	0.000	0.00	0.991	0.67	34.7
2		0.011	0.850	0.48	0.085	0.00	0.998	0.83	14.9
3	313	0.029	0.853	0.50	0.193	0.00	1.006	1.16	9.6
4		0.079	0.863	0.55	0.423	0.00	1.023	2.55	3.9
5		0.085	0.864	0.56	0.426	0.00	1.023	2.58	3.5

The table header "Forward extraction (FE)" spans the physical properties table.

(Table 4.2 continued)

6		0.119	0.870	0.60	0.475	0.00	1.027	3.03	1.6
7	313	0.023	0.852	0.49	0.114	0.03	1.018	0.95	10.8
8		0.083	0.863	0.55	0.337	0.03	1.035	1.99	3.7

Back-extraction (BE)

Exp.		w_{CPL} (aq)	w_{AS} (aq)	$10^{-3} \cdot \rho_c$ kg·m^{-3}	$10^3 \cdot \eta_c$ kg·m^{-1}·s^{-1}	w_{CPL} (org)	$10^{-3} \cdot \rho_d$ kg·m^{-3}	$10^3 \cdot \eta_d$ kg·m^{-1}·s^{-1}	$10^3 \cdot \gamma$ N·m^{-1}
1		0.000	-	0.998	1.02	0.000	0.868	0.59	35.8
2	293	0.091	-	1.006	1.33	0.007	0.869	0.60	15.0
3		0.292	-	1.024	2.80	0.030	0.873	0.63	7.6
4		0.468	-	1.039	5.69	0.090	0.884	0.72	1.9
5		0.087	-	0.998	0.84	0.012	0.850	0.48	14.4
6	313	0.192	-	1.006	1.16	0.029	0.853	0.50	9.6
7		0.461	-	1.026	2.89	0.114	0.869	0.59	1.8

The physical properties of the quaternary system water + caprolactam + ammonium sulfate + toluene as presented in Table 4.2 were correlated by the equations as presented in Chapter 2. These correlations cover the entire range of concentrations and temperatures applied in this study, except for the interfacial tension. The equation for the latter is only valid for concentrations of caprolactam in the organic phase from 0 up to 5 mass %. For experimental conditions with higher concentrations the relation was therefore extrapolated to determine the interfacial tension. The mass fraction of caprolactam in both the organic and aqueous phase and of ammonium sulfate in the aqueous phase was determined as described in Chapter 2.

Data analysis. In the correlation of the hydraulic characteristics the fitted parameters in the model equations might differ for a PDDC compared to the original equations, which were derived for the unified case or for pulsed sieve-plate or Karr columns. These parameters were fitted for a PDDC on the obtained hydraulic data, minimizing the absolute value of the relative error, AARE,[2] defined according to Equation (4–1), where NDP reflects the number of data points.

$$AARE = \frac{1}{NDP} \cdot \sum_{i=1}^{NDP} \frac{\left| \text{fitted value} - \text{experimental value} \right|}{\text{experimental value}} \qquad (4\text{–}1)$$

Operational procedure. All hydraulic experiments were performed at equilibrium concentrations between the aqueous and organic phase. Before carrying out any experiments, both phases were equilibrated. The solvent to feed ratio, total flux, temperature and pulsation frequency and amplitude were set to the desired values. The system was stabilized to achieve steady state condition by maintaining the interface at a given height.

The hydraulic characterises, being Sauter drop diameter, operating regime, hold-up and operational window, were determined using the following experimental procedures:

Drop sizes were determined by taking a digital photo of the column contents using a C-1400 XL digital camera (Olympus, USA) and comparing the drop dimensions with the known size of the column internals as reference. For this comparison two characteristic lengths of the internals were used, being the disc and doughnut thickness and the spacing, *H*. The uncertainty of this method was determined by taking a digital photo of the column contents and measuring the dimensions of the internals on the photo. The size of the internals was then calculated based on each characteristic length and the results were compared with the known sizes. It was found that using the disc and doughnut thickness or spacing, which were situated in the direction of the column length, an average uncertainty of 4.6% in determining the size of the internals was obtained. After the determination of the drop sizes at several positions along the column the Sauter drop diameter, d_{32}, was calculated for the system at the experimental conditions used. A change of the determined drop sizes along the column height was experimentally not observed.

For each operational point the operating regime were established from visual observation simultaneous with the results from the measurements of the drop diameter. Analogue to the observations in the pulsed sieve-plate column operation, a zone without drops in a compartment and a layer of dispersed phase (drops) on the internals was taken as characteristic feature for the mixer-settler regime. A compartment uniformly filled with drops was taken as characteristic for the dispersion regime.[1,3] Accurate visual observation of the transition between the dispersion and emulsion regime was not possible.

The hold-up, *x*, defined as the volume fraction of dispersed phase, was measured by sampling the column contents via ball valves (SP1 to SP4), which were placed in the SS flenses connecting the separate segments of the column. The obtained volume was left to settle after which the volumes of both phases were measured in a measuring cylinder. In order to determine the validity of this method overall column hold-ups were determined as well by shutting down all in- and outlet flows at a given time and determining the total amount of dispersed phase present in the column by displacing the dispersed phase layer into a measuring cylinder after settling. The uncertainty in the results using the overall compared to the ball valve method was 6.9%. The measuring method using the ball valve was used as standard method. The hold-up value was calculated as average from the hold-ups determined at SP1 to SP4, since a change of the hold-up with column height was not observed. Using this method the average uncertainty in a duplo experiment was 4.5%.

The operational window was determined by gradually increasing the pulsation stroke and meanwhile observing the behaviour of the column. For the forward-extraction process the operational window was limited by flooding, which could be observed by the rejection of dispersed phase at the top of the column as a dense layer of droplets. In the back-extraction process, however, an unstable column operation could be observed before the flooding point was reached resulting in phase inversion at increasing pulsation amplitude. Using this method the uncertainty in a duplo experiment was 3.0%.

4.4 Experimental results and data correlation

The column could be operated within a certain window covering a range of operational parameters. First the characteristics within the operational window, being drop diameter, operational regime and hold-up, are described, after which the boundaries of the operational window, being flooding (1) at low pulsation and flooding (2), phase inversion or entrainment at high pulsation, are correlated.

4.4.1 Sauter drop diameter

The experimentally determined Sauter drop diameter values, d_{32}, for the forward and back-extraction of caprolactam are presented in Figure 4.2 (a) and (b), respectively. In Figure 4.2 (a) and (b) it can be seen that an increase in the pulsation intensity resulted in a decrease of the drop diameter, which is the result of increased droplet break-up. An individual influence of frequency and pulsation stroke was, however, not observed. Furthermore it can be seen that an increase in the concentration of caprolactam in the organic phase, either by an increase of the concentration of caprolactam in the aqueous phase, an increase in temperature or addition of ammonium sulfate, resulted in a decrease of the drop diameter. The reason for this behaviour is the strong decrease of the interfacial tension with an increase in the concentration of caprolactam (in the organic phase).

According to the developed model, Equation (3–2) was used to describe the Sauter mean drop diameter. As was experimentally observed, the equation states that hold-up, flow ratio and total flux do not influence the drop diameter. Using this equation the experimentally determined Sauter drop diameter was predicted and the resulting AARE is presented in Table 4.3. In the description of the mean drop diameter, however, the geometrical characteristics, e and H, are different for a PDDC compared to sieve-plate internals and the resulting energy input is thus different as well. Therefore the parameters C_1, C_3, n_1 and n_2 might deviate from the original values.

(a)

$$10^3 \cdot d_{32} \ / \ m$$

$$10^3 \cdot f \cdot S_p \ / \ m \cdot s^{-1}$$

(b)
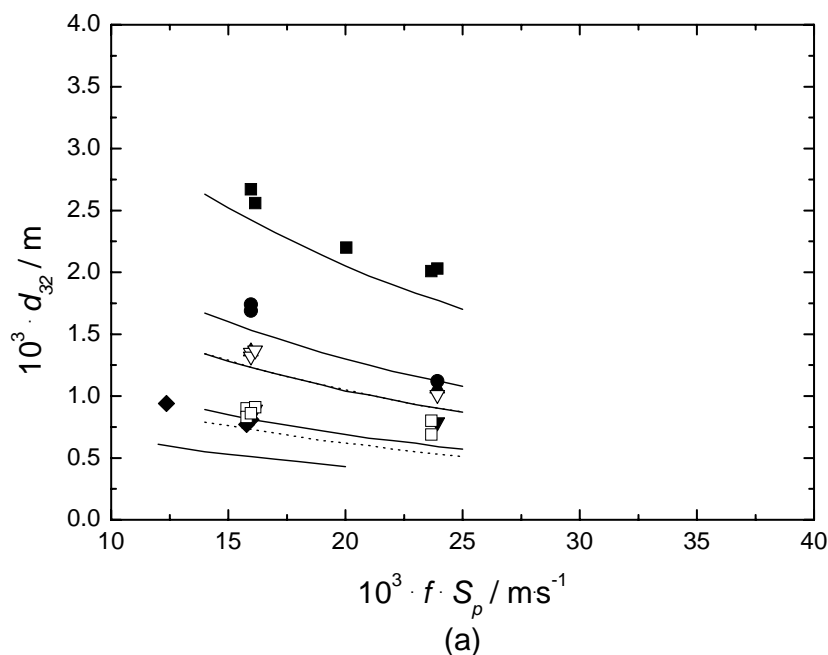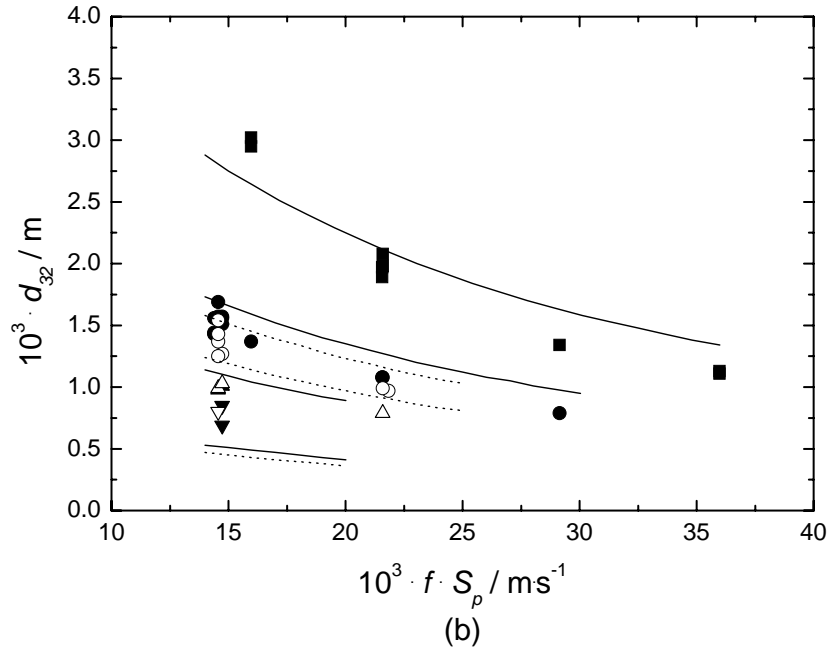
Figure 4.2. Experimental and fitted average drop sizes as function of the pulsation intensity in the forward extraction (a) for: ■, $w_{CPL,aq} = 0.000$; ●, $w_{CPL,aq} = 0.085$; ▲, $w_{CPL,aq} = 0.193$; ▼, $w_{CPL,aq} = 0.426$; ◆, $w_{CPL,aq} = 0.475$; ▽, $w_{CPL,aq} = 0.114$ and $w_{AS,aq} = 0.03$; □, $w_{CPL,aq} = 0.337$ and $w_{AS,aq} = 0.03$; —, fit where $w_{AS,aq} = 0.00$; --, fit where $w_{AS,aq} = 0.03$; and back-extraction (b) at 293 K as function of the pulsation intensity for: ■, $w_{CPL,aq} = 0.000$; ●, $w_{CPL,aq} = 0.091$; ▲, $w_{CPL,aq} = 0.292$; ▼, $w_{CPL,aq} = 0.468$; —, fit; and at 313 K: ○, $w_{CPL,aq} = 0.087$; △, $w_{CPL,aq} = 0.192$; ▽, $w_{CPL,aq} = 0.461$; -- fit. All fits were based on the optimized Equation (3–2).

In the performed experiments, however, the characteristics of the internals, *H* and *e*, were almost the same for the forward and back-extraction. So, the parameters n_1 and n_2 could not be fitted and the original values were thus applied. Finally, Equation (3–2) is valid in all operating regimes, but attention should be paid to the fact that drop coalescence might have influenced the experimentally determined drop sizes in the mixer-settler regime. The parameters C_1 and C_3 were fitted and the results are presented in Table 4.3. Using Equation (3–2) and the fitted values for C_1 and C_3 drop diameter profiles for the forward and back-extraction were calculated and presented in Figure 4.2 (a) and (b), together with the experimentally determined data. From the presented profiles it can be concluded that the determined drop diameter data were correlated accurately. In the figures it can, however, be seen that at low pulsation intensities and low concentrations of caprolactam the determined drop diameters are larger than the fitted values. This is probably the result of increased droplet coalescence in the mixer-settler operating regime and is observed for all drop diameters determined in this regime.

Table 4.3. Original and fitted parameters for the Sauter drop diameter and hold-up equations.

	Fit parameters								NDP	AARE %
d_{32}	C_1	C_2	C_3	n_1	n_2	n_3	n_4			
original	1.38	0.16	-1.25	0.30	0.18	0.14	0.06		68	28.4
fit	2.84	-	-2.59	-	-	-	-		68	14.5
x	C_Π	C_Γ	n_1	n_2	n_3	n_4	n_5	n_7		
original	0.27	6.87	0.78	0.87	3.34	-0.58	0.18	-0.39	349	68.8
fit (x)	2.39	0.45	0.34	-	-	-	-0.08	-0.12	349	12.2
fit (PI)	0.00	6.15	0.38	-	-	-	-	-0.18	141	15.6

4.4.2 Operating regimes

Simultaneous with the drop diameter measurements operating regimes were established from visual observation. Mixer-settler and dispersion regimes were found for both the back-extraction and the forward extraction process at certain pulsation intensities as presented in Figure 4.3 (a) and (b), respectively. In Figure 4.3 the points at which the column is operated are presented as the mixer-settler regime (closed symbols) and the dispersion or emulsion regime (open symbols). From the figures it can be concluded that at constant pulsation intensity the operating regime changes from mixer-settler to dispersion type operation with an increasing concentration of caprolactam. This is probably mainly caused by a decrease of the drop size, since the interfacial tension decreases with increasing concentration of caprolactam. Furthermore it can be seen that at constant concentration of caprolactam the operation changes from mixer-settler to dispersion type operation with increasing pulsation intensity. Since the drop size decreases as well with increased pulsation intensity, this observation is explained accordingly. An individual influence of frequency and amplitude was not observed.

(a)
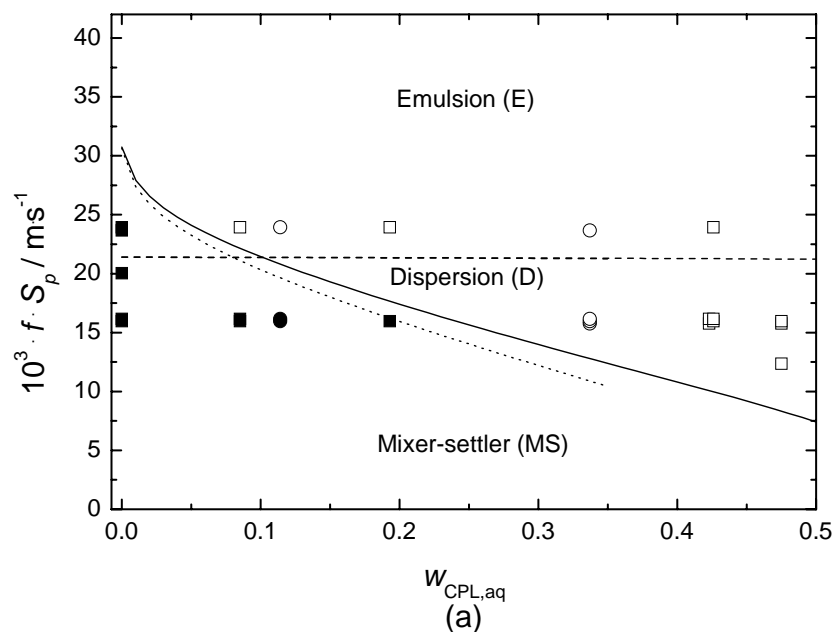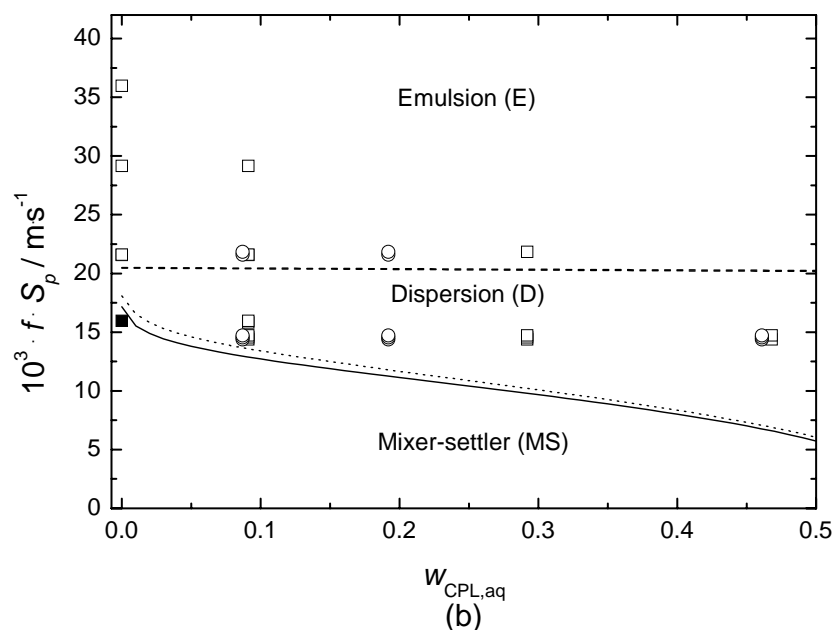
Figure 4.3. Experimental and fitted operating regimes characterized by the pulsation intensity in the forward (a) and back-extraction (b) as function of the aqueous caprolactam weight fraction, where the MS regime was found for: ■, $T/K = 293$ (BE) and $w_{AS,aq} = 0.00$ (FE); ●, $w_{AS,aq} = 0.03$ (FE); and the D or E regime was found for: □, $T/K = 293$ (BE) and $w_{AS,aq} = 0.00$ (FE); ○, $T/K = 313$ (BE) and $w_{AS,aq} = 0.03$ (FE); and fit of MS to D transition using the optimized Equation (3–3a): —, $T/K = 293$ (BE) and $w_{AS,aq} = 0.00$ (FE); --, $T/K = 313$ (BE) and $w_{AS,aq} = 0.03$ (FE); ———, prediction of D to E transition via Equation (3–3b) for all conditions.

The transition from the mixer-settler (MS) to the dispersion (D) regime and the onset for the emulsion regime (E) are predicted by Equation (3–3a) and (b), respectively, according to the derived model. From the observed operating regimes the value for k_3 was fitted at a minimum and maximum value for both the forward and back-extraction. The minimum value was obtained for the conditions at the last observation of the mixer-settler regime. The maximum value was accordingly obtained from the first observation of the dispersion regime. It was found that the regime transition in the forward extraction was represented for $1.43 \times 10^{-2} < k_3 < 1.70 \times 10^{-2}$ and the back-extraction for $7.82 \times 10^{-3} < k_3 < 8.97 \times 10^{-3}$. The determined values corresponded therefore reasonably well with the literature value. Using average values, being $k_3/\text{m·kg}^{-1/6}\text{·s}^{-7/12} = 1.57 \times 10^{-2}$ and 8.40×10^{-3} for the forward and back-extraction, respectively, the fitted regime transitions are presented in Figure 4.3 (a) and (b), together with the experimentally observed regimes. It can be concluded that the mixer-settler to dispersion regime transition is described accurately.

4.4.3 Dispersed phase hold-up

The experimental hold-up data are shown for the forward and back-extraction process in Figure 4.4. Several trends can be observed in the determined hold-up profiles. An increase of flux, flow ratio or pulsation intensity resulted in an increased hold-up. This can be explained by a relative increase of the dispersed phase flow and a decrease of the drop size, resulting in drops being slowed down, respectively. The influence of the physical properties is accounted for by the increase in hold-up with an increasing concentration of caprolactam, whereas the hold-up decreases with increasing temperature. An increasing concentration of caprolactam

results in increased viscosities and a decreased interfacial tension, leading to smaller drops that are slowed down more. An increase in temperature results mainly in strongly decreasing viscosities, which leads to drops moving faster. The influence of physical properties was expected to appear as well for w_{CPLaq} = 0.085, 0.193 and 0.426 in the forward extraction, but the experimentally determined hold-up values were similar. This is probably due to the fact that at low concentrations the column was operated in the mixer-settler regime, see Figure 4.3. This results in an increase of the hold-up compared to operation in the dispersion regime.

(a)

(b)
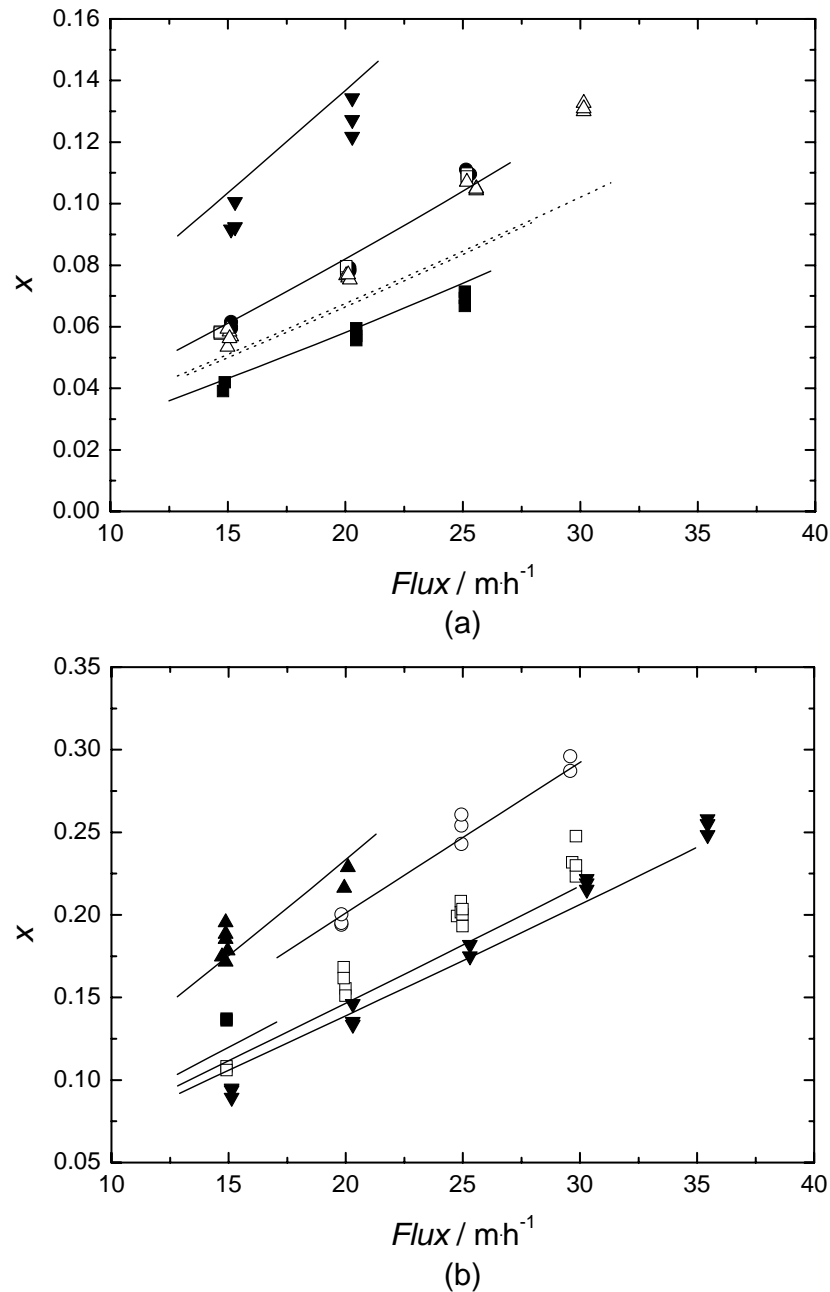
Figure 4.4. Experimental and fitted hold-up data in the forward (FE) (a) and back-extraction (BE) (b) as function of the flux at $f \cdot S_p/\text{m} \cdot \text{s}^{-1}$ = 0.015, R = 0.33 (FE) and R = 1.0 (BE), unless stated otherwise, for FE: ■, $w_{CPL,aq}$ = 0.337, $w_{AS,aq}$ = 0.03 and R = 0.20; ▼, $w_{CPL,aq}$ = 0.337, $w_{AS,aq}$ = 0.03 and R = 1.0; △, $w_{CPL,aq}$ = 0.085; □, $w_{CPL,aq}$ = 0.193; ●, $w_{CPL,aq}$ = 0.426; and for BE at T/K = 293: □, $w_{CPL,aq}$ = 0.091; ○, $w_{CPL,aq}$ = 0.091 and R = 3.0; ▲, $w_{CPL,aq}$ = 0.468; ■, $w_{CPL,aq}$ = 0.091 and $f \cdot S_p/\text{m} \cdot \text{s}^{-1}$ = 0.022; ▼, $w_{CPL,aq}$ = 0.087 and T/K = 313; and: —, fit; --, fit of FE systems in the mixer-settler regime. All fits were based on Equation (3–5).

According to the derived model, the hold-up profiles were described using Equation (3–5), which is a semi-empirical relation valid in the dispersion and emulsion operational regime. The parameter values are presented in Table 4.3, together with the results of the hold-up prediction. However, just as for the drop diameter description, the energy input is different for a PDDC compared to a pulsed sieve-plate or Karr column. Therefore, the parameters C_{Π}, C_{Γ}, n_1 and n_7 might differ for a PDDC. The same accounts for n_5 since the viscosity influence in Equation (3–5) was changed compared to the original equation. Finally, since Equation (3–5) is valid for the dispersion and emulsion regime only, hold-up values measured in the mixer-settler regime were excluded from the fitting procedure. Equation (3–3a) with the average values for k_3 was used to determine the critical pulsation intensity for the transition from the mixer-settler to the dispersion regime. The parameters resulting after fitting are presented in Table 4.3, together with the hold-up description results.

The calculated hold-up profiles using the fitted parameters are presented in Figure 4.4 together with the experimental data. In these figures it can be seen that the experimental data are described well and that the influence of flux, flow ratio, pulsation intensity and physical properties is covered. It can, however, be seen in Figure 4.4 (a) that the description of data in the mixer-settler regime as expected differs from the experimentally determined data.

4.4.4 Operational window

In Chapter 3 it was concluded that several regimes could be limiting for the operation of an extraction column. At low pulsation intensities flooding limits column operation, which is described by the pulsed volume. In our experiments the necessity of a minimum amount of pulsation intensity was also qualitatively observed, but not quantitatively determined. The applicability of presented equation could therefore not be verified, but was used as estimate. At high pulsation intensities flooding (2), phase inversion or entrainment is limiting. The maximum amount of entrainment was neither specified nor determined and is therefore not considered here. Flooding (2) was observed as the limiting process for the forward extraction, which was described by a predictive equation. In the back-extraction process phase inversion was observed to be limiting. The critical hold-up at phase inversion was predicted based on the drop diameter. The corresponding fluxes were described by the hold-up equation.

The determined fluxes at the limiting operating conditions are presented in Figure 4.5 (a) and (b) for the forward and back-extraction process, respectively. From both figures it can be concluded that at increasing pulsation intensities, the total flux at flooding and phase inversion decreases. This is due to a decrease of the drop size with increasing pulsation intensity, which results in an increasing hold-up such that the critical hold-up is reached at a lower total flux. The hold-up also increases with an increasing flow ratio and an increasing concentration of caprolactam in the organic phase, which results in a lower total flux that can be applied as well.

(a)

(b)
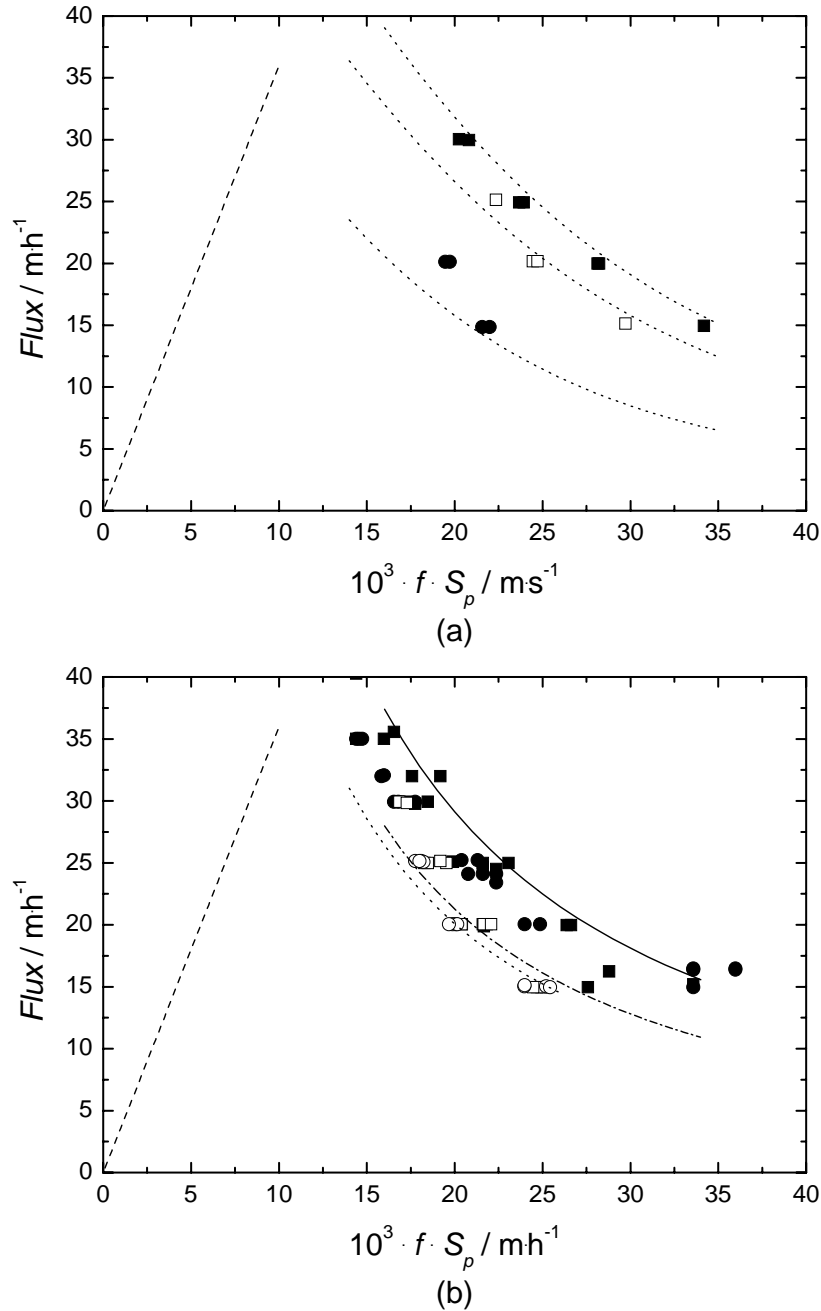
Figure 4.5. Experimentally determined and predicted flooding (2) data in the forward extraction (a) for: ●, $w_{CPL,aq} = 0.475$ and $R = 0.20$; ■, $w_{CPL,aq} = 0.426$ and $R = 0.20$; □, $w_{CPL,aq} = 0.426$ and $R = 0.33$; --, prediction; and phase inversion data in the back-extraction process (b) at $w_{CPL,aq} = 0.091$ and $T/K = 293$: ■, $R = 1.0$; ●, $R = 3.0$; and fit via Equation (3–5) optimized for phase inversion, where: —, $R = 1.0$; — - —, for $R = 3.0$; and at $w_{CPL,aq} = 0.192$ and $T/K = 313$: □, $R = 1.0$; ○, $R = 3.0$; and fit via the optimized Equation (3–5) for: --, $R = 3.0$; and prediction: — —, flooding (1).

At the flooding point the maximum value for the hold-up, x_f, is reached, which was calculated $x_f = 0.14$ to 0.24 for the complete range of experimental conditions. The calculated values represent an acceptable maximum hold-up value compared to the experimentally determined hold-up values at steady state operation. Using these theories the total flux at flooding could be calculated as well with an uncertainty of AARE = 24.7%. It has to be noted, however, that the calculated critical hold-up at flooding is higher than the hold-up calculated using Equation

(3–5) at equal conditions. The AARE of the critical hold-up values compared to Equation (3–5) was over 48%, which is probably caused by the change of the system behaviour near the operational boundary, especially with respect to drop coalescence.[1] Since drop coalescence behaviour changes near the operational boundary, the validity of Equation (3–2) is also questionable, resulting in a larger AARE when prediction flooding data.

The description of the critical hold-up at phase inversion was based on Equation (3–10b). It has to be noted, however, that the calculated critical hold-up at phase inversion is higher than the hold-up calculated using Equation (3–5) at equal conditions, just as for the flooding process. The uncertainty in the calculated critical hold-up values was AARE = 52%. In order to correlate the flux at phase inversion Equation (3–2) or (3–5) need to be fitted for phase inversion conditions especially. The different system behaviour near the operational boundary was accounted for via Equation (3–5) by fitting parameters influencing the interfacial tension and energy input, minimizing the AARE in the flux at phase inversion. The resulting parameter values and flux description are shown in Table 4.3.

4.4.5   Comparison of flooding and phase inversion

For both the theories describing flooding and phase inversion, the critical value for the limiting process to take place is related to the critical hold-up. Therefore critical hold-up values for both limiting processes and the corresponding fluxes were compared both for the back-extraction as for the forward extraction process.

In the forward extraction flooding was observed and critical hold-ups were predicted at $x_f =$ 0.14 to 0.24 and these calculated values represent an acceptable maximum hold-up value compared to the experimentally determined hold-up values at steady state operation. The critical hold-up for phase inversion in the forward extraction process was predicted at $x_{PI} =$ 0.42 to 0.56 for the complete range of experimental conditions. The corresponding predicted total flux at phase inversion was 2.1 times higher than the total flux at flooding at similar conditions.

In the back-extraction phase inversion was observed and critical hold-ups were calculated at $x_{PI} =$ 0.43 to 0.48. The hold-up values measured at pulsation intensities of $f \cdot S_p = 0.9 \cdot (f \cdot S_p)_{PI}$ had an average value of $x = 0.30$ with an AARE of 12.9%. The critical hold-up for flooding in the back-extraction process could only be predicted for systems with an mass fraction of caprolactam in the aqueous phase of $w_{CPL,aq} < 0.20$. At increasing concentrations of caprolactam the drag coefficient, on which the theory is based, increased exponentially, resulting in very low terminal velocities and therefore very low fluxes at flooding. For systems in the back-extraction where $w_{CPL,aq} < 0.20$ the critical hold-up at flooding was predicted at $x_f = 0.24$ to 0.37. The corresponding predicted flux at flooding was 1.2 to 1.06 times lower than the determined total flux at phase inversion at similar conditions.

The experimentally observed limiting processes are not completely predicted correctly by comparison of the critical hold-up values and corresponding fluxes. Based on this approach flooding is expected to be the limiting process for the forward extraction, which was indeed observed experimentally. For the back-extraction phase inversion was observed and flooding

predicted, but the predicted total fluxes for both processes were quite comparable. The uncertainty and limitations in the applied equations result in the fact that the latter prediction is not consistent with the experimental observations, as is the first.

4.4.6   Operational diagram

Experimental data and the derived equations for the description of the operational window, including flooding (1), the different operating regimes and the limiting process were applied to construct an operational diagram specific for a PDDC. For $w_{CPL,aq} = 0.426$ and $R = 0.20$ in the forward extraction and $w_{CPL,aq} = 0.087$ at $T/K = 313$ and $R = 1.0$ in the back-extraction such a diagram is presented in Figure 4.6 (a) and (b), respectively. In this diagram the conditions at steady state operation, experimentally determined and fitted limiting process conditions, being flooding (1), flooding (2) (a) and phase inversion (b), and the critical pulsation intensity required for the transition between the operating regimes, being mixer-settler (MS), dispersion (D) and emulsion (E), are presented. It can be seen that at a constant flux and increasing pulsation intensity first the flooding (1) line is crossed. When the pulsation intensity is increased further, the operational regime changes from mixer-settler to dispersion and emulsion. Increasing the pulsation intensity even more or increasing the flux at a constant pulsation intensity results in reaching the boundary of the operational window. At each operating point the Sauter drop diameter and hold-up values can be calculated using Equation (3–2) or (3–5), respectively. Diagrams as presented in Figure 4.6 (a) and (b) can be constructed for each system in the back- and forward extraction, but are specific with respect to concentrations, temperature and flow ratio.

(a)
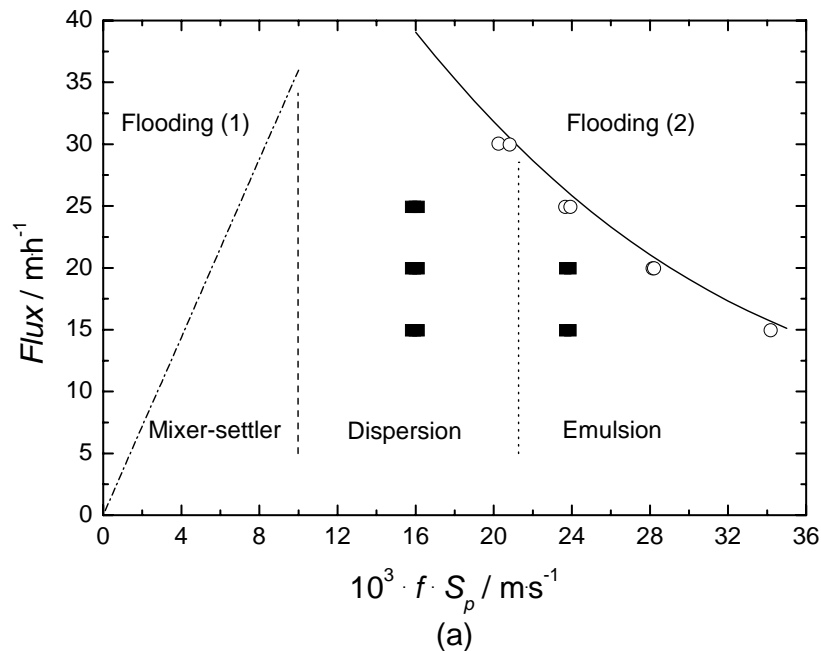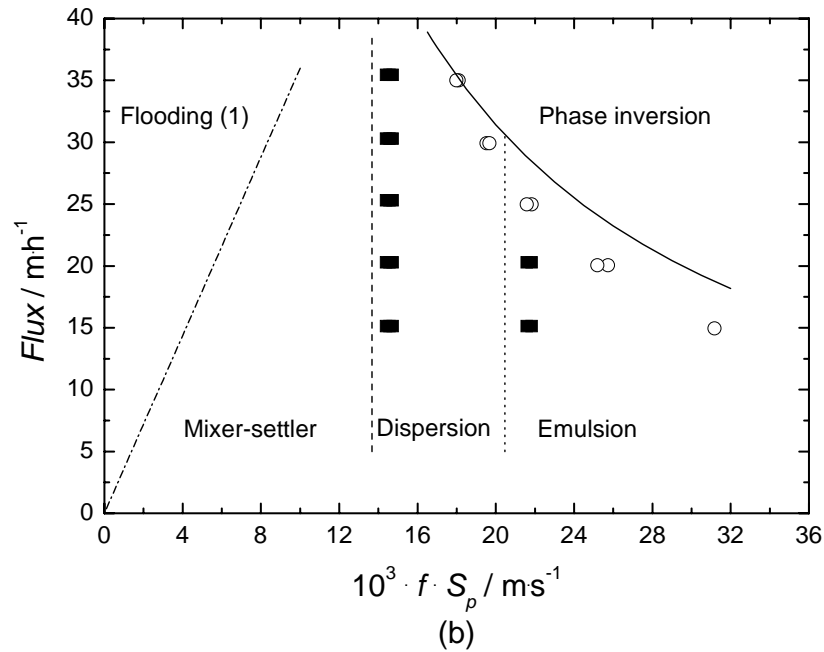
Figure 4.6. Operational diagram for the forward extraction at $w_{CPL,aq} = 0.426$ and $R = 0.20$ (a) and for the back-extraction at $w_{CPL,aq} = 0.087$, $T/K = 313$ and $R = 1.0$ (b), where: ■, steady state operation; ○, flooding (a) and phase inversion (b); —, prediction flooding (2) (a) and fit phase inversion (b); — —, fit MS to D transition; --, prediction D to E transition; — - —, prediction flooding (1).

4.5   Conclusions

The hydraulic operation of a PDDC was evaluated for the back- and forward extraction of caprolactam in a pilot set-up. It was found that a PDDC showed qualitatively comparable operational characteristics to a pulsed sieve-plate column. Mixer-settler and dispersion type operating regimes were observed, as well as flooding due to too low pulsation. The conditions for flooding in the forward extraction and phase inversion in the back-extraction were determined. Hold-up and Sauter drop diameter values were determined in all operating regimes.

The observed trends and determined data were described according to a previously developed model, covering the operational window, operating regimes and a description of drop size and hold-up. It was found that the measured values and observed trends could be described accurately using this model after fitting drop diameter, hold-up and phase inversion data. Using this approach the difference between the back- and forward extraction operation can be understood, just as the influence of the physical properties and operational parameters on the operation.

Using the developed model with the fitted parameters the optimal operating point for caprolactam extraction can be determined, provided that the separation performance and the influence of mass transfer on the hydraulic characteristics is known.

Nomenclature

AARE   Average absolute value of the relative error

D, E, MS	Dispersion, Emulsion and Mixer-settler operating regime, respectively
d_{32}	Sauter drop diameter, m
e	Fractional free cross-sectional area
$f \cdot S_p$	Pulsation intensity, where f/s^{-1} denotes frequency and S_p/m stroke, $m \cdot s^{-1}$
Flux	Total throughput, Flux = $V_d + V_c$, $m \cdot h^{-1}$
H	Disc to doughnut spacing, m
NDP	Number of data points
R	Flow ratio, $R = V_d/V_c$
T	Temperature, K
V_i	Velocity of phase or component i, $m \cdot s^{-1}$
w	Weight fraction
x	Dispersed phase hold-up defined as volume fraction of the dispersed phase

Greek letters

γ	Interfacial tension, $N \cdot m^{-1}$
η	Dynamic viscosity, $kg \cdot m^{-1} \cdot s^{-1}$
ρ	Density, $kg \cdot m^{-3}$

Subscript

aq, org	Aqueous and organic phase, respectively
c, d	Continuous and dispersed phase, respectively
f	Denoting flooding
PI	Denoting phase inversion

Literature cited

1. Godfrey, J.C. Slater, M.J. *Liquid-Liquid Extraction Equipment*; John Wiley & Sons, Inc.: New York, 1994.

2. Kumar, A.; Hartland, S. A Unified Correlation for the Prediction of Dispersed-Phase Hold-up in Liquid-Liquid Extraction Equipment. *Ind. Eng. Chem. Res.* **1995**, *34*, 3925-3940.

3. Klicka, V.; Cermak, J. Zweiphasenströmung in der Pulsier-Extraktionskolonne. *Verfahrenstechnik* **1971**, *5*, 320-327.

Chapter 5

Extraction of caprolactam with toluene in a pulsed disc and doughnut column: mass transfer characteristics

5.1 Introduction

In Chapter 3 a theoretical model was developed describing the hydraulic characteristics of caprolactam extraction in a pulsed disc and doughnut column (PDDC), being Sauter drop diameter, hold-up, operating regimes and operational window. In Chapter 4 pilot plant experiments for the caprolactam forward and back-extraction were performed and evaluated using the theoretical framework of Chapter 3. Hydraulic characteristics were determined as a function of the operating conditions, being total flux, solvent to feed ratio and pulsation frequency and amplitude. The experimental conditions covered the industrial range with respect to the concentrations of caprolactam and ammonium sulfate, temperature and phase continuity. All hydraulic experiments were performed at equilibrium conditions in order to avoid the influence of mass transfer. Application of the in Chapter 3 developed theoretical model for the description of the obtained hydraulic data resulted in an accurate description after fitting.

In this study the contacting efficiency of a PDDC is investigated for caprolactam extraction with toluene, the so-called forward extraction, and its back-extraction with water. In literature some studies are presented on the separation performance of the caprolactam extraction process. Using benzene as extraction solvent the performance of different lay-outs of the industrial EniChem process was studied. The interpretation of the results was based on the two-film model with a contamination factor, accounting for the influence of contaminants on the mass transfer. The overall mass transfer coefficient based on the dispersed phase was determined from single drop mass transfer experiments at k_{od}/m·s^{-1} = 1.5 to 3.0 × 10^{-5}.[1] In a reciprocating plate extraction column caprolactam was extracted with toluene, where the efficiency at different operating conditions was determined at HETS/m = 0.43 to 0.63.[2] Furthermore studies are performed on the extraction of caprolactam using benzene[1,3,4] and trichoroethene[2,5] as solvents. The processes studied include the forward and back-extraction process,[2] extraction from aqueous ammonium sulfate solutions[1,3,5] and effluent water[1,4] and the experiments are performed using single drop experiments,[1] vibrating plate columns,[2,5]

pulsed packed columns[3] and pulsed sieve plate columns.[4] The results are expressed in k_{od},[1] HETS values,[2] concentrations[5] and HTU values.[3,4]

In this study the overall separation performance of a PDDC is investigated for both the forward and back-extraction of caprolactam with and from toluene, respectively. The experimental conditions covered the whole industrial operating range with respect to the concentrations of caprolactam and ammonium sulfate, solvent to feed ratio, temperature and phase continuity. In addition, the influence of operating parameters, being flow rates and pulsation intensity was investigated. Furthermore, the dispersed phase hold-up, Sauter drop diameter and operating regime were determined and compared with the results obtained from previous hydraulic experiments at equilibrium conditions. The concentration profiles were correlated with the backflow model, using a constant overall mass transfer and continuous phase axial dispersion coefficient. The hold-up and drop size, necessary for the description of the interfacial area, were described using the expressions derived for the equilibrium situation, taking into account the relative effect of mass transfer via an additional factor.

5.2   Theory

5.2.1   Backflow model description

In order to describe the separation performance in extraction processes different models, like the plug flow model, are developed. The overall flow pattern in extraction equipment, however, is complex and based on experience it became evident that the description of mass transfer in column extractors with the plug flow model was oversimplified. Therefore, in general, axial dispersion (backmixing) of one or both phases needs to be included in the description, since it shows a major influence on the separation performance.[6] In order to describe this effect Sleicher derived the diffusion model for differential extractors and later gave the corresponding backflow difference equations for mixer-settlers, which are also applicable to stage-wise columns.[6,7] These two distinct types of models represent idealized limiting cases, but in practise the diffusion model is approached by differential extractors, such as packed or baffle-plate columns. The backflow model is to be preferred for multi-compartment columns such as rotary agitated, pulsed plate and reciprocating plate columns.[7] The mass transfer performance in the PDDC is therefore described using the backflow model, although Jahya *et al.* use the diffusion model.[8] Based on these models the main characteristics in the description of column extractors appear to be the axial dispersion and mass transfer, besides the transport by convection.

The basis of the backflow model is graphically presented in Figure 5.1.[7] The model consists of a series of well-mixed stages between which backmixing occurs, characterized by the backflow parameters for phase x and y, α_y and α_x, respectively. Mass transfer takes place in each stage with a flow rate of $(k_{ox} \cdot a \cdot s \cdot h_c)$ where the product of volume mass transfer coefficient and stage volume is constant for each stage. The phases are assumed immiscible, but, in contrast to the original model, the flow rates are dependent on the concentration of caprolactam and therefore change for each stage. The distribution coefficient, finally, is determined from phase equilibria. The corresponding component mass balance for stage n at

steady state for both phase x and y is given by Equation (5–1a) and (b) and the overall mass balance is presented in Equation (5–2).

$$F_{x,n-1} \cdot (1 + \alpha_x) \cdot c_{x,n-1} - F_{x,n} \cdot (1 + 2 \cdot \alpha_x) \cdot c_{x,n} + F_{x,n+1} \cdot \alpha_x \cdot c_{x,n+1}$$
$$- k_{ox} \cdot a \cdot s \cdot h_c \cdot \left(c_{x,n} - c_{x.n}^* \right) = 0 \tag{5–1a}$$

$$F_{y,n-1} \cdot \alpha_y \cdot c_{y,n-1} - F_{y,n} \cdot (1 + 2 \cdot \alpha_y) \cdot c_{y,n} + F_{y,n+1} \cdot (1 + \alpha_y) \cdot c_{y,n+1}$$
$$+ k_{ox} \cdot a \cdot s \cdot h_c \cdot \left(c_{x,n} - c_{x.n}^* \right) = 0 \tag{5–1b}$$

$$(F \cdot c)_{x,feed} + (F \cdot c)_{y,solvent} = (F \cdot c)_{y,extract} + (F \cdot c)_{x,raffinate} \tag{5–2}$$
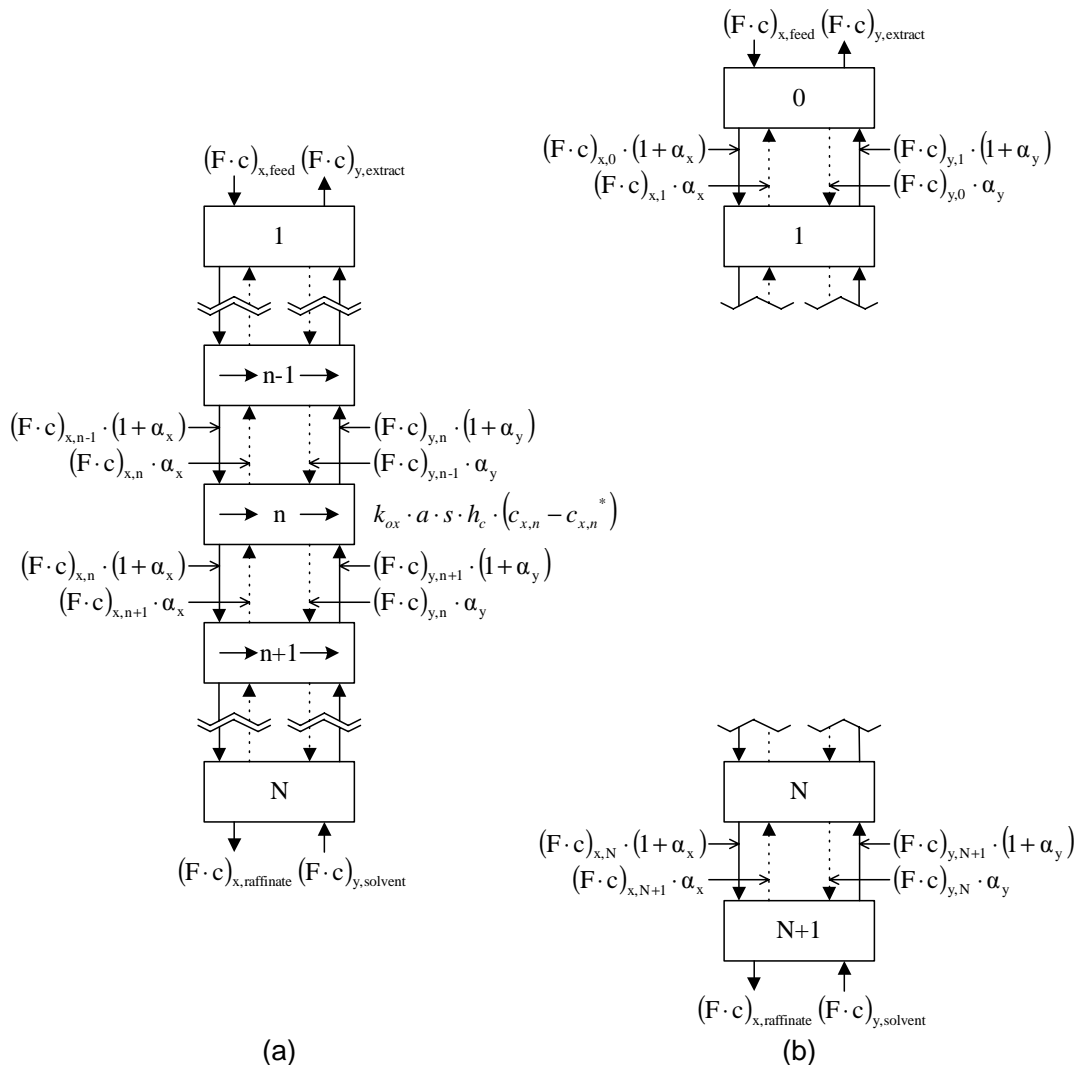
Figure 5.1: Graphical presentation of the backflow model (a) and the arrangement for the description of the feed sides of the column (b).

In Figure 5.1 and Equation (5–1a), (b) and (5–2), the phase flows are presented dependent on the stage number. This approach is necessary since the transfer of caprolactam is so large that it results in a significant change in both phase flows, as well as the system properties, being phase densities, viscosities, interfacial tension and the equilibrium distribution.

The general solution of Equation (5–1a) and (b), i.e. for backmixing in both phases, involves four boundary conditions, two for each phase. Two of these define a concentration jump at the phase inlets due to backmixed solute-depleted feed and solute-enriched solvent. The other two correspond to zero concentration gradients at the phase exits.[6,7]

The concentration jump in the phases fed to the column is accounted for by adding a hypothetical stage 0 before the first column stage at the feed (x) side and a stage N+1 after the last stage N at the solvent (y) side of the column. Via a mass balance the concentration change as a result of the backflow parameter can then be described as expressed via Equation (5–3).[7]

$$F_{x,feed} \cdot c_{x,feed} + F_{x,1} \cdot \alpha_x \cdot c_{x,1} = F_{x,0} \cdot (1 + \alpha_x) \cdot c_{x,0}$$
$$F_{y,solvent} \cdot c_{y,solvent} + F_{y,N} \cdot \alpha_y \cdot c_{y,N} = F_{y,N+1} \cdot (1 + \alpha_y) \cdot c_{y,N+1}$$

(5–3)

Since there is, however, no actual mass transfer taking place over these hypothetical stages, it follows for the exiting phases at these stages that the concentrations remain unchanged as expressed by Equation (5–4).[7]

$$c_{x,raffinate} = c_{x,N+1} = c_{x,N}$$
$$c_{y,extract} = c_{y,0} = c_{y,1}$$

(5–4)

5.2.2 Description of model parameters

According to Equations (5–1) to (5–4) the parameters required to describe the concentration profile in both phases are: phase flow rates, F_x and F_y, the volume of a characteristic column segment, $(s \cdot h_c)$, the specific interfacial area, a, the backflow parameters, α_x and α_y, and the overall mass transfer coefficient based on the feed phase (x), k_{ox}.

The feed and solvent phase flow rates were, evidently, known being operational parameters. As described, these phase flow rates change along the column due to the change in concentration. In the iterative procedure therefore $F_{x,n}$ and $F_{y,n}$ are introduced taking into account the corresponding concentrations. These concentrations are expressed based on the solute containing volume stream. Finally, it was assumed that both phases are completely immiscible.

The cross-sectional column area, s, was determined from the column dimensions. The characteristic height was chosen at $h_c/m = 0.02$, which corresponds to the disc to disc distance of the internals. It is also the step size used in the iterative procedure.

The interfacial area was calculated via the hold-up, x, and Sauter drop diameter, d_{32}, of the dispersed phase, according to Equation (5–5).

$$a = \frac{6 \cdot x}{d_{32}}$$

(5–5)

The hold-up and drop diameter in the caprolactam forward and back-extraction process can be described for the equilibrium situation, as presented in Chapter 3 and Chapter 4. However, mass transfer has also an influence on the drop size and hold-up.[9,10] The drop size increases with mass transfer from the dispersed to the continuous phase, as is the case in the forward and back-extraction of caprolactam, due to enhanced coalescence. According to Kumar and Hartland the relative increase compared to the equilibrium situation varies from 1.0 to 3.0 and is 1.67 for the unified case.[9] The hold-up decreases as result of an increase in the drop diameter. According to Kumar and Hartland the relative decrease is 0.5 to 1.0 and is about 0.6 for pulsed perforated-plate and Karr reciprocating plate columns.[10] It has to be taken into account furthermore that the hold-up description used is not valid in the mixer-settler operating regime, whereas the pulsation intensity required for regime transition in the column increases, because of the increasing drop size, see Chapter 3. The effect of mass transfer on the interfacial area and operating regimes for caprolactam extraction in a PDDC was therefore determined experimentally.

Detailed investigation of the axial dispersion phenomenon is based on concentration gradients, drop residence time or tracer pulse injection studies. The results obtained for the PDDC using these methods are fitted via empirical relations[8-11] or compared with results obtained via numerical simulations.[12-16] In comparison, it is known for reciprocating plate extraction columns that the axial dispersion in liquid-liquid systems has a maximum at low pulsation intensities, stays constant at $f \cdot S_p/\text{m} \cdot \text{s}^{-1} > 0.015$, but increases with increasing pulsation intensity in the emulsion operating regime. At lower dispersed phase velocities, the axial dispersion coefficient increases as well.[17] However, despite extensive studies, there is no complete understanding of this phenomenon such that no expression or model for the prediction or description of axial dispersion coefficients is available. In general, axial backmixing in the continuous phase plays a major role in determining the performance of an extraction column. On the other hand, axial dispersion in the dispersed phase involves both forward mixing and backmixing, though it can usually be disregarded.[6] The dispersed phase backflow ratio was thus chosen at $\alpha_d = 0$ and since the feed phase (x) is the dispersed phase in both the forward and back-extraction process $\alpha_x = 0$. This concept was also applied in previous models for mass transfer in a PDDC when fitting the separation performance.[8]

Various methods exist as well for the determination of the overall mass transfer coefficient, ranging from experiments in mass transfer cells, single drop experiments and pilot studies. Generally accepted expressions exist for the mass transfer coefficient of the continuous phase in single drop systems.[18,19] The liquid inside drops, however, may be stationary, moving in a certain characteristic flow pattern or may be mixing randomly. As a result of this complex behaviour, no reliable models exist to describe the dispersed phase mass transfer coefficient.[18] For the description of mass transfer coefficients in extraction columns, however, Kumar and Hartland developed semi-empirical predictive correlations for the mass transfer coefficient of the continuous and dispersed phase in pulsed, Karr, Kühni and rotating disc columns[19] as presented in Equation (5–6) and (5–7).

$$\frac{\dfrac{Sh_c}{1-x}-Sh_{c,r}}{Sh_{c,\infty}-\dfrac{Sh_c}{1-x}}=0.0526\cdot Re^{\frac{1}{3}+0.066\cdot Re^{0.25}}\cdot Sc_c^{\frac{1}{3}}\cdot\frac{\left(\dfrac{V_{slip}\cdot\eta_c}{\gamma}\right)^{\frac{1}{3}}}{1+\left(\dfrac{\eta_d}{\eta_c}\right)^{1.1}}\cdot\left[1+C_1\left(\frac{\varepsilon}{\gamma}\cdot\left(\frac{\rho_c}{g\cdot\gamma}\right)^{\frac{1}{4}}\right)^{0.33}\right] \qquad (5-6)$$

where

$$Sh_{c,r}=2.43+0.775\cdot Re^{\frac{1}{2}}\cdot Sc_c^{\frac{1}{3}}+0.0103\cdot Re\cdot Sc_c^{\frac{1}{3}}$$

$$Sh_{c,\infty}=50+\frac{2}{\sqrt{\pi}}\cdot\left(Pe_c\right)^{\frac{1}{2}}$$

$$Sh_d=17.7+\frac{0.00319\cdot\left(Re\cdot Sc_d^{\frac{1}{3}}\right)^{1.7}}{1+0.0143\cdot\left(Re\cdot Sc_d^{\frac{1}{3}}\right)^{0.7}}\cdot\left(\frac{\rho_d}{\rho_c}\right)^{\frac{2}{3}}\cdot\frac{1}{1+\left(\dfrac{\eta_d}{\eta_c}\right)^{\frac{2}{3}}}\cdot\left[1+C_2\left(\frac{\varepsilon}{\gamma}\cdot\left(\frac{\rho_c}{g\cdot\gamma}\right)^{\frac{1}{4}}\right)^{0.33}\right] \qquad (5-7)$$

where $C_1 = C_2 = 4.33$ for pulsed columns,[19] which will be used for the description of the mass transfer coefficient in the PDDC. Equation (5–6) and (5–7) are based on corresponding equations for single drops. The presented dimensionless groups in latter equations covered a range of experimental conditions of Re = 0.1-1400, Sc_c = 180-570 000 and Sh_c = 15-1900 for the continuous phase and Re = 6-1300, Sc_d = 130-65 000 and Sh_c = 17-1100 for the dispersed phase.[19] Both mass transfer coefficients can be combined via the two-film model as described via Equation (5–8).

$$\frac{1}{k_{od}}=\frac{m_D}{k_c}+\frac{1}{k_d} \quad \text{where} \quad m_D=\frac{c_d}{c_c} \quad \text{or when } x=d: \quad \frac{1}{k_{ox}}=\frac{m_D}{k_y}+\frac{1}{k_x} \quad \text{with} \quad m_D=\frac{c_x}{c_y} \qquad (5-8)$$

The unknown values of k_{ox} and α_y were determined by fitting a value for k_{ox} at a given value for α_y, assuming $\alpha_x = 0$, in order to comply with the determined concentration profile and raffinate concentration. Performing this procedure for a series of α_y values resulted in a minimized Absolute Average Error (AAE) in the experimentally determined and calculated normalized weight fractions and therefore in optimal values of k_{ox} and α_y. The separation performance of the PDDC for the forward and back-extraction was furthermore interpreted using the Height Equivalent of a Theoretical Stage (HETS), which is calculated based on the determined concentration profiles and the equilibrium data. No evaluation is made based using the well-known Number of Transfer Units, $NTU_{ox} = k_{ox}\cdot a\cdot h_c\cdot s/F_x$,[7] approach, since the values of a, F_x and k_{ox} change for every stage and therefore the NTU_{ox} value changes as well.

The concentration profiles used in the fitting procedure were determined along the column, of which the active section had a length of L_c/m = 4.24. The feed and solvent feed-point, however, are placed 0.18 m from the active column entrance, whereas mass transfer and

backmixing proceeded in this part of the column as well. Therefore the distance from each feed-point to the active section should be taken into account. Since the column contained no internals in this part and the diameter doubled going from the active section to the settler, the mass transfer and backmixing occurred in a different way. The distance of each feed-point to the column entrance should thus be accounted for with an increase of 0.00 m to 0.18 m. Arbitrarily three disc to disc stages were added, resulting in a 0.06 m increase of the active column length on both sides of the column. The final active column length was therefore L_c/m = 4.36.

Finally, it should be noted that in Equations (5–1a), (b) and (5–3) the coefficients α_y and k_{ox} are presented as constants, i.e. average values over the column. It can be concluded from literature on axial dispersion and mass transfer, however, that these processes depend on system properties and operating conditions. The assumption that the coefficients are constant, together with the assumption of the absence of backmixing in the dispersed phase, $\alpha_x = 0$, results therefore in a simplified description of the caprolactam extraction process.

5.3 Experimental set-up and procedure

Experimental set-up. The PDDC pilot set-up is schematically shown in Figure 5.2. Its operation is already explained in Chapter 4. The internals consisted of alternating disc and doughnut baffles (Chapter 3). In contrast to the hydraulic experiments, the phases were after contacting and separation in the top or bottom settler stored in vessel 3 and 4, respectively.
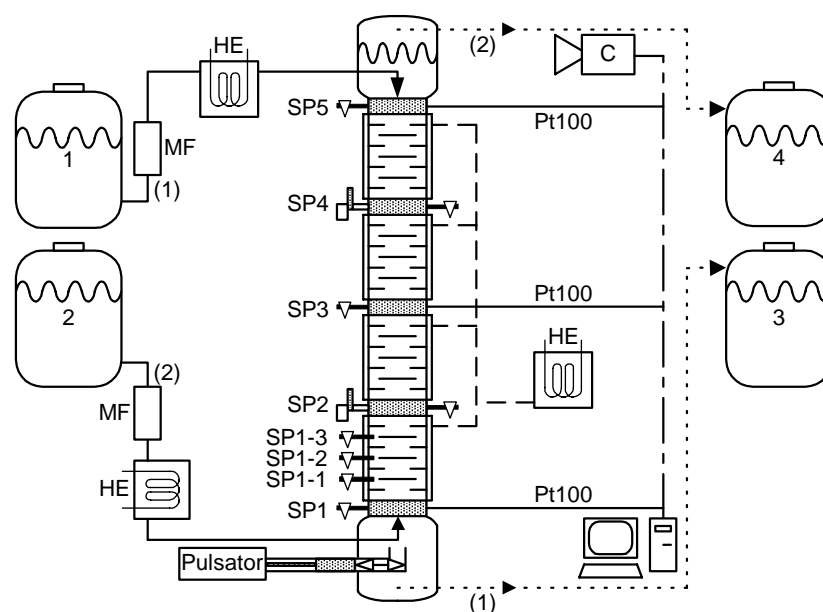
Figure 5.2. Schematic presentation of the PDDC for back-extraction operation.

Experimental procedure. All mass transfer experiments were performed at steady state, which was created by maintaining a constant interface level. In general the time needed to reach a steady state concentration profile was observed to be approximated by the time needed for three to four complete replacements of the column volume.[8] After filling the column and settlers once, this approximation was confirmed by taking samples after 2.5 and 3 column volume replacements and finding no change in the concentration profile.

The hydraulic characteristics, being drop size, operating regime and hold-up, were determined as for the equilibrium situation, see Chapter 4. The drop size was found by comparing the dimensions of the drops on digital photos of the column contents to the reference size of the column internals. Operating regimes were determined from digital images, where a zone without drops accompanied by a dispersed phase layer on the internals were characteristic for mixer-settler operation. A uniform dispersion over the column was taken as characteristic of the dispersion regime. Visual observation of the emulsion regime was, however, not possible. Hold-ups were measured by sampling the column contents via two ball valves (at SP2 and SP4). The obtained volume was left to settle after which the volumes of both phases were measured. Along the column length a change in the drop size and hold-up was found, which was addressed to the effect of mass transfer, since in the equilibrium situation no change along the column length was observed for these parameters.

Concentration profiles were measured via sample ports, which were placed in each flense (SP1 to SP5) and, since a steep concentration gradient was expected, at the feed side of the column three additional sample ports were placed in the glass segment (SP1-1 to SP1-3 for the back-extraction). The sample ports consisted of two separate tubes with an internal diameter of 3 mm. One was wetted by the organic phase and faced downwards, whereas the other was wetted by the aqueous phase and faced up. The phases were thus sampled separately after which the samples were prepared for analysis, see Chapter 2.

Chemicals. All chemicals were used as received. Toluene (purity > 99%) was supplied by Fluka (USA), ε-caprolactam (CPL) (purity grade) by DSM (The Netherlands) and ammonium sulfate (AS) (purity > 99%) by Sigma-Aldrich (USA). Demineralised water was used in all experiments.

Conditions. The experimental conditions covered the full industrial range with respect to the concentrations of caprolactam and ammonium sulfate, solvent to feed ratio, temperature and phase continuity. In Table 5.1 the experimental conditions for both the forward and back-extraction process are presented, where it has to be noted that in the caprolactam process the feed (x) phase is always dispersed (d) as in the industrial case. In order to compare the conditions for the extraction processes, the extraction factor, E, is presented for the feed location, where K_D' represents the equilibrium partition ratio based on the solute mass fraction in the extract and F_y' and F_x' represent the solute free solvent and feed mass flow rates.

In Table 5.2 the physical properties, being densities and viscosities of both separate phases and the interfacial tension between the phases, are presented for the concentrations and temperatures used.

Table 5.1. Experimental feed conditions during mass transfer experiments in the forward and back-extraction process of caprolactam (varied parameters are shown as 'bold' characters).

	w_{CPL} (aq)	w_{AS} (aq)	T K	$10^3 \cdot f \cdot S_p$ m·s^{-1}	Flux=$V_{feed}+V_{solvent}$ m·h^{-1}	$R=V_d/V_c$	$E=K_D'\cdot F_y'/F_x'$
Forward extraction (FE): aqueous feed phase dispersed							
FE-1	0.50	-	313	16.0	20	0.18	1.2
FE-2	0.50	-	313	16.0	**26**	0.18	1.2
FE-3	0.50	-	313	**21.8**	20	0.18	1.2
FE-4	0.50	**0.01**	313	16.0	20	0.18	1.3
FE-3/4	0.50	**0.01**	313	**21.8**	20	0.18	1.3
FE-5	0.50	-	**333**	16.0	20	0.18	1.5
FE-3/5	0.50	-	**333**	**21.8**	20	0.18	1.5

	w_{CPL} (org)		T K	$10^3 \cdot f \cdot S_p$ m·s^{-1}	Flux=$V_{feed}+V_{solvent}$ m·h^{-1}	$R=V_d/V_c$	$E=K_D'\cdot F_y'/F_x'$
Back extraction (BE): organic feed phase dispersed							
BE-1	0.13-0.15		293	16.0	20	2.9	3.4
BE-2	0.13-0.15		293	16.0	**12**	2.9	3.4
BE-3	0.13-0.15		293	**21.8**	20	2.9	3.4
BE-4	0.13-0.15		**313**	16.0	20	2.9	2.4
BE-2/4	0.13-0.15		**313**	16.0	**12**	2.9	2.4
BE-3/4	0.13-0.15		**313**	**21.8**	20	2.9	2.4

Table 5.2. Physical properties regarding the forward and back-extraction of caprolactam covering the maximum concentration range.

	w_{CPL} (aq)	w_{AS} (aq)	w_{CPL} (org)	$10^{-3}\cdot\rho_c$ kg·m^{-3}	$10^3\cdot\eta_c$ kg·m^{-1}·s^{-1}	$10^{-3}\cdot\rho_d$ kg·m^{-3}	$10^3\cdot\eta_d$ kg·m^{-1}·s^{-1}	$10^3\cdot\gamma$ N·m^{-1}
Forward extraction (FE): aqueous feed phase dispersed								
FE-1; FE-2; FE-3	0.50	-	0.10	0.866	0.57	1.029	2.81	2.6
	0.00	-	0.00	0.848	0.47	0.991	0.67	34.7
FE-4; FE-3/4	0.50	0.01	0.10	0.866	0.58	1.035	2.84	2.6
	0.00	0.02	0.00	0.848	0.47	1.003	0.69	34.8
FE-5; FE-3/5	0.50	-	0.10	0.847	0.46	1.011	1.59	2.1
	0.00	-	0.00	0.829	0.38	0.984	0.46	33.5

	w_{CPL} (org)	w_{AS} (aq)	w_{CPL} (aq)	$10^{-3} \cdot \rho_c$ kg·m^{-3}	$10^3 \cdot \eta_c$ kg·m^{-1}·s^{-1}	$10^{-3} \cdot \rho_d$ kg·m^{-3}	$10^3 \cdot \eta_d$ kg·m^{-1}·s^{-1}	$10^3 \cdot \gamma$ N·m^{-1}
	Back-extraction (BE): organic feed phase dispersed							
BE-1; BE-2; BE-3	0.15	-	0.28	1.023	2.65	0.896	0.84	7.3
	0.00	-	0.00	0.998	1.02	0.868	0.59	35.8
BE-4; BE-2/4; BE-3/4	0.15	-	0.28	1.012	1.52	0.876	0.64	7.1
	0.00	-	0.00	0.991	0.67	0.848	0.47	34.7

The physical properties of the quaternary system water + caprolactam + ammonium sulfate + toluene were correlated by the equations as presented in Chapter 2. These correlations cover the entire range of concentrations and temperatures applied in this study, except for the interfacial tension. The equation for the latter is only valid for concentrations of caprolactam in the organic phase from 0 up to 5 mass %. For conditions with higher concentrations of caprolactam the relation was therefore extrapolated to determine the interfacial tension. The equilibrium distribution ratios, m_D and K_D', were based on equilibrium data, see Chapter 2 and described as function of the feed-phase concentration by relevant first or second order polynomials. The mass fraction of caprolactam in both the organic and aqueous phase and of ammonium sulfate in the aqueous phase was determined as described in Chapter 2.

5.4 Experimental results and data correlation

5.4.1 Concentration profiles

The influence of the operational conditions as presented in Table 5.1 on the concentration profiles of both processes was investigated. The resulting experimentally determined concentration profiles for the forward and back-extraction are shown in Figure 5.3.

(a)

(b)
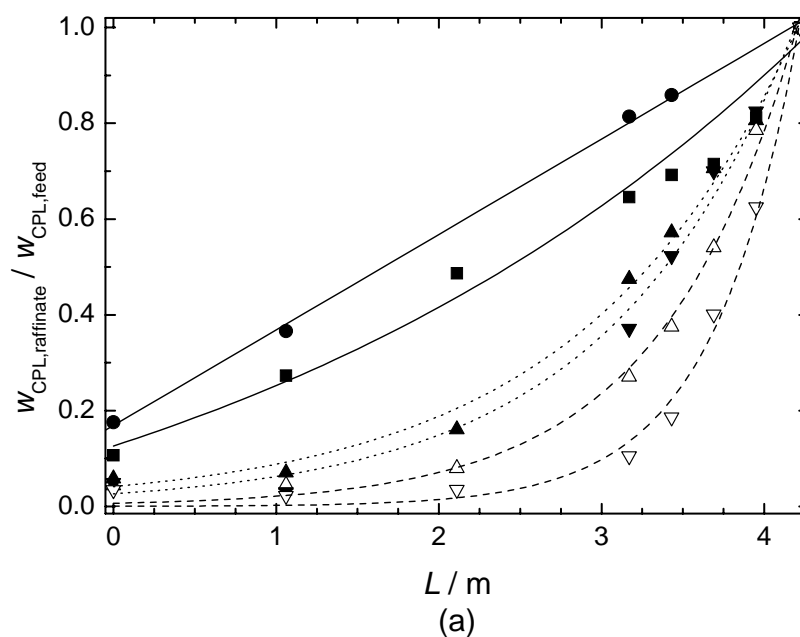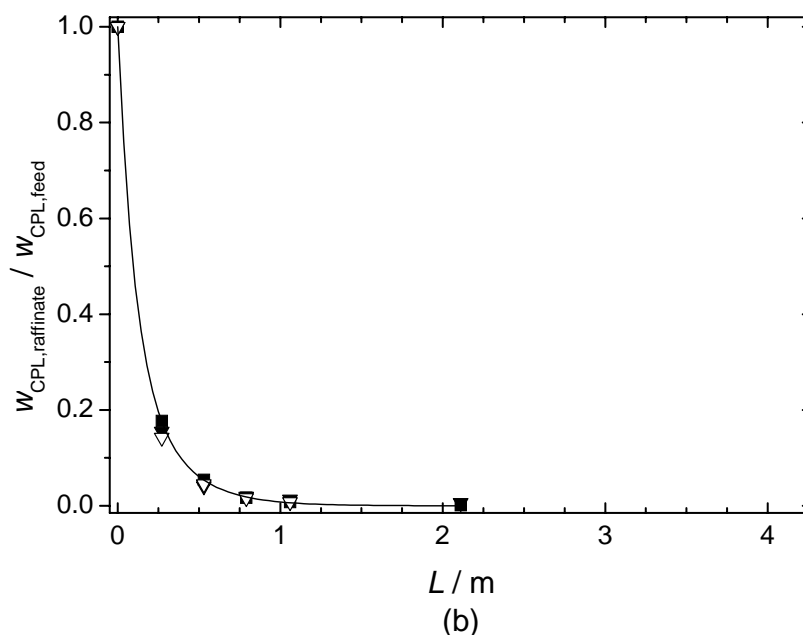
Figure 5.3. Experimental concentration profiles in the forward extraction (a) as function of the position along the column, where $T = 313$, $f \cdot S_p = 0.016$, $w_{AS,aq} = 0.00$ and Flux = 20 (■), unless stated otherwise: ●, Flux = 26; ▲, $w_{AS,aq} = 0.01$; △, $w_{AS,aq} = 0.01$ and $f \cdot S_p = 0.022$; ▼, $T = 333$; ▽, $T = 333$ and $f \cdot S_p = 0.022$; and for the back-extraction (b) where $T = 293$, $f \cdot S_p = 0.016$, and Flux = 20 (■), unless stated otherwise: ▼, $T = 313$; ▽, $T = 313$ and $f \cdot S_p = 0.022$ (where T/K; Flux/m·h^{-1}; $f \cdot S_p$/m·s^{-1}). All presented lines are trend lines.

In the forward extraction process the influence of operational parameters can be distinguished clearly. The influence of flux can be attributed to an increase of the convective flow relative to the mass transfer rate, although the latter increased slightly because of an increase in the hold-up, as expected from the hydraulic tests. The influence of ammonium sulfate and temperature results in a change of system properties. This affects both the hold-up and drop size, but the main influence results from the distribution ratio that increases favourable to the solvent (y) phase, resulting in a larger driving force for mass transfer. It has to be noted that in case ammonium sulfate was present in the feed, its concentration increased with a decreasing concentration of caprolactam, which evidently affected the system properties. The influence of pulsation intensity is directly related to a decrease in the drop size, resulting in an increase of the hold-up and interfacial area and therefore of the mass transfer rate.

In the back-extraction process, the concentration profiles for all operational conditions were comparable. This is probably the result of the highly favourable distribution ratio, resulting in a large driving force for mass transfer.

For the experimental results it was found that the overall mass balance of caprolactam contained an average error of 6.2% and 3.9% for the forward and back-extraction process, respectively. According to the plug flow model the mass balance over the feed and extract side of the column and a random cross-section in the column should fit. Calculating this mass balance based on the experimental results an average error comparable to the error in the overall mass balance should be found. Since the transfer of caprolactam is complete in the back-extraction, the amount of caprolactam in the feed and extract is equal. Therefore, the amount passing a random cross-section in the column in both phases should be equal as well.

Calculating for the back-extraction the error in the amount of caprolactam passing at S1-1, S1-2 and S1-3, reflecting a column position of 0.32 m, 0.58 m and 0.84 m, respectively, average errors of 45%, 44% and 54% are obtained. Calculating for the forward extraction the error in the mass balance of caprolactam over the feed and extract and the streams passing at S4-3, S4-2 and S4-1, reflecting a column position of 4.02 m, 3.76 m and 3.50 m, respectively, average errors of 16%, 14% and 13% are obtained. This strong increase of the error in the mass balance according to the plug flow model is likely to be caused by the effect of backmixing of one or both phases.[7]

5.4.2   Determination of mass transfer influence on the hydraulic parameters

The influence of mass transfer on the drop size, regime transition and hold-up relative to the equilibrium situation, as discussed in Chapter 4, was determined experimentally.

The measured relative increase of the drop size for the forward and back-extraction process was 1.4 ± 0.1 and 1.9 ± 0.1, respectively (accuracy determined as standard deviation). It was furthermore observed that when mass transfer was negligible at the raffinate side of the column, the relative increase of the drop size approached 1.0. The drop size was therefore described using the relation derived for the equilibrium situation including the determined factors to account for the relative increase of the drop size due to mass transfer.

The increase in the required pulsation intensity for the transition from the mixer-settler to the dispersion regime was determined experimentally. From the observed operating regimes the relative increase was fitted at a minimum and maximum value for both the forward and back-extraction. The minimum value was obtained for the conditions at the upper observation of the mixer-settler regime. The maximum value was accordingly obtained for the first observation of the dispersion regime. The relative increase in pulsation intensity for the forward extraction was 1.15 to 1.20 and in the back-extraction 1.5 to 1.6. From experimental observation and the determined relative increase under mass transfer conditions it was found for all experimental conditions in both the forward and the back-extraction that at the feed side of the column the operation started in the emulsion or dispersion regime. Moving along the column, however, the regime changed from dispersion to mixer-settler, except at increased pulsation intensities in the back-extraction. The regime transition was described using the relation derived for the equilibrium situation including the determined factors to account for the influence of mass transfer.

The relative decrease in the hold-up under mass transfer was experimentally determined, where it has to be taken into account that the expression used for the hold-up is not valid in the mixer-settler regime. Hold-up values determined in this regime were therefore excluded, using the equation for regime transition under mass transfer conditions to distinguish between these regimes. In the dispersion or emulsion regime the determined relative decrease of the hold-up for the forward and back-extraction was 0.83 ± 0.08 and 0.88 ± 0.02 (accuracy determined as standard deviation), respectively. As described, for both processes large parts of the column were operated in the mixer-settler regime, which results in an increase of the hold-up (see Chapter 3). Mixer-settler operation and mass transfer therefore counter-act each

other with respect to the hold-up profile. Since insufficient data was available to describe both effects, it was chosen to describe the hold-up profile over the column with the equation derived for the equilibrium situation.

The increase of the drop size under mass transfer conditions resulted in an increase of the pulsation intensity required for regime transition and a decrease of the hold-up compared to the equilibrium system, see Chapter 3 and Chapter 4. An attempt was made to interpret the latter two effects quantitatively from the increase of the drop size. The enhanced drop size coalescence under mass transfer conditions is often interpreted as a result of an interfacial tension gradient.[6,17,20,21] It was now assumed that the overall effect of this gradient, reflected in the relative increase of the drop size, could be described as a result of a relative increase in the interfacial tension. Using this approach the effect of mass transfer on the interfacial tension could be predicted from the determined increase of the drop size via $d_{32} = f(\gamma^{0.5+n_4})$ where $n_4 = 0.06$ (Equation (3–2)). The relative increase in the interfacial tension because of mass transfer was predicted at 1.77 and 3.11 in the forward and back-extraction, respectively. The effect of mass transfer on regime transition and hold-up can now be predicted, introducing the calculated interfacial tension increase in the equations for the equilibrium situation. The relative increase in the pulsation intensity required for the regime transition was predicted at 1.21 for the forward extraction and at 1.45 for the back-extraction. The relative decrease of the hold-up was predicted at 0.89 for the forward extraction and at 0.82 for the back-extraction. Comparing the determined and predicted effects based on the increase of the drop size, it can be seen that the approach used resulted in an accurate interpretation.

5.5   Model results

Back-extraction. In the back-extraction all caprolactam is extracted and the values for the axial dispersion coefficient in the continuous phase, α_y, and the overall mass transfer coefficient, k_{ox}, were fitted by minimizing the value of the absolute average error (AAE), see Table 5.3 for the results. Furthermore, the values of k_{ox} predicted with Equations (5–6) to (5–8) are shown for the experimentally determined range of caprolactam concentrations, together with the determined values of the Height Equivalent of a Theoretical Stage (HETS). The experimental conditions (Exp.) were $T/K = 293$, $f \cdot S_p / \text{m} \cdot \text{s}^{-1} = 0.016$, $\text{Flux} / \text{m} \cdot \text{h}^{-1} = 20$ (BE-1), unless stated otherwise, and the flow ratio was always $R = 2.9$.

From the fit results it was found that the introduction of a fitted value of the backflow parameter for the continuous phase resulted in a decrease of about 50% in the AAE value compared to the case where $\alpha_y = 0$. Furthermore it was found that for all experiments a range existed for $\alpha_y \pm 1.2$ where AAE was within 10% of the minimum AAE value. This observation results partly from the fact that the fitted k_{ox} values are dependent on the set α_y value, since the effect of backmixing and mass transfer on the concentration profile are coupled. It is therefore desirable to determine the backflow parameters, α_x and α_y, from separate experiments. Furthermore it can be questioned whether the measured concentration profiles were determined accurately enough in order to make a viable distinction between the fit results, since all experimentally determined concentration profiles for the back-extraction

were comparable. Finally, it can be seen in Table 5.3 that the fitted values of k_{ox} are within the predicted range based on Equations (5–6) to (5–8) for all experiments.

With respect to the influence of the operational parameters on the fitted and predicted values several observations can be made. It is shown that a decrease in flux resulted in an increase in the backflow parameter while the value for k_{ox} remained unchanged, as was predicted for the latter. The determined increase in HETS points at a decreasing time for mass transfer. A temperature increase, however, did not affect the determined α_y values, but did result in an increase of k_{ox}, which was predicted as well. The trend shown at increased pulsation intensities is controversial. For BE-3 the value for α_y increased slightly compared to BE-1, while the value for k_{ox} was similar. BE-3/4, however, shows the opposite behaviour compared to BE-4. For an increase in the pulsation intensity the value for k_{ox} was expected to increase and an increased overall mass transfer rate was observed based on the HETS values.

Table 5.3. Determined k_{ox} and α_y values at the fitted minimum AAE value in the back-extraction together with the predicted k_{ox} values using Equations (5–6) to (5–8).

	Exp.			α_y	$10^5 \cdot k_{ox}$		HETS
	Flux m·h^{-1}	$f \cdot S_p$ m·s^{-1}	T K	fit	fit m·s^{-1}	predicted m·s^{-1}	m
BE-1	20	0.016	293	4.2	4.5	3.2 - 5.9	0.37
BE-2	12	0.016	293	6.7	5.0	3.0 - 5.5	0.41
BE-3	20	0.022	293	5.1	4.6	3.6 - 6.5	0.33
BE-4	20	0.016	313	4.6	6.8	4.9 - 10.2	0.30
BE-2/4	12	0.016	313	6.4	6.5	5.0 - 9.6	0.35
BE-3/4	20	0.022	313	4.4	5.5	5.7 - 11.3	0.29

From the fitting procedure, profiles in the concentration of caprolactam, Sauter drop diameter and hold-up were obtained for the different operational conditions. These profiles are presented in Figure 5.4 for BE-1 and BE-4 as function of the normalized position within the column, L/L_c. As already concluded from the experimental concentration profiles in Figure 5.3, the influence of operational parameters on these profiles was negligible, which was represented by the model results in Figure 5.4 (a). Furthermore it can be seen that the plug flow model, represented by the dotted line, shows a significant deviation from the optimized fit, especially for the extract phase. As expected, the calculated profiles in drop diameter and hold-up shown in Figure 5.4 (b) change significantly over the column length. This is directly related to the influence of the concentration of caprolactam on the physical properties and the phase flow rates at each stage in the column. The calculated profiles present values in line with the experimental data.

Figure 5.4. Normalized concentration profiles over the normalized column position (a) where in the raffinate phase: ■, $T = 293$, $f \cdot S_p = 0.016$, Flux = 20 and $R = 2.9$ (BE-1); ▲, $T = 313$ (BE-4); and the corresponding open symbols for the extract phase; and the fit of: —, BE-1; --, BE-1 plug flow; ——, BE-4; and the drop diameter (d_{32}) and hold-up (x) profiles over the normalized column position (b) for: ■, d_{32} BE-1; ●, x BE-1; □, d_{32} BE-4; ○, x BE-4 and the fit of d_{32} and x for: —, BE-1; ——, BE-4 (where T/K; Flux/m·h^{-1}; $f \cdot S_p$/m·s^{-1}; d_{32}/m).

Forward extraction. In the forward extraction process the concentration of caprolactam present in the raffinate was not zero. At a set value of the axial dispersion coefficient in the continuous phase, α_y, the value of the overall mass transfer coefficient, k_{ox}, was therefore fitted in order to comply with the determined raffinate concentration. It has to be noted, however, that this approach suffers from the drawback that the uncertainty in the raffinate concentration affects the entire profile. Increasing the value of α_y for $0 < \alpha_y < 6$ results in a decreasing value of AAE. Since an even further increase of the α_y value seemed unrealistic, no minimum AAE value was obtained. The range of fitted k_{ox} values is shown in Table 5.4,

together with the predicted range of k_{ox} values for the experimentally determined range of caprolactam concentrations from Equations (5–6) to (5–8) at $\alpha_y = 3$ and the determined HETS/m values. The experimental conditions (Exp.) were $T/\text{K} = 313$, $f \cdot S_p/\text{m} \cdot \text{s}^{-1} = 0.016$, Flux/m·h^{-1} = 20 (FE-1), unless stated otherwise, and the flow ratio was always $R = 5.5$.

Table 5.4. Determined k_{ox} and HETS values at the investigated range of α_y in the forward extraction, together with the predicted k_{ox} values via Equations (5–6) to (5–8).

	Exp.				α_y	$10^5 \cdot k_{ox}$		HETS
	Flux	$f \cdot S_p$	T	$w_{AS,aq}$	fit	fit	predicted	
	m·h^{-1}	m·s^{-1}	K			m·s^{-1}	m·s^{-1}	m
FE-1	20	0.016	313	-	-	1.1 - 1.3	1.1 - 1.8	0.55
FE-2	26	0.016	313	-	-	0.8 - 0.9	1.2 - 1.9	0.67
FE-3	20	0.022	313	-	-	1.2 - 1.7	1.2 - 2.0	0.42
FE-4	20	0.016	313	0.01	-	1.3 - 1.5	0.9 - 1.8	0.43
FE-3/4	20	0.022	313	0.01	-	1.1 - 1.5	1.0 - 2.0	0.35
FE-5	20	0.016	333	-	-	1.6 - 1.9	1.4 - 2.5	0.47
FE-3/5	20	0.022	333	-	-	1.7 - 2.0	1.6 - 2.8	0.32

From Table 5.4 it can be concluded that the fitted k_{ox} values are comparable to the predicted range according to Equations (5–6) to (5–8) for all experiments. Furthermore an influence of operational conditions on the determined HETS values similar to the trends observed for the back-extraction can be seen. An increase of the flux resulted in an increasing HETS, because of an increase in the convective flow relative to the mass transfer rate, whereas a temperature increase, the addition of ammonium sulfate and a pulsation intensity increase resulted in a decreasing HETS, because of changing system properties for the first two and an increasing interfacial area for the latter. The obtained values and trends are comparable to those obtained for the forward extraction in a reciprocating plate column of 0.05 m diameter and 4.0 m height, with HETS/m values of 0.43 to 0.63, although in that study both higher fluxes and pulsation intensities were used.[2]

From the fitting procedure profiles in the concentration of caprolactam, drop diameter and hold-up were obtained for the different operational conditions and the resulting profiles for FE-1 and FE-3/4 at $\alpha_y = 3$ are presented in Figure 5.5 as function of the normalized position within the column, L/L_c. It can be seen that the raffinate concentration at the column exit was described correctly by the model results. Furthermore it can be seen that the calculated drop diameter and hold-up profiles change significantly over the column length, which is directly related to the influence of the concentration of caprolactam. The calculated drop diameter and hold-up profiles values in Figure 5.5 (b) correlate well with the experimental data.
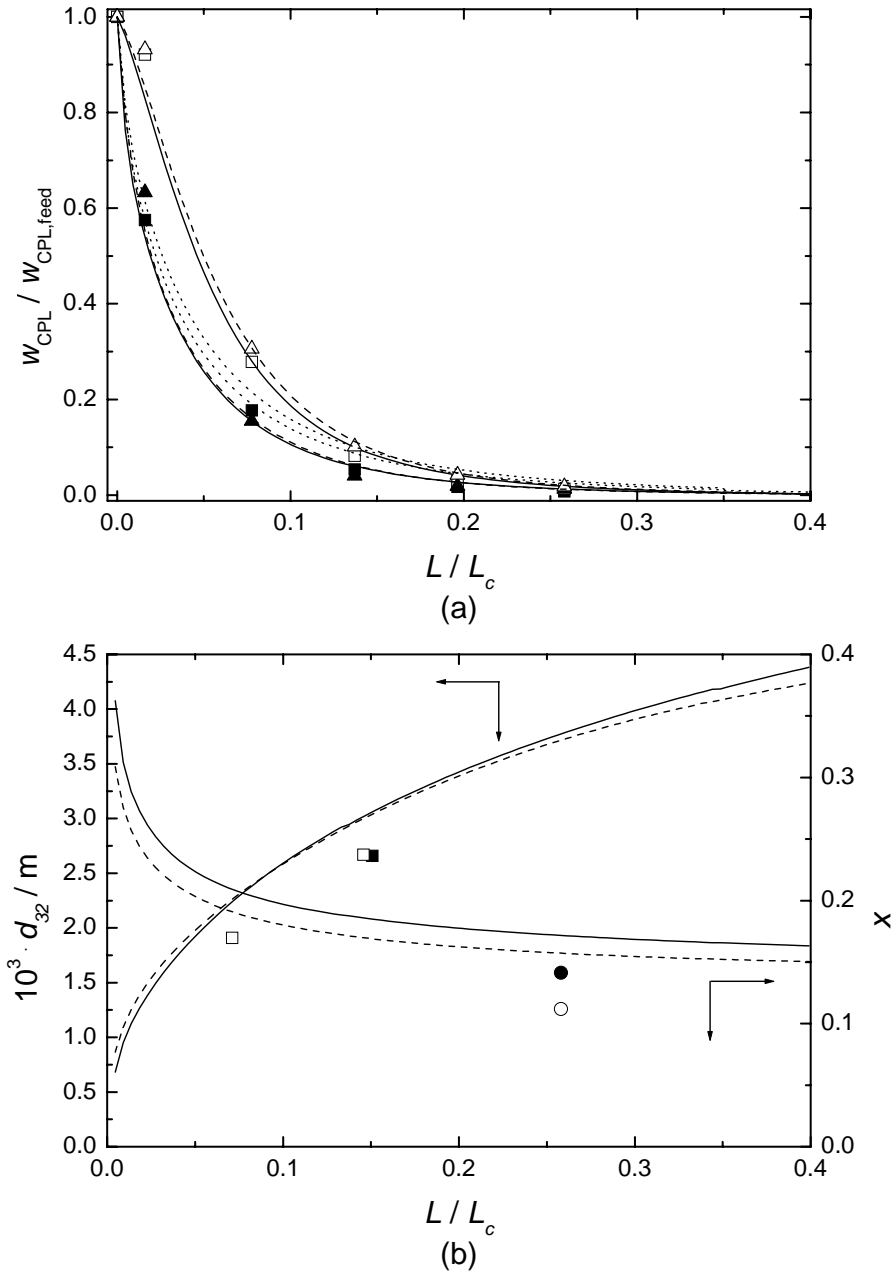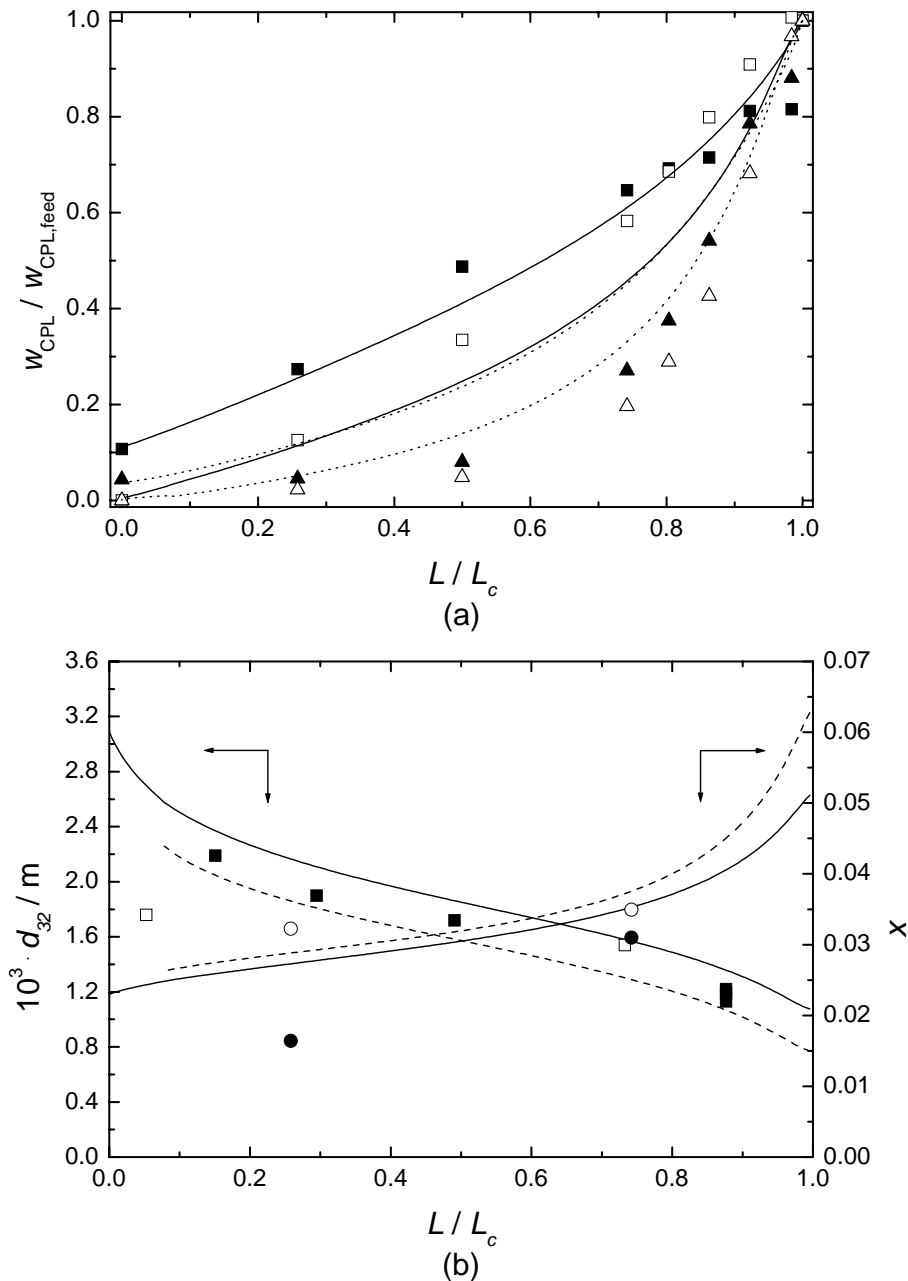
Figure 5.5. Normalized concentration profiles over the normalized column position (a) where in the raffinate phase: ■, $T = 313$, $f \cdot S_p = 0.016$, Flux = 20 and $R = 5.5$ (FE-1); ▲, $T = 313$ and $f \cdot S_p = 0.022$ (FE-3/4); and the corresponding open symbols for the extract phase; and the fit of: —, FE-1; --, FE-3/4; and the drop diameter (d_{32}) and hold-up (x) profiles over the column length (b) for: ■, d_{32} FE-1; ●, x FE-1; □, d_{32} FE-3/4; ○, x FE-3/4 and the fit of d_{32} and x for: —, BE-1; ——, BE-4 (where T/K; Flux/m·h^{-1}; $f \cdot S_p$/m·s^{-1}; d_{32}/m).

In Figure 5.5 the concentration gradient at the feed side of the column is under-predicted, however. This results from the fitting procedure since the k_{ox} value is fitted in order to comply with the experimentally determined raffinate concentration. Minimization of the AAE value resulted in a far better description of the concentration gradient at the feed side of the column. The description of FE-3/4, where AAE was minimized, is shown in Figure 5.6.
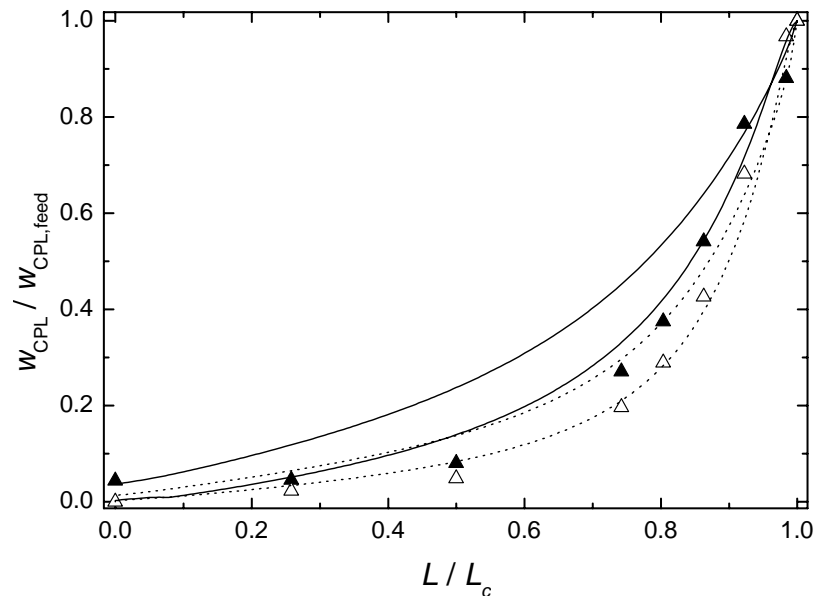
Figure 5.6. Normalized concentration profiles over the normalized column position for FE-3/4 (a) for: ▲, raffinate phase; △, extract phase and their model fits for: —, raffinate concentration fit; --, minimized AAE fit.

From Figure 5.6 it follows that, evidently, the concentration profile in both phases is described more accurately when the AAE value is minimized compared to the case where the α_y and k_{ox} values were fitted on the determined raffinate concentration. However, the calculated raffinate concentration is now 3.5 times lower than the experimentally determined value, which is a larger difference than the experimental uncertainty justifies. Furthermore it can be seen in Figure 5.3 (a) for the experiments in the forward extraction with a steep concentration gradient at the feed side, for $w_{AS,aq} = 0.01$, $f \cdot S_p/\text{m} \cdot \text{s}^{-1} = 0.022$, $T/\text{K} = 333$ or a combination of these, that the slope of the concentration profile at the raffinate end of the column was small. This behaviour was only partly described by minimizing the AAE value.

Another cause for the under-predicted concentration gradient at the feed side or the over-predicted efficiency at the raffinate side is the fact that a simplified model was used to describe the concentration profile. Finally, it should be taken into account that the raffinate side of the column was operated in the mixer-settler regime, which might have an influence as well. In this regime the hold-up increases compared to the dispersion regime (see Chapter 3), but the major part of the time the dispersed phase is situated on the internals as coalesced phase. The interfacial area and thus the mass transfer rate could therefore be decreased drastically. Since this effect was not taken into account in the model, the fitted k_{ox} value might be under-predicted in order to compensate for the over-predicted interfacial area in the raffinate side of the column. This effect might play a role as well in the back-extraction, but is probably masked by the large driving force for mass transfer and the fact that the k_{ox} value could freely be fitted in order to obtain a minimum AAE value.

5.6   Conclusions

The separation efficiency in relation to the operating conditions of a pulsed disc and doughnut column (PDDC) was evaluated for the back- and forward extraction of caprolactam in a pilot

set-up. In the forward extraction the separation efficiency was strongly influenced by the operational parameters, being flux, pulsation intensity, ammonium sulfate and temperature, whereas in the back-extraction the concentration profiles for all operational parameters were similar showing a complete extraction at about the middle of the column.

The PDDC showed qualitatively similar operational characteristics compared to the hydraulic operation at equilibrium, but mass transfer caused an increase of the drop diameter, a decreasing hold-up and a corresponding shift in the operational regime. These parameters could be described using the expressions derived for the hydraulic equilibrium situation including an additional factor to account for the effect of mass transfer.

The concentration profiles in both the forward and back-extraction were described using the backflow model, where a constant value for the overall mass transfer coefficient and the axial dispersion coefficient in the continuous phase was fitted using the derived equations for the Sauter drop diameter and hold-up. The back-extraction was described well using this approach, but in the forward extraction either the concentration gradient at the feed side of the column was under-predicted or the separation efficiency was over-predicted. This might be caused by the experimental uncertainty in the raffinate concentration, assumptions made in the model set-up, but also the mixer-settler operational regime can have an influence on the column performance, which was not taken into account in the model.

HETS values were determined for both the forward and back-extraction. For the latter HETS = 0.28 to 0.41 m. The obtained values in the forward extraction, HETS = 0.32 to 0.67 m, are comparable to those obtained in a reciprocating plate column, where HETS/m = 0.43 to 0.63.

Nomenclature

AAE	Average absolute error
a	Specific interfacial area, $m^2 \cdot m^{-3}$
$c_{i,n}$	Solute concentration at stage n, $kg \cdot m^{-3}$
c_x^*	Theoretical solute concentration in equilibrium with c_y, $kg \cdot m^{-3}$
D	Molecular diffusivity, $m^2 \cdot s^{-1}$
d_{32}	Sauter drop diameter, m
E	Extraction factor, $E = K_D' \cdot F_y' / F_x'$
e	Fractional free cross-sectional area, $e = 1 - D_d^2 / D_c^2$
F	Phase flow rate, $m^3 \cdot s^{-1}$
F_x', F_y'	Feed and solvent phase mass flow rates on solute free basis, $kg \cdot s^{-1}$
$f \cdot S_p$	Pulsation intensity, where f/s^{-1} denotes frequency and S_p/m stroke, $m \cdot s^{-1}$
Flux	Total throughput, $Flux = V_c + V_d$, $m \cdot h^{-1}$
g	Gravitational constant, $g/m^2 \cdot s^{-1} = 9.81$
H	Disc to doughnut spacing, m
h_c	Characteristic height, m
HETS	Height Equivalent of a Theoretical Stage, m

k_i	Mass transfer coefficient, m·s^{-1}
$K_D{}'$	Equilibrium distribution coefficient, $K_D{}' = w_y{}'/w_x{}'$
m_D	Equilibrium distribution coefficient, $m_D = c_x/c_y$
L	Position along the column length, m
L_c	Total column length, m
NTU	Number of Transfer Units, $\text{NTU}_{ox} = k_{ox}·a·h_c·s/F_x$
Pe_i	Peclet number, $\text{Pe}_j = d_{32}·V_{slip}/D_j$
R	Flow ratio, $R = V_d/V_c$
Re	Reynolds number, $\text{Re} = d_{32}·V_{slip}·\rho_c/\eta_c$
s	Column cross-sectional area, m^2
Sc_i	Schmidt number, $\eta_j/\rho_j D_j$
Sh_i	Sherwood number, $\text{Sh}_j = k_j·d_{32}/D_j$
Sh_r, Sh_∞	Sherwood number for rigid and circulating drops, respectively
T	Temperature, K
V_i	Velocity of phase or component i, m·s^{-1}
V_{slip}	Slip velocity, $V_{slip} = V_d/x + V_c/(1-x)$, m·s^{-1}
w	Weight fraction
w'	Weight fraction on solute-free basis
x	Dispersed phase hold-up defined as volume fraction of the dispersed phase

Greek letters

α	Backflow ratio
γ	Interfacial tension, N·m^{-1}
ε	Power dissipation per unit mass, W·kg^{-1}
η	Dynamic viscosity, $\text{kg·m}^{-1}·\text{s}^{-1}$
ρ	Density, kg·m^{-3}

Subscripts

c, d	Continuous and dispersed phase, respectively
extract	Extract phase
feed	Feed phase
i	Denoting phase x or y
o	Overall
raffinate	Raffinate phase
solvent	Solvent phase
x, y	Raffinate and extract phase, respectively

Literature cited

1. Alessi, V.; Penzo, R.; Slater, M. J.; Tessari, R. Caprolactam Production: a Comparison of Different Layouts of the Liquid-Liquid Extraction Section. *Chem. Eng. Tech.* **1997**, *20*, 445-454.

2. Prochazka, J.; Landau, J.; Souhrada, F.; Heyberger, A. Reciprocating-Plate Extraction Column. *British Chem. Eng.* **1971**, *16*, 42-44.

3. Xie, F.; Zhu, M.; Liu, J.; He, C. Extraction of Caprolactam from Aqueous Ammonium Sulfate Solution in Pulsed Packed Column Using 250Y Mellapak Packing. *Chinese J. Chem. Eng.* **2002**, *10*, 677-680.

4. Liu, J.; Xie, F.; He, C.; Zhu, M. Recovery of Caprolactam from Waste Water in Caprolactam Production Using Pulsed-Sieve-Plate Extraction Column. *Chinese J. Chem. Eng.* **2002**, *10*, 371-373.

5. Vasin, A. A.; Legochkina, L. A. Extraction of Caprolactam from an Ammonium Sulfate Solution in a Vibrating Plate Column. *Khim. Prom-st.* **1989**, *21*, 900-903.

6. Pratt, H. R. C. Current and Potential Developments in Methods for the Scale-Up and Design of Column extractors. *Min. Pro. Ext. Met. Rev.* **1998**, *18*, 215-282.

7. Pratt, H. R. C.; Stevens, G. W. Axial Dispersion, in: Thornton, J.D. (Ed.) *Science and Practise of Liquid-Liquid Extraction*. Oxford: Oxford University Press, 1992, pp. 416-491.

8. Jahya, A. B.; Stevens, G. W.; Pratt, H. R. C. Mass Transfer Studies for a Pulsed Disc and Doughnut Extraction Column, In *Proceedings of the International Congress on Mineral Processing and Extractive Metallurgy, 2000*; Australasian Institute of Mining and Metallurgy: Melbourne, 2000, pp. 281-284.

9. Kumar, A.; Hartland, S. Unified Correlations for the Prediction of Drop Size in Liquid-Liquid Extraction Columns. *Ind. Eng. Chem. Res.* **1996**, *35*, 2682-2695.

10. Kumar, A.; Hartland, S. A Unified Correlation for the Prediction of Dispersed-Phase Hold-up in Liquid-Liquid Extraction Columns. *Ind. Eng. Chem. Res.* **1995**, *34*, 3925-3940.

11. Al Khani, S. D.; Gourdon, C.; Gasamatta, G. Simulation of Hydrodynamics and Mass Transfer of a Disks and Rings Pulsed Column. *Ind. Eng. Chem. Res.* **1988**, *27*, 329-333.

12. Toutain, J.; Le Lann, J. M.; Gourdon, C.; Joulia, X. Maxwell-Stefan Approach Coupled Drop Population Model for the Dynamic Simulation of Liquid-Liquid Extraction Pulsed Column. *Comp. Chem. Eng.* **1998**, *22 Suppl.*, S379-S386.

13. Aoun Nabli, M. S.; Guiraud, P.; Gourdon, C. CFD Contribution to a Design Procedure for Discs and Doughnuts Extraction Columns. *Trans. IChemE.* **1998**, *76*, 951-960.

14. Aoun Nabli, M. S.; Guiraud, P.; Gourdon, C. Numerical Experimentation: a Tool to Calculate the Axial Dispersion Coefficient in Discs and Doughnuts Pulsed Extraction Columns. *Chem. Eng. Sci.* **1997**, *52*, 2353-2368.

15. Bardin-Monnier, N.; Guiraud, P.; Gourdon, C. Residence Time Distribution of Droplets within Discs and Doughnuts Pulsed Extraction Columns via Langrangian Experiments and Simulations. *Chem. Eng. J.* **2003**, *94*, 241-254.

16. Bardin-Monnier, N.; Guiraud, P.; Gourdon, C. Langrangian Simulations Contribution to the Knowledge of Discs and Doughnuts Pulsed Solvent Extraction Columns Hydrodynamics. *Chem. Eng. Proc.* **2003**, *42*, 503-516.

17. Hafez, M. M.; Baird, M. H. I.; Nirdosh, I. Flooding and Axial dispersion in Reciprocating Plate Columns. *Can. J. Chem. Eng.* **1979**, *57*, 150-158.

18. Steiner, L. Mass-Transfer Rates from Single Drops and Drop Swarms. *Chem. Eng. Sci.* **1986**, *41*, 1979-1986.

19. Kumar, A.; Hartland, S. Correlations for Prediction of Mass Transfer Coefficients in Single Drop Systems and Liquid-Liquid Extraction Columns. *Trans. IChemE.* **1999**, *77*, 372-384.

20. Baird, M. H. I.; Shen, Z. J. Holdup and Flooding in Reciprocating Plate Extraction Columns. *Can. J. Chem. Eng.* **1984**, *62*, 218-227.

21. Sternling, C. V.; Scriven, L. E. Interfacial Turbulence: Hydrodynamic Instability and the Marangoni Effect. *AIChE J.* **1959**, *5*, 514-523.

Chapter 6

Selection and evaluation of alternative solvents for caprolactam extraction

6.1   Introduction

Caprolactam is recovered from the neutralized Beckmann rearrangement mixture by phase separation followed by solvent extraction of the resulting crude caprolactam and aqueous ammonium sulfate layer. In industry benzene, toluene or chlorinated hydrocarbons are often used as the organic solvent. However, a growing awareness of the negative effects of these solvents on health and environment exists, resulting in extremely strict legislation, as described in Chapter 1.

Therefore the need exists for an environmentally benign solvent as replacement in the caprolactam extraction process. Thereby a solvent is demanded with a capacity towards caprolactam and a mutual solvent solubility comparable to the currently applied solvents or better.[1] Literature on alternative solvents is limited to 1-heptanol and 2-heptanone, where the influence of the concentrations of caprolactam and ammonium sulfate and temperature on phase compositions is described.[2,3] For cyclohexanol the binodal is determined at 293 K.[4] Furthermore the distribution ratio of caprolactam is investigated as function of the carbon chain length for a series of linear alcohols (C_5 to C_8) at limited experimental conditions.[5] These polar systems all show a favourable distribution ratio towards caprolactam, but also a relatively high mutual solvent solubility. Non-polar solvents possess a low mutual solubility, but show a non-favourable capacity towards caprolactam.[6]

The need for the replacement of solvents and the design of substitute candidates, because of strict environmental legislation and required specific solvent properties, resulted in various studies on general solvent selection procedures for the painting, cleaning and extraction industry,[7,8] specific procedures for extraction processes[9,10] and selection procedures for other applications.[11,12] The selection of alternative solvents can be performed empirically, theoretically or experimentally. Empirical methods generally compare one or more properties of the solvents to classify them and to assess the solvent capacity.[13,14] These methods, however, can only identify possible alternative solvent classes, but a specific solvent selection is not possible. Theoretical screening methods are based on a thermodynamic description of

the liquid-liquid system. Here, solvent selection is based on the solute distribution ratio, selectivity and mutual solvent solubility, which are calculated using a thermodynamic model.[13-17] For an overview of possible alternative solvents the Hansen model was used by plotting the δ_p against the δ_h parameter for each solvent, representing the dipole and hydrogen bonding interactions of this solvent, respectively. The comparison of solvent characteristics relative to caprolactam, which is presented as (0,0), is shown in Figure 6.1. Furthermore the Unifac Dortmund model[13,15,17] was initially applied for the prediction of distribution and mutual solubility data. Using the resulting model phase compositions could be calculated for the systems water + caprolactam + benzene, toluene, 1-heptanol or cyclohexane at 293 K. The calculated and experimentally determined concentrations of caprolactam at equilibrium[2] are presented in Figure 6.2.

From Figure 6.1 it can be concluded that several compounds with different functional groups are more polar than the current solvents for caprolactam, whereas the alkanes are less polar. It can also be seen that the structure of a molecule influences the polarity. Furthermore it is shown that no pure solvent is present with a polarity comparable to benzene. The more polar compounds show a larger capacity towards caprolactam and a higher mutual solubility, which is known from literature[2-5] and shown in Figure 6.2. The less polar compounds, the alkanes, show a lower capacity and mutual solubility. Since the characteristics of the alternative solvent should at least be comparable to benzene and toluene, solvent mixtures containing a polar solvent and an alkane are investigated, in order to combine the favourable and eliminate the negative properties of both solvent types. From Figure 6.2 it must be concluded, however, that the results from the Unifac Dortmund model are not accurate enough for solvent screening.
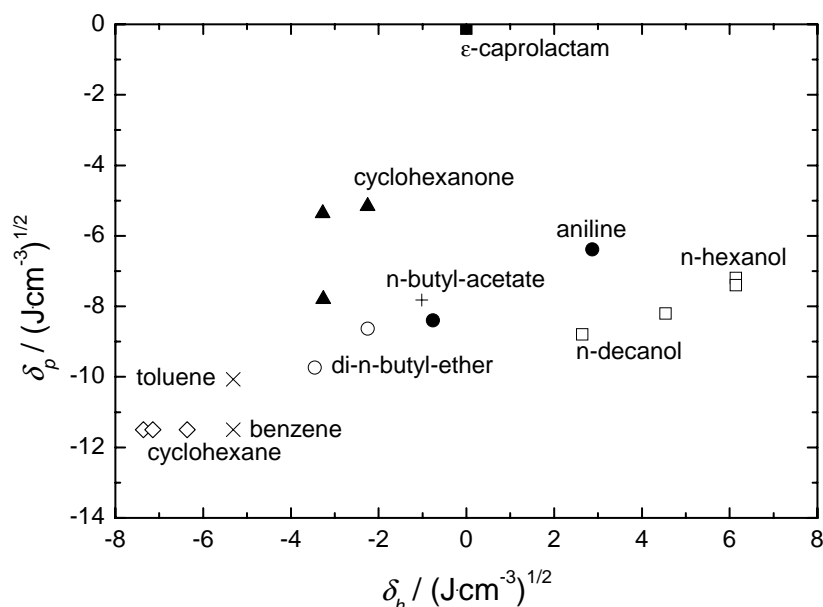
Figure 6.1. Comparison of characteristics based on δ_p and δ_h Hansen solubility parameters relative to caprolactam as origin (0,0), for solvents: ×, current solvents; ●, amines; ○, ethers; ▲, ketones; ◇, alkanes; +, esters; □, alcohols.
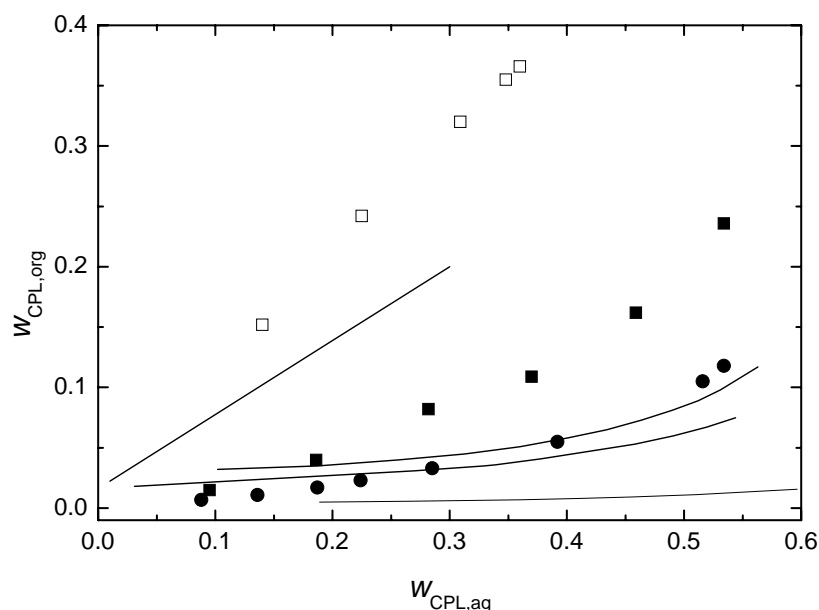
Figure 6.2. Experimentally determined (dots) equilibrium concentrations of caprolactam in the organic and aqueous phase and calculated values using the Unifac Dortmund model (lines) at 293 K for: ■, benzene; □, 1-heptanol;[2] ●, toluene and cyclohexane.

From Figure 6.1 and Figure 6.2 it can therefore be concluded that the solvent screening for an alternative solvent (mixture) needs to be performed experimentally. Next to phase composition data, physical properties, being density and viscosity of the separate liquid phases and interfacial tension of the liquid-liquid system, are needed for the description of extraction equipment.[1] Therefore, these have to be determined for the selection of the final solvent (mixture), taking into account the influence of caprolactam.

In the experimental screening procedure the distribution ratio of caprolactam at equilibrium between the aqueous and (mixed) solvent phase was investigated at 293 K for an initial 10 mass % aqueous caprolactam solution as function of the active group of various polar compounds (alcohol, ketone, ester, ether), their carbon chain length (C_6-C_{12}) and their concentration in a mixture with methylcyclohexane (MCH) or heptane. Solvents or solvent mixtures showing favourable capacities for caprolactam were selected based on the determined distribution ratios compared to benzene and toluene. For these (mixed) solvents the capacity and mutual solvent solubility were determined as function of the mass fraction of caprolactam in the aqueous phase ($w_{CPL,aq}$ = 0.0 to 0.6) at 293 K from which possible alternative solvents were selected. For the remaining alternatives the equilibrium phase compositions of the system water + caprolactam + ammonium sulfate + (mixed) solvent were determined at 293 K, 313 K and 333 K. The experimentally determined phase compositions were described using the NRTL model. Furthermore density and viscosity data of the separate phases and interfacial tension data of the systems studied were determined and correlated.

6.2   Experimental set-up and procedure

Equilibrium and physical properties measurements. To obtain phase equilibrium data the experimental set-up and procedure as described in Chapter 2 were used. The mass fraction of caprolactam in both the organic and the aqueous phase, the mass fraction(s) of the solvent(s) in the aqueous phase and of the polar solvent in the organic phase (in case of a solvent mixture) was determined by gas chromatography (Chapter 2). For each (mixed) solvent the same analytical method was applied, except for the temperature profile and column pressure, which were optimised for each system. The mass fraction of ammonium sulfate in the aqueous phase and of water in the organic phase was determined as described in Chapter 2.

Densities, kinematic viscosities and the interfacial tension were determined as function of the concentration of caprolactam at 293 K, 313 K and 333 K for the selected (mixed) solvents and the ternary systems water + caprolactam + solvent (mixture), respectively, using the procedures as described in Chapter 2.

Chemicals. All chemicals were used as received. These are: ε-caprolactam (purity 99%), ammonium sulfate (purity > 99%), di-propyl-ether (purity > 99%), propyl-butyrate (purity 99%), 2-heptanone (purity 99%), 5-nonanone (purity 98%), methylcyclohexane (purity > 99%) by Sigma-Aldrich (USA), butyl-butyrate (purity > 98%) and n-heptane (purity > 99%) by Merck (Germany), di-hexyl-ether (purity > 97%), di-butyl-ether (purity > 99%) by Fluka (Germany) and di-pentyl-ether (purity 99%), 3-octanone (purity 99%), 2-methylcyclohexanol (purity 99%) and 1-heptanol (purity 98%) by Acros (Belgium). MiliQ water was used in all experiments.

Data analysis. Using the described analytical methods the amount of solute and the mutual solvent solubility (in mass fractions) were determined in the organic and aqueous phase with the described uncertainties. The mass fraction of water in the aqueous phase and of the solvent (in case of a pure solvent) or the alkane fraction in the organic phase (in case of a solvent mixture) was finally determined from the mass balance. The mass fraction of ammonium sulfate in the organic phase was assumed to be negligible. The distribution ratio of a solute i, $K_{D,i}$, is defined as the ratio of the determined solute mass fractions at equilibrium in the organic phase, $w_{i,\text{org}}$, and in the aqueous phase, $w_{i,\text{aq}}$:

$$K_{D,i} = \frac{w_{i,org}}{w_{i,aq}} \qquad\qquad (6\text{--}1)$$

This distribution ratio represents the capacity of a solvent system in the extraction of caprolactam and was used for interpretation and evaluation of the experimental results.

6.3   Solvent screening results

In Figure 6.3 the results are shown for the distribution ratio of caprolactam, $K_{D,\text{CPL}}$, of the systems water + caprolactam + (mixed) solvent at 293 K for an initial 10 mass % aqueous

caprolactam solution as function of the equilibrium polar solvent mass fraction in the organic phase.
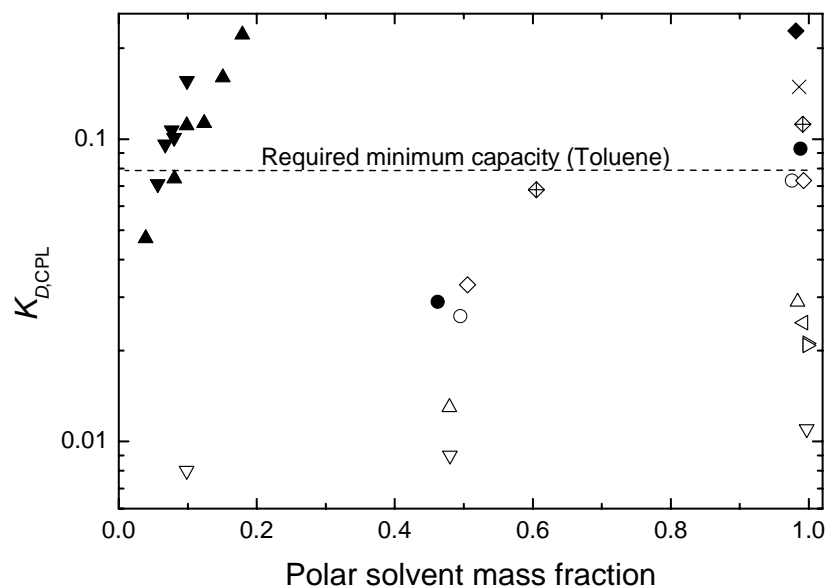
Figure 6.3. $K_{D,CPL}$ as function of the polar solvent fraction in MCH for: ▽, di-hexylether; ▷, di-butylether; ◁, di-pentylether; △, di-propylether; ○, butyl-butyrate; ●, propyl-butyrate; ◇, nonanone, ⊕, octanone; ◆, heptanone; ▼, methylcyclohexanol; ▲, heptanol; ×, benzene and --, toluene as reference at 293 K and $w_{CPL,aq}$ = 0.10 initially.

The data presented in Figure 6.3 are compared with the equilibrium distribution ratio for benzene and toluene at similar conditions. The amount of caprolactam extracted was increased with increasing polarity of the organic phase. This was shown by an increase of the distribution ratio at higher concentrations of polar solvent, at shorter carbon chains, which trend was observed in literature before,[5] and a more polar functional group. The distribution ratio with toluene as solvent, visualised as dashed line, was used to represent the minimal required capacity for a system. From Figure 6.3 it could be concluded that several solvents or solvent mixtures showed an acceptable to favourable distribution ratio relative to toluene. These solvents were heptanone, which was already known to possess a too high mutual solvent solubility,[3] propyl-butyrate, octanone and the solvent mixtures with heptanol and methylcyclohexanol. The latter three solvents were therefore further investigated. The equilibrium distribution ratio and mutual solubility for the solvent systems octanone, MCH-heptanol (15 mass % initially) and MCH-methylcyclohexanol (12 mass % initially) were investigated at 293 K and concentrations of caprolactam in the aqueous phase up at equilibrium to 50 mass %. The distribution ratio for these systems as function of the concentration of caprolactam in the aqueous phase at equilibrium compared to the values for benzene and toluene is shown in Figure 6.4.

From Figure 6.4 it was concluded that, although the selected solvent systems showed favourable capacities at low concentrations of caprolactam, the capacity at high concentrations of caprolactam was below that of toluene. The capacity of the alternative solvent therefore needs to be increased.
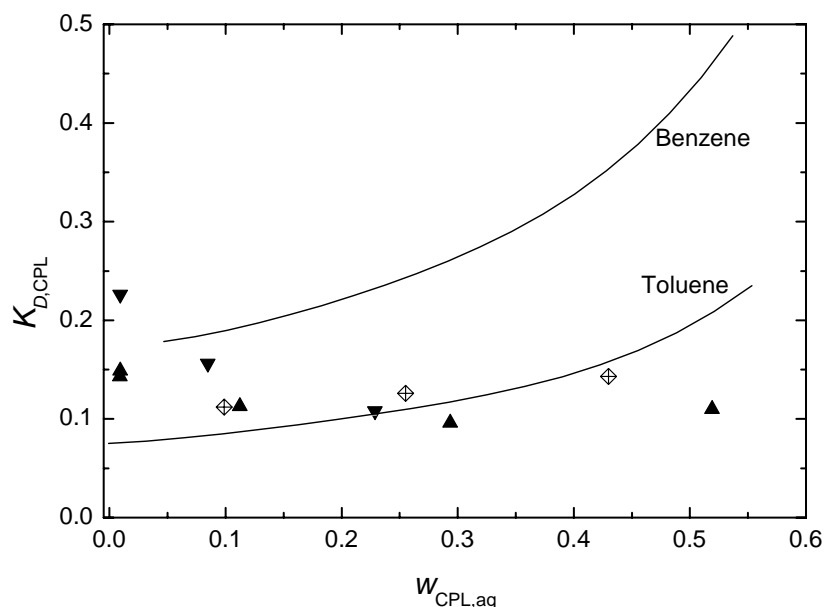
Figure 6.4. $K_{D,CPL}$ as function of $w_{CPL,aq}$ for: ◈, octanone; ▲, MCH-heptanol (15 mass % initially); ▼, MCH-methylcyclohexanol (12 mass % initially); —, benzene and toluene as reference at 293 K.

For the solvent mixtures it was known from Figure 6.3 that the distribution ratio of caprolactam increased with an increasing concentration of polar solvent in the organic phase. For the alcohol mixtures shown in Figure 6.3 the polar solvent fraction could be increased further, whereas octanone already was used as pure solvent. It was therefore investigated whether the concentration of alcohol in the mixed solvents could be increased such that at high concentrations of caprolactam a capacity comparable to benzene and toluene was obtained, without increasing the mutual solvent solubility too much. Since the fractional loss of alcohol to the aqueous phase for the MCH-methylcyclohexanol system was already 0.015 at $w_{CPL,aq} = 0.2$ and an alcohol fraction of 0.1 in the organic phase, it was expected that at higher concentrations of alcohol and caprolactam the mutual solubility would be too high. It was therefore investigated if in the system MCH-heptanol the alcohol content could be increased in order to obtain a suitable solvent concentrations of caprolactam in the aqueous phase up to 50 mass % at equilibrium. The distribution ratio of caprolactam as function of the concentration of caprolactam in the aqueous phase at initial concentrations of alcohol in the organic phase of 5, 15, 20, 30 and 40 mass % at 293 K is shown in Figure 6.5. It can be concluded that the amount of caprolactam extracted to the organic phase increased strongly with the amount of alcohol in the organic phase, as already expected from Figure 6.3. In comparison to the distribution ratio in toluene at 293 K a mixed solvent with initially 40 mass % heptanol showed a higher extraction capacity. Relative to benzene the distribution ratio is comparable. The concentration of alcohol was not increased further, since increasing the alcohol content would, next to an increase of the distribution ratio of caprolactam, also result in a further increase of the mutual solvent solubility. Based on Figure 6.5 the methylcyclohexane-heptanol (40 mass % initially) mixed solvent was selected as candidate alternative solvent for benzene and toluene and this candidate solvent mixture was characterized further.
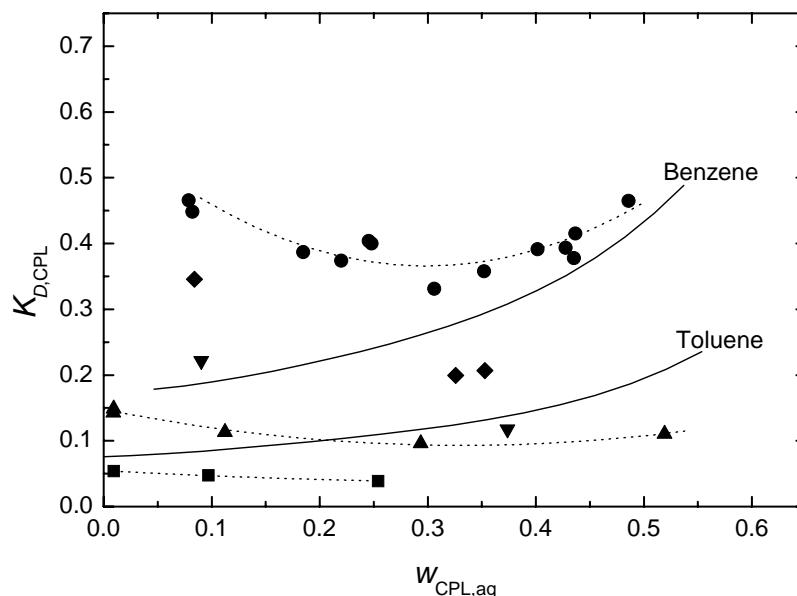
Figure 6.5. $K_{D,CPL}$ as function of the mass fraction of caprolactam in the aqueous phase for MCH-heptanol mixtures having initial heptanol mass fractions of: ■, 0.05; ▲, 0.15; ▼, 0.20; ◆, 0.30; ●, 0.40; —, benzene and toluene as reference at 293 K.

6.4   Solvent characterization results and data correlation

The characterization of the selected mixed solvent was performed by determining phase compositions at equilibrium of the system water + caprolactam + ammonium sulfate + MCH + heptanol (40 mass % initially) at 293 K, 313 K and 333 K. Furthermore the influence of the alkane structure on the system behaviour was determined by replacing methylcyclohexane with heptane. The experimentally determined phase compositions for both mixed solvents were described using the NRTL model. Furthermore density and viscosity data of the separate phases and interfacial tension data for both mixed solvents were determined and correlated.

6.4.1   Equilibrium experiments

Tables B1 and B2 (see Appendix B) present the liquid-liquid equilibrium data of the systems water (1) + caprolactam (2) + ammonium sulfate (3) + methylcyclohexane (4) + heptanol (5), respectively heptane (4) + heptanol (5), at 293 K, 313 K and 333 K. The determined phase equilibrium data for the described systems were correlated with the NRTL model using the approach of De Haan and Niemann, which was used to describe the phase compositions of the quaternary systems water + caprolactam + ammonium sulfate + benzene, respectively toluene, at 293 K to 333 K, as presented in Chapter 2. The influence of ammonium sulfate on the system behaviour was not fitted, since there were not enough data points available. The five NRTL parameters for all component pairs were determined via data regression using ASPEN Plus 11.1. Therefore the quaternary systems water + caprolactam + MCH + heptanol, respectively heptane + heptanol, were simplified to water + caprolactam + solvent, where the solvent was defined as pseudo-component in ASPEN with a mass based average molecular weight and a density, which was determined experimentally. The interactions for the resulting ternary system were determined from the corresponding ternary phase equilibrium data. The

values of the fitted NRTL parameters are listed in Table 6.1, where these parameters were used for the description of both mixed solvents. Initially the values for the CPL-Water interaction were taken as described in Chapter 2, but eventually the interaction parameters were fitted in order to obtain a good description. The different interaction parameters for CPL-Water for this system compared to those for the system water + caprolactam + benzene or toluene are the result of the possible influence of ternary interactions and of the fact that the interactions of the quaternary systems used are simplified to those of ternary systems.

Table 6.1. Fitted NRTL interaction parameters for the description of liquid-liquid phase equilibria of the systems water + caprolactam (CPL) + solvent at 293 K to 333 K, where the solvent is methylcyclohexane-heptanol (40 mass % initially) or heptane-heptanol (40 mass % initially).

Binary parameter	α_{ij}	a_{ij}	a_{ji}	b_{ij}/K	b_{ji}/K
CPL+Water	0.300	273.8	-10.21	-6123	2282
CPL+Solvent	0.300	-5.056	109.5	1170	4400
Water+Solvent	0.200	-16.52	0.227	7444	338.9

Both solvents are well correlated by the NRTL model. The uncertainty in the fitted data was described with the average absolute deviation (AAD) between the experimental and fitted phase compositions at equal concentrations of caprolactam in the aqueous phase. For the MCH-heptanol and heptane-heptanol systems the AAD for the mass fractions of caprolactam in the organic phase was 8.7×10^{-3} and 1.6×10^{-2}, for water in the organic phase it was 4.9×10^{-3} and 7.8×10^{-3}, and for the solvent in the aqueous phase it was 1.6×10^{-2} and 1.3×10^{-2}.

Experimental and calculated phase compositions of the systems water + caprolactam + solvent for MCH + heptanol and heptane + heptanol at 293 K are presented in Figure 6.6.
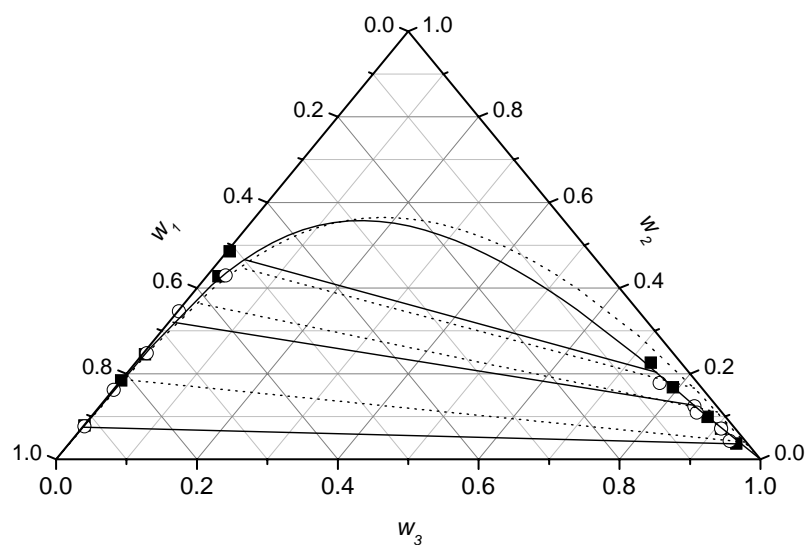
Figure 6.6. Equilibrium phase compositions (mass fractions) at 293 K for the ternary systems water (1) + caprolactam (2) + solvent (3) for the solvents: ■, MCH-heptanol (40 mass % initially); ○, heptane-heptanol (40 mass % initially); —, NRTL fit solvent; --, benzene as reference.

It can be concluded from this figure that the amount of water in the organic phase for both solvents is slightly higher than for benzene and that consequently the two-phase region for both alternative solvents is slightly smaller than for benzene.

The influence of temperature on the experimental and calculated equilibrium data for caprolactam for the MCH + heptanol system is shown in Figure 6.7, relative to benzene. It can be concluded that the concentration of caprolactam in the organic phase is increased considerably at elevated temperatures and that it is higher for the mixed solvent than for benzene at low concentrations of caprolactam ($w_{CPL,aq} < 0.3$) and comparable to benzene at high concentrations of caprolactam ($w_{CPL,aq} > 0.3$).
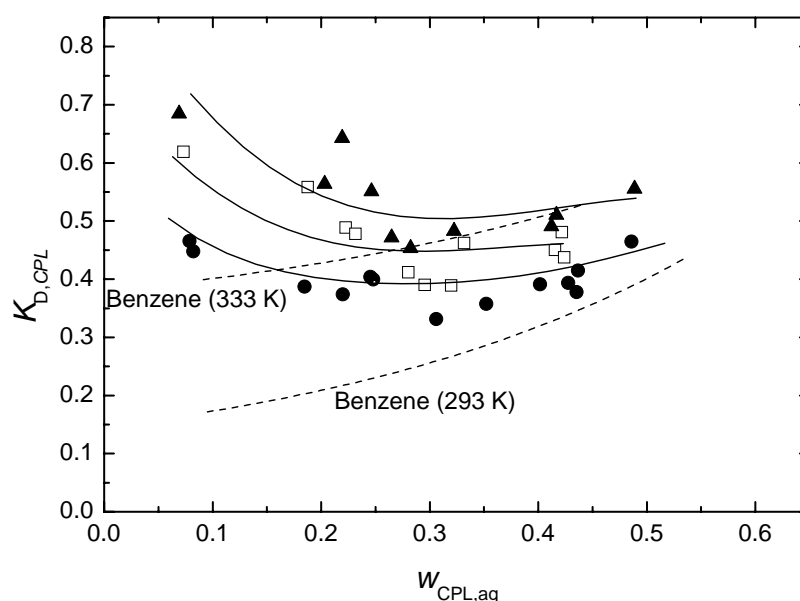
Figure 6.7. $K_{D,CPL}$ as function of the mass fraction of caprolactam in the aqueous phase for MCH-heptanol (40 mass % initially) for: ●, 293 K; □, 313 K; ▲, 333 K; —, NRTL fit solvent; --, benzene as reference at 293 K and 333 K.

The experimental equilibrium data of both alternative solvents are compared in Figure 6.8 at 293 K and 333 K. In this figure it is shown that the influence of the type of alkane on the distribution ratio of caprolactam, by replacing MCH by heptane, is negligible. The influence of ammonium sulfate on the experimental equilibrium data of caprolactam for the MCH + heptanol system is presented in Figure 6.9. It can be concluded that addition of ammonium sulfate to the system causes considerable salting out of caprolactam, resulting in significant changes of the distribution ratio of caprolactam between the two liquid phases, which is similar to the observation for the quaternary systems water + caprolactam + ammonium sulfate + benzene, respectively toluene. The concentration of caprolactam in the organic phase is, however, still higher for the mixed solvent than for benzene at equal conditions. For the 6 mass % ammonium sulfate system with the mixed solvent a three liquid phase equilibrium region was observed at concentrations of caprolactam higher than the presented experimental range in Table B1. This three-phase system was also observed for a 15 mass % ammonium sulfate system with benzene and a 5 mass % ammonium sulfate system with toluene.
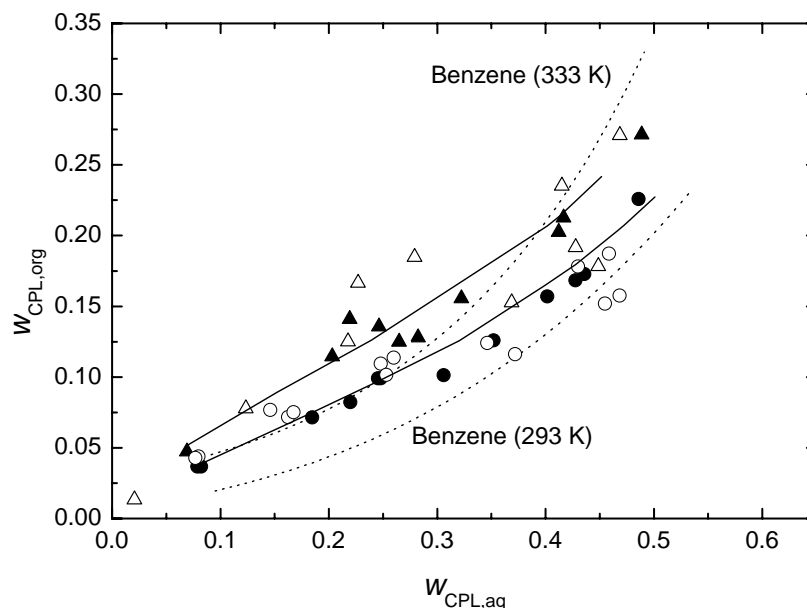
Figure 6.8. The mass fraction of caprolactam in the organic phase as function of that in the aqueous phase for MCH-heptanol (40 mass % initially) for: ●, 293 K; ▲, 333 K; and for heptane-heptanol (40 mass % initially) at: ○, 293 K; △, 333 K; —, NRTL fit solvent; --, benzene as reference at 293 K and 333 K.
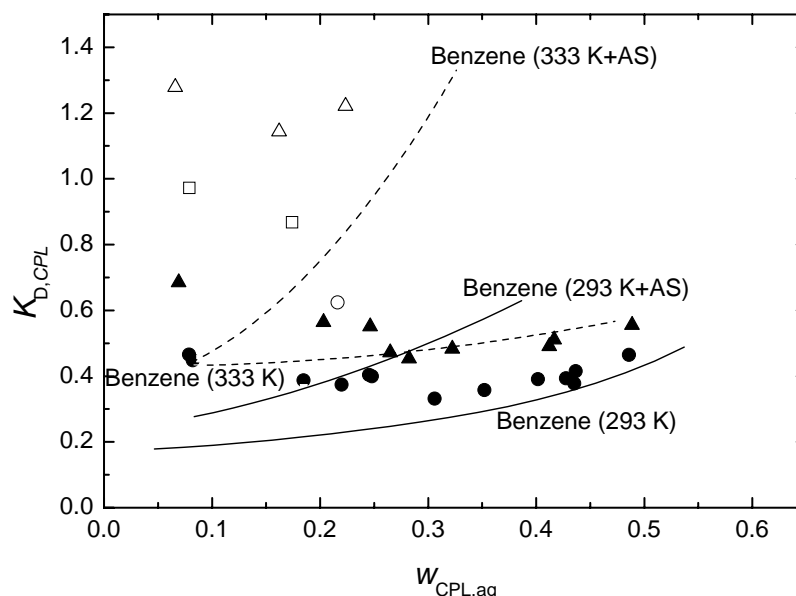
Figure 6.9. $K_{D,CPL}$ as function of $w_{CPL,aq}$ for MCH-heptanol (40 mass % initially) at: ●, 293 K; ▲, 333 K; and MCH-heptanol (40 mass % initially) with 6 mass % ammonium sulfate (AS) at: ○, 293 K; □, 313 K; △, 333 K; and benzene and benzene with 5 mass % AS as reference at: —, 293 K; --, 333 K.

6.4.2   Calculation of the number of theoretical stages

Using the presented results in Figure 6.7 and Figure 6.8, the solvent to feed ratio, *S/F*, and the number of theoretical stages, NTS, needed for the extraction of caprolactam with the proposed mixture alkane + heptanol (40 mass %) according to the industrial DSM process lay-out as reference was calculated and compared to benzene. Since the equilibrium distribution of caprolactam for both mixed solvent systems is similar, the results apply to either the MCH or heptane system. In the forward extraction of caprolactam a 70 mass %

aqueous caprolactam phase is extracted at 313 K with an organic solvent. The solvent to feed ratio for both benzene and the mixed solvent was chosen at $S/F = 3.0$, since the minimum solvent to feed ratio for the mixed solvent and benzene was calculated as $(S/F)_{min} = 2.0$ and 1.9, respectively. The fraction of caprolactam remaining in the raffinate after extraction is shown in Figure 6.10 (a) as function of the number of equilibrium stages. It was thereby assumed that there was no mutual solubility of the solvents, that no ammonium sulfate was present in the feed stream and the extraction of the aqueous ammonium sulfate layer, which is present in the industrial process was not considered. In the back-extraction the caprolactam rich organic phase from the forward extraction is re-extracted at 313 K with water as solvent. Using the extract concentration from the forward extraction, $w_{CPL,extract} = 0.189$, the minimum solvent to feed ratio needed for the back-extraction process at 313 K was calculated for both the mixed solvent and benzene at $(S/F)_{min} = 0.45$. Therefore, using again 1.5 times this amount, $S/F = 0.67$ was selected for both solvents. The fraction of caprolactam remaining in the raffinate after extraction is shown in Figure 6.10 (b) as function of the amount of equilibrium stages.
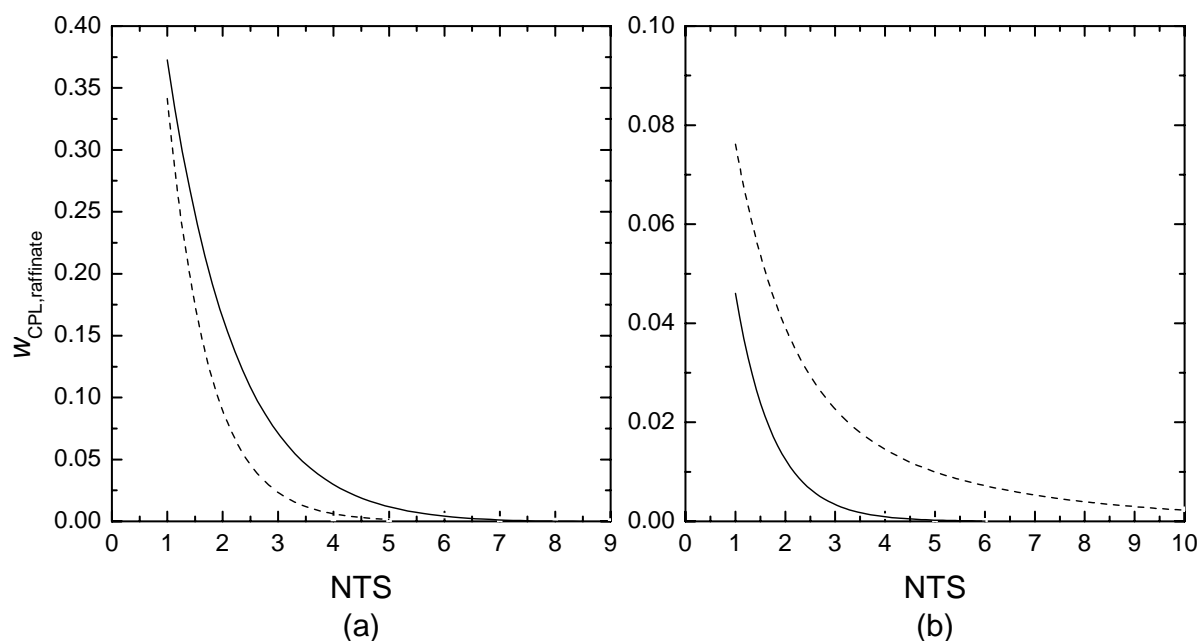
Figure 6.10. Caprolactam raffinate fraction at 313 K as function of NTS used in the forward extraction (a) and back-extraction with water (b) for: — —, both MCH-heptanol (40 mass %) and heptane-heptanol (40 mass %) and --, benzene.

From Figure 6.10 (a) it was concluded that in the forward extraction the mixed solvent with NTS = 5 needs only half of the NTS in order to reach the required raffinate concentration of $w_{CPL,raffinate} = 5 \times 10^{-4}$ relative to benzene under similar conditions. From Figure 6.10 (b) it can, however, be concluded that this trend is reverse. This behaviour can be understood from Figure 6.7. In this figure it can be seen that at high concentrations of caprolactam the behaviour of both solvents is more or less similar, whereas at low concentrations the distribution ratio of caprolactam is higher for the mixed solvent compared to benzene. This results in the mixed solvent being favourable in the forward extraction at low concentrations of caprolactam, but benzene being favourable in the back-extraction at low concentrations.

6.4.3   Physical properties

Density. In Table B3 (see Appendix B) the results are given for the density data of the systems MCH + heptanol (40 mass % initially) + caprolactam and heptane + heptanol (40 mass % initially) + caprolactam at 293 K, 313 K and 333 K. The presented density data were correlated using a linear effect of the solute mass fraction and the volumetric expansion coefficient, as described in Chapter 2. The determined parameters are shown in Table 6.2.

Table 6.2. Fitted parameters for the description of densities, dynamic viscosities and interfacial tensions of the systems alkane + heptanol + caprolactam (CPL) and water + alkane + heptanol + CPL, respectively, at 293 K, 313 K and 333 K, where the alkane is methylcyclohexane or heptane.

Parameters	Methylcyclohexane system	Heptane system
	Density	
$\rho_{0,293}/kg \cdot m^{-3}$	789.4	733.3
$A_{CPL}/kg \cdot m^{-3}$	0.269	0.337
b_{CPL}	1	1
α/K^{-1}	1.07×10^{-3}	1.16×10^{-3}
	Dynamic viscosity	
$\eta_{0,293}/kg \cdot m^{-1} \cdot s^{-1}$	1.45×10^{-3}	0.92×10^{-3}
	$B_{DJ}=k_1 \cdot (T-273)+k_2$	
CPL	$k_1=-15.2 \times 10^{-4}$	$k_1=-5.0 \times 10^{-4}$
	$k_2=0.2660$	$k_2=0.2968$
	$D_{DJ}=m_1 \cdot (T-273)+m_2 \ ; \ F_{DJ}=2$	
CPL	$m_1=2.2 \times 10^{-4}$	$m_1=-5.9 \times 10^{-4}$
	$m_2=0.0614$	$m_2=0.0591$
B_{AG}/K	1659	1334
	Interfacial tension	
$A_{SZ}/mol \cdot l^{-1}$	6.3×10^{-2}	
B_{SZ}	0.294	

The average of the ratio of the measured and calculated density data and its standard deviation is $1.000 \pm 8 \times 10^{-4}$ and $1.000 \pm 7 \times 10^{-4}$ for the MCH and heptane systems, respectively. Experimental and calculated density data for the ternary systems MCH (1) + heptanol (2) + caprolactam (3) and heptane (1) + heptanol (2) + caprolactam (3) as function of the mass fraction of caprolactam at 293 K and 333 K are presented in Figure 6.11 relative to the calculated data for the binary system benzene + caprolactam. Comparison of the calculated and experimental results shows that the experimental data are represented very well and that for all solvents the density at different temperatures increases linearly with increasing solute

mass fraction. It can furthermore be seen that an increase of the temperature resulted in a decrease of density. It can be concluded that the benzene system has the highest density, whereas the heptane-heptanol system has the lowest.
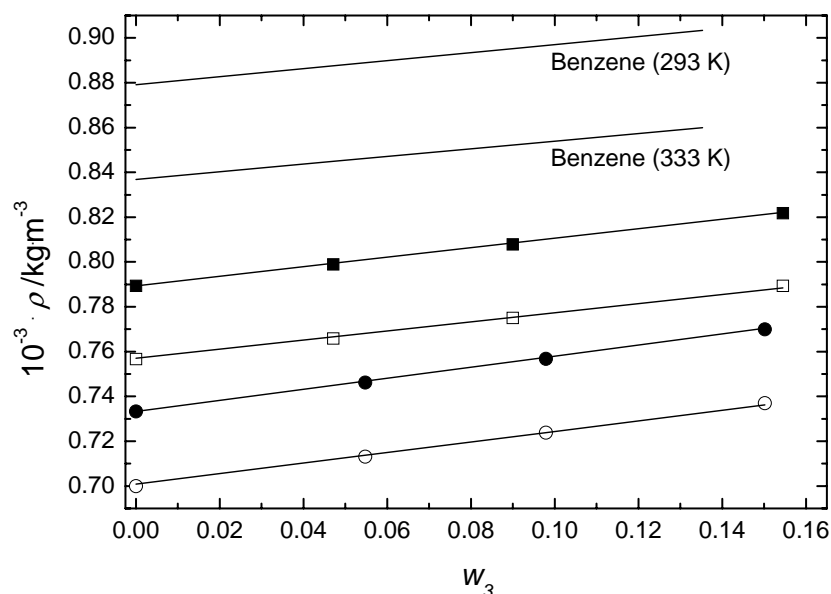
Figure 6.11. Densities as a function of the concentration of caprolactam of the systems solvent + heptanol + caprolactam, where the solvent is MCH or heptane for: ■, MCH at 293 K; □, MCH at 333 K; ●, heptane at 293 K; ○, heptane at 333 K; —, fitted densities of both systems and benzene as reference at 293 K and 333 K.

Dynamic viscosity. In Table B4 (see Appendix B) the results are shown for the kinematic viscosity data of the systems MCH + heptanol (40 mass % initially) + caprolactam and heptane + heptanol (40 mass % initially) + caprolactam at 293 K, 313 K and 333 K. The presented viscosity data were correlated using the (extended) Dole-Jones equation and the Guzman-Andrade equation as described in Chapter 2. The determined parameters are listed in Table 6.2. The average of the ratio of the fitted and measured viscosity data and its standard deviation for the Dole-Jones and Guzman-Andrade equation is $0.99 \pm 1 \times 10^{-2}$ and $1.00 \pm 4 \times 10^{-3}$ for the MCH and heptane systems, respectively. Experimental and fitted dynamic viscosities for MCH (1) + heptanol (2) + caprolactam (3) and heptane (1) + heptanol (2) + caprolactam (3) as function of the concentration of caprolactam at 293 K and 333 K are presented in Figure 6.12 relative to the calculated data for the binary system benzene + caprolactam. Comparison of the calculated and experimental results shows that the experimental data are very well represented with the modified extended Dole-Jones and the Andrade-Guzman equations. Figure 6.12 shows that for all solvents and all solutes the viscosity increases with increasing solute concentration, but the increase is lower at elevated temperatures. Obviously, it can be seen that an increase of temperature results in a decrease of viscosity and that the benzene system has the lowest viscosity, followed by the heptane-heptanol system.
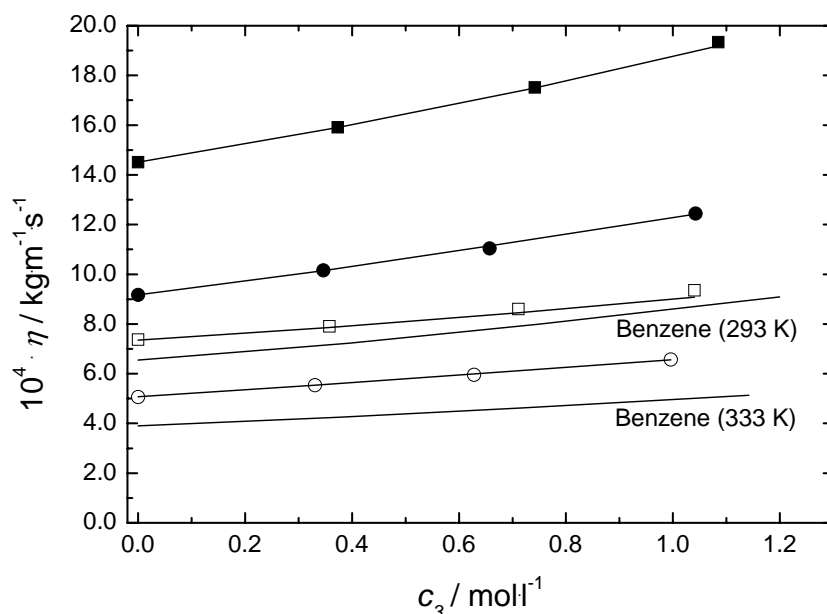
Figure 6.12. Dynamic viscosities as a function of the concentration of caprolactam of the systems solvent + heptanol + caprolactam, where the solvent is MCH or heptane for: ■, MCH at 293 K; □, MCH at 333 K; ●, heptane at 293 K; ○, heptane at 333 K; —, fitted dynamic viscosities of both systems and benzene as reference at 293 K and 333 K.

Interfacial tension. In Table B5 (see Appendix B) the results are shown for the interfacial tension data of the systems water + caprolactam + MCH + heptanol (40 mass % initially) and water + caprolactam + heptane + heptanol (40 mass % initially) at 293 K, 313 K and 333 K. Previous to the experiment a pre-calculated amount of caprolactam was added to both phases in order to obtain initially (nearly) equilibrated systems. The presented interfacial tension data were correlated using the Szyzkowski isotherm, where the influence of the concentration of caprolactam on the interfacial tension of the system was described via the concentration of caprolactam in the organic phase (see Chapter 2). For all temperatures the determined interfacial tension of both solvent systems without caprolactam varied between 11.3 and 12.4 $mN \cdot m^{-1}$. This is probably due to a combined effect of the interfacial tension decrease with increasing temperature for the binary systems water + MCH and water + heptane, the parabolic dependence of the interfacial tension on temperature for the binary system water + heptanol[18] and finally the experimental accuracy. Therefore an average interfacial tension of 11.9 $mN \cdot m^{-1}$ for both ternary solvent systems water + alkane + heptanol (40 mass % initially) and all temperatures was used for the fitting and prediction of interfacial tension data. The determined parameters are shown in Table 6.2. The average of the ratio of the fitted and measured interfacial tension data and its standard deviation for the Szyzkowski equation is 1.0 $\pm$ 6.5 $\times$ 10^{-2} and 1.0 $\pm$ 4.3 $\times$ 10^{-2} for the MCH and heptane systems, respectively. Experimental and calculated interfacial tension data for the systems water (1) + caprolactam (2) + MCH (3) + heptanol (4) and water (1) + caprolactam (2) + heptane (3) + heptanol (4) as function of the concentration of caprolactam in the organic phase at 293 K are presented in Figure 6.13 relative to the calculated interfacial tension data of the ternary system water (1) + caprolactam (2) + toluene (3) at 293 K.

Comparison of the calculated and experimental results shows that the experimental data are very well represented with the Szyzkowski equation. Figure 6.13 shows that the interfacial tension decreased with increasing concentration of caprolactam for the ternary and quaternary systems. It can furthermore be seen that at high concentrations of caprolactam in the organic phase the interfacial tension of all systems is comparable with a decreasing concentration the interfacial tension of the toluene system increases exponentially, whereas it increases slightly for the mixed solvent systems.
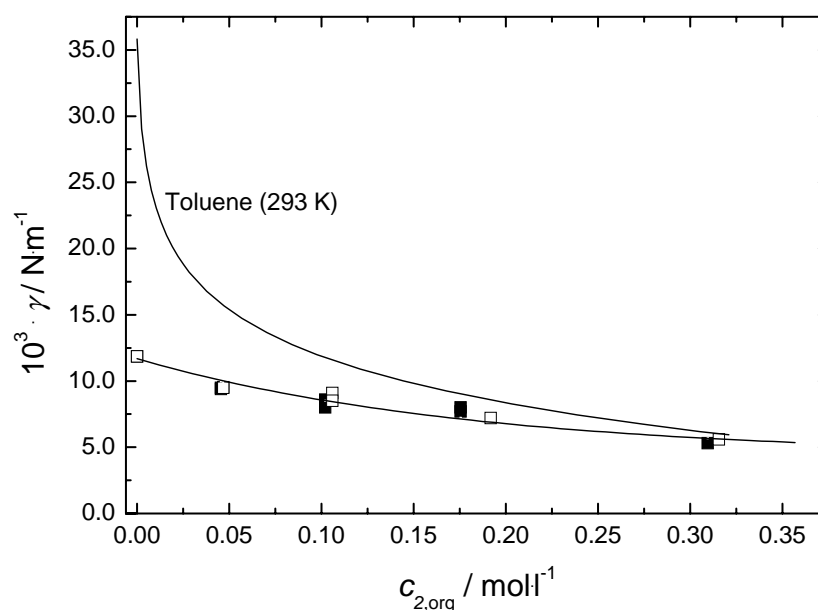
Figure 6.13. Interfacial tension as a function of the concentration of caprolactam in the organic phase of the systems alkane + heptanol + caprolactam, where the alkane is MCH or heptane at 293 K for: ■, MCH; □, heptane; —, fitted interfacial tensions of both systems and toluene as reference.

6.5   Conclusions

Possible alternative solvents for the replacement of benzene and toluene in the caprolactam extraction process were screened using the Hansen solubility model and the Unifac Dortmund model. Using the Hansen model an indication of possible alternative solvent groups was obtained. The results of the Unifac Dortmund model were, however, not accurate enough for in depth solvent selection. Therefore the solvent screening was performed experimentally where it was found that the distribution ratio of caprolactam increased with increasing solvent (mixture) polarity, characterized by a more polar active group (ether, ester, ketone and alcohol), decreasing carbon chain length (C_{12} to C_6) or increasing fraction of polar solvent in the mixture. Based on a high capacity and a low mutual solvent solubility the mixture methylcyclohexane-heptanol (40 mass %) was selected as candidate replacement solvent. The influence of alkane structure on phase compositions was observed to be negligible by replacing methylcyclohexane with heptane, resulting in heptane-heptanol (40 mass %) being selected as second candidate solvent.

Liquid-liquid equilibrium phase compositions were determined for both candidate solvents covering the full concentration and temperature range of the industrial process. Data were

determined for the two liquid phase systems, where three liquid phases were observed for the both systems at 6 mass % of ammonium sulfate. Since the phase compositions of both alternative solvent mixtures are similar they result in equal required *S/F* and NTS values. Phase equilibria were correlated with the classical NRTL model and a good representation was obtained for both systems, where the mixed solvent was treated as one pseudo-component. This approach resulted in a simple and directly applicable model in ASPEN Plus 11.1. Density data were correlated well using a linear relation for the influence of the concentration of solute and the volumetric thermal expansion coefficient. Viscosity data were correlated using the extended Dole-Jones equation and the Andrade-Guzman equation. Interfacial tension data were fitted with the Szyzkowski equation via the concentration of caprolactam in the organic phase, which resulted in good fits.

The interfacial tension of both systems is similar. The density of the heptane + heptanol mixture is however lower than for the MCH + heptanol mixture and benzene, while the viscosity is lower than for MCH + heptanol and comparable to benzene. Lower densities are expected to result in a larger hydraulic capacity in extraction columns and the lower viscosity in a lower drag coefficient when the solvent is the continuous phase. The final selection of heptane + heptanol (40 mass %) as best replacement solvent is therefore based on its beneficial physical properties since the phase compositions of both candidate solvent mixtures are comparable.

Literature cited

1. Ullmann, F. *Ullmann's Encyclopedia of Industrial Chemistry*; Wiley-Interscience: New York, 2004; electronic version.

2. Wijtkamp, M.; van Bochove, G. H.; de Loos, Th. W.; Niemann, S. H. Measurements of Liquid-Liquid Equilibria of Water + ε-Caprolactam + Electrolyte + Organic Solvent Systems. *Fluid Phase Equilib.* **1999**, *158-160*, 939-947.

3. Van Bochove, G. H.; Krooshof, G. J. P.; de Loos, Th. W. Two- and Three-Liquid Phase Equilibria in the System Water + 2-Heptanone + Caprolactam + Ammonium sulfate: Experiments and Modeling. *Fluid Phase Equilib.* **2002**, *194-197*, 1029-1044.

4. Tettamanti, K.; Nogradi, M.; Sawinsky, J. Equilibria of the Ternary System Caprolactam-Water-Organic Solvent, in the Liquid State. *Period. Polytech. Chem. Eng.* **1960**, *4*, 201-218.

5. Poraicu, M.; Davidescu, C.; Pacurariu, C. Studies on Partition Equilibria. The Extraction of ε-Caprolactam from Aqueous Solutions. *Chem. Bull. Politehnica* **1997**, *42*, 139-143.

6. Van Bochove, G. H. *Two- and Three-Liquid Phase Equilibria in Industrial Mixed-Solvent Electrolyte Solutions*. PhD thesis, University of Delft, DUP Science, Delft, 2003, pp. 31.

7. Li, M.; Harten, P. F.; Cabezas, H. Experiences in Designing Solvents for the Environment. *Ind. Eng. Chem. Res*. **2002**, *41*, 5867-5877.

8. Pistikopoulos, E. N.; Stefanis, S. K. Optimal Solvent Design for Environmental Impact Minimization. *Comp. Chem. Eng*. **1998**, *22*, 717-733.

9. Meniai, A.-H.; Newsham, D. M. T. A Computer-Aided Molecular Design of Solvents for Liquid-Liquid Extraction. *Trans. IChemE*. **1996**, *74*, 695-702.

10. Meniai, A.-H.; Newsham, D. M. T.; Khalfaoui, B. Special Papers - Solvent Design for Liquid Extraction Using Calculated Molecular Interaction Parameters. *Trans. IChemE*. **1998**, *76*, 942-950.

11. Barwick, V. J. Strategies for Solvent Selection - A Literature Review. *Trends Anal. Chem*. **1997**, *16*, 293-309.

12. Van Dyk, B.; Nieuwoudt, I. Design of Solvents for Extractive Distillation. *Ind. Eng. Chem. Res*. **2000**, *39*, 1423-1429.

13. Ashton, N. F.; McDermott, C.; Brench, A. Chemistry of Extraction of Nonreacting Solutes, In *Handbook of Solvent Extraction*; Lo, T. C., Baird, M. H. I., Hanson, C., Eds.; Wiley: New York, 1983, pp. 3-35.

14. Aten, W. C. Solvent Reaction and Measurement, In *Directory of Solvents*. B.P. Whim, P.G. Johnson, Eds.; Blackie Academic & Professional, London, 1996, pp. 10-47.

15. Newsham, D. M. T. Liquid-Liquid Equilibria, In *Science and Practice of Liquid-Liquid Extraction*; Thornton, J. D., Eds.; Clarendon Press: Oxford, 1992, pp. 1-39.

16. Hansen, C. M. The Three Dimensional Solubility Parameter – Key to Paint Component Affinities: I. Solvents, Plasticizers, Polymers, and Resins. *J. Paint Tech*. **1967**, *39*, 104-117.

17. Weidlich, U.; Gmehling, J. A Modified UNIFAC Model. 1. Prediction of VLE, h^E, and γ^∞. *Ind. Eng. Chem. Res*. **1987**, *26*, 1372-1381.

18. Chavepeyer, G.; Salajan, M.; Platten, J. K.; Smet, P. Interfacial Tension and Surface Adsorption in i-Heptanol/Water Systems. *J. Colloid Interface Sci*. **1995**, *174*, 112-116.

Chapter 7

Impurity distribution behaviour in caprolactam extraction with environmentally benign mixed solvents

7.1   Introduction

Caprolactam is recovered from the neutralized Beckmann rearrangement mixture by phase separation, where both streams contain various impurities, followed by solvent extraction of the resulting crude caprolactam phase, the so-called forward extraction, and the aqueous ammonium sulfate layer, as described in Chapter 1. Currently, benzene, toluene and chlorinated hydrocarbons are used as solvents in the caprolactam extraction process. Because of the negative effects on health and environment of these solvents and the resulting strict legislation, the need exists for an alternative solvent. In Chapter 6 a mixed solvent composed of an alkane, being heptane or methylcyclohexane, and an alcohol, 40 mass % heptanol, was selected from an experimental screening procedure. The solvent mixture heptane + heptanol (40 mass %) was finally selected as replacement solvent based on its beneficial physical properties, since the phase compositions of both candidate solvent mixtures are similar and satisfying relative to the conventional solvents.

The impurities entering the forward extraction process reside from the feedstock (benzene, toluene, phenol, cyclohexane, etc.), by-products formed in the reaction steps (oxidation, hydrogenation, dehydrogenation, Beckmann rearrangement, etc.) and additional compounds introduced in the different process steps (neutralization, extraction, etc.). They are of both inorganic and organic nature,[1,2,3] of which mainly the latter are extracted along with caprolactam in the forward extraction.[1]

The specifications for fibre-grade commercial caprolactam are severe, resulting in a required high purity (> 99.9%). The impurities present in the crude caprolactam need therefore to be reduced to a very low level.[1,2,4] After the first separation step, being extraction, a series of purification steps, including chemical treatment and vacuum distillation, is applied to obtain the required purity.[1] Changing the solvent in the extraction process might result in a different impurity profile in the extract and therefore a different composition of the feed for the final purification, which needs to be identified before the implementation of the alternative solvent.

Therefore, in the present study the equilibrium distribution ratio of caprolactam and four model impurities of organic nature was studied at 293 K, 313 K and 333 K for toluene as reference solvent and both alternative mixed solvents, in order to determine the effect of different solvent mixtures on the distribution ratio. The experimental conditions covered the industrial operating range with respect to the concentrations of caprolactam and ammonium sulfate. The phase equilibria results were interpreted using the equilibrium stages model for a conceptual extraction column design.

In Chapter 8 the extraction performance of the best alternative solvent with respect to phase compositions, physical properties and impurity distribution ratio is experimentally evaluated and compared to that of toluene.

7.2 Experimental set-up and procedure

Model impurities. In the crude caprolactam phase a large amount of impurities can be detected.[3] These are represented by four model impurities detected in crude caprolactam covering (I) impurities with low boiling points compared to caprolactam, (II) impurities with a moderate boiling point, (III), derivatives of caprolactam, (IV) impurities with a boiling point higher than caprolactam. The selected model impurities were cyclohexanone (I),[2,3] aniline (II),[2] n-methylcaprolactam (III)[2,4] and cyclohexane-carboxamide (IV),[3] which are structures comparable to those used in other model studies.[4] The structural formulas of these model impurities are shown in Figure 7.1
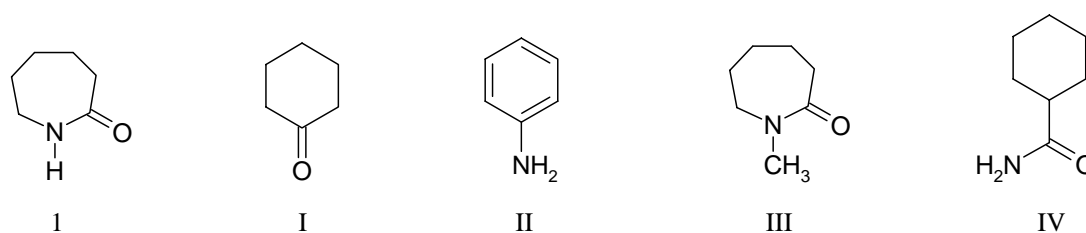
Figure 7.1. Structural formulas of: 1, Caprolactam; I, Cyclohexanone; II, Aniline; III, N-methylcaprolactam; IV, Cyclohexane-carboxamide.

Equilibrium measurements. To obtain experimental phase equilibrium data the same procedure as described in Chapter 2 was followed. The initial mass fraction of caprolactam in the aqueous phase ranged from $w_{CPL,aq} = 0.3$ to 0.7 and the initial organic heptanol mass fraction was $w_{heptanol,org} = 0.4$. To the aqueous mixture 0.5 mass % of each impurity was added and 1.5 mass % ammonium sulfate if required. The mixtures were stirred for at least 45 min to be sure that equilibrium was reached and then allowed to settle for at least 1 h after which the phases were completely separated. Then samples were taken from both phases with a syringe. The samples were diluted and prepared for analysis. The determined equilibrium data were interpreted using the distribution ratio, $K_{D,i}$, as introduced in Chapter 6.

Chemicals. All chemicals were used as received. These are: ε-caprolactam (purity 99%), ammonium sulfate (purity > 99%), methylcyclohexane and n-methylcaprolactam (purity 99%) by Sigma-Aldrich (USA), 1-heptanol (purity 98%) and cyclohexane-carboxamide (purity 97%) by Acros (Belgium), cyclohexanone (purity > 99%), aniline (purity > 99.5%) and n-heptane (purity > 99%) by Merck (Germany). MiliQ water was used in all experiments.

Chemical analysis. The mass fraction of caprolactam and the impurities in both the organic and the aqueous phase was determined by gas chromatography. The same analytical procedure as described in Chapter 2 and Chapter 6 was applied for both phases and each solvent. An aqueous mixture containing 0.5 mass % of the four impurities was analyzed four times with an uncertainty of 0.01 mass %. The mass fraction of ammonium sulfate in the aqueous phase was determined as described in Chapter 2 and the amount distributed to the organic phase was assumed negligible.

7.3   Experimental results and discussion

7.3.1   Toluene

In Figure 7.2 the results are shown for the distribution ratio of all four model impurities and caprolactam with toluene as benchmark solvent at 293 K and 333 K. The data measured are compared with the equilibrium distribution ratio for toluene at similar conditions.
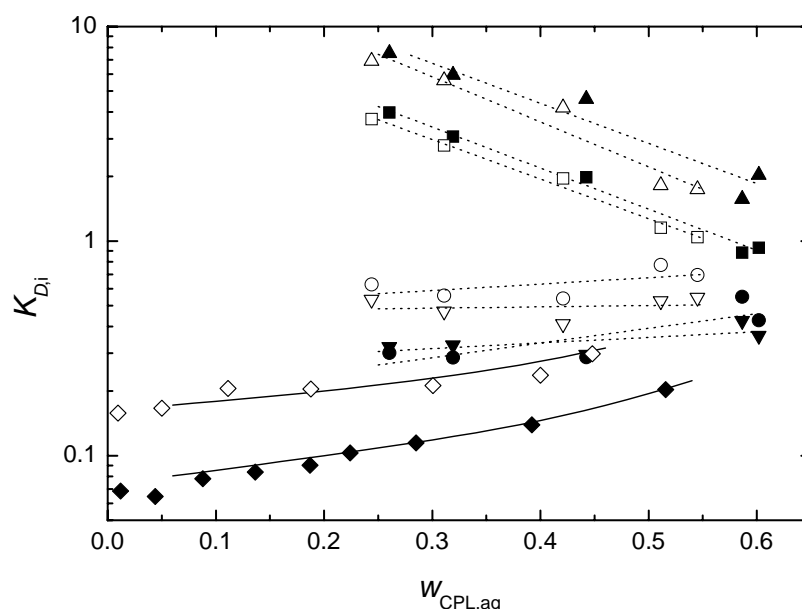
Figure 7.2. Equilibrium distribution ratio as function of $w_{CPL,aq}$ with toluene as solvent at 293 K: ◆, caprolactam; ■, aniline; ●, n-methylcaprolactam; ▲, cyclohexanone; ▼, cyclohexane-carboxamide; at 333 K: corresponding open symbols; and: —, NRTL fit of the distribution ratio of caprolactam (Chapter 2); --, trend lines.

In Figure 7.2 it can be seen that all impurities at both temperatures showed a distribution ratio higher than the distribution ratio of caprolactam. Furthermore, it follows that the model impurities show different behaviour in the liquid-liquid system due to differences in the chemical structure. N-methylcaprolactam, as derivative of caprolactam, and cyclohexane-carboxamide, because of the strong amide-water interaction, showed a low distribution ratio that was slightly increasing with an increasign concentration of caprolactam in the aqueous phase, which is comparable to the behaviour of caprolactam itself. The less polar aniline and cyclohexanone showed high distribution ratios that were decreasing with the concentration of caprolactam. The dependence of the distribution ratios on the amount of caprolactam present in the system is explained by the fact that both phases become more alike at higher concentrations of caprolactam. An increasing temperature resulted in a slight increase of the

distribution ratio of n-methylcaprolactam and cyclohexane-carboxamide, which is comparable for caprolactam, while the distribution ratio of aniline and cyclohexanone decreased. This first observation is explained by the weakening of hydrogen bond formation in the aqueous phase with increasing temperature, whereas in this phase the repelling forces to non-polar organic components decrease, explaining the latter observation.

In the crude lactam phase 1 to 1.5 mass % ammonium sulfate is present. It is known that its presence increases the distribution ratio of caprolactam because of the salting-out effect. The influence of this effect on the distribution ratio of the impurities was investigated at 293 K, 313 K and 333 K by addition of an initial amount of 1.5 mass % ammonium sulfate to the above aqueous mixture before extraction. This resulted in equilibrium concentrations of 1.5 to 2.0 mass %. The impurity distribution ratio at 313 K with and without ammonium sulfate is shown in Figure 7.3, compared to caprolactam.
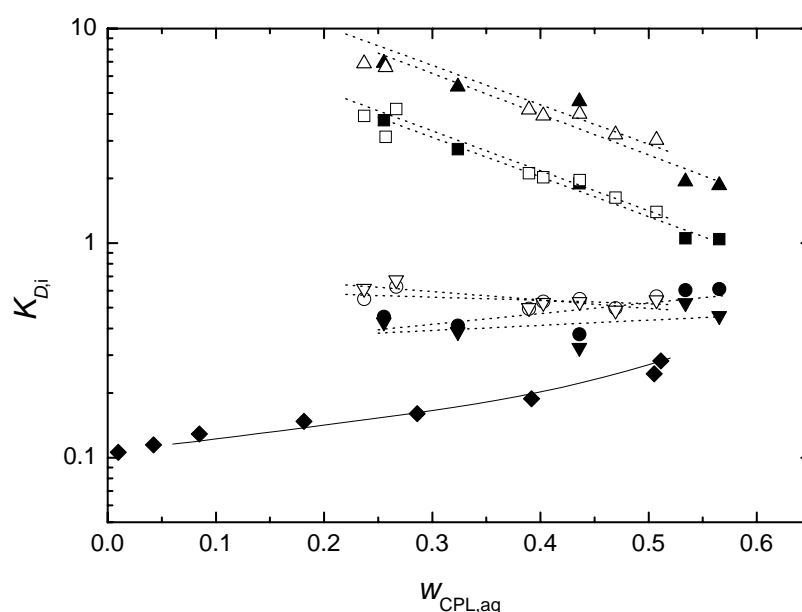
Figure 7.3. Equilibrium distribution ratio as function of $w_{CPL,aq}$ with toluene as solvent at 313 K: ◆, caprolactam; ■, aniline; ●, n-methylcaprolactam; ▲, cyclohexanone; ▼, cyclohexane-carboxamide; and with 1.5 mass % ammonium sulfate: corresponding open symbols; and: —, NRTL fit of the distribution ratio of caprolactam (Chapter 2); --, trend lines.

From Figure 7.3 it can be concluded that with ammonium sulfate present the distribution ratio of the impurities seems to be increased slightly. Similar to caprolactam the increase is caused by salting-out. The effect shown in this figure is, however, not very large and will therefore not be investigated further in this study, although it has to be taken into account for process design. Furthermore it can be seen that all trends observed were similar to those already shown in Figure 7.2, which was also the case for the determined temperature effect.

7.3.2   Mixed solvents

Whether and how the impurity distribution ratio changes when applying both selected mixed solvents, being heptane + heptanol (40 mass %) and methylcyclohexane + heptanol (40 mass %) is shown in Figure 7.4 at 293 K, 313 K and 333 K.

Figure 7.4. Equilibrium distribution ratio as function of $w_{CPL,aq}$ with heptane + heptanol (40 mass %) as solvent at 313 K: ◆, caprolactam; ■, aniline; ●, n-methylcaprolactam; ▲, cyclohexanone; ▼, cyclohexane-carboxamide; and for methylcyclohexane + heptanol (40 mass %): corresponding open symbols; and: —, NRTL fit of the distribution ratio of caprolactam (Chapter 6); — —, trend lines.

In Figure 7.4 it can be seen that, as for toluene, the impurity distribution ratio is comparable or higher than the distribution ratio of caprolactam in both mixed solvents. Furthermore, it is shown that the impurity distribution ratio was similar for both mixed solvents used. In Chapter 6 the solvent mixture heptane + heptanol (40 mass %) was selected as candidate solvent based on its beneficial physical properties, since the distribution ratio of caprolactam and the mutual solvent solubility were similar for both solvents. As the impurity distribution ratio is equal for both solvent mixtures as well, the previously selected solvent was investigated further as best alternative solvent for the extraction of caprolactam.

The caprolactam and impurity distribution ratio for heptane + heptanol (40 mass %) at 313 K are shown in Figure 7.5 (a) and (b), compared to those in toluene. In this figure it can be seen that the distribution ratio for some impurities differed compared to the distribution in toluene. The equilibrium data for aniline and n-methylcaprolactam were more or less comparable to toluene showing a slight decrease and increase, respectively, but the distribution ratio of cyclohexanone decreased strongly, whereas the distribution ratio of cyclohexane-carboxamide increased significantly. From the equilibrium distribution ratio of caprolactam it is known that it is higher for the mixed solvents compared to toluene, because of the heptanol present, which is capable of hydrogen bond formation. This influence seems the same now for n-methylcaprolactam and especially for cyclohexane-carboxamide, while aniline and particularly cyclohexanone are more repelled by the more polar organic phase.

In Figure 7.6 the influence of the temperature on the impurity distribution ratio is shown using heptane + heptanol (40 mass %) as solvent relative to the fitted distribution ratio of caprolactam. It can be concluded that the distribution ratio decreased with increasing temperature for aniline and cyclohexanone, as also found for toluene, and in addition also for

cyclohexane-carboxamide, whereas it increased for n-methylcaprolactam, as was the case with toluene. The presented influence can be explained by the lower hydrogen bonding strength at elevated temperatures. Furthermore, the non-polar organic compounds are less repelled by the aqueous phase. Finally it can be seen that the distribution ratio of the impurities is comparable or higher than that of caprolactam, as also found for toluene.
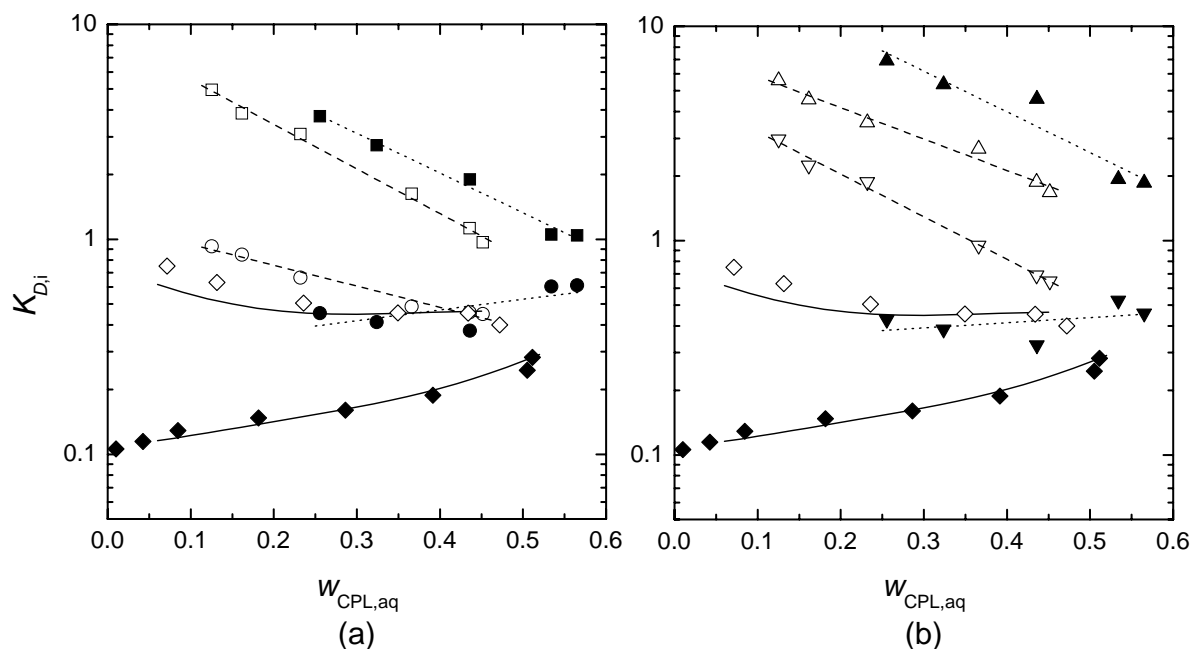
Figure 7.5. Equilibrium distribution ratio as function of $w_{CPL,aq}$ with toluene as solvent at 313 K: ◆, caprolactam; ■, aniline (a); ●, n-methylcaprolactam (a); ▲, cyclohexanone (b); ▼, cyclohexane-carboxamide (b); and for heptane + heptanol (40 mass %): corresponding open symbols; and: —, NRTL fit of the distribution ratio of caprolactam (Chapter 2 and Chapter 6); --, trend lines for toluene; — —, trend lines for mixed solvent.
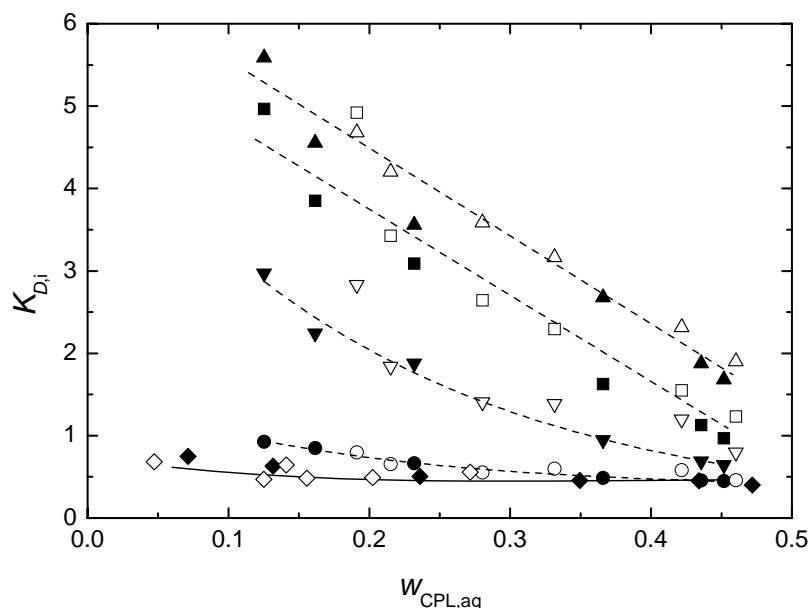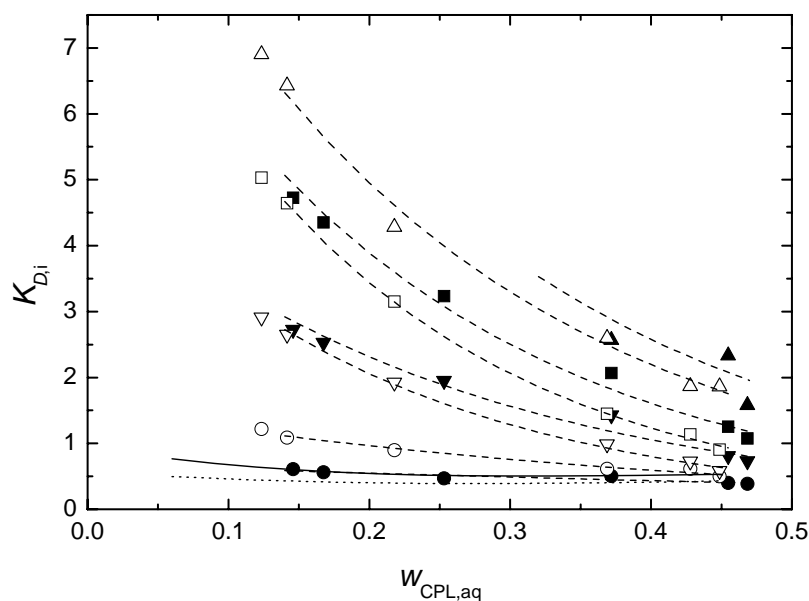

Figure 7.6. Equilibrium distribution ratio as function of $w_{CPL,aq}$ with heptane + heptanol (40 mass %) as solvent at 293 K: ■, aniline; ●, n-methylcaprolactam; ▲, cyclohexanone; ▼, cyclohexane-carboxamide; and at 333 K: corresponding open symbols; — —, trend lines; and NRTL fit of the distribution ratio of caprolactam (Chapter 6): --, 293 K; —, 333 K.

7.4   Equilibrium calculations

Using equilibrium data and the solvent to feed ratio, *S/F*, the number of theoretical stages, NTS, needed for the extraction of caprolactam according to the industrial DSM process layout[1] with toluene and the proposed best solvent mixture heptane + heptanol (40 mass %) was calculated. Furthermore the fraction of impurities extracted was calculated. In the calculations the influence of the extracted fraction of caprolactam on the mass flows was taken into account, but the influence of the impurities was assumed negligible. Furthermore, it was assumed that there was no mutual solubility of both phases, no ammonium sulfate was present in the feed stream, whereas the extraction of the aqueous ammonium sulfate layer, which is present in the reference process, was not taken into account.

In the forward extraction of caprolactam a 70 mass % aqueous caprolactam phase is extracted at 313 K with an organic solvent. The solvent to feed ratio for toluene and the mixed solvent was calculated at $S/F = 5.0$ and 3.0, both equal to 1.5 times the minimum solvent to feed ratio. In Figure 7.7 the fraction of impurities extracted along with caprolactam is shown as function of the NTS for toluene (a) and the mixed solvent (b). It can be seen that for both solvents all impurities (100%) are present in the extract after NTS = 5 and 4, respectively. In this figure furthermore the caprolactam raffinate concentration is shown as function of the NTS. It was calculated that the mixed solvent with NTS = 5 only needs one half of the NTS in order to reach the required raffinate concentration of $w_{CPL,raffinate} < 5 \times 10^{-4}$ relative to toluene under equal conditions. Based on these calculated values of NTS it can therefore be concluded that for both solvents in the forward extraction process the total fraction of impurities, 100%, is present in the extract. This can be explained by the fact that all impurities possess a distribution coefficient higher than caprolactam.
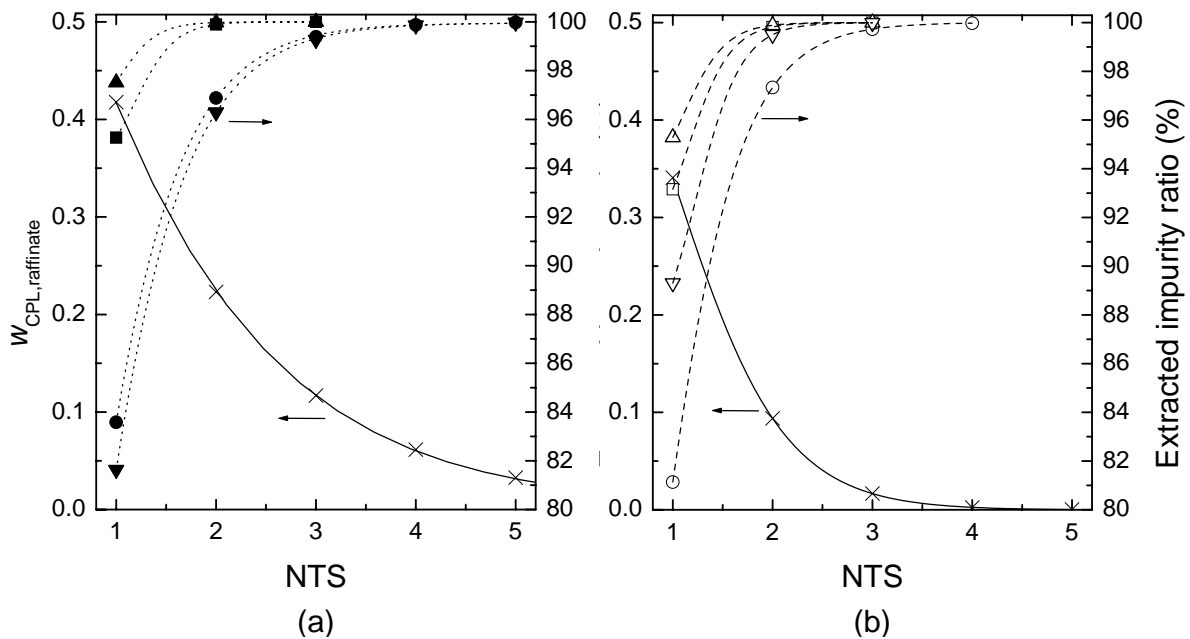
Figure 7.7. Calculated concentration of caprolactam in the raffinate as function of the NTS with toluene (a) and heptane + heptanol (40 mass %) (b) as solvent in the forward extraction: ×, caprolactam; —, trend line; and the extracted impurity ratio (a): ■, aniline; ●, n-methylcaprolactam; ▲, cyclohexanone; ▼, cyclohexane-carboxamide; --, trend line; and (b): corresponding open symbols; — —, trend line.

In the back-extraction the caprolactam-rich organic phase from the forward extraction is re-extracted at 313 K with water as solvent. Using the extract concentration from the forward extraction, $w_{CPL,extract}$ = 0.123 and 0.189 for toluene and the mixed solvent, respectively, the minimum solvent to feed ratio was calculated at $(S/F)_{min}$ = 0.26 and 0.45, respectively, resulting in S/F = 0.39 and 0.67 for toluene and the mixed solvent. The calculated raffinate fraction of caprolactam as function of the amount of equilibrium stages is shown in Figure 7.8 (a) and (b) for toluene and the solvent mixture, respectively. Furthermore the extracted impurity ratio is presented as function of the amount of equilibrium stages.
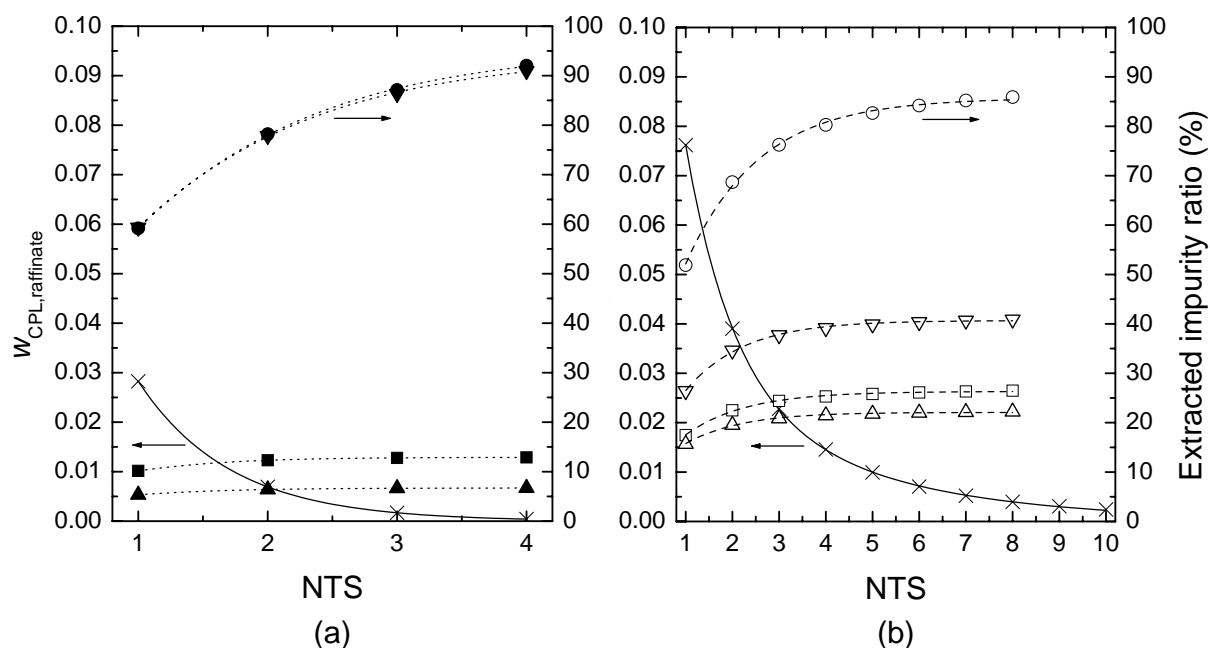
Figure 7.8. Calculated concentration of caprolactam in the raffinate as function of the NTS with toluene (a) and heptane + heptanol (40 mass %) (b) as feed phase in the back-extraction: ×, caprolactam; —, trend line; and the extracted impurity ratio (a): ■, aniline; ●, n-methylcaprolactam; ▲, cyclohexanone; ▼, cyclohexane-carboxamide; --, trend line; and (b): corresponding open symbols; — —, trend line.

From Figure 7.8 it can be concluded that the trend shown for the required amount of equilibrium stages for caprolactam extraction is reversed. This behaviour can be understood from the equilibrium distribution ratio of caprolactam, which is higher for the mixed solvent compared to toluene. This results furthermore in a reduced amount of mixed solvent required in the forward extraction, while in the back-extraction the toluene process can operate with a lower solvent to feed ratio. Since, however, the amount of toluene used in the forward extraction is 1.7 times higher than the amount of mixed solvent and the solvent to feed ratio for the toluene process in the back-extraction is 1.7 times lower, the absolute amount of water required in the back-extraction is similar for both processes. In the back-extraction, furthermore, the distribution coefficient towards the solvent is favourable for caprolactam and since the distribution coefficients differ for the impurities and for each impurity in the different solvents according to Figure 7.5, different profiles are calculated. The resulting impurity amount in the extract of the back-extraction compared to the initial amount fed in the forward extraction using toluene and heptane + heptanol (40 mass %) is shown in Table 7.1.

Table 7.1. Calculated extracted impurity ratio for toluene and mixed solvent as feed in the back-extraction.

	Cyclohexanone	Aniline	N-methyl-caprolactam	Cyclohexane-carboxamide	Total
Toluene	6.7%	12.9%	92.0%	91.0%	50.6%
Mixed solvent	22.2%	26.5%	85.9%	40.9%	43.9%

7.5   Conclusions

The equilibrium distribution ratio of caprolactam and four model impurities of organic nature was studied at 293 K, 313 K and 333 K for toluene as reference solvent and two alternative solvents, being heptane or methylcyclohexane + heptanol (40 mass %). The selected model impurities were aniline, n-methylcaprolactam, cyclohexanone and cyclohexane-carboxamide.

For the model impurities at all conditions it was found that the distribution to the organic phase was higher compared to caprolactam. Furthermore it can be concluded that changing the alkane structure in the mixed solvent from heptane to methylcyclohexane did not influence the impurity distribution ratio. The salting-out effect caused by the presence of an initial 1.5 mass % ammonium sulfate was determined for the toluene system, but the effect on the impurity distribution ratio was not large. The temperature influence was measured, but the effect differed depending on the solvent system and chemical structure of the impurities.

The required solvent to feed ratio, *S/F*, and number of theoretical stages, NTS, for the forward extraction of caprolactam followed by back-extraction using toluene and heptane + heptanol (40 mass %) were calculated. For the forward extraction *S/F* = 5.0 and 3.0 and NTS = 11 and 5, respectively, and for the back-extraction *S/F* = 0.39 and 0.67 and NTS = 4 and 10, respectively. Based on the equilibrium calculations it was found that the impurities representing group I and II were present in a higher ratio using the mixed solvent. For group III the fraction was comparable, while of group IV a significantly lower amount was present compared to toluene. Overall it can be concluded that the fraction of impurities co-extracted with toluene was higher than with the new environmentally benign mixed solvent.

Literature cited

1. Simons, A. J. F.; Haasen, N. F. Extraction of Caprolactam. In *Handbook of Solvent Extraction*; Lo, T. C.; Baird, M. H. I.; Hanson, C., Eds.; Wiley: New York, 1983; pp 557-566.

2. Alessi, V.; Penzo, R.; Slater, M. J.; Tessari, R. Caprolactam Production: a Comparison of Different Layouts of the Liquid-Liquid Extraction Section. *Chem. Eng. Tech.* **1997**, *20*, 445-454.

3. Usova, E. P.; Mitina, L. I., Sergeeva, G. S.; Sizova, G. S.; Znamenskaya, A. P. Gas-Chromatographic Determination of Impurities in Caprolactam Produced from Toluene. *J. Analyt. Chem. (USSR)* **1987**, *42*, 1661-1665.

4. Van der Gun, M. A. *Production and Purification of Crystalline Particles in a Melt - Development of a Novel Melt Crystallization Process*. PhD thesis. University of Delft, Bruno Production B.V., Delft, 2002.

Chapter 8

Extraction of caprolactam with an alternative benign solvent in a pulsed disc and doughnut column

8.1   Introduction

In Chapter 6 and Chapter 7 an alternative benign solvent for the extraction of caprolactam was developed. The mixed solvent heptane-heptanol (40 mass %) was selected via an experimental screening procedure based on a relatively high distribution ratio of caprolactam, a low mutual solvent solubility, beneficial physical properties and a low distribution ratio of impurities. From the phase compositions it was calculated that when using the mixed solvent less theoretical stages are required in the forward extraction compared to benzene and toluene, NTS = 5 relative to 9 and 11, respectively, whereas this trend was reverse in the back-extraction, NTS = 10 compared to 5 and 4, respectively. The physical properties showed slightly higher viscosities, but lower densities and interfacial tensions for the mixed solvent. The first two effects are expected to counteract each other with respect to their influence on the hold-up and operational window of an extraction column. However, the lower interfacial tension will result in smaller drops, which are expected to have a large influence on the extractor performance. The overall effect on the operational characteristics, capacity and separation efficiency of the caprolactam extraction process when applying the mixed solvent instead of the currently used solvents needs, therefore, to be investigated experimentally in a pilot scale column.

The applicability of the developed alternative solvent for caprolactam extraction was therefore experimentally validated in a pulsed disc and doughnut column (PDDC). First, pilot plant experiments were performed in the PDDC to determine the hydraulic characteristics, being Sauter drop diameter, hold-up, operating regimes and operational window, at equilibrium conditions for the forward and back-extraction configuration. These characteristics were determined as a function of the operating conditions and the experimental conditions covered the industrially applied range. The results were compared with those obtained for toluene as benchmark solvent (Chapter 4) and interpreted using a previously developed theoretical model (Chapter 3), which was fitted to the obtained toluene data. Furthermore, the overall separation performance in a PDDC was investigated for the forward and back-extraction of caprolactam with and from the mixed solvent, respectively. The experimental conditions and

operating parameters were similar to those in the hydraulic experiments. Additionally, from the above the influence of mass transfer on the hydraulic characteristics could be determined and compared with the results at equilibrium conditions. The determined separation efficiency and mass transfer influence were compared with those obtained for toluene as benchmark solvent (Chapter 5) and the concentration profiles were correlated with the backflow model.

8.2   Experimental set-up and procedure

Experimental set-up. The PDDC pilot set-up and its operation are shown and explained in Chapter 4 concerning the hydraulic characteristics and Chapter 5 for the separation performance. All hydraulic and mass transfer experiments were performed at steady state, which was created by maintaining a constant interface level. The time needed to reach a constant concentration profile is approximated by the time needed for three to four column volume replacements, which was already confirmed for extraction with toluene. Drop sizes were determined by comparing drops on digital photos of the column contents with the known size of the column internals as reference and from the digital images simultaneously the operating regimes were determined. Hold-ups were measured by sampling the column contents via two ball valves (at SP2 and SP4). The obtained volumes were left to settle after which the volume of both phases was measured. Along the column length no change in drop size and hold-up was found for the hydraulic experiments at equilibrium, but for the mass transfer experiments a profile was observed. Concentration profiles were determined from chemical analysis of separate samples of both phases, which were obtained via 8 sample ports placed along the column.

Chemicals. All chemicals were used as received. Heptane (purity 99 %) and heptanol (purity 99 %) were supplied by Fluka (USA) and ε-caprolactam (CPL) (purity grade) by DSM (The Netherlands). Demineralised water was used in all experiments.

Conditions. The experimental conditions for the determination of hydraulic characteristics and separation performance were derived from the full industrial range with respect to the concentration of caprolactam, flow ratio, temperature and phase continuity. In Table 8.1 (a) the studied operational conditions for the hydraulic characteristics in both the forward and back-extraction process are presented for each experiment (Exp.) and in Table 8.1 (b) the corresponding physical properties are presented. The hydraulic experiments were performed at equilibrium conditions to avoid the influence of mass transfer.

Table 8.1a. Experimental conditions for the determination of the hydraulic characteristics in the forward and back-extraction of caprolactam.

Exp.	Pulsation intensity			Phase flows		
	$10^3 \cdot S_p$	f	$10^3 \cdot f \cdot S_p$	Phase	Flux $= V_d + V_c$	$R = V_d/V_c$
	m	s^{-1}	m·s^{-1}	[c]	m·h^{-1}	
Forward extraction						
1,2	8.8-15.8	1.80-2.49	15.8-39.4	org	5.3-60.5	0.20; 0.33

			Back-extraction			
1,2	8.0-14.4	1.50-2.49	12.0-36.0	aq	5.3-25.0	1.0; 3.0

Table 8.1b. Physical properties for the determination of the hydraulic characteristics in the forward and back-extraction of caprolactam.

			Organic phase			Aqueous phase		
Exp.	T	w_{CPL}	$10^{-3}\cdot\rho_{org}$	$10^3\cdot\eta_{org}$	w_{CPL}	$10^{-3}\cdot\rho_{aq}$	$10^3\cdot\eta_{aq}$	$10^3\cdot\gamma$
	K	(org)	$kg\cdot m^{-3}$	$kg\cdot m^{-1}\cdot s^{-1}$	(aq)	$kg\cdot m^{-3}$	$kg\cdot m^{-1}\cdot s^{-1}$	$N\cdot m^{-1}$
1	313	0.000	0.717	0.67	0.000	0.991	0.67	11.9
2	313	0.159	0.755	0.89	0.389	1.020	2.28	1.8

In Table 8.2 (a) and (b) the experimental conditions and corresponding physical properties are presented as used in the mass transfer experiments for both the forward and back-extraction. The conditions for both FE-1 and BE-1 are directly derived from toluene experiments. In the forward extraction it was further investigated whether the column could be operated at a lower energy input and higher flux, which was expected based on the determined phase compositions and physical properties. In the back-extraction the effect of a temperature decrease was determined, since this beneficially reduces the required number of theoretical stages. In order to compare the conditions for the extraction processes, the extraction factor, *E*, is presented for the feed location, where K_D' represents the equilibrium partition ratio based on the solute mass fraction in the extract and *Fy'* and *Fx'* represent the solute-free solvent and feed mass flow rates.

Table 8.2a. Experimental feed conditions during mass transfer experiments in the forward and back-extraction process of caprolactam (varied parameters are shown as 'bold' characters).

				Forward extraction (FE): aqueous feed phase dispersed			
	w_{CPL}	w_{AS}	T	$10^3\cdot f\cdot S_p$	Flux=V_{feed}+$V_{solvent}$	R=V_d/V_c	E=$K_D'\cdot F_y'/F_x'$
	(aq)	(aq)	K	$m\cdot s^{-1}$	$m\cdot h^{-1}$		
FE-1	0.50	-	313	16.5	20.4	0.23	1.7
FE-2	0.50	-	313	**12.7**	20.6	0.23	1.7
FE-3	0.50	-	313	**12.7**	**30.1**	0.23	1.7
				Back extraction (BE): organic feed phase dispersed			
	w_{CPL}		T	$10^3\cdot f\cdot S_p$	Flux=V_{feed}+$V_{solvent}$	R=V_d/V_c	E=$K_D'\cdot F_y'/F_x'$
	(org)		K	$m\cdot s^{-1}$	$m\cdot h^{-1}$		
BE-1	0.15		313	16.0	20.8	2.1	1.7
BE-2	0.15		**293**	16.0	20.6	2.1	1.8

Table 8.2b. Physical properties regarding the forward and back-extraction of caprolactam covering the maximum concentration range.

	$w_{CPL,d}$ (aq)	$w_{AS,d}$ (aq)	$w_{CPL,c}$ (org)	$10^{-3} \cdot \rho_c$ kg·m^{-3}	$10^{3} \cdot \eta_c$ kg·m^{-1}·s^{-1}	$10^{-3} \cdot \rho_d$ kg·m^{-3}	$10^{3} \cdot \eta_d$ kg·m^{-1}·s^{-1}	$10^{3} \cdot \gamma$ N·m^{-1}
Forward extraction (FE): aqueous feed phase dispersed								
FE-1; FE-2; FE-3	0.50	-	0.14	0.751	0.87	1.029	2.81	11.9
	0.00	-	0.00	0.717	0.67	0.991	0.67	2.3

	$w_{CPL,d}$ (org)	$w_{AS,c}$ (aq)	$w_{CPL,c}$ (aq)	$10^{-3} \cdot \rho_c$ kg·m^{-3}	$10^{3} \cdot \eta_c$ kg·m^{-1}·s^{-1}	$10^{-3} \cdot \rho_d$ kg·m^{-3}	$10^{3} \cdot \eta_d$ kg·m^{-1}·s^{-1}	$10^{3} \cdot \gamma$ N·m^{-1}
Back-extraction (BE): organic feed phase dispersed								
BE-1	0.15	-	0.19	1.006	1.17	0.771	0.89	3.4
	0.00	-	0.00	0.991	0.67	0.717	0.67	11.9
BE-2	0.15	-	0.20	1.016	1.95	0.754	1.24	3.6
	0.00	-	0.00	0.998	1.02	0.733	0.92	11.9

In Table 8.1 (b) and Table 8.2 (b) the physical properties, being densities and viscosities of both separate phases and the interfacial tension between the phases, are presented for the concentrations and temperatures used. The physical properties of the quaternary systems water + caprolactam (CPL) + mixed solvent were correlated by the equations as presented in Chapter 2. These correlations cover the entire range of concentrations and temperatures applied in this study, except for the interfacial tension. The latter is only valid for concentrations of caprolactam in the organic phase from 0 up to 5 mass %. For experimental conditions with higher concentrations the relation was therefore extrapolated to determine the interfacial tension. The equilibrium distribution ratio, K_D', was based on equilibrium data (Chapter 6) and fitted as function of the feed-phase concentration by relevant first or second order polynomials. The mass fraction of caprolactam in both the organic and the aqueous phase and of heptanol in the organic phase was determined by gas chromatography, where the same analytical method was applied for both phases, as described in Chapter 2 and Chapter 6.

8.3   Hydraulic experiments: experimental results and data correlation

The column could be operated within a certain window covering a range of operational parameters as described in Chapter 3 and as determined and correlated in Chapter 4. First the characteristics within the operational window, being drop diameter, operational regime and hold-up, are described, after which the boundaries of the operational window, being flooding (1) at low pulsation and flooding (2) or phase inversion at high pulsation, are correlated.

8.3.1 Sauter drop diameter.

The experimentally determined Sauter drop diameter values, d_{32}, for the forward and back-extraction of caprolactam with the mixed solvent are presented in Figure 8.1 (a) and (b), respectively, and compared with data obtained for toluene (Chapter 4).
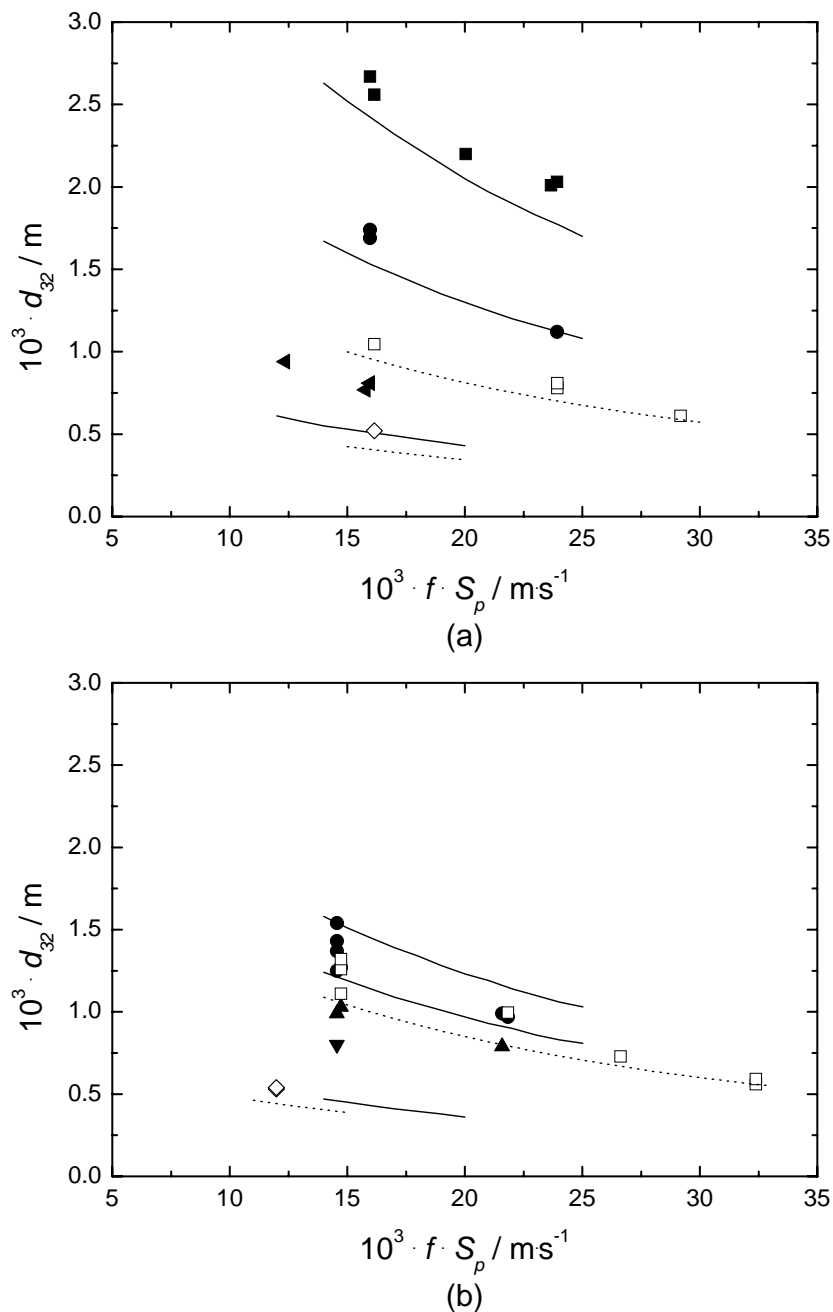
Figure 8.1. Experimental and fitted average drop sizes in the forward (a) and back-extraction (b) as function of the pulsation intensity at 313 K at various caprolactam concentrations for toluene: ■, $w_{CPL,aq} = 0.000$; ●, $w_{CPL,aq} = 0.086$; ▲, $w_{CPL,aq} = 0.192$; ▼, $w_{CPL,aq} = 0.461$; ◄, $w_{CPL,aq} = 0.475$; and for the mixed solvent: □, $w_{CPL,aq} = 0.000$; ◇, $w_{CPL,aq} = 0.389$; and: —, fit toluene; -- fit mixed solvent.

In Figure 8.1 (a) and (b) it can be seen that the determined drop diameter data show comparable trends to the drop diameter data for the toluene system (Chapter 4). An increase in the pulsation intensity or concentration of caprolactam resulted in a decreasing drop diameter, because of increased droplet break-up or a strong reduction of the interfacial tension

with an increase in the concentration of caprolactam (in the organic phase), respectively. It was furthermore found that a change in the flow ratio or total flux did not affect the Sauter drop diameter and an individual influence of frequency and amplitude was not observed. Finally, it can be seen that at similar conditions the drop size for the mixed solvent system is much smaller than for the toluene system, especially when the concentration of caprolactam is low. This is caused by the lower interfacial tension of the mixed solvent system.

The drop diameter data determined for the mixed solvent was described according to the developed model for a hydraulic system in a PDDC (Chapter 3), using parameter values fitted on drop diameter data obtained for toluene as solvent. Application of the derived equation resulted in an uncertainty of AARE = 12.1% for NDP = 14. The resulting drop diameter profiles for both solvents in the forward and back-extraction are presented in Figure 8.1 (a) and (b), together with the experimentally determined data. From the presented profiles it can be concluded that the determined drop diameter data were correlated accurately.

8.3.2   Operating regimes

Simultaneous with the drop diameter measurements operating regimes were established from visual observation. Mixer-settler and dispersion regimes were found for both the back-extraction and the forward extraction process at certain pulsation intensities as presented in Figure 8.2 (a) and (b), respectively. The points at which the column is operated, are presented as the mixer-settler region (closed symbols) and the dispersion or emulsion region (open symbols). It can be concluded that at constant pulsation intensity the operating regime changes from mixer-settler to dispersion regime with an increasing concentration of caprolactam. This is mainly caused by a decrease of the drop size. Since the latter decreases as well with increased pulsation intensity at a constant concentration of caprolactam, the operation changes from mixer-settler to dispersion regime with increasing pulsation intensity. Since the drop size for the mixed solvent system is smaller compared to the toluene system, the mixer-settler regime transists to the dispersion regime at lower pulsation intensities.

(a)
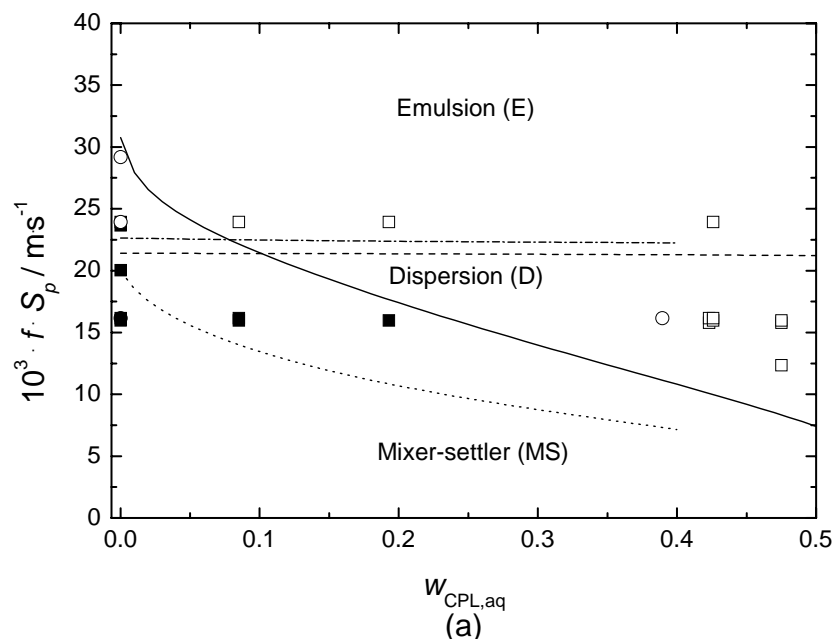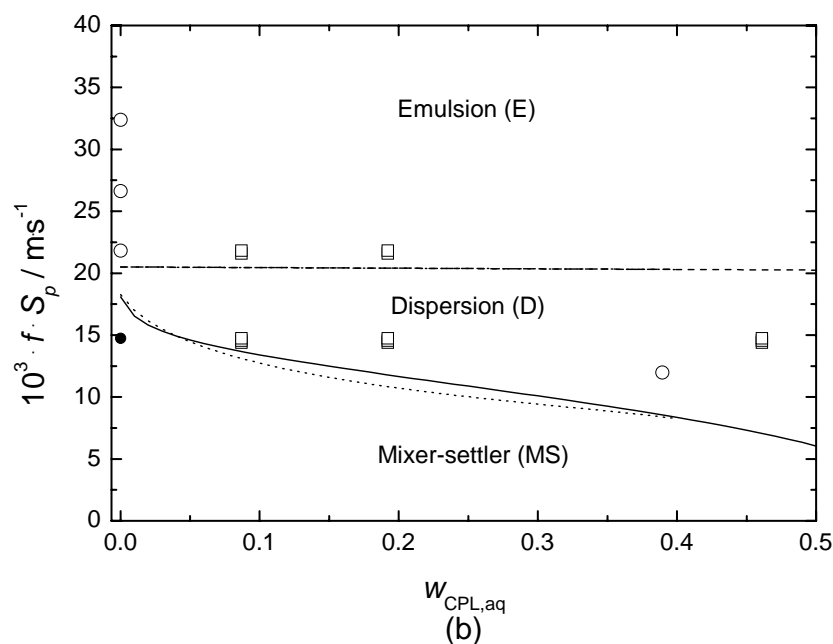
Figure 8.2. Experimental and fitted operating regimes characterized by the pulsation intensity in the forward (a) and back-extraction (b) as function of the aqueous caprolactam weight fraction, where the MS regime was found for: ■, toluene; ●, mixed solvent; and D or E regime: □, toluene; ○, mixed solvent; and fit of MS to D transition: —, toluene; --, mixed solvent; prediction of D to E transfer: — —, toluene; — - —, mixed solvent.

The transitions from the mixer-settler to the dispersion regime and from the dispersion to the emulsion regime were correlated according to the developed model (Chapter 3). The latter is based on a predictive equation, but the correlation of the first contains an empirical constant, $k_3/\text{m·kg}^{-1/6}\text{·s}^{-7/12} = 9.69\cdot10^{-3}$, which was fitted on regime transition data in the PDDC with toluene as solvent for the forward and back-extraction within a range of $1.43\cdot10^{-2} < k_3 < 1.70\cdot10^{-2}$ and $7.82\cdot10^{-3} < k_3 < 8.97\cdot10^{-3}$, respectively (Chapter 4). Based on the regime transition data for the mixed solvent system this range could be fitted for the forward and back-extraction at $1.11\cdot10^{-2} < k_3 < 1.65\cdot10^{-2}$ and $1.01\cdot10^{-2} < k_3 < 1.50\cdot10^{-2}$, respectively. It can be concluded that the determined values for both solvents correspond well. In the back-extraction, however, only the upper boundary for the toluene and the lower boundary for the mixed solvent system are comparable. Using an average value, being $k_3/\text{m·kg}^{-1/6}\text{·s}^{-7/12} = 1.57\cdot10^{-2}$ and $8.40\cdot10^{-3}$ for toluene and $k_3/\text{m·kg}^{-1/6}\text{·s}^{-7/12} = 1.38\cdot10^{-2}$ and $1.25\cdot10^{-2}$ for the mixed solvent in the forward and back-extraction, respectively, the calculated regime transitions are presented in Figure 8.2 (a) and (b), together with the experimentally observed regimes. It can be concluded from these figures that the observed mixer-settler to dispersion regime transition is described accurately.

8.3.3 Dispersed phase hold-up

The experimentally determined hold-up data for the mixed solvent in comparison to toluene (Chapter 4) are shown for the forward and back-extraction in Figure 8.3 (a) and (b), respectively.

(a)

(b)
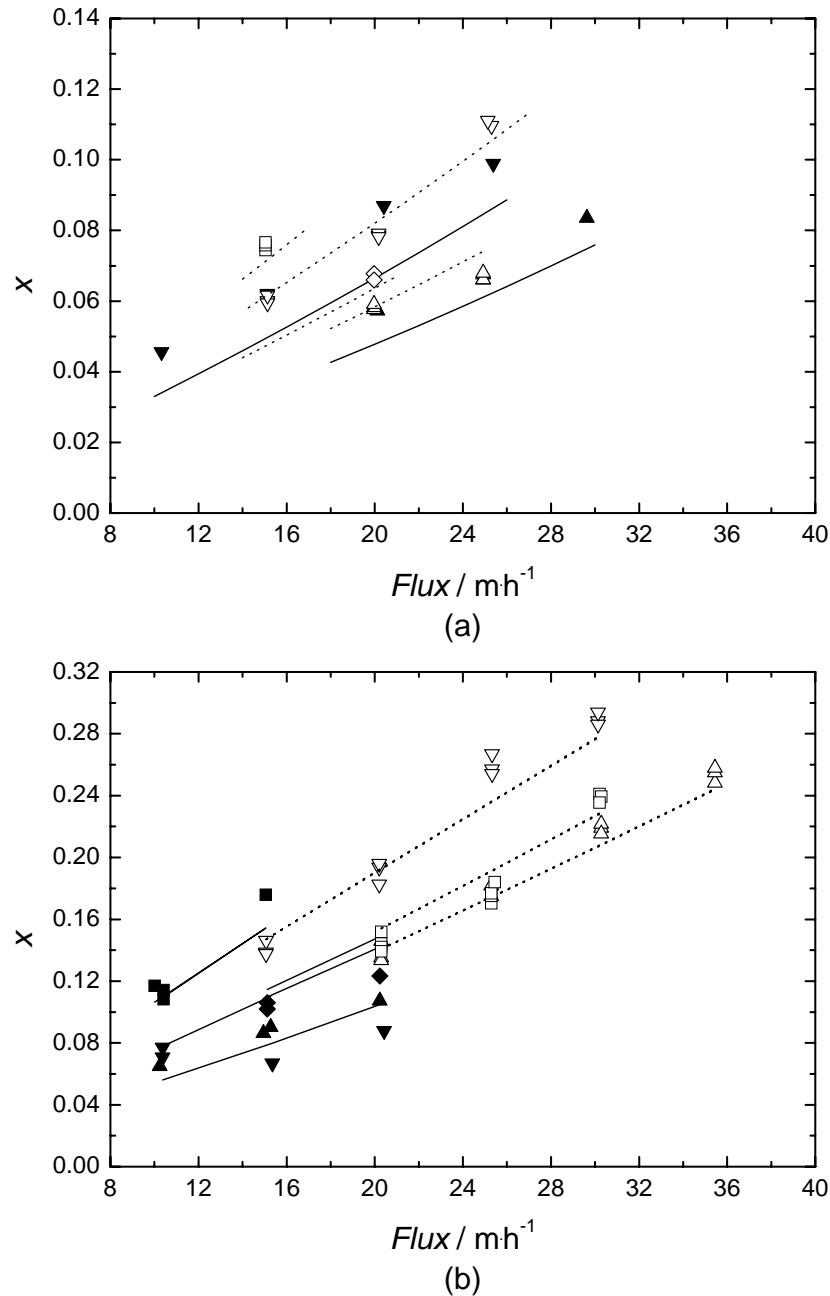
Figure 8.3 Experimentally determined and fitted hold-up data in the forward (FE) (a) and back-extraction (BE) (b) as function of the flux, where in FE for toluene: $R = 0.20$, $w_{\text{CPL,aq}} = 0.43$ and $f \cdot S_p = 0.016$ ($\triangle$), unless stated otherwise; $\diamondsuit$, $f \cdot S_p = 0.016$; $\triangledown$, $R = 3.0$, $\square$, $w_{\text{CPL,aq}} = 0.47$; for the mixed solvent: $R = 0.20$, $w_{\text{CPL,aq}} = 0.39$ and $f \cdot S_p = 0.016$ ($\blacktriangle$), unless stated otherwise; $\blacktriangledown$, $R = 0.33$; in BE for toluene: $R = 1.0$, $w_{\text{CPL,aq}} = 0.09$ and $f \cdot S_p = 0.015$ ($\triangle$), unless stated otherwise; $\triangledown$, $R = 3.0$, $\square$, $w_{\text{CPL,aq}} = 0.19$; for the mixed solvent: $R = 3.0$, $w_{\text{CPL,aq}} = 0.0$ and $f \cdot S_p = 0.022$ ($\blacktriangle$), unless stated otherwise, $\blacktriangledown$, $R = 1.0$, $\blacklozenge$, $f \cdot S_p = 0.027$; $\blacksquare$, $w_{\text{CPL,aq}} = 0.39$; and: --, fit toluene; —, fit mixed solvent (where $f \cdot S_p/\text{m} \cdot \text{s}^{-1}$).

In Figure 8.3 (a) and (b) several trends can be observed in the determined hold-up, x, profiles. An increase of the flux, flow ratio, R, or the pulsation intensity, $f \cdot S_p$, resulted in an increasing hold-up. This can be explained by a (relative) increase of the flow rate of dispersed phase compared to continuous phase and a decreasing drop size, resulting in the drops being slowed down. The influence of the physical properties is accounted for by the increase of the hold-up with an increasing concentration of caprolactam, which results in increased viscosities and a

reduction in interfacial tension. This leads to smaller drop velocities. Furthermore, it can be seen that at similar conditions, the hold-up for the mixed solvent is comparable in the forward extraction and smaller in the back-extraction than for the toluene system, which is caused by the counter-acting effects of a smaller interfacial tension, larger viscosity and lower density for the mixed solvent.

The hold-up profiles determined for the mixed solvent were correlated according to the developed model for a hydraulic system in a PDDC (Chapter 3), using parameter values fitted on hold-up data obtained for toluene as solvent (Chapter 4). Application of this correlation resulted in an uncertainty of AARE = 21.6%, where NDP = 81. The main contribution to the AARE resulted from the hold-up data in the forward extraction at $w_{CPL,aq}$ = 0.000, where the hold-up data were very low and the relative error therefore large. The calculated hold-up profiles for the toluene and mixed solvent system are presented in Figure 8.3 (a) and (b) together with the experimentally determined data. From this figure it can be concluded that the description of the data is accurate.

8.3.4   Operational range

In the model development (Chapter 3) it was concluded that several regimes could be limiting for operation of the extraction column, being flooding (1) due to a too low pulsation intensity, flooding (2) due to a too low relative velocity between the phases or phase inversion. Flooding at low pulsation is described by the pulsed volume and was in our experiments qualitatively observed, but not quantitatively determined. For the forward and back-extraction flooding (2) was observed as the limiting process. The determined fluxes at flooding (2) conditions are presented in Figure 8.4 (a) and (b) for the forward and back-extraction process, respectively.

(a)

(b)
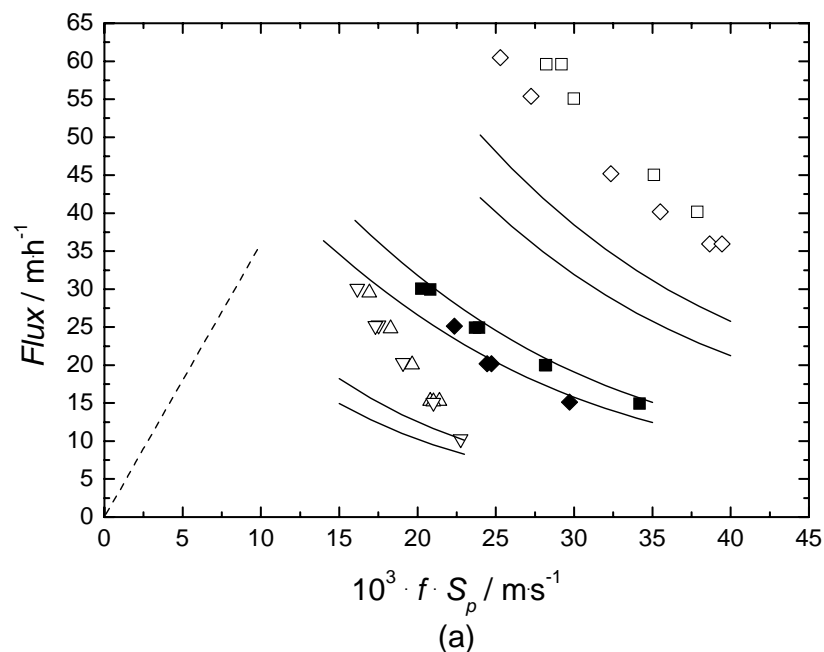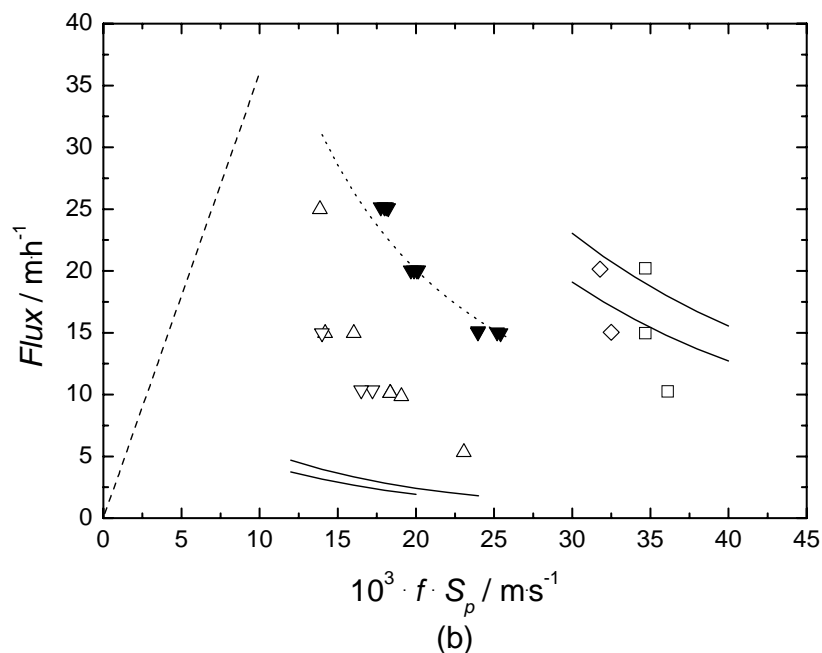
Figure 8.4 Experimentally determined and predicted flooding (2) data in the forward extraction (a) for toluene at $w_{CPL,aq} = 0.086$: ■, $R = 0.20$; ◆, $R = 0.33$; and for the mixed solvent at $w_{CPL,aq} = 0.000$: □, $R = 0.20$; ◇, $R = 0.33$; and at $w_{CPL,aq} = 0.389$: △, $R = 0.20$; ▽, $R = 0.33$; and in the back-extraction phase inversion data for toluene: ▼, $w_{CPL,aq} = 0.39$ with $R = 3.0$; and flooding (2) data for the mixed solvent: at $w_{CPL,aq} = 0.000$: □, $R = 0.20$; ◇, $R = 0.33$; and at $w_{CPL,aq} = 0.389$: △, $R = 0.20$; ▽, $R = 0.33$; —, flooding (2) prediction; --, phase inversion fit; — —, flooding (1) prediction.

In Figure 8.4 (a) and (b) it can be seen that at increasing pulsation intensities, the total flux at flooding and phase inversion (for toluene in the back-extraction) decreases. This is due to a decrease of the drop size with increasing pulsation intensity, which results in an increase of the hold-up, such that the critical hold-up is reached at a lower total flux. The hold-up also increases with an increasing flow ratio and an increasing concentration of caprolactam in the organic phase, which results in a lower total flux that can be applied as well.

At flooding the maximum value for the hold-up, x_f, is reached, which was calculated at $x_f = 0.10$ to 0.25 for the complete range of experimental conditions investigated. These are acceptable maximum hold-up values compared to the experimentally determined hold-up data at steady state operation. A high mass fraction of caprolactam in the aqueous phase, $w_{CPL,aq} = 0.389$, in the back-extraction, however, results in a high drag coefficient in the applied theory, corresponding to an unrealistic prediction of the flux at flooding, as presented in Figure 8.4 (b) and as concluded previously for the toluene system (Chapter 3 and Chapter 4). Removing these unreliable data the uncertainty was AARE = 30.7% at NDP = 28.

In back-extraction flooding (2) was found as limiting process for the mixed solvent, while phase inversion was found for toluene. In the comparison of the conditions at which the respective limiting processes occurred, the critical hold-up at flooding (2) and phase inversion and the resulting fluxes were considered (Chapter 3 and Chapter 4). The critical hold-up at phase inversion for the mixed solvent was calculated at $x_{PI} = 0.49$ to 0.52, compared to $x_f = 0.10$ to 0.25 for the experimental conditions investigated. The corresponding fluxes are 1.2 to 3.2 times larger for phase inversion compared to flooding (2), which results in the conclusion

that flooding (2) could be expected as limiting process for the mixed solvent in the back-extraction.

Comparing the operational windows limited by flooding (2) for toluene and the mixed solvent, several parameters have an effect on the flux that can be reached, which are d_{32}, $\Delta\rho$, x, η_c and ρ_c, and of these d_{32} and $\Delta\rho$ change the most for the different solvents. The smaller drop diameter for the mixed solvent would result in a smaller operational window, but the larger density difference compensates for this effect. Therefore there is not a large difference in the size of the operational window for both solvents. The comparison of the effects of different parameters on phase inversion for toluene and flooding (2) for the mixed solvent in the back-extraction is more complicated. For toluene it was, however, calculated according to the respective theories that the flux at phase inversion and flooding (2) are almost equal (Chapter 4). In accordance with the discussion for the forward extraction a comparable operational window can be expected for both solvents in the back-extraction as well. However, flooding (2) can not be predicted accurately for $w_{CPL,aq} > 0.2$ in the back-extraction, since the drag coefficient used in the applied theories increases exponentially for higher concentrations.

8.3.5 Operational window

Experimental data and the derived equations for the description of the operational window, including flooding (1), the different operating regimes and the limiting process were applied to construct an operational diagram. For $w_{CPL,aq} = 0.389$ at $R = 0.20$ and 0.33 in the forward and $w_{CPL,aq} = 0.000$ at $R = 1.0$ and 3.0 in the back-extraction such a diagram is presented in Figure 8.5 (a) and (b). In this diagram the conditions at steady state operation, experimentally determined and fitted limiting process conditions, being flooding (1) and flooding (2), and the critical pulsation intensity required for the transition between the operating regimes, being mixer-settler, dispersion and emulsion, are presented.

(a)
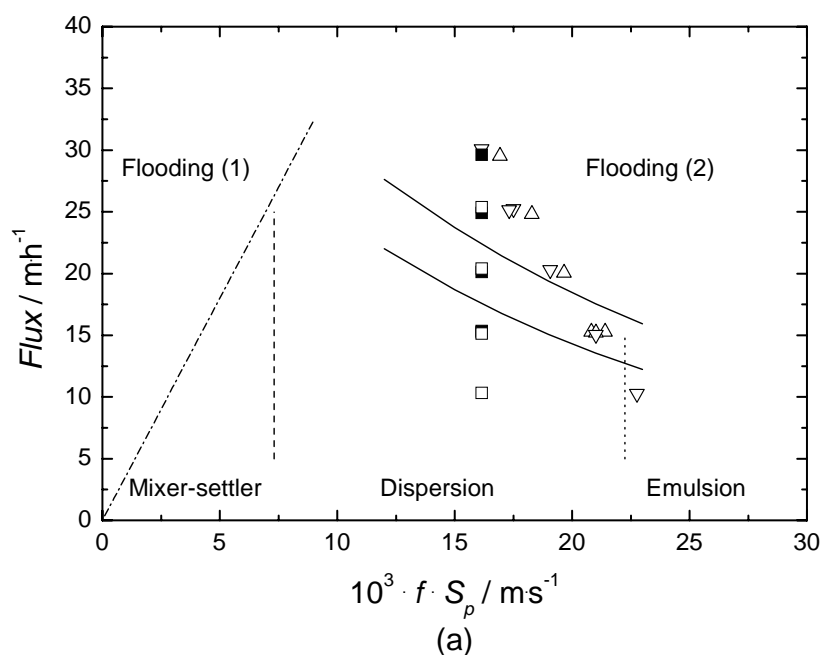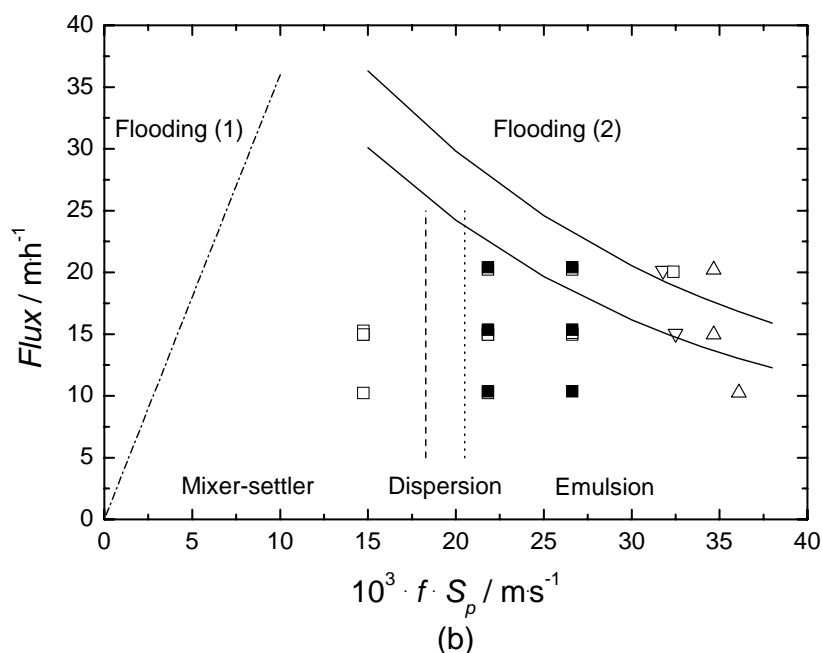
Figure 8.5. Operational diagram for $w_{\text{CPL,aq}} = 0.389$ in the forward (a) and $w_{\text{CPL,aq}} = 0.000$ in the back-extraction (b), where for $R = 0.20$ (FE) and 1.0 (BE): ■, steady state operation; △, flooding (2) and for $R = 0.33$ (FE) and 3.0 (BE): □, steady state operation; ▽, flooding (2); and : —, prediction flooding (2), — —, fit MS to D transition; --, prediction D to E transition; — - —, prediction flooding (1)

It can be seen that at a constant flux and increasing pulsation intensity first the flooding (1) line is crossed after which the operational regime transits from mixer-settler to dispersion and emulsion. Increasing the pulsation intensity even more or increasing the flux at a constant pulsation intensity results in reaching the boundary of the operational window. At each operating point Sauter drop diameter and hold-up values can be calculated. Diagrams as presented in Figure 8.5 (a) and (b) can be constructed for each system in the back- and forward extraction, but are specific with respect to concentrations, temperature and flow ratio.

Comparing the operational window and especially the operational range, it can be concluded that using toluene as solvent results in a slightly larger operational window compared to the mixed solvent. The extraction process with toluene can therefore be operated at higher fluxes and pulsation intensities, which is beneficial for the column capacity and the interfacial area, respectively. However, for the treatment of a set feed stream in the forward extraction a lower amount of mixed solvent is required relative to toluene, resulting in a lower flux. For the back-extraction the mixed solvent system operates with a larger solvent to feed ratio than toluene. However, since the feed, being the extract stream from the forward extraction, is lower for the mixed solvent system, the absolute amount of solvent required in the back-extraction is comparable for both solvent systems and the resulting flux for the toluene system is even higher. Finally, the lower interfacial tension of the mixed solvent system results in smaller drops compared to toluene, which result in a relatively high interfacial area even at lower pulsation intensities. Despite the slightly smaller operational window, it can therefore be concluded that the experimentally determined hydraulic characteristics at equilibrium are beneficial for the mixed solvent relative to toluene.

8.4   Mass transfer experiments

8.4.1   Experimental results

The influence of the operational conditions as presented in Table 8.2 (a) on the concentration profiles of both processes using the mixed solvent was investigated and compared to results obtained with toluene (Chapter 5). The resulting experimentally determined concentration profiles for the forward and back-extraction are shown in Figure 8.6 (a) and (b), respectively.

(a)

(b)
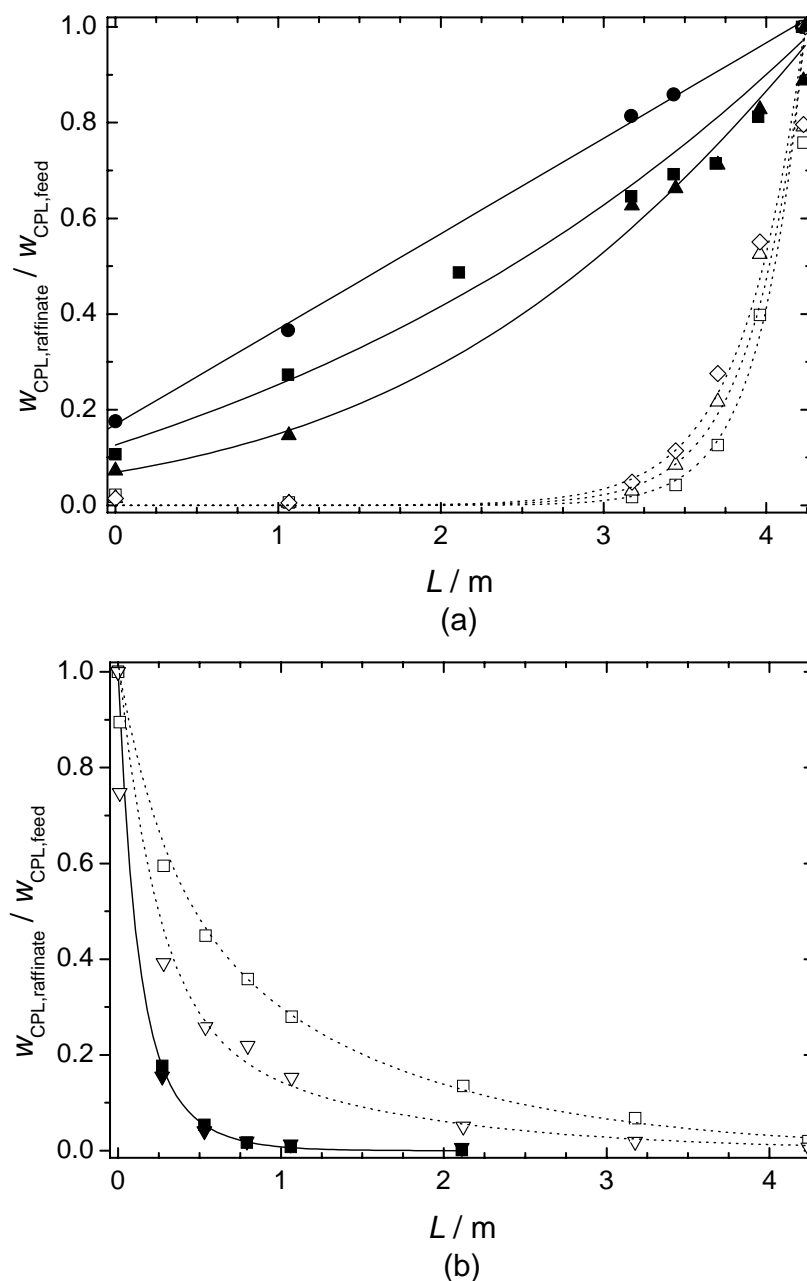
Figure 8.6. Experimental concentration profiles in the forward extraction (a) as function of the position along the column at Flux = 20, $f \cdot S_p$ = 0.016 and T = 313, unless stated otherwise: for toluene (■): ●, Flux = 26; ▲, $f \cdot S_p$ = 0.022; and for the mixed solvent (□): △, $f \cdot S_p$ = 0.013; ◇, $f \cdot S_p$ = 0.013 and Flux = 30; and in the back-extraction (b) at Flux = 20, $f \cdot S_p$ = 0.016 and T = 293, unless stated otherwise: for toluene (■): ▼, T = 313; and for the mixed solvent (▽): □, T = 313 (presented lines are trend lines; where Flux/m·h^{-1}; $f \cdot S_p$/m·s^{-1} and T/K).

137

In Figure 8.6 (a) and (b) the determined concentration profiles for the forward and back-extraction of caprolactam with toluene and the mixed solvent are presented. It is obvious that the mixed solvent is superior in the forward extraction, while toluene is favourable in the back-extraction. This is the result of the phase equilibria of both systems, which result in a higher equilibrium distribution coefficient, K_D', for the mixed solvent. In the forward extraction the driving force for mass transfer is therefore higher for the mixed solvent, while it is lower in the back-extraction. In both processes the influence of operational parameters can be distinguished clearly. An increasing flux resulted in a relatively poor separation performance. This can be attributed to a reduction in residence time relative to mass transfer time, although the mass transfer rate increased slightly because of an increase in the hold-up, as expected from the hydraulic tests. The influence of pulsation intensity is directly related to a changing drop size and hold-up and therefore interfacial area, resulting in an influence on the mass transfer rate. The influence of temperature in the back-extraction resulted in a change of system properties. This affected the hold-up, drop size, and the distribution ratio, resulting in a change of the driving force for mass transfer. For the mixed solvent a temperature increase resulted in an unfavourable process, but for toluene the concentration profiles for all operational conditions were comparable. This is probably the result of the highly favourable distribution ratio under all conditions, resulting in a large driving force for mass transfer.

8.4.2   Backflow model

Mass transfer profiles for caprolactam extraction with toluene in a PDDC were correlated via the backflow model (Chapter 5). The basis of the backflow model consists of a series of well-mixed stages, between which backmixing occurs. The parameters required to describe the concentration profile in both phases are: phase flow rates, F_x and F_y, the volume of a characteristic column segment, $(s \cdot h_c)$, the specific interfacial area, a, the backflow parameters, α_x and α_y, and the overall mass transfer coefficient based on feed phase (x), k_{ox}.

According to the developed model, the phase flow rates $F_{x,n}$ and $F_{y,n}$ are introduced in the iterative procedure, since the flow rates change along the column due to the change in the concentrations. These concentrations are expressed based on the solute-containing volume streams for which it was assumed that both phases are immiscible. The cross-sectional column area, s, was determined from the column dimensions. The characteristic height was chosen at $h_c/m = 0.02$, which corresponds to the disc to disc distance of the internals. It is also the step size used in the iterative procedure. The interfacial area was calculated via the hold-up, x, and Sauter drop diameter, d_{32}. The hold-up and drop diameter are influenced by mass transfer, resulting in an increasing drop size and a decreasing hold-up compared to the hydraulic characteristics at equilibrium conditions. The effect of mass transfer on the interfacial area and operating regimes for caprolactam extraction in a PDDC was therefore determined experimentally. The backflow parameters for phase x and y, α_x and α_y, respectively, and the overall mass transfer coefficient, k_{ox}, were assumed constant over the length of the column, where $\alpha_x = 0$, since in general the effect of axial dispersion in the dispersed phase is small.

The unknown values of k_{ox} and α_y were determined by fitting a value for k_{ox} at a given value for α_y, assuming $\alpha_x = 0$, in order to comply with the determined concentration profile and raffinate concentration. Performing this procedure for a series of α_y values resulted in a minimized Absolute Average Error (AAE) in the experimentally determined and calculated normalized weight fractions and therefore in optimal values of k_{ox} and α_y. The separation performance of the PDDC for the forward and back-extraction was furthermore interpreted using the Height Equivalent of a Theoretical Stage (HETS), which is calculated based on the determined concentration profiles and the equilibrium data.

8.4.3 Determination of mass transfer influence on the hydraulic parameters

The hold-up and Sauter drop diameter in the caprolactam forward and back-extraction process can be described for the hydraulic situation. The experimentally determined increase of the drop size under mass transfer conditions was 1.3 ± 0.1 and 1.8 ± 0.1 (accuracy determined as standard deviation) for the forward and back-extraction, respectively, compared to 1.4 ± 0.1 and 1.9 ± 0.1 for the toluene system. It was furthermore observed that when mass transfer was negligible, the factor describing the relative increase of the drop size approached 1.0. The drop size was thus described using the relation derived for the hydraulic situation including the determined factors to account for the relative drop size increase due to mass transfer.

Since the drop size changes under mass transfer conditions, the transition between the operating regions changes as well compared to the hydraulic conditions. The experimentally determined increase in the required pulsation intensity for the transition from the mixer-settler to the dispersion regime was 0.94 to 1.15 for the forward extraction and 1.3 to 1.4 for the back-extraction. From experimental observation and the derived increase in the pulsation intensity required for regime transition, it was found for all experimental conditions that at the feed side of the column the operation started in the emulsion or dispersion region. Moving along the column, however, the operating regime changed from dispersion to mixer-settler.

The hold-up decreases as a result of a drop diameter increase under mass transfer conditions, but operation in the mixer-settler regime results in an increase of the hold-up compared to operation in the dispersion regime. Mixer-settler operation and mass transfer therefore counter-act each other with respect to the hold-up profile and since insufficient data was available to describe both effects, it was chosen to describe the hold-up profile over the column with the equation derived for the equilibrium situation.

The increase of the drop size under mass transfer conditions resulted in an increase of the pulsation intensity required for regime transition and a decrease of the hold-up compared to the equilibrium system. As for the toluene system, the increase of the drop size was assumed to result from an average interfacial tension increase. Using this approach the effect of mass transfer on the regime transition and hold-up could be predicted from the determined drop diameter increase. The increase in the pulsation intensity required for regime transition was predicted at 1.17 and 1.4 and the decrease in hold-up at 0.90 and 0.83 for the forward and back-extraction, respectively. Comparing the determined and predicted effects based on the drop size increase, it can be seen that the approach used resulted in an accurate interpretation.

8.4.4   Model results: forward extraction

In the forward extraction using the mixed solvent all caprolactam is extracted and the values for the axial dispersion coefficient in the continuous phase, α_y, and the overall mass transfer coefficient, k_{ox}, were fitted by minimizing the value of the absolute average error (AAE) in the experimentally determined and calculated normalized weight fractions, see Table 8.3 for the results. Furthermore, the predicted values of k_{ox} are shown for the experimentally determined range of caprolactam concentrations, together with the determined values of the Height Equivalent of a Theoretical Stage (HETS). The experimental conditions (Exp.) were $T/K = 313$, $f \cdot S_p / m \cdot s^{-1} = 0.016$, Flux$/m \cdot h^{-1} = 20$ (FE-1), unless stated otherwise, and the flow ratio was always $R = 0.23$.

Table 8.3. Determined k_{ox} and α_y values at the fitted minimum AAE value in the forward extraction together with the predicted k_{ox} values.

	Exp.			α_y	$10^5 \cdot k_{ox}$		HETS
	Flux	$f \cdot S_p$	T	fit	fit	predicted	
	$m \cdot h^{-1}$	$m \cdot s^{-1}$	K		$m \cdot s^{-1}$	$m \cdot s^{-1}$	m
FE-1	20	0.016	313	2.0	3.3	1.7 - 3.8	0.26
FE-2	21	0.013	313	2.4	3.1	1.5 - 3.5	0.32
FE-3	30	0.013	313	1.0	2.5	1.6 - 3.7	0.37

The results obtained as presented in Table 8.3, show partly similar trends to those obtained for the back-extraction process with toluene as solvent (Chapter 5). The introduction of a backflow parameter for the continuous phase, α_y, resulted as well in a significant decrease in the AAE value compared to the case where $\alpha_y = 0$ and for all experiments a range existed for $\alpha_y \pm 1.2$ where AAE was within 10% of the minimum AAE value. Finally, it can be seen that the fitted k_{ox} values are within the predicted range for all experiments. Since all fitted values are more or less comparable and since a large range of possible α_y values exists, no conclusions can be drawn about the influence of the operational parameters on the fitted values. It is therefore desirable to determine the values of the backflow parameters, α_x and α_y, from separate experiments.

Comparing the fitted values to those obtained for toluene it has to be noted that for toluene no minimum AAE value was obtained for $0 < \alpha_y < 6$. Fitted values for α_y can therefore not be obtained. The fitted and predicted values of k_{ox} are higher for the mixed solvent, which might be a part of the explanation of the faster extraction using this solvent compared to toluene.

In the table HETS values are presented as well, which are calculated based on the determined concentration profiles and equilibrium data. The influence of operational conditions can be seen clearly on the determined values as for toluene, where the decrease in pulsation intensity and the increase in flux resulted in an increase of HETS. This was mainly caused by less interfacial area and an increased ratio of flow rates to mass transfer rate, respectively. For

toluene at Flux/m·h^{-1} = 20 and $f \cdot S_p$/m·s^{-1} = 0.016 it was calculated that HETS/m = 0.55 compared to 0.26 for the mixed solvent. Changing the conditions for toluene to Flux/m·h^{-1} = 26 or $f \cdot S_p$/m·s^{-1} = 0.022 resulted in HETS/m = 0.67 and 0.42, respectively. It can therefore be concluded that in the forward extraction the mixed solvent not only needs less theoretical stages relative to toluene, but that these are obtained over a smaller column height as well.

From the fitting procedure caprolactam concentration, Sauter drop diameter and hold-up profiles were obtained for the different operational conditions and the resulting profiles for FE-1 are presented in Figure 8.7 as function of the normalized column length, L/L_c.
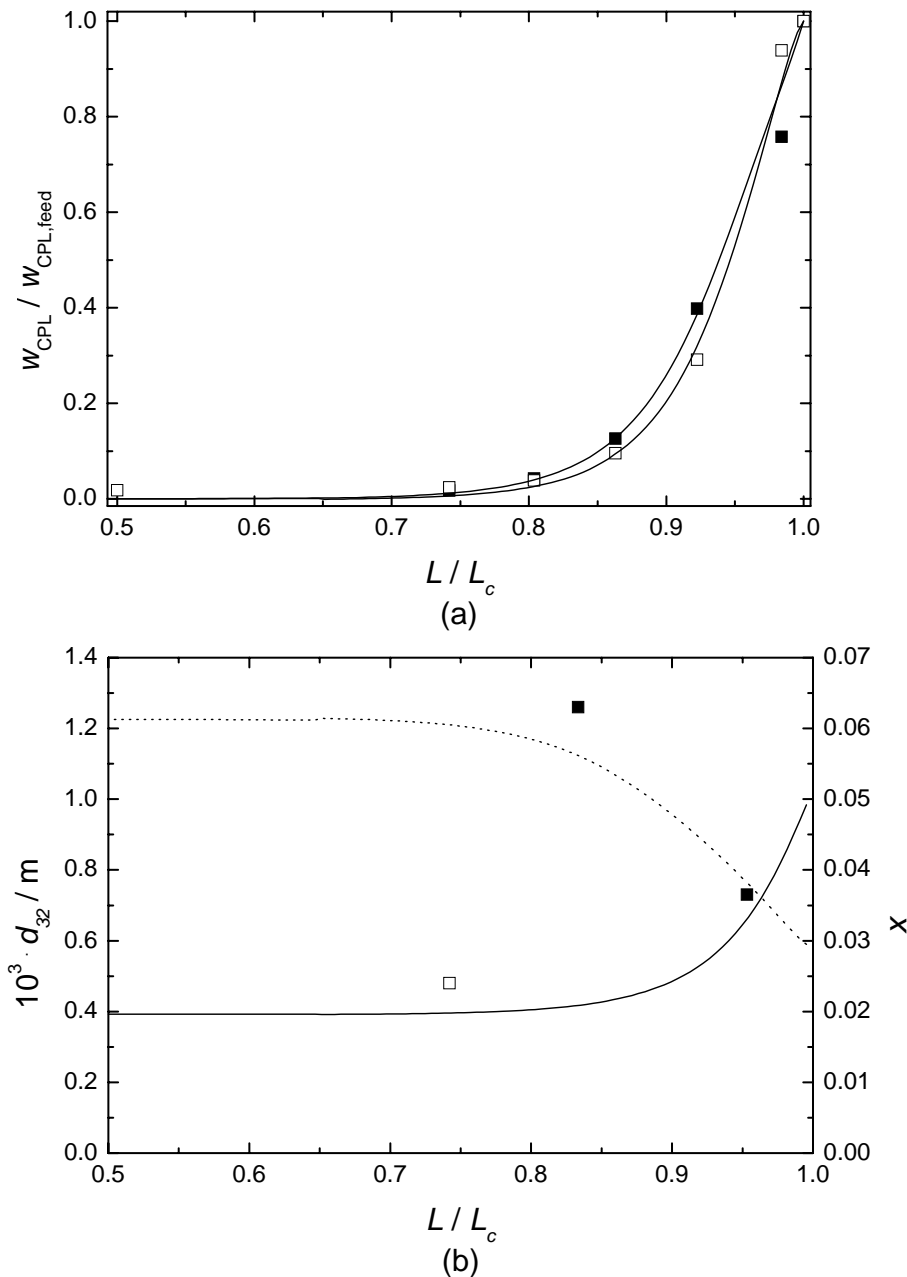
Figure 8.7. Normalized concentration profiles along the normalized column position (a), where T/K = 313, $f \cdot S_p$/m·s^{-1} = 0.016, Flux/m·h^{-1} = 20 and R = 0.23 (FE-1): ■, raffinate phase; □, extract phase; —, model fit; and the drop diameter (d_{32}/m) and hold-up (x) profiles along the normalized column position (b) for: ■, d_{32}/m; □, x; and model fits for: —, x; --, d_{32}/m.

From Figure 8.7 it can be concluded that the description of the concentration profiles in the forward extraction with the mixed solvent is accurate. As expected, the calculated drop diameter and hold-up profiles change significantly over the column length, which is directly related to the influence of the concentration of caprolactam on the physical properties and phase flow rates at each stage in the column. The calculated drop diameter and hold-up profiles present values in line with the experimental data. The hold-up profile is comparable to the one calculated for toluene, but the drop diameter profile shows for toluene values that are more than two times higher relative to the mixed solvent, which overall results in a higher interfacial area.

From Figure 8.6 (a) it was already concluded that the forward extraction proceeds much faster for the mixed solvent than for toluene. This is expressed by the lower HETS values, while the mixed solvent requires less theoretical stages as well. The reduced HETS values for the solvent mixture can be explained by the higher k_{ox} values and the larger interfacial area, although the α_y values could not be compared.

8.4.5   Model results: back-extraction

In the forward extraction using the mixed solvent practically all caprolactam is extracted, $w_{CPL,org} < 0.003$, and the values for the axial dispersion coefficient in the continuous phase, α_y, and the overall mass transfer coefficient, k_{ox}, were fitted by minimizing the value of the absolute average error (AAE), see Table 8.4 for the results. Furthermore, the predicted values of k_{ox} are shown for the experimentally determined range of caprolactam concentrations, together with the determined HETS values. The experimental conditions (Exp.) were T/K = 313, $f \cdot S_p$/m·s^{-1} = 0.016, Flux/m·h^{-1} = 21 (BE-1), unless stated otherwise, and the flow ratio was always $R = 2.1$.

Table 8.4. Determined k_{ox}/m·s^{-1} and α_y values at the fitted minimum AAE value in the back-extraction together with the predicted k_{ox}/m·s^{-1} values.

	Exp.			α_y	$10^5 \cdot k_{ox}$		HETS
	Flux	$f \cdot S_p$	T	fit	fit	predicted	
	m·h^{-1}	m·s^{-1}	K		m·s^{-1}	m·s^{-1}	m
BE-1	21	0.016	313	4.1	8.6	5.2 - 6.2	0.33
BE-2	21	0.016	293	4.0	4.5	4.1 - 5.3	0.40

From the results presented in Table 8.4 similar trends can be observed as for the forward extraction. It can be concluded that the fitted k_{ox} values are comparable to the predicted range, although the fitted temperature influence is stronger than predicted. The introduction of a backflow parameter for the continuous phase, α_y, resulted in a significant decrease of AARE and no influence of temperature on α_y was found. Comparing the fitted values to those obtained for toluene it was found that both the fitted α_y and k_{ox} values are comparable.

The influence of a temperature decrease on the separation performance resulted in an increasing HETS value, because of changing system properties. For toluene at Flux/m·h^{-1} = 20, $f·S_p$/m·s^{-1} = 0.016 and T/K = 313 it was calculated that HETS/m = 0.30 compared to 0.33 for the mixed solvent. Changing the conditions for toluene to T/K = 293 resulted in HETS/m = 0.37. It can therefore be concluded that in the back-extraction the mixed solvent needs more theoretical stages relative to toluene, but that each stage requires a similar column height.

From the fitting procedure concentration, drop diameter and hold-up profiles were obtained for the different operational conditions and the resulting profiles for BE-2 are presented in Figure 8.8 as function of the normalized column length, L/L_c.
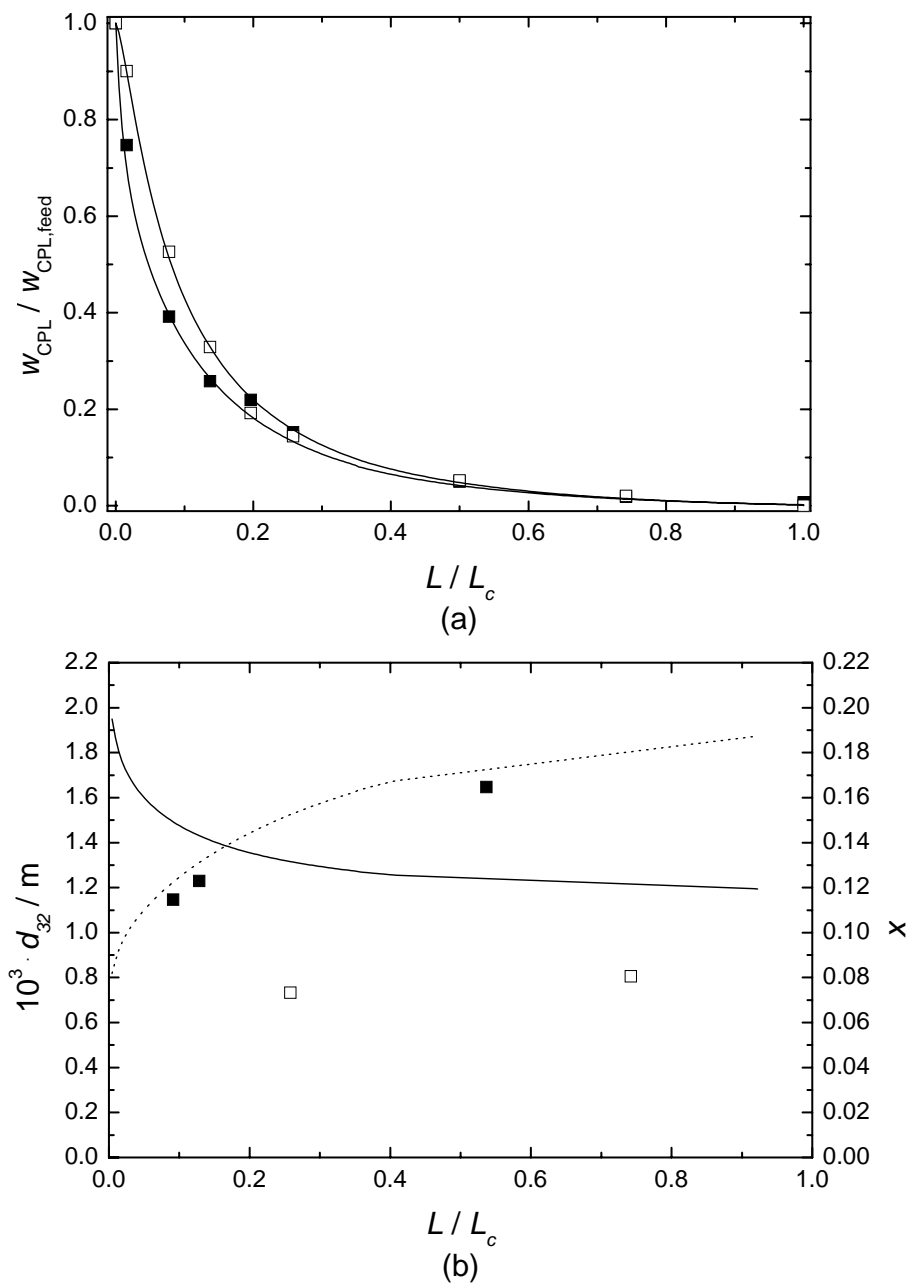
Figure 8.8. Normalized concentration profiles along the normalized column position (a), where T/K = 293, $f·S_p$/m·s^{-1} = 0.016, Flux/m·h^{-1} = 21 and R = 2.1 (BE-2): ■, raffinate phase; □, extract phase; —, model fit; and the drop diameter (d_{32}/m) and hold-up (x) profiles along the normalized column position (b) for: ■, d_{32}/m; □, x; and model fits for: —, x; --, d_{32}/m.

In Figure 8.8 it can be seen that both concentration profiles are described accurately. It can furthermore be seen that the calculated drop diameter and hold-up profiles change significantly over the column length, as observed for the forward extraction, and the model results present profiles in line with the experimental data. Compared to toluene the drop diameter and hold-up profiles show lower values, therefore, counter acting each other with respect to their influence on the interfacial area.

According to the model description, however, all caprolactam is extracted and the concentration gradient is almost zero for $L/L_c > 0.7$. The caprolactam concentrations as calculated from the model are lower than experimentally determined, which is caused by the fitting procedure since the k_{ox} value is fitted in order to minimize the AAE. Fitting the k_{ox} value in order to comply with the raffinate concentration would result in an exact description of the raffinate side of the column, as performed for the forward extraction with toluene, but also results in an under-prediction of the concentration gradient at the feed-side of the column. This observation might be explained partly from the model assumptions, but might also be influenced by the fact that the column at the raffinate side was operated in the mixer-settler regime, resulting in a decreasing column efficiency, which was not taken into account.

From Figure 8.6 (b) it was already concluded that the back-extraction proceeds faster for toluene than for the mixed solvent. This is caused by the increased amount of theoretical stages the mixed solvent requires relative to toluene, whereas the HETS values are comparable.

8.5 Conclusions

The performance of a PDDC was evaluated for the forward and back-extraction of caprolactam in a pilot set-up with an alternative mixed solvent compared to toluene. The PDDC showed qualitatively comparable operational characteristics for both solvents.

In the hydraulic experiments the mixed solvent showed smaller drop diameters, mainly because of a lower interfacial tension of this system, and slightly smaller hold-ups, which is the result of a combined effect of the interfacial tension, phase viscosities and densities. The pulsation intensities required for the transition from the mixer-settler to the dispersion regime are lower for the mixed solvent system, while the pulsation intensities for the dispersion to emulsion transition are more or less comparable for both solvent systems. The operational windows are slightly smaller for the mixed solvent where flooding was observed as limiting process for both the forward and back-extraction, while phase inversion was observed for toluene in the back-extraction. However, based on the treatment of a set feed stream the experimentally determined hydraulic characteristics at equilibrium conditions are beneficial for the mixed solvent, despite the slightly smaller operational window.

For both solvents mass transfer resulted in an increasing drop diameter and pulsation intensity required for regime transition. In the forward extraction the mixed solvent was superior, which is expressed by the lower HETS/m values, being 0.26 to 0.37 for the mixed solvent and 0.42 to 0.67 for toluene, while the mixed solvent requires less theoretical stages as well. For the back-extraction the determined HETS/m values are comparable, being 0.33 to 0.40 for the

mixed solvent and 0.30 to 0.37 for toluene, but toluene is favourable with respect to the required column length, because of the lower amount of theoretical stages required.

The hydraulic characteristics at equilibrium and concentration profiles in both the forward and back-extraction were described accurately using the developed models.

Nomenclature

a	Specific interfacial area, $m^2 \cdot m^{-3}$
AARE	Average absolute value of the relative error
AAE	Average absolute error
D, E, MS	Dispersion, Emulsion and Mixer-settler operating regime, respectively
d_{32}	Sauter drop diameter, m
E	Extraction factor, $E = K_D' \cdot F_y'/F_x'$
F	Phase flow rate, $m^3 \cdot s^{-1}$
f	Frequency, s^{-1}
F_x', F_y'	Feed and solvent phase mass flow rates on solute free basis, $kg \cdot s^{-1}$
$f \cdot S_p$	Pulsation intensity, where f/s^{-1} denotes frequency and S_p/m stroke, $m \cdot s^{-1}$
Flux	Total throughput, Flux $= V_c + V_d$, $m \cdot h^{-1}$
h_c	Characteristic column height, m
HETS	Height Equivalent of a Theoretical Stage, m
k_j	Mass transfer coefficient, $m \cdot s^{-1}$
K_D'	Equilibrium distribution coefficient, $K_D' = w_y'/w_x'$
L	Length, m
L_c	Total column length, m
NDP	Number of data points
R	Flow ratio, $R = V_d/V_c$
s	Column cross-sectional area, m^2
S_p	Stroke of pulsation (twice the pulsation amplitude), m
T	Temperature, K
V_i	Velocity of phase or component i, $m \cdot s^{-1}$
w	Weight fraction
x	Dispersed phase hold-up defined as volume fraction of the dispersed phase

Greek letters

α	Backflow ratio
γ	Interfacial tension, $N \cdot m^{-1}$
η	Dynamic viscosity, $kg \cdot m^{-1} \cdot s^{-1}$

ρ	Density, kg·m^{-3}
$\Delta\rho$	Density difference, kg·m^{-3}

Subscript

aq	Denoting aqueous phase
c	Denoting continuous phase
d	Denoting dispersed phase
f	Denoting flooding
feed	Feed phase
o	Overall
org	Denoting organic phase
PI	Denoting phase inversion
raffinate	Raffinate phase
x, y	Raffinate and extract phase, respectively

Chapter 9

Conclusions, outlook and recommendations

9.1   Conclusions

From the current market situation it follows that in the near future existing technology will remain the dominating production route for caprolactam. The current recovery route uses solvent extraction as initial step, but in this extraction process toxic and carcinogenic solvents are used.

The first objective of research was the characterisation of the Bateman pulsed disc and doughnut column (Bateman Advanced Technologies, Israel) for its applicability in the extraction of caprolactam. The second objective was the selection and characterization of alternative environmentally benign solvents for caprolactam extraction. Finally, caprolactam extraction with the selected alternative solvent has been compared with toluene.

9.1.1   Pulsed disc and doughnut column characterization

For the hydraulic characteristics of caprolactam extraction with toluene in a pulsed disc and doughnut column (PDDC) it was found that the operation of a PDDC could be characterized by the operational window and regimes, which are mainly dependent on the Sauter drop diameter and hold-up and are qualitatively comparable to those of a pulsed sieve-plate column. The measured properties described above and observed trends could be described accurately after fitting drop diameter, hold-up and phase inversion data, using a theoretical model based on the system physical properties, operational parameters and geometrical characteristics of the column and internals. Using this approach, the difference between the back- and forward extraction operation can be understood, just as the influence of the physical parameters on the operation.

The HETS values obtained from mass transfer experiments in the forward extraction were HETS/m = 0.32 to 0.67, whereas in the back-extraction HETS/m = 0.28 to 0.41. Mass transfer caused a drop diameter increase, a decreasing hold-up and a corresponding shift in the operational regime. Concentration profiles were described using the backflow model.

9.1.2   Selection and characterization of alternative environmentally benign solvents

Based on an experimentally determined high capacity, low mutual solvent solubility and beneficial physical properties, the mixture heptane-heptanol (40 mass %) was selected as best candidate solvent for the replacement of benzene and toluene in the extraction of caprolactam.

For the equilibrium distribution of caprolactam and four model impurities of organic nature, being cyclohexanone (I), aniline (II), n-methylcaprolactam (III) and cyclohexane-carboxamide (IV), it was found at all conditions that the distribution ratio of the impurities to the solvents, being toluene or heptane + heptanol (40 mass %), was higher than that of caprolactam. Based on equilibrium calculations for the back-extraction, it was found that group I and II impurities are present in a higher ratio in the mixed solvent. For group III components the fraction was comparable, while for group IV species a lower amount was present. In total a lower amount of impurities was extracted using the mixed solvent compared to toluene.

The selected mixture was applied in the PDDC for caprolactam extraction where the operational characteristics were found to be qualitatively comparable to toluene. Smaller drop diameters and slightly smaller hold-ups and operational windows were determined for the mixed solvent. However, for the treatment of a particular feed stream relative to toluene the mixed solvent shows hydraulic characteristics beneficial for caprolactam extraction.

In the forward and back-extraction the determined HETS/m values were 0.26 to 0.37 and 0.33 to 0.40, respectively. In the forward extraction the mixed solvent is therefore superior compared to toluene with respect to the required column length, while the mixed solvent requires less theoretical stages as well. Toluene is favourable in the back-extraction, because of the lower amount of theoretical stages required.

9.2   Outlook

The selection of the solvent mixture heptane-heptanol (40 mass %) as best candidate solvent was based on a high distribution ratio of caprolactam relative to benzene and toluene as well as beneficial physical properties, but the mutual solvent solubility was slightly higher for water in the organic phase. The latter in itself it not a problem, since back-extraction is performed with water as solvent. The mixed solvent feed is thus freed from the dissolved water, because it is transferred to the aqueous phase. With the dissolved water, however, inorganic impurities might be transferred as well, resulting in a different feed composition for the purification section. The feed composition is furthermore influenced by the different impurity distribution ratio for the mixed solvent relative to toluene.

Other considerations on the use of the developed solvent mixture might be of economical nature or on the ease with which it can be recovered or freed from impurities. It might be economically interesting to apply a mixed solvent composed of other compounds when these are cheaper to purchase or already available. The recovery of the solvent, freeing it from impurities, is often performed with distillation, which was possible for benzene and toluene with boiling points of 353.2 K and 383.8 K, respectively, while that of the low-boiling organic impurities (cyclohexanone) is 428.2 K. Heptane has a boiling point of 371.6 K, which

is between the values of benzene and toluene, but that of 1-heptanol is 449.2 K. Freeing the binary solvent mixture partly or completely from impurities might therefore prove more complex than for the currently used solvents.

From the used solvent selection approach it follows, however, that by changing the composition of a mixture, its properties can be adjusted as required. Taking into account the extra requirements, water solubility in the organic phase, process economics, impurity distribution behaviour and solvent recovery, the developed solvent mixture might be improved even further by changing the mixture composition without losing the obtained beneficial properties.

Finally, in this thesis it has been demonstrated that the use of solvent mixtures offers a possibility to create environmentally benign solvents, which can replace currently used toxic solvents in a technical and economical feasible way. Although studied for caprolactam in this thesis, it is expected that solvent mixtures can be used in a beneficial way for many other applications where pure solvents are not able to replace the currently used hazardous solvents. Furthermore it is expected that mixed solvents can be designed to perform better than pure solvents and/or to obtain economically attractive designer solvents without the need of custom synthesizes.

For the application of the selected solvent mixture in the PDDC qualitatively comparable operational characteristics were found relative to toluene, whereas smaller drop diameters and slightly smaller hold-ups and operational windows were measured. Between the currently used solvents benzene and toluene only minor differences exists between the physical properties and therefore comparable hydraulic characteristics are expected for these two solvents. Furthermore, because of almost equal physical properties, HETS values comparable to toluene are expected for benzene, although an influence might exist of the different flow ratio.

In the forward extraction the column length required using the mixed solvent is less than half of the column length required when using benzene and toluene, because of the lower amount of theoretical stages required, whereas the HETS values are much lower as well. In the back-extraction the column length required using the mixed solvent is twice the column length required for benzene and toluene, because of comparable HETS values and the double amount of theoretical stages required. The column throughput in both processes using the mixed solvent is comparable to benzene but smaller than for toluene. Therefore, using the mixed solvent, an environmentally benign alternative is obtained for benzene and toluene with column throughputs comparable to benzene and a much smaller column for the forward and a larger column for the back-extraction.

Since the operational diagrams of all solvents do not show large differences with respect to the fluxes that can be obtained, it is expected that the columns can be operated at comparable capacities. Because of a comparable interfacial tension, benzene and toluene will require a similar energy input, while the solvent mixture requires less as result of the lower interfacial tension of this system.

From the performed mass transfer experiments it follows that changing experimental conditions influences the extraction process beneficially. This is the case for an increased energy input, resulting in an increased interfacial area, but also for a temperature change. The forward extraction with toluene and the back-extraction from the mixed solvent especially were influenced beneficially by a temperature increase and decrease, respectively, compared to the operational temperature of 313 K, because of a beneficial change of the system properties. Performing the forward extraction at 333 K and the back-extraction at 293 K will therefore prove beneficial for caprolactam extraction, whatever solvent and column is used.

In the extraction process large concentration changes are obtained along the column, especially for the forward extraction of caprolactam where $0.0 < w_{CPL,aq} < 0.7$. This concentration decrease results in enormous changes of the system properties, but process operation and column design are dominated by the concentrations at the feed-section only. The column length required to reach the desired raffinate concentration is, however, dominated by the raffinate-side of the column, which is operated in the unfavourable mixer-settler regime in case of the PDDC. Keeping the process as it is, a different design of the column internals might result in a more efficient operation. The basis of the alternative design is a less intensified energy input in the top (feed-section) and a more intensified input in the bottom (raffinate-section), created by a specific internal design along the column length. For a PDDC this might be obtained by decreasing disc sizes, increasing doughnut aperture sizes and a larger distance between the discs and doughnuts towards the top of the column. For an RDC decreasing disc sizes and an increased distance between the discs towards the top of the column can be applied.

In agitated columns a better distribution of the mechanical energy leads to a smaller drop size distribution, resulting amongst others in less emulsion formation. A PDDC might prove beneficial compared to a RDC, since the latter shows a high energy input at the disc-tips.

In the column operation emulsion formation was observed, but not quantified, for both toluene as for the mixed solvent, especially at high concentrations of caprolactam and therefore low interfacial tensions. This effect of emulsion formation on the extract quality of especially the forward extraction might prove necessary to take into account in the comparison of the solvents.

9.3 Recommendations for further research on the extraction of caprolactam

In the presented work an environmentally benign mixed solvent is presented as candidate solvent for the replacement for benzene and toluene in caprolactam extraction, based on a high distribution ratio of caprolactam relative to benzene and toluene and beneficial physical properties. Further attention might be paid to solvent optimization with respect to the mutual solvent solubility, solvent recovery, economics and the impurity distribution behaviour.

Furthermore it is interesting to investigate the optimal experimental conditions for caprolactam extraction, with respect to caprolactam yield, solvent requirement, column dimensions, energy input, solvent loss, solvent recovery, impurity distribution behaviour and the purification section. Thereby emulsion formation deserves further investigation as well, in

combination with the development of a (predictive) model, especially when it proves of importance for the product quality or results in a strong influence on the purification section.

The PDDC is described via the backflow model, using a constant overall mass transfer coefficient and a constant backflow parameter for the continuous phase. The latter effect should, however, be investigated for both phases separately as function of the operational parameters and experimental conditions in order to make a valid distinction between the influence of mass transfer and backmixing on the separation efficiency.

From the presented work it follows that the extraction operation is affected by numerous effects. A predictive model describing extraction operation or its separate characteristics, being hold-up drop diameter and operational window, from first principles should therefore prove an enormous asset.

Appendix A

System properties of the reference systems

Table A1. Liquid-liquid equilibria of the quaternary system water (1) + caprolactam (2) + ammonium sulfate (3) + benzene (4) at 293 K, 313 K and 333 K.

Organic phase			Aqueous phase			
$10^2 w_1$	$10^2 w_2$	$10^2 w_4$	$10^2 w_1$	$10^2 w_2$	$10^2 w_3$	$10^2 w_4$
293 K						
0.04	0.00	99.96	99.87	0.00	0.00	0.13
0.09	1.53	98.38	90.28	9.51	0.00	0.21
0.18	4.02	95.80	81.03	18.60	0.00	0.37
0.42	8.24	91.34	71.13	28.20	0.00	0.67
0.71	10.90	88.39	61.66	37.00	0.00	1.34
1.20	16.20	82.60	51.08	45.90	0.00	3.02
2.39	23.60	74.01	39.53	53.40	0.00	7.07
0.04	0.00	99.96	94.85	0.00	5.07	0.08
0.14	2.47	97.39	84.60	9.39	5.85	0.16
0.38	7.39	92.23	76.15	18.50	5.16	0.19
0.80	13.20	86.00	66.91	27.40	5.01	0.68
1.70	20.30	78.00	57.14	36.00	5.07	1.79
2.08	22.70	75.22	54.97	37.60	5.21	2.22
0.06	0.00	99.94	84.77	0.00	15.20	0.03
0.40	8.46	91.14	76.46	7.95	15.50	0.09
1.61	19.50	78.89	69.29	15.70	14.70	0.31
0.06	0.00	99.94	60.00	0.00	40.00	0.00
3.13	32.20	64.67	58.53	0.57	40.90	0.00
8.32	51.10	40.58	56.59	0.61	42.80	0.00
11.00	55.90	33.10	58.48	0.72	40.80	0.00
13.80	58.90	27.30	59.85	0.85	39.30	0.00
313 K						
0.05	0.00	99.95	99.89	0.00	0.00	0.11
0.15	2.55	97.30	90.22	9.55	0.00	0.23
0.31	5.78	93.91	80.78	18.80	0.00	0.42
0.72	9.86	89.42	70.75	28.30	0.00	0.95
1.08	14.50	84.42	60.83	37.10	0.00	2.07
1.85	19.80	78.35	49.69	45.70	0.00	4.61
4.02	28.10	67.88	37.80	51.50	0.00	10.70
0.06	0.00	99.94	94.83	0.00	5.08	0.09
0.19	3.75	96.06	84.80	9.09	5.96	0.15
0.69	10.30	89.01	76.46	17.80	5.35	0.39
(313 K continued)						
1.67	17.90	80.43	67.53	26.50	5.06	0.91
3.74	27.30	68.96	57.83	34.50	5.15	2.52
4.88	31.30	63.82	55.72	35.80	5.33	3.15
0.09	0.00	99.91	84.97	0.00	15.00	0.03
0.83	11.60	87.57	77.14	6.97	15.80	0.09
3.93	28.50	67.57	71.35	12.70	15.70	0.25
0.05	0.00	99.95	60.20	0.00	39.80	0.00
3.29	31.90	64.81	59.40	0.60	40.00	0.00
9.30	50.00	40.70	58.53	0.67	40.80	0.00
10.80	55.70	33.50	57.82	0.68	41.50	0.00
13.70	58.00	28.30	59.56	0.84	39.60	0.00
333 K						
0.07	0.00	99.93	99.88	0.00	0.00	0.12
0.22	3.61	96.17	90.56	9.15	0.00	0.29
0.62	7.82	91.56	81.19	18.20	0.00	0.61
1.09	12.50	86.41	71.22	27.50	0.00	1.28
1.71	17.50	80.79	60.48	36.40	0.00	3.12
3.08	23.60	73.32	49.25	44.30	0.00	6.45
7.74	34.40	57.86	36.90	49.10	0.00	14.00
0.04	0.00	99.96	94.79	0.00	5.12	0.09
0.19	3.70	96.11	85.13	8.89	5.82	0.16
1.22	13.70	85.08	76.71	17.60	5.23	0.46
3.08	24.50	72.42	68.13	25.60	5.22	1.05
9.00	39.10	51.90	59.61	31.80	5.47	3.12
0.05	0.00	99.95	85.27	0.00	14.70	0.03
1.37	14.70	83.93	77.56	6.46	15.90	0.08
7.09	36.90	56.01	73.97	9.64	16.20	0.19
0.10	0.00	99.90	59.50	0.00	40.50	0.00
3.66	32.70	63.64	59.22	0.58	40.20	0.00
10.40	56.40	33.20	57.56	0.64	41.80	0.00
11.20	55.70	33.10	58.42	0.68	40.90	0.00
13.10	59.50	27.40	58.15	0.75	41.10	0.00

Table A2. Liquid-liquid equilibria of the quaternary system water (1) + caprolactam (2) + ammonium sulfate (3) + toluene (4) at 293 K, 313 K and 333 K.

Organic phase			Aqueous phase				Organic phase			Aqueous phase			
10^2w_1	10^2w_2	10^2w_4	10^2w_1	10^2w_2	10^2w_3	10^2w_4	10^2w_1	10^2w_2	10^2w_4	10^2w_1	10^2w_2	10^2w_3	10^2w_4
293 K							(313 K continued)						
0.04	0.08	99.87	98.54	1.20	0.00	0.26	0.05	0.15	99.80	93.80	0.98	5.07	0.16
0.06	0.28	99.66	95.38	4.41	0.00	0.21	0.08	1.11	98.81	89.09	5.87	4.84	0.20
0.07	0.69	99.25	90.99	8.79	0.00	0.22	0.11	1.68	98.21	86.51	8.35	4.98	0.16
0.08	1.14	98.78	86.13	13.63	0.00	0.24	0.28	4.92	94.80	75.89	18.87	4.83	0.41
0.10	1.69	98.21	81.07	18.69	0.00	0.24	0.59	8.61	90.80	65.91	27.70	4.85	1.55
0.12	2.31	97.57	77.19	22.40	0.00	0.41	0.80	12.79	86.41	55.62	37.58	5.16	1.63
0.16	3.27	96.57	70.97	28.51	0.00	0.52	0.06	0.47	99.47	59.72	0.12	40.16	0.00
0.28	5.46	94.26	59.69	39.20	0.00	1.11	0.06	0.93	99.00	60.35	0.17	39.45	0.03
0.58	10.49	88.93	45.41	51.58	0.00	3.01	0.08	1.31	98.61	59.82	0.20	39.92	0.05
0.79	11.81	87.40	41.16	53.44	0.00	5.40	0.16	4.06	95.78	57.96	0.28	41.72	0.04
3.26	24.93	71.82	17.41	60.21	0.00	22.38	0.48	11.09	88.43	59.22	0.65	40.13	0.00
0.05	0.09	99.87	93.70	1.02	5.10	0.18	1.42	20.67	77.91	58.93	0.81	40.25	0.01
0.06	0.51	99.44	90.77	4.00	5.03	0.20	2.92	31.03	66.05	59.46	0.82	39.70	0.02
0.07	1.24	98.69	85.65	9.16	4.98	0.22	333 K						
0.17	3.63	96.21	75.19	19.24	5.07	0.50	0.06	0.15	99.79	98.73	0.96	0.00	0.32
0.31	7.02	92.67	63.77	30.46	5.05	0.73	0.08	0.83	99.09	94.84	5.01	0.00	0.15
0.50	10.62	88.88	53.08	40.45	5.00	1.46	0.11	2.29	97.60	88.46	11.12	0.00	0.42
0.04	0.40	99.56	59.96	0.14	39.86	0.04	0.19	3.84	95.97	80.77	18.79	0.00	0.44
0.05	0.86	99.09	59.76	0.18	40.02	0.04	0.32	6.38	93.31	68.89	30.08	0.00	1.04
0.06	1.24	98.70	60.13	0.21	39.60	0.06	0.49	9.48	90.03	58.13	40.00	0.00	1.87
0.15	4.59	95.26	59.02	0.39	40.58	0.01	1.05	13.38	85.57	49.91	44.78	0.00	5.31
0.37	10.16	89.47	57.13	0.54	42.32	0.01	3.63	24.35	72.02	24.08	52.54	0.00	23.38
0.72	14.87	84.41	56.95	0.58	42.44	0.02	0.05	0.24	99.71	93.64	0.91	5.04	0.41
0.65	14.55	84.80	58.73	0.61	40.65	0.00	0.09	1.42	98.49	89.92	5.07	4.81	0.21
1.30	20.55	78.15	59.16	0.93	39.90	0.01	0.16	3.11	96.73	84.65	9.92	5.06	0.37
2.88	29.96	67.16	59.61	0.97	39.35	0.06	0.80	12.68	86.52	62.50	31.35	4.97	1.17
313 K							1.20	17.57	81.23	55.46	37.14	5.30	2.10
0.06	0.10	99.84	98.80	0.99	0.00	0.21	0.06	0.48	99.46	60.98	0.10	38.92	0.00
0.07	0.49	99.44	95.56	4.24	0.00	0.20	0.07	0.97	98.96	60.56	0.13	39.30	0.01
0.12	1.09	98.79	91.33	8.47	0.00	0.20	0.08	1.37	98.54	60.56	0.16	39.27	0.02
0.15	2.68	97.17	81.50	18.14	0.00	0.36	0.18	4.26	95.56	56.97	0.26	42.77	0.00
0.23	4.59	95.17	70.73	28.60	0.00	0.67	0.37	8.86	90.77	56.24	0.39	43.35	0.01
0.37	7.37	92.26	59.40	39.16	0.00	1.44	0.51	10.92	88.57	59.03	0.57	40.39	0.00
0.75	12.41	86.84	45.70	50.50	0.00	3.80	1.46	21.77	76.77	59.42	0.73	39.82	0.03
1.17	14.45	84.38	40.48	51.12	0.00	8.39	3.10	32.22	64.68	58.06	0.78	41.13	0.03
4.48	26.36	69.16	17.63	56.27	0.00	26.10							

Table A3. Densities of the systems solvent (1) + caprolactam (2) + ammonium sulfate (3) at 293 K, 313 K and 333 K, where the solvent is water, benzene or toluene.

$100 \cdot w_2$	$100 \cdot w_3$	$10^{-3} \cdot \rho / \text{kg} \cdot \text{m}^{-3}$			$100 \cdot w_2$	$100 \cdot w_3$	$10^{-3} \cdot \rho / \text{kg} \cdot \text{m}^{-3}$		
		293 K	313 K	333 K			293 K	313 K	333 K
Water system[a]					*(Water system[a] continued)*				
0.00	0.00	0.9984	0.9924	0.9833	19.98	5.00	1.0447	1.0349	1.0232
10.31	0.00	1.0070	0.9994	0.9892	30.10	4.99	1.0534	1.0417	1.0288
20.31	0.00	1.0165	1.0069	0.9948	39.38	5.04	1.0609	1.0477	1.0337
29.99	0.00	1.0256	1.0140	1.0008	Benzene system[b]				
39.92	0.00	1.0344	1.0210	1.0064	0.00	-	0.8790	0.8580	0.8358
50.29	0.00	1.0428	1.0279	1.0116	4.84	-	0.8872	0.8661	0.8447
60.09	0.00	1.0495	1.0337	1.0170	9.21	-	0.8947	0.8739	0.8528
0.00	4.96	1.0276	1.0210	1.0119	13.53	-	0.9020	0.8815	0.8608
0.00	10.02	1.0569	1.0498	1.0401	Toluene system[c]				
0.00	19.96	1.1141	1.1065	1.0982	0.00	-	0.8676	0.8483	0.8293
0.00	30.13	1.1724	1.1647	1.1551	5.14	-	0.8773	0.8574	0.8386
0.00	39.82	1.2269	1.2198	1.2126	9.38	-	0.8852	0.8650	0.8463
9.93	4.99	1.0357	1.0277	1.0174	14.44	-	0.8948	0.8741	0.8557

[a] water (1) + caprolactam (2) + ammonium sulfate (3); [b] benzene (1) + caprolactam (2); [c] toluene (1) + caprolactam (2)

Table A4. Kinematic viscosities of the systems solvent (1) + caprolactam (2) + ammonium sulfate (3) at 293 K, 313 K and 333 K, where the solvent is water, benzene or toluene.

$100 \cdot w_2$	$100 \cdot w_3$	$10^{6} \cdot \nu / \text{m}^2 \cdot \text{s}^{-1}$			$100 \cdot w_2$	$100 \cdot w_3$	$10^{6} \cdot \nu / \text{m}^2 \cdot \text{s}^{-1}$		
		293 K	313 K	333 K			293 K	313 K	333 K
Water system[a]					*(Water system[a] continued)*				
0.00	0.00	1.02	0.67	0.48	19.88	5.00	2.14	1.28	0.87
10.00	0.00	1.44	0.88	0.61	30.03	5.03	3.17	1.78	1.17
19.93	0.00	1.96	1.16	0.77	39.38	5.04	4.72	2.50	1.56
30.05	0.00	2.74	1.56	1.00	Benzene system[b]				
39.92	0.00	4.04	2.12	1.31	0.00	-	0.75	0.58	0.47
50.29	0.00	5.98	2.88	1.69	5.05	-	0.82	0.63	0.51
60.08	0.00	9.36	4.15	2.28	9.49	-	0.89	0.68	0.54
0.00	5.06	1.08	0.72	0.53	14.98	-	1.01	0.76	0.60
0.00	10.00	1.13	0.77	0.56	Toluene system[c]				
0.00	19.72	1.29	0.90	0.67	0.00	-	0.68	0.55	0.46
0.00	31.62	1.69	1.15	0.86	5.14	-	0.75	0.60	0.50
0.00	40.01	2.07	1.46	1.06	9.76	-	0.84	0.65	0.54
10.28	4.97	1.52	0.95	0.67	14.97	-	0.94	0.73	0.59

[a] water (1) + caprolactam (2) + ammonium sulfate (3); [b] benzene (1) + caprolactam (2); [c] toluene (1) + caprolactam (2)

Table A5. Interfacial tensions dependent on the concentration of solute in the aqueous (aq) and organic (org) phase for the systems water (1) + caprolactam (2) + ammonium sulfate (3) + toluene (4) at 293 K, 313 K and 333 K.

$100 \cdot w_{2,aq}$	$100 \cdot w_{3,aq}$ [a]	$100 \cdot w_{2,org}$	$\gamma/N \cdot m^{-1}$	$100 \cdot w_{2,aq}$	$100 \cdot w_{3,aq}$ [a]	$100 \cdot w_{2,org}$	$\gamma/N \cdot m^{-1}$
	293 K				*(313 K continued)*		
0.00	0.00	0.00	0.0357	0.00	36.95	0.00	0.0385
0.00	5.00	0.00	0.0364	0.00	40.02	0.00	0.0392
0.00	9.38	0.00	0.0367	2.67	0.00	0.32	0.0206
0.00	17.33	0.00	0.0371	5.34	0.00	0.64	0.0170
0.00	19.96	0.00	0.0378	9.95	0.00	1.27	0.0133
0.00	22.45	0.00	0.0377	14.96	0.00	2.05	0.0103
0.00	34.72	0.00	0.0389	19.90	0.00	2.92	0.0083
0.00	36.95	0.00	0.0392	29.66	0.00	4.96	0.0053
0.00	40.02	0.00	0.0400	2.55	4.99	0.43	0.0198
2.50	0.00	0.17	0.0224	5.09	5.03	0.93	0.0155
5.41	0.00	0.37	0.0180	10.09	5.00	2.11	0.0108
9.87	0.00	0.74	0.0152	15.17	4.98	3.57	0.0088
14.92	0.00	1.27	0.0114	20.15	5.00	5.26	0.0059
21.77	0.00	2.18	0.0100		333 K		
29.95	0.00	3.55	0.0073				
33.08	0.00	4.15	0.0057	0.00	0.00	0.00	0.0334
2.54	5.05	0.28	0.0203	0.00	5.00	0.00	0.0338
5.04	4.99	0.60	0.0172	0.00	9.98	0.00	0.0346
10.08	5.03	1.42	0.0111	0.00	20.07	0.00	0.0356
15.09	5.00	2.44	0.0091	0.00	29.24	0.00	0.0373
20.05	5.00	3.67	0.0078	0.00	40.02	0.00	0.0375
25.12	5.02	5.14	0.0058	2.63	0.00	0.48	0.0196
30.25	5.00	6.85	0.0048	5.06	0.00	0.92	0.0171
	313 K			9.85	0.00	1.85	0.0119
				19.32	0.00	3.91	0.0082
0.00	0.00	0.00	0.0349	23.33	0.00	4.86	0.0070
0.00	5.00	0.00	0.0352	2.56	5.02	0.69	0.0180
0.00	9.97	0.00	0.0359	5.11	4.99	1.45	0.0146
0.00	20.05	0.00	0.0370	9.86	5.03	3.05	0.0096
0.00	30.77	0.00	0.0387	15.11	5.00	5.10	0.0067

[a] $100 \cdot w_{2,org}$ assumed to be zero

Appendix B

System properties of the alternative solvent systems

Table B1. Liquid-liquid equilibria of the systems water (1) + caprolactam (2) + ammonium sulfate (3) + methylcyclohexane (4) + heptanol (5) at 293 K, 313 K and 333 K.

Organic phase				Aqueous phase				
$10^2 w_1$	$10^2 w_2$	$10^2 w_4$	$10^2 w_5$	$10^2 w_1$	$10^2 w_2$	$10^2 w_3$	$10^2 w_4$	$10^2 w_5$
293 K								
1.58	3.67	57.77	36.99	92.04	7.88	0.00	0.02	0.07
2.00	7.14	51.63	39.23	81.53	18.45	0.00	0.00	0.02
2.53	9.91	52.23	35.32	75.10	24.54	0.00	0.04	0.32
4.00	16.83	48.50	30.67	55.57	42.76	0.00	0.18	1.49
4.27	22.59	43.43	29.71	51.04	48.59	0.00	0.01	0.36
3.20	13.49	57.75	33.64	72.25	21.61	5.84	0.04	0.26
313 K								
1.78	4.52	56.75	36.95	92.43	7.31	0.00	0.20	0.06
1.19	9.07	49.85	39.89	81.23	18.74	0.00	0.00	0.02
1.45	12.16	53.46	32.93	77.33	22.25	0.00	0.02	0.40
2.93	11.53	49.12	36.42	69.97	29.53	0.00	0.08	0.42
-	12.45	-	36.29	67.12	31.97	0.00	0.24	0.67
4.89	18.70	46.26	30.15	55.97	41.53	0.00	0.32	2.18
1.78	7.67	64.72	38.20	86.05	7.89	5.94	0.02	0.10
3.69	15.11	52.64	32.50	75.62	17.40	6.70	0.02	0.26
333 K								
1.75	4.73	56.24	37.29	92.89	6.92	0.00	0.12	0.07
3.54	14.09	48.47	33.89	77.54	21.93	0.00	0.02	0.51
3.15	12.50	55.30	34.58	72.92	26.50	0.00	0.08	0.50
-	15.57	-	37.04	67.08	32.23	0.00	0.08	0.67
5.74	20.24	45.75	28.27	55.45	41.23	0.00	0.49	2.84
5.27	27.15	39.00	28.59	50.35	48.88	0.00	0.02	0.75
1.70	8.43	63.46	38.98	87.05	6.59	6.22	0.03	0.11
3.72	18.55	54.36	33.56	76.42	16.21	6.97	0.06	0.34
8.36	27.29	36.65	24.71	70.60	22.35	5.60	0.48	0.97

Table B2. Liquid-liquid equilibria of the systems water (1) + caprolactam (2) + ammonium sulfate (3) + heptane (4) + heptanol (5) at 293 K, 313 K and 333 K.

	Organic phase				Aqueous phase				
10^2w_1	10^2w_2	10^2w_4	10^2w_5	10^2w_1	10^2w_2	10^2w_3	10^2w_4	10^2w_5
				293 K					
2.20	4.29	48.43	45.08	92.12	7.68	0.00	0.04	0.16
1.99	7.18	48.09	42.74	83.70	16.24	0.00	0.00	0.06
3.58	10.94	44.09	41.38	74.74	24.78	0.00	0.05	0.43
3.17	12.41	48.03	36.40	65.25	34.61	0.00	0.00	0.13
5.41	17.82	40.57	36.20	54.41	42.98	0.00	0.26	2.35
				313 K					
2.27	5.35	44.64	47.74	92.68	7.13	0.00	0.03	0.16
2.15	8.30	50.60	38.96	86.74	13.16	0.00	0.00	0.10
4.11	11.92	41.71	42.26	75.75	23.59	0.00	0.10	0.56
3.73	15.89	42.45	37.93	71.30	34.94	0.00	0.00	0.16
6.23	19.65	39.36	34.76	52.52	43.40	0.00	0.45	3.63
5.27	18.85	47.95	27.93	51.87	47.19	0.00	0.02	0.93
				333 K					
1.32	1.35	52.32	45.01	97.60	2.07	0.00	0.32	0.01
5.06	16.67	38.23	40.04	76.40	22.71	0.00	0.12	0.77
4.19	18.49	39.47	37.85	71.75	27.92	0.00	0.00	0.32
6.38	23.53	34.66	35.43	52.67	41.51	0.00	0.76	5.06
6.27	27.09	39.16	27.48	52.00	46.85	0.00	0.03	1.13

Table B3. Densities of the systems alkane (1) + heptanol (2) + caprolactam (3) at 293 K, 313 K and 333 K, where the alkane is methylcyclohexane or heptane.

$100 \cdot w_2$	$100 \cdot w_3$	$10^{-3} \cdot \rho/\mathrm{kg \cdot m^{-3}}$			$100 \cdot w_2$	$100 \cdot w_3$	$10^{-3} \cdot \rho/\mathrm{kg \cdot m^{-3}}$		
		293 K	313 K	333 K			293 K	313 K	333 K
	Methylcyclohexane system					Heptane system			
0.00	0.00	0.7692	0.7517	0.7341	0.00	0.00	0.6838	0.6667	0.6491
100.00	0.00	0.8232	0.8084	0.7936	100.00	0.00	0.8232	0.8084	0.7936
40.11	0.00	0.7894	0.7736	0.7566	39.51	0.00	0.7333	0.7168	0.7000
38.22	4.71	0.7989	0.7824	0.7658	37.35	5.48	0.7462	0.7298	0.7131
36.50	9.00	0.8078	0.7916	0.7751	35.65	9.79	0.7568	0.7403	0.7238
33.91	15.45	0.8218	0.8058	0.7894	33.58	15.02	0.7699	0.7534	0.7370

Table B4. Kinematic viscosities of the systems alkane (1) + heptanol (2) + caprolactam (3) at 293 K, 313 K and 333 K, where the alkane is methylcyclohexane or heptane.

$100 \cdot w_2$	$100 \cdot w_3$	$10^6 \cdot \nu/\mathrm{m}^2 \cdot \mathrm{s}^{-1}$			$100 \cdot w_2$	$100 \cdot w_3$	$10^6 \cdot \nu/\mathrm{m}^2 \cdot \mathrm{s}^{-1}$		
		293 K	313 K	333 K			293 K	313 K	333 K
Methylcyclohexane system					Heptane system				
0.00	0.00	0.95	0.75	0.61	0.00	0.00	0.60	0.50	0.43
100.00	0.00	8.52	4.59	2.72	100.00	0.00	8.52	4.59	2.72
39.70	0.00	1.84	1.30	0.97	40.30	0.00	1.25	0.94	0.72
37.61	5.27	1.99	1.40	1.03	38.18	5.25	1.36	1.01	0.78
35.59	10.34	2.16	1.50	1.11	36.34	9.82	1.46	1.07	0.82
33.77	14.95	2.36	1.64	1.19	34.13	15.30	1.61	1.17	0.89

Table B5. Interfacial tensions dependent on the concentration of caprolactam in the aqueous (aq) and organic (org) phase for the systems water (1) + caprolactam (2) + alkane (3) + 1-heptanol (4) at 293 K, 313 K and 333 K, where the alkane is methylcyclohexane or heptane.

$100 \cdot w_{2,\mathrm{aq}}$	$100 \cdot w_{2,\mathrm{org}}$	$100 \cdot w_{4,\mathrm{org}}$	$10^3 \gamma/\mathrm{N} \cdot \mathrm{m}^{-1}$	$100 \cdot w_{2,\mathrm{aq}}$	$100 \cdot w_{2,\mathrm{org}}$	$100 \cdot w_{4,\mathrm{org}}$	$10^3 \gamma/\mathrm{N} \cdot \mathrm{m}^{-1}$
Methylcyclohexane system at 293 K				Heptane system at 313 K			
1.03	0.65	39.87	9.5	0.99	0.72	39.61	9.5
2.66	1.46	39.36	8.3	2.51	1.63	39.60	8.8
5.10	2.50	38.98	7.9	4.97	2.93	38.73	7.2
10.24	4.39	38.22	5.3	8.87	4.80	40.82	5.6

$100 \cdot w_{4,\mathrm{org}}$	$10^3 \gamma/\mathrm{N} \cdot \mathrm{m}^{-1}$			$100 \cdot w_{4,\mathrm{org}}$	$10^3 \gamma/\mathrm{N} \cdot \mathrm{m}^{-1}$		
	293 K	313 K	333 K		293 K	313 K	333 K
Methylcyclohexane system (no caprolactam present)				Heptane system (no caprolactam present)			
0.00	49.0	47.2	44.8	0.00	50.0	48.6	46.0
39.80	12.3	11.4	12.4	40.25	11.5	11.3	12.4
100.00	7.3	8.3	8.1	100.00	7.3	8.3	8.1